

**CDCA Activation of CFTR-Dependent Cl<sup>-</sup> Secretion Requires a Complex Network of Signaling Cascades**

BY

JADA CECILIA DOMINGUE  
B.S., University of California Irvine, 2010

THESIS

Submitted as partial fulfillment of the requirements  
for the degree of Doctor of Philosophy in Physiology and Biophysics  
in the Graduate College of the  
University of Illinois at Chicago, 2016

Chicago, Illinois

Defense Committee:

Mark M. Rasenick, Chair  
Mrinalini C. Rao, Advisor  
Carlos O. Stocco, Physiology and Biophysics  
Waddah A. Alrefai, Medicine  
Giamila Fantuzzi, Kinesiology and Nutrition  
Jayashree Sarathy, Physiology and Biophysics

This thesis is dedicated to my nieces and nephews, Miles, Sophie, Ellis, and Mae Domingue, and Mavrick Graniel, may they know that you can overcome any limitations as long as you are willing to put in hard work.

## ACKNOWLEDGMENTS

I cannot begin this section without first thanking my parents and family for their continuous support over these last six years. It has not been easy being so far away from them, but their love for me and support of my education has never wavered. They have managed only seeing me a few times a year, they have put up with my attitude when things have not been going well, they have had patience when they didn't hear from me for several days or weeks because I was swamped with work, and they have always comforted me when I called crying when I was on the verge of cracking under the pressures of this program. They are my biggest cheer leaders and my confidants, and this thesis and the woman I am today is because of their love and support. This is truly their accomplishment just as much as it is mine.

Thinking back on beginning this program and not knowing if I would succeed, I was constantly reminded of my potential by my undergraduate mentors from the Minority Science Program at the University of California, Irvine, Drs. Marlene de la Cruz and Luis Mota-Bravo. I cannot thank them and the program enough for their contribution to this degree. MSP was absolutely crucial in laying the foundation for me to enter and excel in graduate school. I joined their program late in my Junior year at Irvine and they quickly helped me gain as much biomedical research experience as possible before applying to graduate school. I was very hesitant to even apply but they constantly encouraged me to strive for a higher education. Dr. de la Cruz reminds me to this day that I didn't believe in myself and that now I should look and be proud of everything I have accomplished.

I'd next like to acknowledge my committee members, Drs. Mark Rasenick, Giamila Fantuzzi, Carlos Stocco, and Waddah Alrefai for taking this journey with me. Thank you for always being present (both physically and mentally) at all of my meetings and presentations. Thank you for challenging me to think critically, for critiquing me in a constructive manner, and for guiding me in asking the right questions to create this dissertation. Also thank you for your

patience and encouragement in this last year, without your input this thesis would not be what it is today. I promise your letters of recommendation will not be taken for granted and I will represent you to the best of my abilities. Especially thank you to Dr. Alrefai for contributing to intellectual discussions that we had about my project over lab meetings during the first half of the program. Not only was my committee crucial to my evolution over the last few years, but my peers, faculty, and staff in the Department of Physiology and Biophysics truly made my time here very memorable. This is a wonderful department to train in. I'd especially like to thank Drs. John Solaro, Jesús García-Martínez, and John Kennedy for their support in all of my applications and for always being there for the students.

Thank you also to my colleagues at Erasmus University Medical Center in Rotterdam, Netherlands. Thank you Dr. Hugo de Jonge for giving me the opportunity to come and train in your lab. Thank you to Dr. Marcel Bijvelds and Yuebang Yin for your patience, guidance, and trust in culturing the organoids. My time in the Netherlands would have not have been the same without Kelly Meijsen and Anna Weijler. We shared many frustrations with these organoids and you both helped the difficult days pass easy and the good days pass even easier. Also thank you to Leonie Moree for your support and friendship during my time in Rotterdam.

To the people I have spent most of my time with, my wonderful lab members, Mei Ao, Alvin George, and Shreya Shanker, thank you. Mei you taught me almost all of the techniques used in this thesis and have been there with me each and every day to trouble shoot or to listen to my frustrations when one of my experiments hasn't gone as I had hoped. Thank you for laughing with me, for singing with me, smiling with me, and comforting me each day in the lab. You are so smart and kind, it's been a privilege to work with you all these years. I will miss you so much. To the students that I have trained or helped train, you have all challenged me to think better and smarter so that I can convey things to you that you may have not understood. The three of you brought so much spirit and youth to the lab, I would have smiled less if it wasn't for you three. Being involved in your training has been one of the most rewarding experiences

during my graduate studies. I know you all are going to go on and do great things and I can't wait to hear about it. I cannot finish thanking my lab without thanking Dr. Jayashree Sarathy. I honestly don't know if I have the words to express how grateful I am for your mentorship, "mother-ship", and friendship you have showed me. I look up to you in so many ways and I admire the way you have handled your career. You are such an intelligent, beautiful, and loving individual, I truly don't know what I would have done without you and I hope you know how much you have positively influenced my life.

Meena, what can I say but wow, it's been a fun ride. I have always admired your strength, your intelligence, your wit, and your compassion. We have had many ups and downs over the years but your support for me as a scientist, as a minority, and as an individual has been second to none. We butt heads, but we laugh, we cry, but we smile and in the end I couldn't have imagined being trained and mentored by anyone else. You have challenged me and pushed me to my limits so that I may realize my potential. I may have not always had my priorities in the order you thought best, but I cannot thank you enough for your time, patience, and guidance in research and in life. You have always had my best interests in mind, and though our conversations may have been repetitive and difficult at times because I wasn't rising to my challenges, I always walked away from them knowing that you always made time for me because of how much you cared. I don't think most students have advisors that care about them as much as you did for me, and I hope all of your mentees see your value, I know I did. You are more than a research advisor, you have been my mentor in research and in diversity, you have been like a second mother, and you have become a friend that I didn't realize I would gain out of an advisor-advisee relationship. Thank you for making me the scientist and woman I am today; I am a better person because of you.

I have to credit my survival through this program to those that I didn't share a bench with, to the people who have been with me every step of the way, my friends: Drs. Ruby Ana Fernandez, Melissa Geyer, Shweta Dambal, Jesus Banuelos, Juan Jimenez, and Franklin

Garcia. We all started this grad school journey together, and now we are finally all done. The bond that was created through the challenges we faced together will never be broken. In one way or another you have all been my confidants, drinking buddies, eating buddies, crying buddies, and burn-out buddies. From our late night study sessions during our first year, to supporting each other at presentations, to all the birthdays we celebrated together, you are much more than friends, you are, and will always be, my family. Ruby and Jesus, we didn't know each other that well when we decided to be Chicago roommates, but your friendship has meant the world to me. We cooked for each other, protected each other, and celebrated each other; I know our parents were glad we had each other when we moved here. Ruby you are my closest friend and a sister to me, and Jesus you are the brother I never had. I can't wait to see where life takes all of us.

Last, but certainly not least, Dr. Leonid Serebryannyy. I had absolutely no idea what Chicago would bring, but never did I think it would be you. You are possibly the smartest, hardest working, and caring individual that I know and I have been so blessed to have you by my side through every second of this journey. You have been with me at my lowest of lows, and my highest of highs and I know I will always have you to count on when I feel lost. You are my best friend and probably a bigger cheerleader of mine than my family. We started this as peers and I was very intimidated by your intelligence; I saw you as my competition. We became friends and I teased you, while you challenged me to be better and have faith in myself. And while those aspects of our relationship have not changed, our relationship has evolved into so much more. You are more than my best friend and I am forever grateful for experiencing this chapter of our lives together. Thank you for loving me, thank you for the time and effort that you have put into us, and thank you for making me a better scientist and a better human being. We have so much more ahead of us and I can't wait to be by your side for all that we will accomplish and fail at. You aren't my competition anymore; you are my partner.

## CONTRIBUTION OF AUTHORS

Some of the data presented in **Chapter III** represent part of the work that I contributed to our laboratory's manuscript (Ao M, Sarathy J, **Domingue J**, Alrefai WA, and Rao MC. 2013. Chenodeoxycholic acid stimulates Cl<sup>-</sup> secretion via cAMP signaling and increases cystic fibrosis transmembrane conductance regulator phosphorylation in T84 cells. *Am J Physiol Cell Physiol.* 305:C447–C456) for which I was the third author and assisted the drafting and revisions of the manuscript. I performed the immunoblots and the TGR5 mRNA transcript studies in **Figure 8**. I also elucidated the role of muscarinic receptors presented in **Figure 10**. **Chapter IV** represents a series of my own experiments directed at answering which second messenger pathways are involved in CDCA action. **Figure 23A** was also used from the same manuscript (above) and the data was reanalyzed for this thesis. Additionally, experiments for **Figure 28B** were designed by me but performed by our colleague Dr. J. Sarathy at Benedictine University (Lisle, IL). **Chapter V** includes data from my primary author manuscript (**Domingue JC**, Ao M, Sarathy J, George A, Alrefai WA, Nelson DJ, and Rao MC. HEK-293 cells expressing the cystic fibrosis transmembrane conductance regulator (CFTR): a model for studying regulation of Cl<sup>-</sup> transport. *Physiological reports* 2: 2014) in an attempt to utilize the HEK-293 cell line as another model to investigate bile acid action. Mei Ao assisted in the generation of the HEK-CFTR cell line and helped perform the CFTR trafficking experiments in **Figure 36**. Alvin George helped perform the iodide efflux and Ca<sup>2+</sup> measurements shown in **Figure 41**. The data presented in **Table III** was recently published (Ao M, **Domingue JC**, Khan N, Javed F, Osmani K, Sarathy J, and Rao MC. Lithocholic acid attenuates cAMP-dependent Cl<sup>-</sup> secretion in human colonic epithelial T84 cells. *American journal of physiology Cell physiology* 310: C1010-1023, 2016). Finally, studies shown in **Chapter VI** were performed with the help of Dr. M. Bijvelds and Kelly Meijssen under Dr. H. de Jonge at Erasmus Medical Center in Rotterdam, Netherlands. The future directions and implications of this work are discussed in **Chapter VII**.

## TABLE OF CONTENTS

CHAPTER	PAGE
I. Introduction .....	1
A. Bile Acid Physiology .....	3
1. Synthesis .....	3
2. Lipid Digestion and Enterohepatic Circulation .....	4
3. Bile Acids and the Gut Microbiota .....	8
4. Role of Bile Acid as Signaling Molecules .....	11
i. Activation of Nuclear Receptors .....	11
ii. Activation of Membrane Receptors .....	13
iii. Direct Membrane Perturbations .....	17
B. Mammalian Colon .....	18
1. Structure .....	19
2. Function .....	22
C. Bile Acids and the Regulation of Epithelial Ion Transport .....	23
1. Establishment of the Driving Force for Cl <sup>-</sup> Secretion .....	23
2. Cl <sup>-</sup> Channels .....	24
3. Intracellular Signaling Pathways .....	28
i. Intracellular Signaling Pathways: cAMP .....	28
ii. Intracellular Signaling Pathways: Ca <sup>2+</sup> .....	29
iii. Intracellular Signaling Pathways: Store Operated cAMP Signaling .....	31
iv. Intracellular Signaling Pathways: EGFR and Associated Kinases .....	32
v. CDCA Action in T84 Cells .....	34
D. Bile Acids and Pathophysiology .....	34
1. Bile Acids and Colorectal Cancer .....	35
2. Bile Acids and the Metabolic Syndrome .....	36
3. Bile Acid Malabsorption and Bile Acid-Associated Diarrhea .....	36
E. Models for Ion Transport .....	40
1. Human Colonic T84 Cells .....	40
2. Human Embryonic Kidney-293 Cells .....	42
3. Intestinal Organoids Cultures .....	43
F. Hypothesis, Objective, and Specific Aims .....	45
II. Materials and Methods .....	47
A. Materials .....	48
B. Tissue Culture .....	49
C. Transfection .....	50
1. CFTR Over-Expression .....	50
2. EGFR siRNA .....	51
D. RNA Isolation and Reverse Transcriptase Polymerase Chain Reaction (RT-PCR) .....	52
E. Protein Isolation, SDS-polyacrylamide gel electrophoresis, and Immunoblotting .....	53
F. Human Phosphokinase Array .....	54
G. Preparation of Detergent-Soluble and Insoluble Tubulin .....	54
H. Cell Surface Biotinylation .....	55
I. Live Cell Imaging and Vesicle Trafficking .....	56
J. Intracellular Ca <sup>2+</sup> ([Ca <sup>2+</sup> ] <sub>i</sub> ) Measurements .....	57
K. Intracellular cAMP ([cAMP] <sub>i</sub> ) Measurements .....	58
L. IP <sub>3</sub> Measurements .....	58
M. Ussing Chambers .....	59
N. Iodide Efflux .....	62
O. Rap Activation Assay .....	63

## TABLE OF CONTENTS (CONTINUED)

CHAPTER	PAGE
P. Organoids.....	64
1. Generation and Maintenance.....	64
2. Swelling Assay.....	66
Q. Statistics.....	66
III. Results: Bile Acid Activation of Cl <sup>-</sup> Transport in T84 Cells.....	68
A. Rationale and Aim.....	69
B. Bile Acid Specificity and Sidedness of Action.....	69
C. Bile Acid Specific Receptors.....	72
1. FXR and TGR5 Expression.....	72
2. Bile Acid Receptor Agonists and I <sub>sc</sub> .....	74
D. Role of Putative Bile Acid Receptors in CDCA Action.....	76
1. Effect of Inhibition of Muscarinic Receptors by Atropine.....	76
2. Effect of Inhibition of EGFR by AG1478.....	76
E. CDCA Activation of EGFR.....	78
1. EGFR phosphorylation.....	78
2. Effect of EGFR Knockdown on CDCA-Induced Cl <sup>-</sup> transport.....	80
3. Involvement of Matrix Metalloproteinases.....	82
F. Membrane Perturbations.....	83
G. Discussion.....	84
IV. Results: CDCA activation of 2 <sup>nd</sup> Messenger Signaling Pathways.....	89
A. Rationale and Aim.....	90
B. The Role of Ca <sup>2+</sup> in CDCA Action.....	90
C. PLC Activation in CDCA Action.....	93
1. The Role of IP <sub>3</sub> in CDCA Action.....	93
2. The Role of PKC in CDCA Action.....	95
D. The Role of EGFR-Related Kinases in CDCA Action.....	97
1. Human Phosphokinase Array.....	97
2. Src Kinase and CDCA Activation of I <sub>sc</sub> .....	99
3. p38 and ERK 1/2 Kinases in CDCA Signaling.....	100
4. PI3K in CDCA Action.....	103
E. The Role of cAMP in CDCA Action.....	105
1. Rap1 Signaling in CDCA-Stimulated I <sub>sc</sub> .....	112
2. Rap2 Signaling in CDCA Action.....	114
F. Discussion.....	116
V. Results: Characterization of Cl <sup>-</sup> Transport in HEK-293 Cells.....	121
A. Rationale and Aim.....	122
B. Expression of Cl <sup>-</sup> channels in HEK.....	122
C. Establishment and Characterization of HEK-CFTR cell line.....	123
1. Forskolin Dose Response in HEK-CFTR.....	125
2. Forskolin Responses in HEK and HEK-CFTR Cells.....	127
3. Effect of CFTRinh172 on Forskolin-Induced Iodide Efflux.....	127
4. Forkolin-Induced cAMP Signaling in HEK-CFTR Cells.....	129
5. The Role of MRP4 in HEK-CFTR Cells.....	131
6. Effect of Ca <sup>2+</sup> Chelation on the Forskolin Response in HEK-CFTR Cells.....	133
7. Effect of Forskolin on CFTR Surface Expression of CFTR.....	134
8. Effect of Nocodazole in HEK-CFTR cells.....	135
i. Effect of Nocodazole on Tubulin.....	135
ii. Effect of Nocodazole on Forskolin-Induced Iodide Efflux.....	137

## TABLE OF CONTENTS (CONTINUED)

<u>CHAPTER</u>	<u>PAGE</u>
D. Bile Acid Signaling in HEK-293 Cells .....	139
1. Expression of TGR5 in HEK Cells .....	139
2. CDCA-Induced Iodide Efflux in HEK v HEK-CFTR Cells .....	139
i. CDCA Dose Response.....	139
ii. Microtubule Destabilization in CDCA Action in HEK-CFTR Cells.....	142
iii. Effect of CFTRinh172 on CDCA Action in HEK Cells.....	142
iv. CDCA and Ca <sup>2+</sup> Signaling in HEK Cells .....	144
3. LCA Action in HEK and HEK-CFTR Cells.....	146
i. LCA Dose Response.....	146
ii. Effect of LCA Pretreatment on Iodide Efflux.....	146
iii. LCA and 2 <sup>nd</sup> Messenger Production .....	148
E. Discussion .....	149
VI. Results: CDCA Action in Intestinal Organoids .....	156
A. Rationale and Aim .....	157
B. Relevance of Organoid Cultures .....	157
C. Region Specific Organoid Swelling .....	158
D. EPAC and CDCA-Induced Organoid Swelling .....	160
E. Discussion .....	162
VII. General Conclusions and Future Directions.....	165
VIII. Cited Literature .....	180
IX. Appendices.....	203
A. Appendix A: Permissions .....	203
B. Appendix B: Letter to the Graduate College from Dr. Mary Bowman.....	204
IX. Vita .....	205

## LIST OF TABLES

<u>TABLE</u>		<u>PAGE</u>
I. Reverse Transcriptase Polymerase Chain Reaction primers .....		52
II. Sidedness of conjugated and unconjugated bile acids .....		70
III. Effect of LCA in T84 cells .....		147

## LIST OF FIGURES

<u>FIGURE</u>	<u>PAGE</u>
1. Structures of the major bile acids .....	5
2. Enterohepatic circulation of bile acids .....	7
3. Bile acid transporters and negative feedback.....	10
4. Epithelial Cl <sup>-</sup> secretion .....	27
5. Typical Ussing chamber protocol.....	61
6. Depiction of crypt isolation to organoid maturation.....	67
7. Specificity of bile acids on Cl <sup>-</sup> secretion.....	71
8. Bile acid receptor expression.....	73
9. Effect of bile acid receptor agonists on I <sub>sc</sub> .....	75
10. Effect of putative bile acid receptor antagonists on CDCA-induced I <sub>sc</sub> .....	77
11. Effect of CDCA on EGFR phosphorylation .....	79
12. Effect of EGFR siRNA on EGFR expression and CDCA-induced Cl <sup>-</sup> Transport .....	81
13. Effect of MMP inhibition on the CDCA response .....	83
14. Receptor involvement in CDCA action .....	88
15. The role of Ca <sup>2+</sup> in CDCA action.....	92
16. The role of PLC in CDCA action .....	94
17. Effect of PKC inhibition on CDCA-induced I <sub>sc</sub> .....	96
18. Kinase phosphorylation by CDCA .....	98
19. Effect of Src inhibition on CDCA-induced I <sub>sc</sub> .....	99
20. The role of p38 in CDCA action .....	101
21. The role of ERK1/2 signaling in CDCA action .....	102
22. Effect of inhibition of PI3K and AKT on CDCA action.....	104
23. Effect of inhibition of PKA on I <sub>sc</sub> .....	105
24. Effect of EPAC inhibition on the CDCA response.....	107
25. EPAC involvement in apical Cl <sup>-</sup> currents .....	109
26. The effect of inhibition of PKA and EPAC on CDCA action.....	111
27. Rap1 signaling in CDCA action .....	113
28. Rap2 activation in CDCA action .....	115
29. Summary of intracellular signaling initiated by CDCA .....	120
30. Cl <sup>-</sup> channel expression in HEK-293 and HEK-CFTR cells.....	124
31. Forskolin-induced iodide efflux in HEK-CFTR cells.....	126
32. Effect of forskolin on iodide efflux in HEK-CFTR and HEK-293 cells .....	128
33. The role of CFTR and cAMP signaling in forskolin-induced iodide efflux .....	130
34. MRP expression and function in HEK-CFTR cells.....	132
35. Effect of BAPTA-AM on forskolin-induced iodide efflux.....	133
36. Effect of forskolin on the surface expression of CFTR .....	136
37. Effect of nocodazole treatment in HEK-CFTR cells.....	138
38. Expression of TGR5 in HEK-293/CFTR cells .....	140
39. CDCA-induced iodide efflux in HEK-293 and HEK-CFTR cells.....	141
40. Effects of nocodazole and CFTRinh172 on CDCA action in HEK-CFTR cells .....	143
41. Ca <sup>2+</sup> in CDCA action in HEK-293 cells .....	145
42. LCA action in HEK-CFTR cells .....	147
43. Measurements of 2 <sup>nd</sup> messenger production by LCA in HEK-CFTR cells.....	148
44. Mouse intestinal region specific organoid swelling .....	159
45. Effect of ESI-09 on mouse colonic organoid swelling.....	161
46. Summary of the complex network of signaling cascade induced by CDCA .....	179

## LIST OF ABBREVIATIONS

[Ca <sup>2+</sup> ] <sub>i</sub>	intracellular Ca <sup>2+</sup>
[Ca <sup>2+</sup> ] <sub>o</sub>	extracellular Ca <sup>2+</sup>
[cAMP] <sub>i</sub>	intracellular cAMP
AKT	protein kinase B
ASBT	apical sodium-dependent bile acid transporter
ATP	adenosine triphosphate
BSH	bile salt hydrolase
CA	cholic acid
CaCC	calcium activated Cl <sup>-</sup> channel
cAMP	3',5'-cyclic adenosine monophosphate
CAR	constitutive androstane receptor
CDCA	chenodeoxycholic acid
CF	cystic fibrosis
CFTR	cystic fibrosis transmembrane conductance regulator
cGMP	cyclic guanosine monophosphate
CYP7A1	cholesterol 7 $\alpha$ -hydroxylase
DCA	deoxycholic acid
DNA	deoxyribonucleic acid
EGF	epidermal growth factor
EGFP	enhanced green fluorescent protein
EGFR	epidermal growth factor receptor
EPAC	exchange protein directly activated by cAMP
ERK	extracellular signal-regulated kinase
FGF	fibroblast growth factor
FXR	farnesoid X receptor
GDP	guanosine diphosphate
GPCR	G-protein coupled receptor
GTP	guanosine triphosphate
HB-EGF	heparin binding-EGF-like growth factor
HEK-293	human embryonic kidney 293 cells
HEK-CFTR	CFTR transfected HEK-293 cells
HRP	horse radish peroxidase
IBD	inflammatory bowel disease
IBS	irritable bowel syndrome
IP <sub>3</sub>	inositol (1, 4, 5) triphosphate
I <sub>sc</sub>	short circuit current
I $\kappa$ B $\alpha$	inhibitor of nuclear factor of kappa light polypeptide gene enhancer in B cells
LCA	lithocholic acid
MAPK	mitogen activated protein kinase
MEK	MAPK kinase to ERK 1/2
MKK	MAPK kinase
MMP	matrix metalloproteinase
MRP	multidrug resistance-associated protein
M $\#$ R	muscarinic (isoform) receptor
NEC	necrotizing enterocolitis
NF- $\kappa$ B	nuclear factor of kappa light polypeptide gene enhancer in B cells

## LIST OF ABBREVIATIONS (CONTINUED)

NHE	Na <sup>+</sup> /H <sup>+</sup> exchanger
PBS	phosphate buffered saline
PDZ	PSD95, DlgA, ZO-1
PGC-1 $\alpha$	peroxisome proliferator-activated receptor gamma coactivator 1 $\alpha$
PI3K	phosphatidylinositol-4,5-bisphosphate 3-kinase
PKA	protein kinase A
PKC	protein kinase C
PLC	phospholipase c
PXR	pregnane X receptor
RNA	ribonucleic acid
ROCK	Rho-associated protein kinase
S1PR2	sphingosine 1 phosphate receptor 2
SHP	small heterodimer partner
siRNA	small interfering RNA
SOcAMPS	store-operated cAMP signaling
SOCE	store-operated Ca <sup>2+</sup> entry
TER	transepithelial electrical resistance
TGR5	transmembrane G-protein coupled receptor 5
TMEM16	transmembrane member 16
TRPC	transient receptor potential proteins
UDCA	ursodeoxycholic acid
VDR	vitamin D receptor
VIP	vasoactive intestinal peptide

## SUMMARY

Bile acids are synthesized in the liver and secreted into the small intestine to aid in lipid digestion and absorption. Approximately 95% of bile acids are reabsorbed in the terminal ileum and recycled back to the liver by enterohepatic circulation. The remaining 5% enter the colon and may be reabsorbed or excreted. Bile acid malabsorption, such as seen in irritable bowel syndrome, greatly increases colonic bile acid concentrations leading to excess fluid secretion and diarrhea. Of the approximately 90 million irritable bowel syndrome patients worldwide, annually over 10 million suffer from bile acid-associated diarrhea. Despite the prevalence of bile acid-associated diarrhea, the molecular mechanisms underlying bile acid action have yet to be fully elucidated. Previous work in our laboratory established that the primary, 7 $\alpha$ -dihydroxy bile acid, chenodeoxycholic acid (CDCA), activates Cl<sup>-</sup> secretion via the cystic fibrosis transmembrane conductance regulator (CFTR) in human colonic cells, and was partially dependent on protein kinase A (PKA) activation (Ao, Sarathy, Domingue, Alrefai, and Rao, *AJP*:305:C447-C456, 2013). Based on this, we hypothesized that CDCA utilizes a membrane receptor-mediated activation of multiple intracellular signaling cascades to stimulate CFTR-dependent Cl<sup>-</sup> secretion. We tested our hypothesis in the human colonic T84 cell line, HEK-293 cells and in mouse intestinal organoids. Cl<sup>-</sup> transport was measured by changes in short-circuit current ( $I_{sc}$ ), iodide efflux assay, and by organoid swelling. We find that in T84 cells, CDCA does not act through any of the well-established bile acid receptors: the nuclear farnesoid X receptor, or the G-protein coupled receptors, transmembrane G-protein coupled receptor 5 or the muscarinic receptor. However, CDCA transactivates the epidermal growth factor receptor (EGFR), increasing its phosphorylation. Intracellularly, CDCA action involves intricate crosstalk between cAMP, Ca<sup>2+</sup>, and EGFR signaling cascades to activate CFTR. CDCA activates cAMP signaling, leading to activation of PKA and the exchange protein directly activated by cAMP (EPAC). While PKA phosphorylates CFTR, CDCA also activates Rap2 via EPAC, which may be leading to the changes in intracellular Ca<sup>2+</sup> that we observe. Furthermore, cAMP signaling

mediates CDCA-induced EGFR activation. In an attempt to better understand the molecular mechanisms involved in CDCA's regulation of CFTR, we developed a stable CFTR-expressing HEK-293 cell line. While CFTR is functional and regulated in its canonical manner by cAMP and PKA, CDCA stimulates Cl<sup>-</sup> transport independently of CFTR in HEK-293 cells, suggesting a cell type specific activation of Cl<sup>-</sup> transport by CDCA. Although cell lines are useful to study regulation of Cl<sup>-</sup> secretion, they may not represent the in vivo situation. Therefore, we examined CDCA responsiveness in intestinal organoids derived from intestinal crypt stem cells. Preliminary findings reveal that CDCA increases fluid transport, measured by organoid swelling, especially in colon-derived organoids and is partially dependent on EPAC activation, paralleling our findings in T84 cells. The data presented here reveal the complex network of signaling cascades initiated by bile acids, underlying the secretory processes that contribute to bile acid-associated diarrhea, and lay the foundation for identification of new therapeutic targets to alleviate diarrheal symptoms.

## **Chapter I: Introduction**

Under normal physiological conditions, bile acids are essential for the emulsification and absorption of lipids. The primary bile acids are synthesized from cholesterol in the liver and secreted into the small intestine. Because bile acids are the primary exit pathway for cholesterol metabolism, it is critical that the bile acid pool be tightly regulated. This regulation of the pool is maintained by synthesis of new bile acids by the liver, efficient reabsorption of bile acids in the terminal small intestine to recycle back to the liver, and the excretion of remaining luminal bile acids into the feces. Some intestinal disorders that affect bile acid metabolism, such as irritable bowel syndrome and inflammatory bowel diseases, result in bile acid malabsorption.

The consequence of bile acid malabsorption is an increase in the colonic luminal concentration of bile acids. The colon normally functions to absorb the majority of fluid that was not absorbed in the small intestine, and to decrease the fluid content of the feces. This function is achieved by a tightly regulated balance of the secretory and absorptive processes of the colonic epithelium. When there is an influx of pathological concentrations of bile acids into the colon, the bile acids impact normal colonic functioning by decreasing absorption and increasing secretion of fluid, resulting in secretory diarrhea. It has been well established in a variety of species that bile acids increase colonic fluid secretion by activating  $\text{Cl}^-$  channels on the apical membrane of colonic epithelial cells. While our laboratory previously published that this occurs via  $\text{Ca}^{2+}$  and protein kinase C (PKC)- $\delta$  signaling in the rabbit (118, 250), we have also found species differences in signaling. In contrast to the rabbit, bile acids, specifically chenodeoxycholic acid (CDCA), stimulate the apical  $\text{Cl}^-$  channel, the cystic fibrosis transmembrane conductance regulator (CFTR), partially via a protein kinase A (PKA)-dependent mechanism in the human colonic epithelial cell line, T84 (15). The partial involvement of PKA suggested the potential contribution of other, as yet unresolved, signaling cascades in the action of CDCA on  $\text{Cl}^-$  secretion. Thus, the purpose of this study was to further investigate the molecular mechanisms underlying CDCA activation of  $\text{Cl}^-$  secretion, to contribute to our knowledge of bile acid physiology and our understanding of bile acid-induced diarrhea.

To establish the foundation on which this investigation was based, the remaining sections of the introduction provide background on the following: bile acid physiology, including their role as signaling molecules; a description of the colonic epithelial cell architecture and secretory function; cellular signaling pathways that are known to be involved in Cl<sup>-</sup> secretion and in bile acid action; and the impact of bile acids on intestinal pathophysiology. Furthermore, we establish the use of T84 cells, human embryonic kidney-293 cells, and mouse-derived intestinal organoids as models to study bile acid action on ion transport.

## **A. Bile Acid Physiology**

### **1. Synthesis**

Bile acids are the end products of cholesterol metabolism in the liver. The synthesis of the two primary bile acids, cholic acid (CA) and CDCA, is the result of several enzymatic modifications of the sterol nucleus of cholesterol. Classically, degradation of cholesterol into the primary bile acids begins with cholesterol 7 $\alpha$ -hydroxylase (CYP7A1), the rate-limiting step of bile acid synthesis in hepatocytes. CA is trihydroxylated, with hydroxyl groups at positions 3 $\alpha$ , 7 $\alpha$ , and 12 $\alpha$ , whereas CDCA is dihydroxylated, with hydroxyl groups at positions 3 $\alpha$  and 7 $\alpha$  (**Figure 1**). In the mouse, CDCA is modified by 6 $\alpha/\beta$ -hydroxylase epimerase into the trihydroxylated muricholic acid (3 $\alpha$ , 6 $\alpha/\beta$ , 7 $\alpha/\beta$ ). Within hepatocytes, bile acids are conjugated with taurine or glycine by bile acid coenzyme A synthase and the bile acid amino acid N-acyl transferase, to render them more water-soluble. The predominant species, accounting for 95% of the bile acid pool in the human liver and biliary secretions, are the taurine and glycine conjugates of CDCA, CA, and deoxycholic acid (DCA). The other 5% is made up of sulfated or glucuronidated bile acids including sulfolithocholyglycine and sulfolithocholy taurine, which are largely excreted from the body (106). In the intestinal lumen, bacterial bile salt hydrolase removes the taurine or glycine (**Figure 2**). Further modification by bacterial 7 $\alpha$ -dehydroxylase converts the primary bile

acids into the secondary bile acids. CA is converted to DCA, with hydroxyl groups remaining at the 3 $\alpha$  and 12 $\alpha$  positions. CDCA is converted to lithocholic acid (LCA), which is monohydroxylated at position 3 $\alpha$ . It is noteworthy that deconjugation must precede dehydroxylation as the 7 $\alpha$ -dehydroxylases cannot act on conjugated bile acids. In addition to dehydroxylation of CDCA, bacterial epimerization of CDCA results in production of ursodeoxycholic acid (UDCA; 3 $\alpha$  and 7 $\beta$ ), which was originally discovered in bear bile (**Figure 1**) (52, 65, 161). These intestinal bacterial modifications are reflected in the bile acid composition of human plasma. As determined by ultra-performance liquid chromatography, mass spectrometry, and multiple reaction monitoring, the bile acid composition of human plasma is 52% unconjugated bile acids, 42% glycine-conjugated, and 6% taurine-conjugated bile acids. The dominant bile acid species in human serum are DCA (19%), CA (16%), CDCA (15%), and of the conjugated species, glycine conjugated-CDCA make up 24%, with the remaining species a mix of glycine and taurine conjugated forms ( $\leq 5\%$  each) (94). Ahlberg et al. reported that the portal venous content was  $6.14 \pm 1.20\mu\text{M}$  CA,  $8.4 \pm 1.84\mu\text{M}$  CDCA, and  $6.18 \pm 2.27\mu\text{M}$  DCA (2).

## **2. Lipid Digestion and Enterohepatic Circulation**

Post-synthesis, bile acids are moved in and out of cells via a variety of transporters (6). They are transported from the hepatocyte into the bile duct via the bile salt export pump (**Figure 3**). The bile acids combine with water, bilirubin, and cholesterol to form bile that is stored and concentrated in the gallbladder. Upon digestion of a meal, the gastrointestinal hormone cholecystokinin stimulates gallbladder contraction and release of bile into the small intestine. Here, bile acids assist in the emulsification of lipids and the absorption of fat-soluble vitamins. Because bile acids are amphipathic in nature, they form micelles around lipid droplets and allow pancreatic lipase to breakdown triglycerides to be absorbed by small intestinal enterocytes (24).

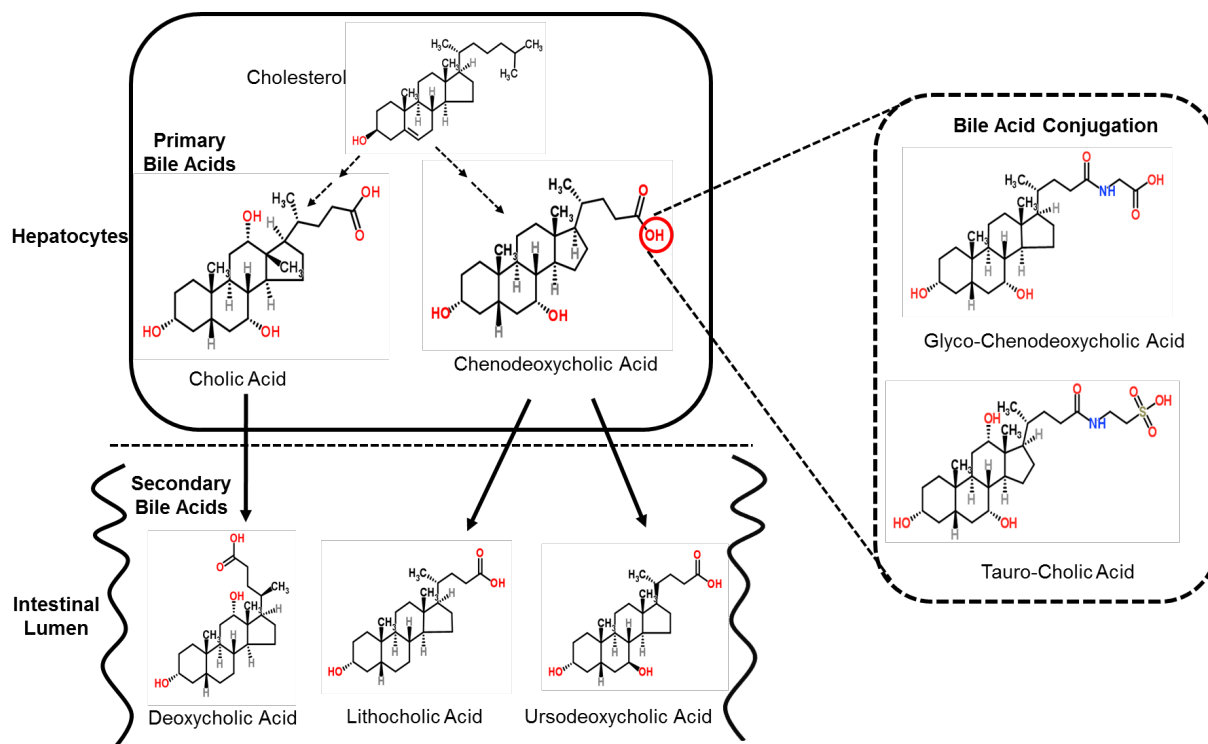


**Figure 1:** Structures of the major bile acids. Bile acids are derived from cholesterol by a series of enzymatic reactions, including 7 $\alpha$ -hydroxylase and 12 $\alpha$ -hydroxylase, in the liver into the primary bile acids cholic acid (hydroxyl positions: 3 $\alpha$ , 7 $\alpha$ , and 12 $\alpha$ ) and chenodeoxycholic acid (hydroxyl positions: 3 $\alpha$  and 7 $\alpha$ ). Intestinal bacteria modify the primary bile acids into the secondary bile acids deoxycholic acid, lithocholic acid, and ursodeoxycholic acid. Bile acids can also be conjugated to glycine or taurine as depicted in the representation (right hand box) of glycine conjugated chenodeoxycholic acid and taurine conjugated cholic acid.

In order to form micelles, bile acids must reach their critical micellar concentration. In water, CDCA has a critical micellar concentration of 9mM and CA 13mM. These critical micellar concentrations are reduced if the bile acids are conjugated or if they are in a 0.15M Na<sup>+</sup> solution (181). Any unconjugated bile acids traveling down the length of the small intestine enter enterocytes by passive diffusion, but the majority (95%) of conjugated bile acids are actively transported in the distal ileum by the apical sodium-dependent bile acid transporter (ASBT). From there, they are exported into the portal circulation by the organic solute transporters  $\alpha/\beta$  (**Figure 3**). Once they reach the liver, they are absorbed by hepatocytes through the Na<sup>+</sup>-taurocholic acid cotransporting polypeptide or the organic anion transporting polypeptides (**Figure 3**). The bile acids are then re-conjugated or re-epimerized to be used again (2-6 times/day), thus establishing enterohepatic recirculation of bile acids (**Figure 2**) and maintenance of the bile acid pool, which is ~2-3g in adult humans (106). Of note, rehydroxylation of the C-7 position does not occur in humans, so new CDCA and CA must be synthesized; ~0.3g/day (106, 235). Although some passive absorption occurs in the colon, the remaining 5% is excreted in the feces (65, 161).

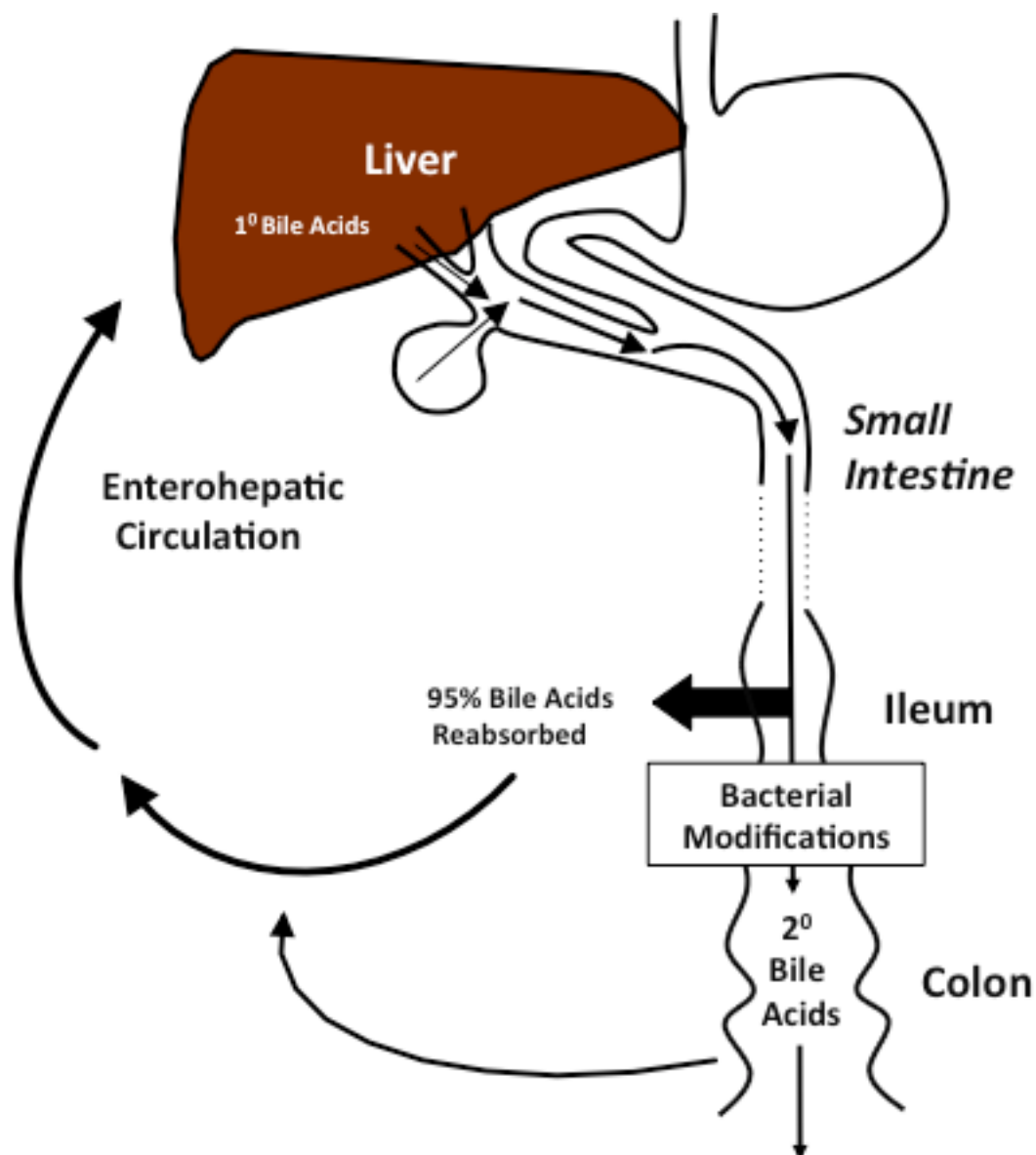


**Figure 2:** Enterohepatic circulation of bile acids. Primary bile acids in the small intestine facilitate lipid digestion and absorption. Modifications by bacteria result in the formation of secondary bile acids in the intestinal lumen. The majority of bile acids are absorbed in the distal ileum. Conjugated bile acids are transported by ASBT on the ileal enterocytes and unconjugated bile acids enter enterohepatic circulation via passive diffusion across the epithelial layer. When the bile acids return to the liver, they are reconstituted and re-epimerized to be used for the next round of digestion. Any remaining bile acids in the colon may be passively absorbed, or excreted in the feces.

### **3. Bile Acids and the Gut Microbiota**

Gut microbiota play a critical role in bile acid biology, being long recognized both for bile acid deconjugation and formation of secondary bile acids. The gut microbiota increase significantly in the first year of life. Prior to the maturation of the gut microbiome, the bile acid pool mainly consists of primary bile acids. As the microbiota colonize the intestinal lumen there is an increase in the amount of secondary bile acids in the bile acid pool (106). Recent insights into the influence of the gut microbiota on normal and pathological physiology are proving the importance of the interactions between bacteria and host. It is estimated that  $10^{14}$  microorganisms live along the length of the human gastrointestinal tract, with 500-1000 different species of bacteria, although the microbiota are largely concentrated in the colon ( $\sim 10^{12}$  bacteria/g wet fecal weight). In addition to bacteria, the microbiota community is composed of Archaea, bacteriophages, viruses, and eukaryotic microorganisms, which function as their own organ-like system (87, 211). Bacterial modifications, specifically  $7\alpha/\beta$  hydroxylation, of primary bile acids are necessary for the production of secondary bile acids (205). In fact, Sayin et al. (213) showed that mice lacking gut microbiota have no secondary bile acids and have an increased bile acid pool. The increase in the bile acid pool is due to the lack of bacterial degradation of  $\beta$  muricholic acid, which is the predominant bile acid in mice.  $\beta$  muricholic acid negatively regulates the bile acid specific nuclear receptor, the farnesoid X receptor (FXR), and under normal conditions FXR regulates the synthesis of new bile acids. Thus, inhibition of FXR by  $\beta$  muricholic acid increases bile acid synthesis. Prior to the conversion to secondary bile acids, the intestinal microbiota first modify bile acids by deconjugating the glycine and taurine side chains with the enzyme bile salt hydrolase. Joyce et al. (116) colonized germ free mice, which normally don't produce secondary bile acids, with a strain of *E. coli* that express bile salt hydrolase 1. These mice then had a reduced bile acid pool and had increased amounts of free CA and muricholic acid. Although a variety of microbial species have this hydrolase1 activity,

only a small set of *Clostridium* species have the enzymes that can dehydroxylate the primary bile acids (260, 261). However, bile acids that are sulfated by sulfotransferase in distal ileal epithelial cells are resistant to bacterial modifications, allowing for their excretion from the body (62, 82). Despite taurine and glycine, released by deconjugation of bile acids, serving as metabolic substrates for the bacteria, bile acids can also be detrimental to bacteria in a number of ways. Bile acids can act as antimicrobial agents by inhibiting bacterial growth (136, 150), by causing damage to the bacterial cell membrane, and by disrupting normal bacterial functions (63, 168, 238). Interestingly, CDCA can act in an antimicrobial manner by inhibiting tauro-CA-induced spore germination of *Clostridium difficile*, a species well known to cause diarrhea (231).

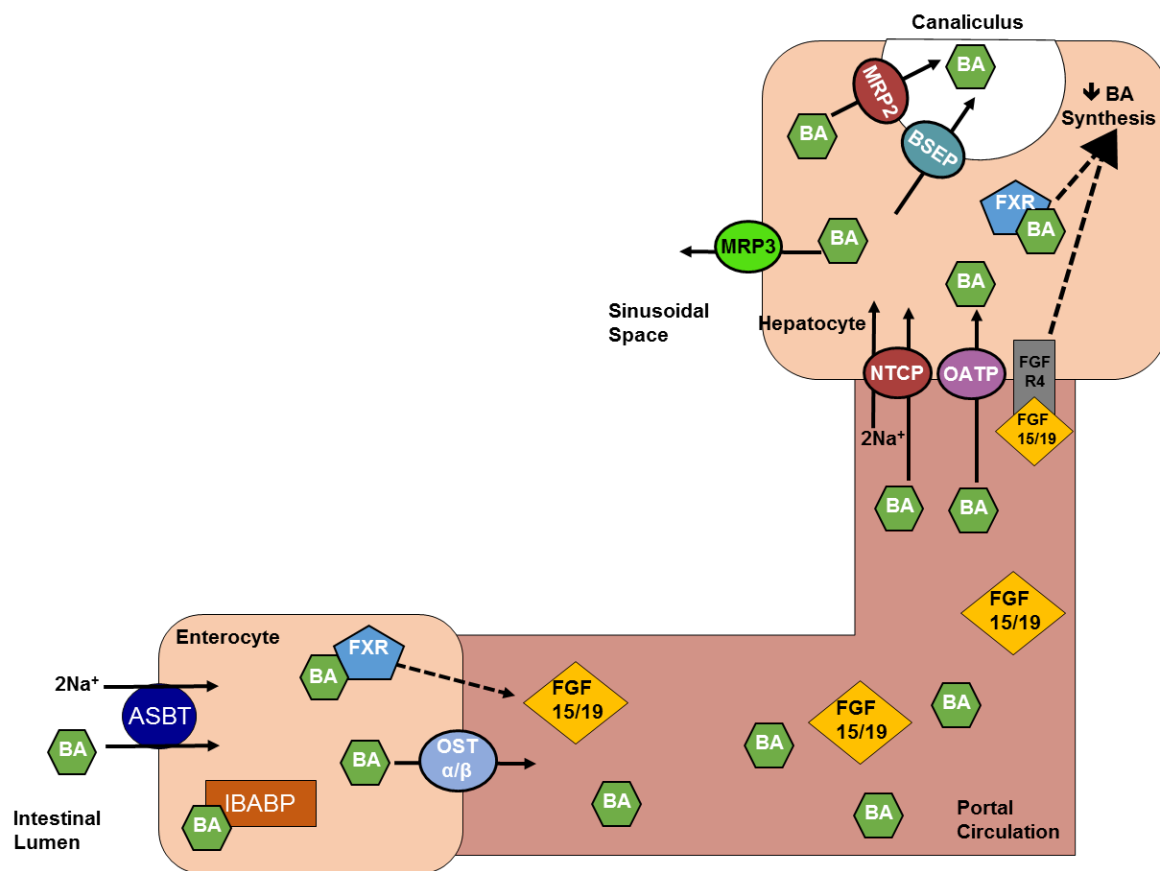


**Figure 3:** Bile acid transporters and negative feedback. Conjugated bile acids (BA) in the terminal ileum are absorbed by the apical Na<sup>+</sup>-dependent bile acid transporter (ASBT). They are transported intracellularly by the ileal bile acid binding protein (IBABP). Bile acids are effluxed from the enterocyte by the basolateral transporters, the organic solute transporter proteins α and β (OSTα/β). Bile acids can also activate the nuclear receptor, the farnesoid X receptor (FXR), in the enterocytes to produce fibroblast growth factor 15/19 (FGF15/19). Bile acids and FGF15/19 travel through portal circulation back to the hepatocytes. The Na<sup>+</sup>-dependent taurocholic cotransporting polypeptide (NTCP) and the organic anion transporting polypeptide (OATP), located on the basolateral membrane, transport bile acids into hepatocytes. Bile acids leave the hepatocytes into the sinusoidal space by multidrug resistance-associated protein (MRP), MRP3, or into the canaliculus via the bile salt export protein (BSEP) and MRP2. FGF15/19 binds to its receptor, FGF4, and leads to down regulation of bile acid synthesis. Bile acid binding to FXR in hepatocytes also decreases bile acid synthesis.

#### **4. Role of Bile Acids as Signaling Molecules**

Aside from their role in lipid digestion and their interactions with the microbiota, there has been accumulating evidence for bile acids to be considered as signaling molecules. The majority of this evidence lies in the discovery of bile acid-activated receptors, specifically the. The lipophilic nature of bile acids allows for passive diffusion across the plasma membrane to activate nuclear receptors. Additionally, bile acids can bind and activate plasma membrane bound receptors. Activation of these bile acid specific (e.g. FXR or the transmembrane G-protein coupled receptor 5, TGR5) and non-specific receptors [e.g. vitamin D receptor (VDR), muscarinic 3 receptor (M3R)] exert genomic and non-genomic effects as described below.

##### **i. Activation of Nuclear Receptors**

Signaling by bile acid-activated nuclear receptors regulates bile acid synthesis, metabolism and toxicity, and promotes detoxification of bile acids and removal of bile acids from the body. The discovery of FXR (encoded by the *NR1H4* gene) as a nuclear receptor specific for bile acids in 1999 provided the first evidence for the “hormone-like” signaling properties of bile acids. FXR is a prototypical nuclear receptor with a DNA-binding domain, a ligand-independent activation domain, and a ligand-binding domain with a ligand-dependent activation domain. The human *NR1H4* gene is composed of 10 introns and 11 exons and the gene is widely conserved across species. There are four known isoforms of FXR,  $\alpha$ 1-4, which exhibit tissue and species specificity. For example, in the human,  $\alpha$ 1 and  $\alpha$ 2 are largely expressed in the liver,  $\alpha$ 1-4 are found in the small intestine, and  $\alpha$ 3 and  $\alpha$ 4 dominate in the kidney and colon. FXR has the highest affinity for CDCA ( $EC_{50} \approx 10 \mu M$ ) with decreased affinity for DCA, and even less for LCA and CA (155, 188). Three FXR<sup>-/-</sup> mouse models have been studied and were derived as follows: 1. Deletion of a DNA fragment that encodes the ligand-binding domain and the 3' untranslated region; 2. Deletion of a portion of exon 2, which encodes the DNA-binding domain; and 3. Deletion of exon 9 containing part of the ligand-binding domain. Depending on

the knockout model used, FXR<sup>-/-</sup> mice exhibit a variety of phenotypes that underscore the pleiotropic roles of FXR. They may display alterations in bile acid transport, in the bile acid pool, in cholesterol and triglycerides concentrations in the liver, and in glucose metabolism, to name a few. The system-wide effects of FXR deletion establish the role that FXR plays in maintenance of metabolism, and manipulation of FXR signaling can prove beneficial for those suffering from metabolic disorders (87, 161).

Within hepatocytes, bile acids bind to FXR in the cytosol, leading to its translocation to the nucleus. Once in the nucleus, FXR heterodimerizes with the retinoid X receptor, binds to DNA, and regulates expression of specific genes. The most commonly studied gene regulated by FXR is *CYP7A1*, which encodes the rate-limiting enzyme in bile acid synthesis, and is the target for negative feedback action of bile acids. Thus, when the bile acid pool is large, activation of FXR leads to the expression of the small heterodimer partner (SHP) (161). SHP then binds to and inhibits liver receptor homolog-1 and liver x receptor to down regulate *CYP7A1*, resulting in a decrease in *CYP7A1*-dependent bile acid synthesis (**Figure 3**) (87, 161). In intestinal epithelial cells, FXR activation leads to upregulation of fibroblast growth factor 15/19 (FGF; 15 in the mouse, and 19 in human and other species). FGF15/19 then travels through the portal circulation back to the hepatocytes where it binds to FGF receptor 4 (**Figure 3**), leading to further induction of SHP via extracellular signal-regulated kinase 1/2 (ERK 1/2). Interestingly, SHP inhibits ASBT in enterocytes, thus reducing uptake of bile acids into portal circulation, and SHP also inhibits uptake of bile acids into hepatocytes via Na<sup>+</sup>-taurocholic acid cotransporting polypeptide transport (87, 161).

Although FXR is the bile acid specific nuclear receptor, bile acids can directly activate the VDR and the pregnane X receptor (PXR), and indirectly activate the constitutive androstane receptor (CAR), to further assist in regulation of bile acid metabolism. The common goal of bile acid-activated nuclear receptors is to modulate the activity of critical enzymes in

hydroxylation, conjugation, and transport of bile acids, with a goal to minimize the potential toxic effects of bile acids. VDR and PXR are potently activated by LCA ( $EC_{50}=100\text{nM}$ ), with DCA and CA showing decreased potencies (52, 87, 144). VDR mainly acts as a bile acid sensor in the intestine. Both PXR and CAR, which mainly regulate detoxification and excretion of foreign substances such as drugs, are primarily activated in hepatocytes. Activation of any of these non-specific bile acid nuclear receptors leads to a decrease in *CYP7A1*. Interestingly, the CAR binds to the same sequences of DNA as PXR, and therefore regulates the same genes. Activation of PXR in hepatocytes reduces *CYP7A1* transcription via an inhibition of complex formation between hepatocyte nuclear factor 4 $\alpha$  and peroxisome proliferator-activated receptor gamma coactivator 1 $\alpha$ , which are required for *CYP7A1* transcription. The decrease in transcription of *CYP7A1* was absent in PXR knockout mice (27, 143, 234). Even though its expression in hepatocytes is low as compared to its expression in the intestine, VDR has been shown to also reduce *CYP7A1* gene activation, possibly by competing with proliferator-activated receptor gamma coactivator 1 $\alpha$  complexing with hepatocyte nuclear factor 4 $\alpha$ . In the intestine, activation of these nuclear receptors upregulates FGF15/19 to feed back to the liver to further reduce *CYP7A1*. Interestingly, in a similar manner to FGF15/19 regulation of *CYP7A1*, a cell surface bound VDR leads to ERK 1/2 signaling and repression of *CYP7A1*. Transcription of cytochrome P450 3A, needed for hydroxylation of bile acids, and bile salt sulfotransferase is increased by these nuclear receptors in the liver. Additionally, PXR increases multidrug resistance-associated protein (MRP) 2, which excretes bile acids from hepatocytes across the canalicular membrane, while VDR promotes removal of bile acids via MRP3 expression at the hepatocyte sinusoidal membrane. In the intestine, VDR increases expression of ASBT to facilitate reabsorption of bile acids and transport back to the liver (144). Overall, signaling by bile acid-activated nuclear receptors cooperate to regulate bile acid metabolism and toxicity, to promote detoxification and removal of bile acids from the body.

## **ii. Activation of Membrane Receptors**

Many physiological effects of bile acids occur irrespective of gene transcription initiated by the nuclear receptors. These effects range from induction of cell proliferation (203), regulation of hormone release (5, 120, 134, 244), smooth muscle contraction (137), to modulation of ion transport (72, 118, 124, 250). The majority of these effects can be attributed to membrane bound receptors such as the TGR5, muscarinic receptors, as well as the sphingosine 1 phosphate receptor 2 (S1PR2), and recently  $\alpha 5\beta 1$ -integrin (65, 87).

Maruyama et al. (160) and Kawamata et al. (121) first identified TGR5 by screening for orphan G protein-coupled receptor (GPCRs) that could bind bile acids using the GenBank database. This receptor is encoded by one exon of 993 base pairs, leading to the translation of 330 amino acids that make up the canonical seven membrane spanning domains of GPCRs. The human form has the largest sequence homology to rabbit (90%), followed by bovine (86%), mouse (83%), and rat (82%). Receptor mRNA is ubiquitously expressed across tissues including the brain, spleen, kidney, liver, heart, and intestine, with high expression in leukocytes and macrophages (121). Northern blot analysis showed expression of TGR5 along the entire length of the human digestive tract, with the exception of the esophagus and rectum (160). Further probing of common intestinal cell lines revealed expression of TGR5 in NCI-H716, STC-1, and GLUTag enteroendocrine cells, but not in HT-29 and Caco-2 epithelial cells (160). Both groups cloned the TGR5 cDNA into expression vectors and transfected cells to examine 3',5'-cyclic adenosine monophosphate (cAMP) production. Of the >1,000 compounds screened for receptor activation, tauro-LCA, LCA, DCA, and CDCA were able to increase cAMP at low concentrations (2-25 $\mu$ M) and in a rapid manner (<20 mins). From this data the rank order of potency for TGR5 activation was determined to be tauro-LCA =LCA> DCA> CDCA> CA (EC<sub>50</sub> in  $\mu$ M: 0.33, 0.53, 1.01, 4.43, and 7.72 respectively) (121, 160). In addition to cAMP activation,

Kawamata et al. showed that TGR5 transiently expressed in CHO cells is internalized upon activation and leads to an increase in ERK 1/2 phosphorylation (121).

The initial investigation into a bile acid-specific membrane receptor was an attempt to better explain the rapid, and therefore presumably non-genomic effects of bile acids, such as their modulation of ion transport reported in the rabbit colon (60, 191, 250) or their effects on macrophage activity (40, 101). Kawamata et al. were the first to establish that activation of TGR5 by tauro-LCA reduces LPS-induced cytokine production in rabbit alveolar macrophages, as well as in TGR5 over-expressing THP-1 monocytic cells (121). THP-1 cells, which have naturally low levels of TGR5 expression, did not show an inhibition of cytokine production by tauro-LCA (121). This anti-inflammatory effect was further supported by Wang et al., who showed that activation of TGR5 reduces phosphorylation of the inhibitor (I $\kappa$ B $\alpha$ ) of the nuclear factor of kappa light polypeptide gene enhancer in B-cells (NF- $\kappa$ B) by increasing I $\kappa$ B $\alpha$  interaction with  $\beta$ -arrestin 2 (254). This stabilizes the NF- $\kappa$ B- I $\kappa$ B $\alpha$  complex and prevents translocation of NF- $\kappa$ B to the nucleus where it activates inflammatory target genes (254). Similar findings were reported in a model of atherosclerosis, where TGR5 action reduced macrophage-dependent inflammation and lipid loading, which may contribute to the role TGR5 plays in the metabolic syndrome (190).

In addition to its role in modulation of macrophage function, activation of TGR5 impacts muscle contraction, release of hormones related to metabolic disorders, and ion transport. In the gall bladder, Lavoie et al. showed that bile acids cause membrane hyperpolarization in a PKA-dependent activation of K<sup>+</sup> channels, resulting in smooth muscle relaxation (137). Furthermore, bile acids decreased smooth muscle contraction, and promoted gall bladder filling (145). Similarly, in gastric smooth muscle cells, activation of TGR5 by oleanolic acid activates PKA and the exchange protein directly activated by cAMP (EPAC), to increase myosin light chain phosphatase activity, leading to smooth muscle relaxation. This

effect is absent in TGR5<sup>-/-</sup> mice (199). Some of the most significant discoveries involving TGR5 have been elucidating its role in metabolism. In 2005, Katsuma et al. (120) first showed that LCA and DCA stimulate secretion of glucagon like peptide-1 from the mouse enteroendocrine cell line STC-1, but not from cells transfected with TGR5 shRNA. TGR5's role in glucose homeostasis was further supported by Thomas et al. in showing that TGR5 activation by its specific agonist, INT-777, in obese mice improves hepatic and pancreatic function and glucose tolerance by increasing glucagon like peptide-1 release (244). Interestingly, mice fed a high fat diet supplemented with CA showed increased energy expenditure in brown adipose tissue via a TGR5-cAMP-dependent activation of the type 2 iodothyronine deiodinase, which activates thyroid hormone (257). Hence, these actions of TGR5 can improve metabolic disorders such as diabetes and obesity. Furthermore, TGR5 also regulates ion transport in epithelial tissues. In human gall bladder epithelium, TGR5 activation of cAMP production is coupled to Cl<sup>-</sup> secretion via CFTR (126). This increase in fluid secretion from the gall bladder epithelium is thought to aid in the prevention of gall stone formation. In rat colonocytes, activation of TGR5 by INT-777 regulated basal ion transport activity and inhibited cholinergic-stimulated secretory responses (256). Overall, activation of TGR5 stimulates cAMP production and regulates a variety of physiological functions, providing further evidence for the pleiotropic effects of bile acids.

Bile acids can also exert their effects through non-bile acid-specific membrane-bound receptors. These include the MRs, S1PR2, and  $\alpha 5\beta 1$ -integrin. Studies elucidating bile acid interaction with muscarinic receptors have largely been conducted by J.P. Raufman and colleagues. This group first identified that tauro-LCA partially activated acetylcholine receptors on guinea pig gastric chief cells (204). It was later identified that tauro-LCA preferentially binds to M3Rs, whereas sulfated LCA prefers the M1R. The rank order of potency for M3R is tauro-LCA > -DCA > -CA (202). Further investigation by this group found that in the human colon cancer cell line H508, taurine- and glycine-conjugated LCA and DCA activate M3Rs to stimulate

proliferation via transactivation of the epidermal growth factor (EGF) receptor (EGFR). Thus, M3R binding to bile acids results in the activation of matrix metalloproteinase (MMP) 7 and cleavage of heparin binding- EGF-like growth factor (HB-EGF), to release the mature form of HB-EGF. This soluble HB-EGF is then free to bind to EGFR (50) and activates ERK 1/2 (49). Activation of muscarinic receptors is not limited to the M3R and M1R isoforms as tauro-CA induces arrhythmia in rat neonatal cardiomyocytes in an M2R-dependent manner (221).

New insights into bile acid physiology has led to the identification of S1PR2 and  $\alpha 5\beta 1$ -integrin as bile acid activated membrane receptors. S1PR2, another GPCR, when activated specifically by conjugated bile acids leads to downstream signaling via ERK1/2 and protein kinase B (AKT) in rodent hepatocytes (236). Furthermore, conjugated bile acids can regulate lipid metabolism via S1PR2 modulation of hepatic gene expression (176). Similar to the findings that bile acids can promote colon carcinoma by inducing cell proliferation (49), Liu et al. suggested a role for conjugated bile acids in promoting cholangiocarcinomas in an S1PR2-dependent manner (148). Finally, the most recent receptor associated with bile acids is  $\alpha 5\beta 1$ -integrin. Integrins are heterodimeric transmembrane spanning proteins that serve as bridges for cell-cell and cell-matrix interactions. The  $\alpha 5\beta 1$ -integrin is the primary receptor for the extracellular matrix glycoprotein, fibronectin. UDCA has long been used as a choleric agent but the mechanisms remained unresolved. Gohlke et al. determined that within rat hepatocytes, tauro-UDCA binds directly to  $\alpha 5\beta 1$ -integrin, causes a conformational change that activates the  $\beta 1$  subunit, which then signals downstream through ERK 1/2 (98). This leads to increases in expression of MRP2 and bile salt export pump at the canalicular membrane, and promotion of choleresis.

### **iii. Direct Membrane Perturbations**

Although bile acids are capable of binding directly to plasma membrane bound receptors, it is important to remember that they are amphipathic derivatives of cholesterol. The

more hydrophobic the bile acid molecule, the more capable it is of incorporating into the plasma membrane and affecting intracellular signaling. While there is no evidence for direct interaction of bile acids with EGFR, it is common for EGFR to be transactivated via other receptors. Interestingly, there is some evidence for ligand-independent activation of EGFR. In rat hepatocytes DCA induces EGFR phosphorylation and downstream signaling via mitogen activated protein kinases (MAPKs), however this induction is not blocked by neutralizing antibodies to EGFR ligands (196). In fact, a thorough investigation of the effects of DCA on membrane dynamics suggests that hydrophobic bile acids, DCA and possibly CDCA, cause plasma membrane cholesterol aggregation via membrane perturbations, resulting in receptor activation. In this regard, membrane perturbation by DCA may be causing EGFR to autophosphorylate and activate downstream signaling pathways (114).

In summary, it is evident that bile acids mediate their physiological effects through a variety of ways. They negatively regulate their own metabolism through nuclear receptor modulation of gene expression. By activation of GPCRs, bile acids can elicit more rapid effects such as smooth muscle relaxation, hormone release, and inhibition of proinflammatory cytokine release from macrophages. Their role in the intestinal epithelium is of significance because of the potential harmful effects of excess bile acids on barrier function, and even more so on the dysregulation of absorptive and secretory processes in the colonic epithelium that promote diarrhea.

## **B. Mammalian Colon**

The effects of bile acids on ion transport in the mammalian colon were originally reported in the 1970s by Binder and Rawlins, who investigated the effect of glycine and taurine-conjugated CDCA on rat colon and found that there was an increase in secretion and a decrease in

absorption (32). Additionally, Conley et al. demonstrated that DCA activates basolateral adenylyl cyclase to increase net secretion in the rabbit colon (60). Further studies in the rabbit colon established that tauro-CDCA increases  $\text{Cl}^-$  secretion and decreases  $\text{Na}^+$  absorption (90) and that tauro-DCA increases  $\text{Cl}^-$  secretion in a  $\text{Ca}^{2+}$ - and PKC-dependent manner (118, 250). Moreover, it was demonstrated that the adult human colon absorbs a significant amount of dihydroxy bile acids by passive diffusion (165). Studies in T84 cells by Dharmasathaphorn et al. showed that tauro-DCA increases  $\text{Cl}^-$  secretion in a  $\text{Ca}^{2+}$ -dependent manner (72). More recent studies have determined that TGR5 activation in enteric neurons and enteroendocrine cells promotes normal defecation in mice (5). Thus, it is critical to understand the context in which bile acids act in the colon. With this in mind, the following sections describe the colonic architecture, discuss the cellular mechanisms involved in electrolyte and fluid transport, and expand on known bile acid activated pathways that were briefly discussed in previous sections.

## **1. Structure**

As reviewed in Rao et al. (201), the gastrointestinal tract is a long tube running from the mouth to the anus that serves as a conduit for exchange to occur between the external world and the internal environment of the body. The large intestine (the colon) is comprised of the cecum, ascending colon, transverse colon, descending colon, rectum, and the anus. Like other regions of the gastrointestinal tract, the colon has several structural layers beginning with (from the lumen outward) the epithelial layer, lamina propria, and the muscularis mucosa that form the mucosal layer, followed by the submucosal layer, submucosal nerve plexus, muscularis externa comprised of the circular muscle, myenteric nerve plexus and longitudinal muscles and finally the serosa. Specific to the colon are the tenia coli, which are extra strips of longitudinal muscle, and haustra, which are small pouches formed when the regions of the circular muscle are contracted. Of structural importance is that, unlike the crypt-villus structures of the small intestine, the colonic mucosa exhibits crypts and a flat surface topography. The epithelial layer

lining the luminal surface is composed of a variety of cell types including the colonocytes, enterochromaffin cells, goblet cells, and stem cells (201). Paneth cells, an intestinal epithelial cell type involved in the production of antimicrobial peptides, are chiefly expressed in the small intestine. In healthy individuals Paneth cells can be found in the cecum and proximal colon, but not in the distal colon, however under inflammatory conditions, such as inflammatory bowel disease, Paneth cell expression along the colon increases (227). Additionally, as described earlier, a major component of the colonic environment is the presence of the microbiota ( $\sim 10^{14}$  microorganisms), which are crucial to colonic function (87). All the cell types are derived from intestinal stem cells located towards the base of the crypts. As the cells divide and move up the crypt-surface axis, the cells differentiate and express different proteins that are essential to their specific function (201). The *Lgr5* gene was identified as the intestinal crypt cell marker, and encodes a GPCR that binds to the Wnt signaling agonist R-spondin (19). Wnt signaling maintains the proliferative and crypt-like nature of the epithelial cells and decreases with differentiation (59). In 2009, Sato et al. took advantage of *Lgr5* identification and revolutionized the field of gastrointestinal physiology by developing the intestinal organoid methodology (210).

The cells lining the length of the colonic lumen are columnar epithelial cells, with the exception of the rectum, which is lined with a squamous epithelium. The hallmark of an epithelial cell is its polarity, which is essential for vectorial transport to occur. Polarity of epithelial cells is determined by the distribution of specific proteins and lipids to distinctive regions of the plasma membrane, supported by subcellular scaffolding matrices and defined by the localization of tight junction complexes that connect adjacent cells. Tight junctions form a partition between the apical membrane (mucosal surface) and the basolateral membrane (serosal surface) of intestinal epithelial cells. This gating mechanism prevents lateral diffusion of transmembrane spanning proteins and of lipids, and helps establish the asymmetry between the apical and basolateral membranes. Vectorial transport is achieved either transcellularly or

paracellularly, where the tight junctions help determine the specificity (size and charge) of molecules that pass between cells (**Figure 4**) (201).

In terms of asymmetry, the apical membrane of intestinal epithelial cells is composed of ~37% glycosphingolipids, 32% phospholipids, 31% cholesterol, with very little phosphatidylcholine. In contrast, the basolateral membrane composition is more similar to non-polarized cells, with the dominant lipid being phosphatidylcholine (~30%), a much smaller contribution by glycosphingolipids (~10%), and the remaining being comprised of phospholipids and cholesterol (~60%) (228). With regard to membrane specific transporter expression, there is variation in the surface-crypt axis as well as along the cephalocaudal axis. However, in all colonic epithelial cells, the  $\text{Na}^+/\text{K}^+$ -ATPase is expressed on the basolateral membrane. This essential transporter utilizes ATP as an energy source to transport  $2\text{K}^+$  into the cell with simultaneous transport of  $3\text{Na}^+$  out of the cell against their concentration gradients. A vast array of secondary active symporters and antiporters, and other transporters, utilize the driving force provided by the  $\text{Na}^+/\text{K}^+$ -ATPase to transport ions and small molecules across both membranes. While the apical membrane of all colonocytes express alkaline phosphatase, the distribution of specific transporters varies. For example, CFTR is predominantly expressed on the apical membrane of colonic crypt epithelia where it contributes to  $\text{Cl}^-$  and  $\text{HCO}_3^-$  secretion, whereas the epithelial  $\text{Na}^+$  channel is expressed on the apical membrane of colonic surface cells (201).

Tight junctions are important components of the intestinal epithelial barrier, which functions to prevent the translocation of an array of pathogens and xenobiotics into the blood. Protein-protein interactions between epithelial cells regulate passive paracellular transport. The proteins that form tight junctions include the claudins, junctional adhesion molecules, occludins, and the zonula occludens. There are 24 isoforms in the claudin family, which are transmembrane spanning proteins that interact with other claudins on adjacent cells to form pores. Of the different proteins comprising tight junctions, the claudins largely regulate the

charge and size selectivity of molecules that can pass paracellularly. The cytoplasmic tail of claudins can interact with regulatory proteins, such as the zonula occludens (1-3), via PDZ (PSD95, DlgA, ZO-1) binding domains. Zonula occludens were the first proteins of the tight junctions to be discovered, and are intracellular peripheral proteins that connect the tight junctions complex to the underlying actin cytoskeleton. The architecture of the cell depends on the influence of the cytoskeleton and scaffolding proteins on the intercellular connections (201). It is well established that contraction of the actin cytoskeleton by myosin, due to an increase in the phosphorylation of myosin light chain by myosin light chain kinase, modifies junctional permeability (157). The regulation of tight junctional proteins determines the permeability (leakiness) of the intestinal barrier, measured as transepithelial electrical resistance (TER;  $\Omega \cdot \text{cm}^2$ ), with low TER correlating with high permeability and high TER with low permeability. The colon mainly functions to absorb fluid and is considered moderately tight (TER  $\sim 50\text{-}60 \Omega \cdot \text{cm}^2$ ). Dysregulation of barrier function and disruption of tight junctions is a common characteristic of many intestinal disorders (201).

## **2. Function**

Content of the colonic lumen include undigested macromolecules, fluid and electrolytes not absorbed by the small intestine, as well as vitamin K and short chain fatty acids. The colon primarily functions to reabsorb the majority of the fluid and to store any undigested and unabsorbed waste until excretion. Goblet cells located throughout the surface-crypt axis have high expression of mucin proteins, specifically mucin 2, and secrete mucus to help protect the epithelial lining of the colon. The mucus serves as a lubricant for the luminal contents and is another barrier preventing noxious stimuli, such as pathogenic bacteria, from reaching the epithelium and translocating into the blood stream (201). Although the number of Paneth cells in the colon is low compared to the small intestine, these cells contain secretory granules that release antimicrobial proteins. These microbe-killing proteins include defensins, lysozyme, and

phospholipase A2 (26). It makes sense that as Paneth cell expression decreases down the length of the colon, the microbial content increases. The colonic epithelium also has enterochromaffin cells, which are endocrine and neurocrine in nature. For example, they synthesize and release the neurotransmitter serotonin which influences the functions of the surrounding cells leading to contraction of the smooth muscle layer, and regulation of ion secretory processes (201). Surface colonocytes express transporters such as the epithelial  $\text{Na}^+$  channel,  $\text{Na}^+/\text{H}^+$  exchangers (NHE), and the  $\text{Cl}^-/\text{HCO}_3^-$  exchanger down regulated in adenoma to promote fluid absorption. From the surface to the crypt, the expression of pro-absorptive transporters decrease, and there is a contrasting increase in pro-secretory transporters. For example, CFTR is a major contributor to  $\text{Cl}^-$  secretion and is highly expressed in the crypts compared surface colonocytes. For the purpose of this thesis, we focus on the function of secretory colonic cells.

## **C. Bile Acids and the Regulation of Epithelial Ion Transport**

### **1. Establishment of the Driving Force for $\text{Cl}^-$ Secretion**

The electrolyte composition and amount of fluid in the intestinal lumen is determined by the balance of absorptive and secretory processes. Fluxes of electrolytes and nutrients across the epithelium are dependent on the establishment of electrochemical gradients. The primary contributor to movement of ions and fluid in or out of the lumen is the  $\text{Na}^+/\text{K}^+$ -ATPase located on the basolateral membrane (**Figure 4**). The activity of the  $\text{Na}^+/\text{K}^+$ -ATPase is coupled to the recycling of  $\text{K}^+$  via  $\text{K}^+$  channels, which is a secondary active transport process that allows export of  $\text{K}^+$  down its electrochemical gradient. Finally, the  $\text{Na}^+/\text{K}^+/\text{2Cl}^-$  cotransporter 1, also located on the basolateral membrane, utilizes the  $\text{Na}^+$  gradient generated by the  $\text{Na}^+/\text{K}^+$ -ATPase to bring  $\text{Cl}^-$  into the cell. Thus, with the activity of these three transporters,  $\text{Cl}^-$  accumulates in the cell

above its electrochemical equilibrium, and establishes the driving force needed for  $\text{Cl}^-$  to be extruded via apical  $\text{Cl}^-$  channels (**Figure 4**). Activation or interruption of the activity of any of these transporters will respectively stimulate or prevent  $\text{Cl}^-$  secretion (20, 201).  $\text{Cl}^-$  secretion is necessary for proper hydration of the intestinal lumen, to facilitate the movement of luminal contents down the intestine. As  $\text{Cl}^-$  is secreted into the lumen it creates an electrical gradient for  $\text{Na}^+$  to follow, which creates a transepithelial osmotic pressure gradient that pulls water into the lumen.

## **2. $\text{Cl}^-$ Channels**

There are currently 3 types of  $\text{Cl}^-$  channels known to be expressed in secretory epithelial cells. The first is CIC-2, a member of the CIC family which has 9 isoforms. CIC-2 is an inwardly rectifying  $\text{Cl}^-$  channel that has been shown to play a role in modulating intracellular  $\text{Cl}^-$ , in maintenance of intracellular pH, as well as in regulation of cell volume. Studies in the Caco-2 and T84 intestinal cell lines have shown that CIC-2 can be located on the apical and lateral membranes, whereas it is located basolaterally in the mouse colon (201). The evidence for it contributing to  $\text{Cl}^-$  secretion across the apical membrane of epithelial cells is controversial. Patch clamp studies in Caco-2 cells showed that decreasing CIC-2 expression by antisense methodology resulted in a decrease in hyperpolarization and hypotonic-activated  $\text{Cl}^-$  currents (170). In the pig ileum CIC-2 was found responsible for the prostaglandin-induced  $\text{Cl}^-$  secretion that contributes to barrier function recovery after ischemia injury (169). Because of such studies showing that CIC-2 can play a role in  $\text{Cl}^-$  secretion, it was hypothesized that it could be therapeutically targeted as an alternative exit pathway in cases of cystic fibrosis (CF) where CFTR is dysfunctional. Interestingly, in CFTR<sup>-/-</sup> mice, CIC-2 cannot recover the CF phenotype seen in the intestine (276). The constipation alleviating agent lubiprostone had been reported as an activator of CIC-2 (64), however the physiological relevance of this is debatable. Thus, our laboratory demonstrated that lubiprostone increased  $\text{Cl}^-$  secretion in T84 cells in a cAMP-

dependent manner and the increase in secretion was inhibited by the CFTRinh172 but not by the CIC-2 inhibitor CdCl<sub>2</sub> (16). Additionally, lubiprostone increased CFTR membrane expression (16). Furthermore, in CF mice, as well as CF patients, lubiprostone was unable to increase Cl<sup>-</sup> secretion, suggesting that CIC-2 is not a major contributor to Cl<sup>-</sup> secretion in the intestine (28).

A second type of Cl<sup>-</sup> channel is the Ca<sup>2+</sup>-activated Cl<sup>-</sup> channel (CaCC). In contrast to the CICs, CaCCs are outwardly rectifying, and as their name states, are regulated by changes in Ca<sup>2+</sup>. The transmembrane member 16 (TMEM16; anoctamins) gene family was first discovered in 2004 and follow up studies by three different groups (43, 217, 268) found that of the 10 members of this family, TMEM16A and TMEM16B (aka ANO1 and ANO2) are indeed CaCCs. These CaCCs have eight predicted transmembrane spanning domains, and TMEM16A traffics to the plasma membrane as a homodimer, and possibly forms oligomers with its own isoform or others (79, 83, 224). Interestingly, TMEM16A can be activated by Ca<sup>2+</sup> and voltage changes, despite it lacking typical binding sites for Ca<sup>2+</sup>, or transmembrane helices with charged amino acids to sense voltage (266). TMEM16A is expressed in a variety of tissues including the mammary gland, airway epithelium, and the intestine (43, 268). Several studies using T84 cells have shown that TMEM16A exhibits Ca<sup>2+</sup>-dependent Cl<sup>-</sup> transport (174, 179, 237). In TMEM16A<sup>-/-</sup> mice, Ca<sup>2+</sup>-stimulated Cl<sup>-</sup> secretion is absent or decreased across several epithelia including the trachea, colon, and hepatocytes (185). Interestingly, rotavirus-induced diarrhea, which has been associated with CaCC (172), has now been linked to TMEM16A (186).

TMEM16A was thought to be a potential therapeutic target for those who suffer from CF, however its expression in human airways is very low compared to its expression in pig and mouse airways (218). Defects in CFTR results in meconium ileus and/or obstruction of the intestine in CF patients and has been long associated with secretory diarrheas. CFTR is the primary mechanism for Cl<sup>-</sup> secretion across the apical membrane of secretory epithelia and in the intestine, its expression increases down the villus/surface →crypt axis, where crypts are the

major sites of secretion. CFTR is an ATP-binding cassette protein, in that it utilizes ATP hydrolysis for full channel activity. The gene encoding CFTR is 24 exons in length, leading to the transcription of the protein containing 12 (in 2 clusters of six each) transmembrane spanning domains, 2 nucleotide binding domains (sites of ATP hydrolysis), and a regulatory domain with multiple consensus sequences for kinase specific phosphorylation. Topologically the protein has two halves, separated by the regulatory domain; each half has one transmembrane cluster and a nucleotide binding domain. Mutations in the gene result in CF. The twelve transmembrane domains make up the channel pore with an anion selectivity of  $\text{Br}^- > \text{Cl}^- > \text{I}^- > \text{F}^-$  and an ability to also transport  $\text{HCO}_3^-$  and ATP. The majority of the kinase consensus sites are for PKA and CFTR activation is dependent on cAMP production. PKA phosphorylation of the regulatory domain causes a conformational change in the nucleotide binding domain 1 and ATP hydrolysis, further phosphorylation of the regulatory domain changes the conformation of the second nucleotide binding domain and hydrolysis of ATP at this site, resulting in full opening of the channel. Additionally, the probability of channel opening can be regulated through its association with other proteins via protein-protein interactions in the N-terminus or via PDZ interactions in the C-terminus, or through increasing its expression at the plasma membrane (142, 180, 201, 206). For example, CFTR colocalizes with the MRP4, which regulates the spatiotemporal coupling of CFTR with cAMP (141). Other than CF, CFTR plays a role in various pathological conditions such as cholera and pertussis. Both cholera and pertussis toxins hijack the cAMP signaling pathway that is required for CFTR activation. In the case of cholera toxin, it causes an over activation of adenylyl cyclase by causing  $\text{G}\alpha_s$  to lose its catalytic guanosine triphosphate (GTP)-ase activity so that it remains in its active conformation to stimulate adenylyl cyclase. In contrast, pertussis toxin inhibits  $\text{G}\alpha_i$ , so that it remains inactive and cannot inhibit cAMP production by adenylyl cyclase (201). With regard to bile acid signaling, taurine conjugated CA is absorbed by ASBT in the terminal ileum and activates CFTR-

dependent  $\text{Cl}^-$  secretion. This activation of CFTR was irrespective of canonical cAMP-PKA and cyclic guanosine monophosphate (cGMP) protein kinase signaling pathways (29).

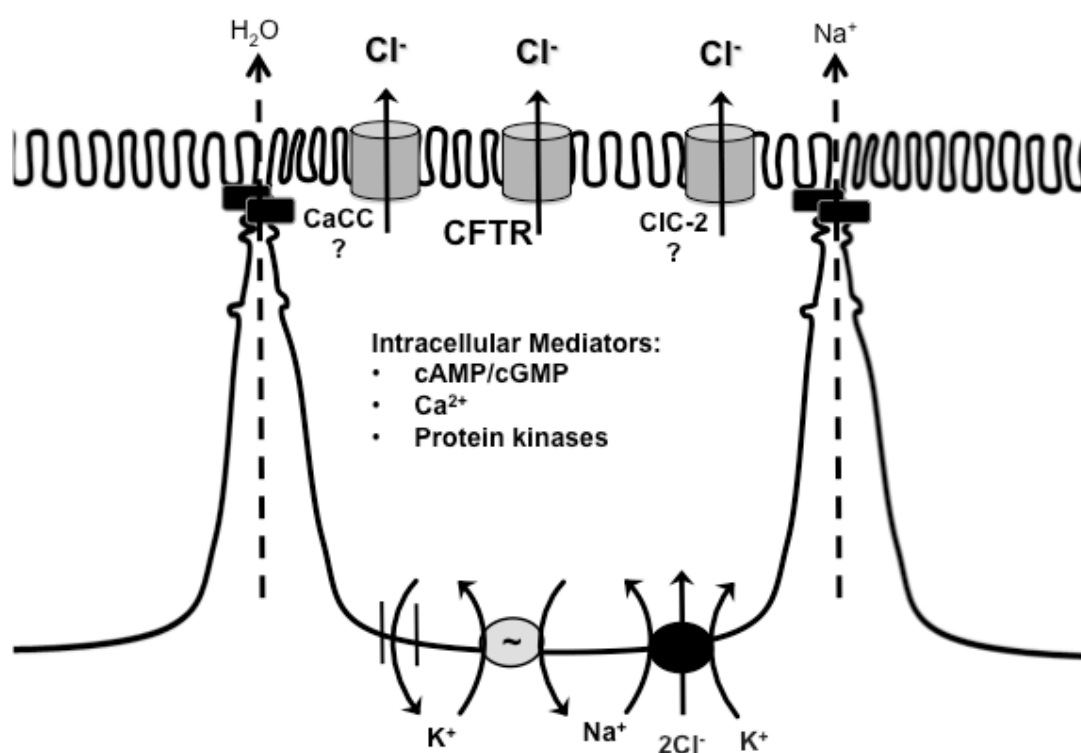


**Figure 4:** Epithelial  $\text{Cl}^-$  secretion. For  $\text{Cl}^-$  secretion to occur in colonocytes,  $\text{Cl}^-$  must accumulate within the cell above its electrochemical equilibrium. The combined efforts of basolaterally expressed  $\text{K}^+$  channels, the  $\text{Na}^+/\text{K}^+$ -ATPase, and the  $\text{Na}^+/\text{K}^+/\text{2Cl}^-$  cotransporter bring  $\text{Cl}^-$  into the cell. Exit occurs across the apical membrane. CFTR is the primary  $\text{Cl}^-$  channel expressed on the apical membrane, and most  $\text{Cl}^-$  exits via this channel. The function of  $\text{Ca}^{2+}$ -activated  $\text{Cl}^-$  channels (CaCCs) and CIC-2 in contributing to  $\text{Cl}^-$  secretion in the intestine is still being elucidated.  $\text{Cl}^-$  secretion creates an electrical gradient for  $\text{Na}^+$  to follow paracellularly. This sets up an osmotic pressure gradient and water movement follows. Activation of the various transporters underlying  $\text{Cl}^-$  secretion are regulated by intracellular mediators including cAMP, cyclic guanosine monophosphate (cGMP),  $\text{Ca}^{2+}$ , and protein kinases.

### **3. Intracellular Signaling Pathways:**

Underlying the activation of Cl<sup>-</sup> channels, as well as the transporters that establish the driving force for Cl<sup>-</sup> secretion, are a variety of intracellular second messenger signaling cascades, including cAMP, Ca<sup>2+</sup>, store-operated cAMP signaling, and EGFR-associated kinases.

#### **i. Intracellular Signaling Pathways: cAMP**

The first step in the cAMP pathway is activation of Gα<sub>s</sub> (stimulatory G protein α). Gα<sub>s</sub> is coupled to a GPCR, and upon ligand binding to the receptor, a conformational change occurs, and guanosine diphosphate (GDP) bound to Gα<sub>s</sub> is exchanged for GTP, rendering Gα<sub>s</sub> active. Gα<sub>s</sub> can now activate adenylyl cyclase, which catalyzes the formation of cAMP from ATP (201). There are ten isoforms of adenylyl cyclase, the first nine being plasma membrane bound, with adenylyl cyclase 10 identified as the soluble/cytoplasmic isoform (207). Fractionation of epithelial cells via discontinuous sucrose gradient resulted in a co-purification of adenylyl cyclase with the Na<sup>+</sup>/K<sup>+</sup>-ATPase, implying basolateral localization of adenylyl cyclase (175). Adenylyl cyclase and regulatory Gα proteins have been found to colocalize in caveolin rich regions of the plasma membrane. Localization to caveolin rich regions is not essential for adenylyl cyclase function, since cells lacking caveolin still exhibit cAMP signaling (61, 103, 109). Levels of cAMP are also regulated by the activity of cyclic nucleotide phosphodiesterases that degrade cAMP into AMP, also by binding of Gα<sub>i</sub> (inhibitory G protein α) to adenylyl cyclase (4, 208), or by efflux of cAMP out of the cell by MRP4 (141).

Once cAMP is produced it can bind to its effector proteins, including PKA and EPAC. PKA is activated when four molecules of cAMP bind to sites in the two regulatory subunits (two molecules cAMP per regulatory unit). This results in a conformational change and release of the two catalytic subunits which can phosphorylate target proteins at serine and threonine residues

(4, 208). For example, CFTR's regulatory domain has at least 10 serine residues that can be phosphorylated by PKA (93). Additionally, PKA can translocate into the nucleus where it can phosphorylate and activate the cAMP response element-binding protein, which in turn will bind to cAMP response elements in the DNA and activate transcription of cAMP regulated genes. Unlike PKA which regulates its substrates by phosphorylation, EPAC acts as a guanine nucleotide exchange factor. When EPAC binds to cAMP, there is a conformational change to reveal EPAC's active site, allowing it to facilitate the exchange of GDP for GTP to activate the Rap GTPases (214). Interestingly, EPAC has been shown to be a point of crosstalk between cAMP and  $Ca^{2+}$  signaling in a variety of systems (119, 215).

The cAMP pathway has been shown to regulate the action of ion transporters, including many that contribute to the driving force of  $Cl^-$  secretion. Activity of the  $Na^+-K^+-2Cl^-$  cotransporter and  $K^+$  channels on the basolateral membrane increase with rising concentrations of cAMP (201). Some colonic epithelial cells also possess apical  $K^+$  conductances, and cAMP is known to stimulate these channels (222). In the human bile duct epithelium, bile acids activate TGR5 to increase cAMP and stimulate CFTR-dependent  $Cl^-$  secretion (126). Furthermore, we established that CDCA is dependent on cAMP-PKA signaling to phosphorylate and activate CFTR in T84 cells (15). Aside from its effects on transporters that promote electrolyte secretion, cAMP also negatively regulates apical  $Na^+$  absorption via a CFTR-related mechanism. This phenomenon was evidenced by a rise in cAMP inhibiting  $Na^+$  absorption in wild-type mice jejunum, but not in CFTR<sup>-/-</sup> mice (58).

## **ii. Intracellular Signaling Pathways: $Ca^{2+}$**

$Ca^{2+}$  is one of the most tightly regulated second messengers; it is not synthesized or degraded by the cell, but sequestered in different compartments to control its action. Rises in free cytosolic  $Ca^{2+}$  ( $[Ca^{2+}]_i$ ) modulate a variety of cellular functions including enzymatic activity, cytoskeletal rearrangements, and ion transport. Cytosolic  $Ca^{2+}$  increases due to influx via  $Ca^{2+}$

channels on the plasma membrane, or due to a signal transduction pathway activated by molecules that bind to  $G\alpha_q$ -coupled GPCRs.  $G\alpha_q$  activates phospholipase C (PLC), which hydrolyzes phosphatidyl inositol bisphosphate into diacyl glycerol and inositol triphosphate ( $IP_3$ ). Diacyl glycerol is needed for activation of PKC, which phosphorylates downstream substrates on serine and threonine residues, similar to PKA. For  $[Ca^{2+}]_i$  to increase,  $IP_3$  must bind to its receptor ( $IP_3Rs$ ) on the endoplasmic reticulum, allowing for free movement of  $Ca^{2+}$  into the cytosol (201). When  $Ca^{2+}$  levels in the store drop, an endoplasmic reticulum  $Ca^{2+}$  sensor translocates and activates  $Ca^{2+}$  channels on the plasma membrane. Activation of these channels is dependent on store depletion and results in  $Ca^{2+}$  entry to replenish the empty stores. This influx of  $Ca^{2+}$  from the extracellular fluid is termed store-operated  $Ca^{2+}$  entry (SOCE) (107).

$Ca^{2+}$  elicits its effects either by direct binding to target proteins, or through the  $Ca^{2+}$  binding protein calmodulin, which serves as a signal transducer to proteins that can't bind  $Ca^{2+}$  directly. The calmodulin protein consists of two globular regions separated by a flexible linker region. Each globular domain has two  $Ca^{2+}$  binding motifs to hold a total of four  $Ca^{2+}$  ions. Binding of  $Ca^{2+}$  causes an "opening" of calmodulin, exposing hydrophobic residues that can interact with target proteins. One such protein is the  $Ca^{2+}$ -calmodulin specific serine/threonine protein kinase,  $Ca^{2+}$ -calmodulin kinase. This tetradecameric (14 subunits) serine/threonine kinase increases in activity as more subunits bind to  $Ca^{2+}$ -calmodulin complexes, resulting in autophosphorylation and prolonged activation (54). Interestingly,  $Ca^{2+}$ -calmodulin activity has been controversially associated with regulation of  $Cl^-$  transport via TMEM16A (245, 273, 274).

It is well documented that DCA and its taurine conjugate utilize the  $Ca^{2+}$  signaling pathway to activate  $Cl^-$  secretion. Studies in T84 cells by Dharmasathaphorn et al. showed that tauro-DCA increase cytosolic  $Ca^{2+}$  from extracellular sources to increase electrolyte transport (72). Devor et al. then established the involvement of  $IP_3$  in activation of  $K^+$  and  $Cl^-$

conductances (70). Studies in the rabbit colon showed both age and segment specificity of tauro-DCA action. While tauro-DCA utilized  $IP_3$ ,  $Ca^{2+}$  (250), and PKC- $\delta$  (118) in stimulation of  $Cl^-$  secretion in the adult distal colon, it had no effect in the weanling and newborn colon. Interestingly, tauro-DCA had no effect on the proximal colon, but neurotensin stimulated  $Cl^-$  transport in a PLC-dependent manner and involved Src tyrosine kinases. Neither tauro-DCA nor neurotensin altered  $Cl^-$  secretion in weanling and newborn distal colon (192). In contrast, the cAMP activator prostaglandin E2, was able to increase  $Cl^-$  transport in the distal colon of all ages, suggesting that  $Ca^{2+}$ -induced, but not cAMP-induced,  $Cl^-$  transport is developmentally regulated (250). It remains to be investigated if  $Ca^{2+}$  is required only for DCA-induced signaling, or if it is utilized by CDCA to increase  $Cl^-$  secretion either in the rabbit or human colon. To further increase the complexity of bile acid handling in the young vs. adult rabbit intestine, our laboratory found that the weanling colon is similar to the adult ileum with regard to expression of ASBT, lipid binding protein, and FXR. Additionally, it was found that, in contrast to the adult colon, which secretes fluid in response to bile acids, the weanling colon absorbs bile acids (259). Although the pro-secretory actions are thought to be exclusively initiated by the  $7\alpha$ -dihydroxy bile acids DCA and CDCA, a study of  $Cl^-$  secretion in mouse cholangiocytes found that the  $7\beta$  dihydroxy bile acid, UDCA, not commonly considered pro-secretory, stimulated  $Cl^-$  and fluid secretion indirectly via ATP release, which then increases  $[Ca^{2+}]_i$  (86). This ATP- $Ca^{2+}$ -dependent  $Cl^-$  secretion was in contrast to another study that showed utilization of the cAMP pathway for bile acid-induced secretion in cholangiocytes (126).

### **iii. Intracellular Signaling Pathways: Store-Operated cAMP Signaling**

Typically, when  $Ca^{2+}$  levels in the endoplasmic reticulum drop, there is activation of store-operated  $Ca^{2+}$  channels, and  $Ca^{2+}$  enters the cytosol to replenish the empty stores (SOCE, see above). A.M.Hofer and colleagues demonstrated a novel signaling pathway that occurs when the  $Ca^{2+}$  stores are depleted. In the absence of extracellular  $Ca^{2+}$  to replenish the stores,

there is recruitment of adenylyl cyclase and increased cAMP production (138). This new store-operated activation of cAMP was coined as store-operated cAMP signaling (SOcAMPS). Further investigation from this laboratory using the colonic cell line NCM460 established that adenylyl cyclase 3 accounts for cAMP production in SOcAMPS, but  $\text{Ca}^{2+}$  entry via the  $\text{Ca}^{2+}$  channel Orai1 inhibits this pathway. Thus, SOcAMPS only occurs when the  $\text{Ca}^{2+}$  store remains depleted and does not involve  $\text{Ca}^{2+}$  activated adenylyl cyclases, but requires translocation of the endoplasmic reticulum  $\text{Ca}^{2+}$  sensor and indirect activation of adenylyl cyclase 3 (154). Furthermore, in human colonic T84 cells they validated that SOcAMPS can be activated by the muscarinic agonist carbachol, which is known to increase  $\text{Ca}^{2+}$ , and addition of carbachol lead to an increase in PKA activation. The increase in SOcAMPS by carbachol lead to activation of  $\text{Cl}^-$  secretion via CFTR. They concluded that part of the  $\text{Ca}^{2+}$ -dependent  $\text{Cl}^-$  secretion in the colon can be attributed to SOcAMPS (182).

#### **iv. Intracellular Signaling Pathways: EGFR and Associated Kinases**

EGFR has been implicated in the functions of a variety of cell types and cell signaling pathways. EGFR is a tyrosine kinase receptor that can be activated in several ways, including binding of its ligands as well as via plasma membrane perturbations. Some of its ligands include EGF, transforming growth factor (TGF)  $\alpha$ , and HB-EGF. Upon activation, the receptor dimerizes, and transphosphorylation occurs between the monomers. Phosphorylation of the C-terminal domain allows for docking of proteins with phosphotyrosine binding domains and initiation of signal transduction pathways. These pathways include the MAPKs ERK1/2 and p38, Src kinase, and phosphatidylinositol-4,5-bisphosphate 3-kinase (PI3K)-AKT signaling to mediate downstream effects of EGFR (104, 130).

It is not surprising that EGFR, with its ubiquitous expression, has been implicated in both  $\text{Cl}^-$  secretion and bile acid signaling in a variety of cell types. Our laboratory demonstrated that in the rabbit, stimulation of colonic epithelial cells with EGF elicits a  $\text{Cl}^-$  secretory response

(44). In addition to direct binding of EGFR ligands, EGFR can be transactivated by GPCRs. Bertelsen et al. delineated that vasoactive intestinal peptide (VIP), a potent activator of cAMP-dependent Cl<sup>-</sup> secretion via CFTR, stimulates EGFR in a PKA-dependent manner (25). Downstream of EGFR, PI3K activity contributed to the VIP-induced secretory response. Whether EGFR acts in a pro-secretory or anti-secretory manner seems to depend on the agonist. In contrast to cAMP-dependent Cl<sup>-</sup> secretion, studies examining Ca<sup>2+</sup>-dependent Cl<sup>-</sup> secretion showed that EGFR was acting to inhibit Cl<sup>-</sup> transport (247). Additional studies from the same laboratory implicated several of EGFR's effector proteins including PI3K (248), MAPKs (125), PKC $\epsilon$  (55), and p38 (123) in mediating the inhibitory effect on Ca<sup>2+</sup>-dependent Cl<sup>-</sup> secretion. Interestingly, in contrast to the inhibitory role of EGFR on ion transport in T84 cells, studies in mouse models of colitis demonstrated that EGFR activation could restore ion transport responses. Consistent with their laboratory's findings in T84 cells, EGF pretreatment inhibited carbachol and forskolin responses in normal mouse distal colon; however, the pretreatment potentiated the forskolin and carbachol responses in the dextran sulfate sodium and multidrug resistance protein 1a knockout models of colitis (162).

Among its pleiotropic effects, EGFR has been implicated in bile acid action. Tauro-DCA stimulates transactivation of EGFR via MRs (49, 50) in regulation of colon cancer cell proliferation. Depending on the cell type, bile acids can transactivate EGFR by cleavage of a variety of EGFR ligands. For example, activation of EGFR by bile acids in cholangiocytes is dependent on binding of TGF $\alpha$  (262). Although the EGFR ligand was undefined, low doses of DCA, at short time points (<30 minutes), lead to increases in EGFR, ERK 1/2, and p38 phosphorylation (122). Interestingly, the unconjugated and more hydrophobic form of this bile acid, DCA, is able to activate EGFR via a MR- and EGFR ligand-independent mechanism; these results imply that bile acids are either binding directly to EGFR (an unsubstantiated possibility), or perturbing the membrane to activate EGFR and its downstream signaling

cascades (114, 196). While the majority of studies linking bile acids and EGFR have been performed with DCA, it remains to be investigated whether these pathways also apply to CDCA action.

#### **v. CDCA Action in T84 Cells**

In our previously published investigation on the action of CDCA in T84 cells, we found that CDCA acts in a rapid manner to increase  $\text{Cl}^-$  transport as measured by iodide efflux as well as short circuit current. CDCA was more effective when added basolaterally. Interestingly, pretreatment of T84 cells with a cytokine cocktail potentiated the effect of apical addition of CDCA on  $\text{Cl}^-$  transport. Additionally, we found that CDCA directly increased activation of apical  $\text{Cl}^-$  currents, but not basolateral  $\text{K}^+$  currents. CDCA action in intact monolayers was sensitive to bumetanide ( $\text{Na}^+/\text{K}^+/\text{2Cl}^-$  inhibitor),  $\text{BaCl}_2$  ( $\text{K}^+$  channel inhibitor), CFTRinh172, MDL12330A (adenylyl cyclase inhibitor) and H89 (PKA inhibitor). Furthermore, we found that CDCA increased phosphorylation of CFTR. These findings suggested that CDCA required action of the basolateral transporters, as well as the cAMP pathway and PKA phosphorylation of CFTR to stimulate  $\text{Cl}^-$  secretion. The side-dependent action of CDCA, as well as the lack of complete inhibition by H89, implied the involvement of a membrane receptor and the possibility of other signaling kinases (15).

#### **D. Bile Acids and Pathophysiology**

Considering their central role in lipid absorption and as signaling molecules, perturbations in bile acid biology have been linked to a variety of disease states. Provided here are two brief examples, cancer and the metabolic syndrome, followed by a more detailed section on bile acid associated diarrheas, a topic most relevant to this dissertation.

## **1. Bile Acids and Colorectal Cancer**

Bile acids have been shown to increase proliferation associated with gastrointestinal cancers. Thus, chronic exposure to high concentrations of bile acids is an increased risk factor underlying cancers of the gastrointestinal tract. Interestingly, bile acid malabsorption in patients with inflammatory bowel disease with colitis predisposes them to developing colon cancer later in life. High fat diets, typical of Western culture, also increases the chance of developing colorectal cancer, as there is an increased need for bile acid synthesis to counteract the excessive amount of fat in the diet. Bile acids, specifically the secondary bile acids DCA and LCA, can exert a number of pro-cancerous effects including increasing reactive oxygen species, disruption of mitochondrial function, induction of DNA damage, as well as reducing apoptotic capabilities and increasing cell proliferation (3). In fact, DCA levels were found to be higher in the serum of patients with colorectal cancer (22, 23). As mentioned above in the section on membrane receptors (A.4.ii.) Raufman and colleagues have shown that an M3R → HB-EGF → EGFR cascade underlies bile acid stimulation of cell proliferation leading to colonic tumor development (49, 50, 203). In contrast to these deleterious effects, activation of bile acid specific nuclear receptors, including FXR and VDR, protect against bile acid carcinogenic effects. Although activation of FXR promotes apoptosis, which is beneficial in preventing cancer cell proliferation, DCA and LCA are not potent activators of FXR. Thus, a specific FXR agonist could be used to counter DCA and LCA's cancer promoting effects (156). Interestingly, vitamin D is protective against cancer and its deficiency contributes to colon cancer risk. LCA is a potent activator of VDR, and binding of LCA to VDR leads to its detoxification (3). It is possible that targeting the bile acid-activated nuclear receptors could have beneficial effects for colon cancer patients.

## **2. Bile Acids and the Metabolic Syndrome**

There is increasing evidence that bile acids may play a beneficial role in aspects of the metabolic syndrome. Both TGR5 and FXR contribute to the effects of bile acids on metabolism. Activation of TGR5 leads to secretion of glucagon like peptide-1 from intestinal L cells and leads to an increase in insulin release (42, 51, 120) and also contributes to increased pancreatic and liver function. Furthermore, this improved the glucose tolerance in obese mice (51, 244). Additionally, activation of TGR5 in brown adipose tissue stimulated the conversion of thyroid hormone T4 to T3 and thereby increase energy metabolism. However, there is little brown adipose tissue in adult humans, so this may be a species-specific effect of bile acids (51, 257). Interestingly, FGF15, a FXR effector, causes a switch from white adipose tissue to brown adipose tissue in diet-induced obese mice, suggesting that FG15 and TGR5 could be working together to increase metabolism (42). FXR also regulates energy substrate use and storage in hepatocytes. Activation of FXR inhibits glycolysis and lipogenesis and promotes weight loss after bariatric surgery in mice (133). In contrast, in diabetic mice, FXR inhibited gluconeogenesis, but increased glycolysis and glycogenesis. This effect on metabolic pathways provided evidence for a role of FXR in increasing glucose tolerance and insulin sensitivity (51, 57, 152, 277). Targeting FXR and TGR5 could be beneficial in the treatment of metabolic disorders.

## **3. Bile Acid Malabsorption and Bile Acid-Associated Diarrhea**

Physiologically the colon functions to absorb the fluid and electrolytes in the lumen (4.5-5 liters of fluid per day) and to concentrate the feces. Circumstances that disturb the absorptive and secretory processes of the colonic epithelium may result in diarrhea. In addition, disruption of the epithelial barrier, dysbiosis of the gut microbiota, and alterations in transport functions may contribute to the etiology of diarrhea (85, 251). It is well established that bile acids can influence all of these factors and the bile acid pool must be tightly regulated as changes in bile

acid homeostasis can result in diarrhea. While physiological concentrations of bile acids can be anti-secretory (122), high pathophysiological concentrations of bile acids (>3mM in the human) result in excessive colonic fluid secretion and bile acid-associated diarrhea (75).

The etiology of bile acid diarrhea is multifactorial and may be due to dysregulation of bile acid recycling or of bile acid synthesis. Traditionally, a majority, if not all, of bile acid diarrhea was presumed to be a consequence of bile acid malabsorption. However, there is recent evidence that a subset of chronic bile acid-diarrhea patients have normal ileal bile acid absorption, and therefore recycling. However, they have low serum FGF19 levels suggesting that the consequent lack of inhibition of bile acid synthesis leads to excess bile acid production leading to the disease etiology (251). Clinically bile acid malabsorption is classified as follows: Type 1: Disruption of ileal functioning (e.g. ileal disease or ileal resection); Type 2: Primary idiopathic bile acid malabsorption; and Type 3: Malabsorption due to celiac disease, peptic ulcer surgery, cholecystectomy, chronic pancreatitis, or diabetes (251). In Type 1, ileal resection (>100cm) due to damage can cause the bile acid pool to shrink dramatically and bile acid synthesis to increase (85). In Type 2, pathological conditions leading to disruption of the absorptive processes of the ileum, primarily mediated by ASBT, also result in bile acid malabsorption and increased concentration of luminal bile acids (38, 105). Although strictly not a “malabsorption” Type 2 has also been used to describe the diarrhea associated with excessive bile acid production due to dysregulation of FGF19 signaling. Type 3 is considered an indirect consequence of other gastrointestinal diseases.

Diagnosis of bile acid malabsorption is often overlooked but can be determined by fecal bile acid content, the <sup>75</sup>Se-homo-taurocholic acid test, measurements of bile acid metabolites in the plasma, or by circulating FGF19 levels (41). The efficacy of the <sup>75</sup>Se-homo-taurocholic acid test is very high (sensitivity: >80%; specificity: >70%) but it is not approved by the Food and Drug Administration in the United States. Most clinical practitioners use therapy-resistant watery

diarrhea as an indication of bile acid malabsorption instead of performing a diagnostic test, allowing for many patients with bile acid malabsorption to go undiagnosed (251). Those that are diagnosed with mild bile acid malabsorption and bile acid-associated diarrhea can be treated with the bile acid sequestrant cholestyramine (85).

Several mechanisms may contribute to the pro-diarrheal environment in patients with bile acid malabsorption. Two major mechanisms by which bile acids act are by regulating the ion transport proteins in the membrane, resulting in a net stimulation of secretion via CFTR (5, 15, 72, 124, 166) and an inhibition of absorption via Na/H and Cl/HCO<sub>3</sub> exchangers (31). When the majority of bile acids are lost in the stool, de novo synthesis cannot compensate for the loss to the bile acid pool. Therefore, lipid digestion and absorption is impaired resulting in increased fat in the colonic lumen which leads to steatorrhea. Increased fatty acids in the colon are themselves potent secretagogues (37). Increased inflammation of the intestine, such as that seen in patients with inflammatory bowel disease (IBD), can compromise the epithelial barrier. The epithelial barrier may be further perturbed by bile acids increasing tight junction permeability (84, 198). Bile acids also contribute to diarrhea by increasing colonic motility; allowing less time for electrolyte absorption, resulting in more fluid in the colonic lumen and subsequent diarrhea (5).

Excess luminal bile acids contributes to the pathogenesis of several intestinal disorders that have diarrheal symptoms such as idiopathic diarrhea, IBD, necrotizing enterocolitis (NEC), and irritable bowel syndrome (IBS). At least 50% of patients with functional diarrhea, have bile acid malabsorption that contributes to their symptoms. IBD is a chronic inflammatory condition of the intestine, whose symptoms include dysfunction of ion transport, disruption of the barrier, and dysmotility. The causes of IBD are multifactorial, and clinically identified as two major types: 1. Crohn's disease which can affect various regions of the intestine; and 2. Ulcerative colitis which is chronic inflammation localized to the colon. Bile acid malabsorption is often seen in

people that suffer from Crohn's disease localized to the ileum, since ASBT-dependent recycling is disrupted. Therefore it is not surprising that 85% of Crohn's patients suffer from diarrheal symptoms (251). IBD patients show a potent dysregulation of NaCl absorption (194), processes which are also negatively regulated by bile acids (187).

A second pathological condition associated with bile acid malabsorption and bile acid-associated diarrhea is NEC. As its name suggests, NEC is the necrosis of inflamed bowel, found primarily in preterm infants. The severity of NEC can be influenced by a variety of factors including the susceptibility of the host, inflammatory responses, ischemia, the development of the intestinal microflora, as well as enteral feedings. The necrosis is often localized to the ileum and proximal colon, resulting in disruption of transport processes in these regions (153). Using the neonatal rat model of NEC, it was found that total bile acid levels in the ileum were increased and were positively correlated to the severity of NEC. This was alleviated by cholestyramine treatment. It is well documented that ASBT expression is tightly regulated during development, with expression being low in the neonate and weanling ileum and achieving adult levels in post-weaning animals (226, 259). Interestingly, ASBT expression is low in non-NEC rats, but induction of NEC causes an increase in ileal ASBT expression, potentially as a compensatory mechanism to the high luminal bile acid content. This suggests that uptake of bile acids could be potentiating enterocyte injury under the inflammatory conditions of NEC. Thus it seems that the inflamed environment of NEC neonates can result in bile acid mishandling, which results in further damage to the epithelium and potentially diarrhea (102).

About 30% of IBS patients suffer from diarrhea and account for 30 million people worldwide (75, 258). Of these IBS diarrheal cases, 30% ( $\approx$ 10 million people) are due to bile acid malabsorption. Although most of these patients respond to treatments with bile acid sequestrants, such as cholestyramine or colesevelam, their malabsorption did not seem to be due to malfunctioning of ileal transport of bile acids. This phenomenon suggested that there

must be dysregulation in another part of bile acid metabolism, perhaps synthesis. Attention focused on the discovery that FGF15/19, (15 in mouse and 19 in human), produced by enterocytes, recycles to the liver where it binds to FGF receptor 4, and its binding partner  $\beta$ klotho, to negatively regulate bile acid synthesis (110). Interestingly, patients with primary bile acid diarrhea, had FGF19 levels about 50% compared to healthy volunteers (253) and a subset of diarrhea-predominant IBS patients carried single nucleotide polymorphisms in FGF receptor 4 and  $\beta$ klotho genes (75).

In summary, bile acid malabsorption and the accompanying diarrhea are rather prevalent in segments of the current population suffering from gastrointestinal disorders. However, the underlying signaling mechanisms remain to be defined.

## **E. Models for Ion Transport**

Despite the abundance of knowledge on bile acid signaling in metabolism, colon cancer, and diarrhea, there remains more to be investigated. In the context of bile acid malabsorption and the resulting diarrhea, the underlying mechanisms are poorly understood. Elucidating these mechanisms in models of ion transport will prove beneficial in the understanding of bile acid action in intestinal disorders like IBS and IBD.

### **1. Human Colonic T84 Cells**

A number of reductionist human cell line models have been used to study solute transport function in intestinal epithelial cells. Three in particular, derived from human colon carcinoma cells, have been used extensively to study ion transport as they form confluent monolayers exhibiting transepithelial resistance similar to that observed in native tissues. Caco-2 cells have been used to study absorptive properties more representative of small intestinal villar and colonic surface cells, whereas, HT-29 and T84 cells have been used to study

secretory functions more representative of crypt cells (10, 15, 141). Human colonic T84 cells are derived from a lung metastasis of a colon carcinoma that was injected into BALB/c nude mice before propagation in tissue culture (74). T84 cells grow slowly, often taking 2.5 to 3 days to double in numbers. T84 cells exhibit typical epithelial polarity when grown on rat-tail collagen-coated filters and tight junctions are fully formed after ~18 hours. In contrast, T84 cells grown on flat dishes have less distinct polarity, lack uniformity of tight junctions, and have less distinct apical and basolateral membranes (73).

Culturing the T84 cell line on semi-permeable filters allows for the elucidation of sidedness of action in altering transport mechanisms and measurement of vectorial transport. Vectorial transport can be measured in an Ussing chamber, which is an apparatus, in which an epithelial monolayer can be clamped between two chambers containing a physiological buffer. T84 cells grown on semi-permeable Transwell filters can be mounted between these two chambers and vectorial transport of ions can be measured as a current (see Methods). Transwell filters are microporous membranes that permit polarized cells to differentiate into a columnar epithelial cell layer and exhibit vectorial transport with directional movement across their basolateral and apical surfaces. Cells grown on Transwells better represents the activity of these cells in vivo as compared to their behavior when grown on flat surfaces. The benefit of utilizing the T84 cell line is that it has been established that transepithelial current measured in Ussing chambers is due to the activation of  $\text{Cl}^-$  channels on the apical membrane (74). Dharmsathaphorn et al. have described the presence and activity of the hallmark transporters that contribute to  $\text{Cl}^-$  secretion. Namely, the basolateral  $\text{Na}^+/\text{K}^+-2\text{Cl}^-$  cotransporter,  $\text{Na}^+/\text{K}^+$ -ATPase, cAMP- and  $\text{Ca}^{2+}$ -dependent  $\text{K}^+$  channels (45), and apical  $\text{Cl}^-$  channels (**Figure 4**) (73). T84 cells respond to a variety of physiological secretory stimuli such as VIP, prostaglandin 1, carbachol, and A23187, as well as the inhibitors somatostatin and verapamil (74). Similar to previous findings in the rabbit colon (60), it was found that tauro-DCA increased net  $\text{Cl}^-$

secretion from the basolateral side of T84 cells at a lower concentration than what was required to elicit a secretory response when applied to the apical side. Tauro-DCA did not increase cyclic nucleotides but did increase intracellular  $\text{Ca}^{2+}$ . It was proposed that in conditions where the luminal concentration of bile acids exceed 1mM, there is an increase in tight junction permeability and bile acids reach the basolateral membrane to initiate signaling cascades (72). Our lab has utilized this cell line and published that T84 cells can reach a TER of  $\geq 950 \Omega \cdot \text{cm}^2$  in contrast to the TER of the small intestinal like cell line, Caco-2 ( $\sim 300\text{-}500 \Omega \cdot \text{cm}^2$ ) (15, 239). The ability to achieve high TER indicates a well-differentiated monolayer and allows for the easy measurement of transepithelial electrical parameters. Although three  $\text{Cl}^-$  channels,  $\text{ClC-2}$  (18),  $\text{TMEM16A}$  (174) and  $\text{CFTR}$  (15), are present in T84 cells, the predominant apical membrane channel responsible for secretion is  $\text{CFTR}$ . Despite T84 cells being extremely useful for measurements of ion transport, their slow growth and disruption of polarity and function after being subjected to routine genetic manipulations, including stable transfection, calls for the use of other models.

## **2. Human Embryonic Kidney (HEK-293) Cells**

In a seminal paper, Graham et al. demonstrated the versatility of the Human Embryonic Kidney 293 (HEK-293) cell line as a model for genetic manipulations. HEK-293 cells were established by transfecting human embryonic kidney cells either as primary, or secondary cultures in early passages with sheared adenovirus (type 5) DNA in the presence of calcium phosphate (100). Because of their susceptibility to genetic manipulations we utilized the HEK-293 cells as a reductionist model to study bile acid signaling. This cell line has become the preferred tool of mammalian cell and molecular physiologists as they are of human origin and express foreign proteins readily. Amongst their advantages are the ease with which they can be cultured, transfected, and molecularly manipulated to study cloned protein function and associated signal transduction pathways. The use of HEK-293 cells has ranged from being a

mammalian cell factory for protein over-expression to being used as a tool to study structure-function correlations of a given protein. Li et al. used HEK-293 cells to over-express MRP4 to study spatiotemporal coupling of MRP4, PDZK1 scaffolding protein, and CFTR (141). HEK-293 cells stably transfected with ASBT have been used to study the roles of lipid rafts and protein trafficking in ASBT regulation (11-13). In a recent study, Jensen et al. used HEK-293 cells stably transfected with the bile acid receptor, TGR5, and transiently transfected with protease receptor 2 or  $\beta$ -arrestins 1 and 2 to study TGR5 function and trafficking (115). It is important to note that the endogenously expressed HEK-293 cell proteins may contribute to function as well as trafficking of the over-expressed protein of interest. Therefore, there is a need to examine the function of transfected proteins against the backdrop of endogenous proteins. Given the limitations of the T84 epithelial cell line we chose to study the regulation of  $\text{Cl}^-$  secretion in HEK-293 cells and in HEK-293 cells transfected with an EGFP-CFTR construct (described in Methods).

### **3. Intestinal Organoid Cultures**

The culturing of primary intestinal cells has been a difficult technique to perfect due to the short life span of mature intestinal epithelial cells, potential contamination with the gut microflora, and the variety of cell types that are expressed in the epithelium (73). With the discovery of LGR5 as a marker of intestinal stem cells, and the subsequent definition of conditions for growth and differentiation, the gastrointestinal physiology field entered a new era of investigation into the native intestinal epithelium (19). Consequently, two types of “mini guts” in culture have been developed: those derived from intestinal pluripotent stem cells and those derived from the stem cells present in the mature intestinal crypts. The “mini guts” derived from induced pluripotent stem cells display an enclosed lumen surrounded by both epithelial and mesenchymal layers and are sometimes referred to as “organoids”, while the “mini guts” derived from small intestinal or colonic crypts are sometimes referred to as enteroids or colonoids,

respectively. The enteroids and colonoids similarly form an enclosed lumen and are lined with a monolayer of epithelial cells, lacking a mesenchymal layer. The epithelial-only organoids also require culturing in a 3D matrigel suspension, with media containing specific growth factors including R-spondin, Wnt3a, and Noggin for their development. The nomenclature of these *ex vivo* preparations is under debate, as the original studies from the H. Clevers laboratory (210) used “organoids” to refer to the cultures of the epithelial-only mini guts while others refer to them as enteroids or colonoids. For the purpose of this study, we refer to crypt-derived cultures as organoids in **Chapter VI**. Upon isolation and culturing of intestinal crypts, the crypts close to form simple spherical structures. As cells begin to proliferate and differentiate the spheres form bud-like structures and resemble the crypt and surface/villi of the native intestine. Similar to cell lines, organoids can be passaged, and continuously cultured over many passages (59). Although most studies derive their organoids from isolated tissue, Sato et al. demonstrated that isolation of single LGR5+ stem cells can give rise to full organoid structures (210). Addition of the aforementioned Wnt signaling agonists helps maintain the proliferative phenotype (“stemness”) that is typical of the stem cells. Removal of Wnt agonists results in differentiation and the cells lose their proliferative capacity (210).

Development of this self-renewing primary culture system has become the hallmark technique for new approaches to advancing personalized medicine and looking at microbe and host interactions in an *ex vivo* culture system. Using crypt-derived mouse intestinal organoids, Zhang et al. were able to assess the bacterial invasiveness and dysregulation of the epithelium after Salmonella infection (278). Microinjection of *Clostridium difficile* into the organoids derived from human induced pluripotent stem cells, resulted in bacterial colonization and disruption of barrier function (139). Because the organoids possess all the intestinal epithelial cell types, it is possible to observe the effect of bacteria on specific cell types. Additionally, in organoids

derived from human small intestinal biopsies, Saxena et al. were able to study the susceptibility of specific patients to rotavirus infection (212).

Since the majority of epithelial cells along the intestine function to transport electrolytes it was important to know that these transport processes could be recapitulated in the organoid cultures. Using organoids derived from normal and cystic fibrosis human and mouse tissue, Dekkers et al. developed the forskolin-induced swelling assay to monitor activation of CFTR (67). In this assay, addition of CFTR agonists, such as forskolin, induce swelling of the organoids, indicative of Cl<sup>-</sup> secretion into the lumen. This assay was used to test the responsiveness of cystic fibrosis patients to novel CFTR potentiators and correctors, verifying the utility of the organoid system in developing personalized therapies. In addition to organoid swelling to study Cl<sup>-</sup> transport, NHE and pH regulation can be measured (89, 252). Continued use of these methodologies will emphasize the regulation of ion transporters in normal and pathological conditions in the gastrointestinal tract.

#### **F. Hypothesis, Objective, and Specific Aims**

Bile acids, specifically the 7 $\alpha$ -dihydroxy CDCA and DCA, act on colonic epithelia in a rapid, side-dependent manner to activate CFTR and stimulate Cl<sup>-</sup> secretion, suggesting the involvement of a plasma membrane receptor-signaling cascade. While bile acid-activated receptors in intestinal secretory epithelia have been related to a variety of cellular responses, their link to Cl<sup>-</sup> secretion has yet to be identified. Thus, **I hypothesized that the primary, dihydroxy bile acid, CDCA, stimulates Cl<sup>-</sup> secretion in the colonic epithelium via a receptor-mediated activation of CFTR using multiple intracellular signaling pathways.** The objective of this study is to determine the regulatory cascades by which CDCA induces

colonic Cl<sup>-</sup> secretion using the human colon carcinoma cell line T84, HEK-293 cells, and intestinal organoid cultures. To accomplish this, I identified three specific aims:

- **Aim 1.** Determine the initial step by which CDCA acts to modulate Cl<sup>-</sup> secretion in a cell model of the human colonic epithelium (**Chapter III**);
- **Aim 2.** Elucidate the second messenger signaling cascades by which CDCA induces Cl<sup>-</sup> transport in cultured cell lines (**Chapters IV and V**); and
- **Aim 3.** Delineate CDCA activation of CFTR *ex vivo* using native intestinal epithelial cultures (**Chapter VI**).

The overall goal of this research plan is to contribute significantly to our understanding of the molecular basis of bile acid-stimulated Cl<sup>-</sup> secretion. This study will enhance our knowledge of bile acid-associated diarrhea in poorly understood intestinal disorders like irritable bowel syndrome.

## **Chapter II: Materials and Methods**

## **A. Materials**

Tissue culture media included: Dulbecco's Modified Eagle Medium, Minimum Essential Media, Ham's F12 nutrient mixture, bovine calf serum, fetal bovine serum, and G418, purchased from Invitrogen (Carlsbad, CA). For HEK-293 transfection experiments, DH5alpha competent *E. coli* was obtained from Invitrogen (Carlsbad, CA), X-tremeGENE 9 DNA Transfection Reagent and Lipofectamine 2000 were from Roche (San Francisco, CA). Opti-MEM media for EGFR transfections was purchased from Thermo Fisher Scientific (Asheville, NC). EGFR specific siRNA (HsEGFR 11) and negative control siRNA were synthesized by and purchased from Qiagen (Valencia, CA). Rat-tail collagen, bovine serum albumin, and Poly-L lysine were obtained from Sigma-Aldrich Corp (St. Louis, MO). Secretagogues and inhibitors used were of analytical grade and included: chenodeoxycholic acid, forskolin, carbachol, lithocholic acid, ciprofloxacin, GW4064, H89, CFTR<sub>inh</sub>172, nocodazole, MK571, AG1478, ESI-09, nystatin, U73122, PD98059, LY294002, wortmannin, T16Ainh-AO1, protease inhibitor cocktail P8340, and phosphatase inhibitor cocktails 2 and 3 purchased from Sigma-Aldrich Corp. (St. Louis, MO). BAPTA-AM and Fura2-AM were purchased from Molecular Probes of Thermo Fisher Scientific Inc. (Hanover Park, IL). H1152 was purchased from Enzo Life Sciences (Farmingdale, NY). GGTI298 was purchased from Tocris Bioscience (Pittsburgh, PA). The protein kinase C inhibitors rottlerin and chelerythrine were obtained from Millipore Calbiochem (Danvers, MA). The IP<sub>3</sub> receptor inhibitor 2-APB was bought from Santa Cruz Biotech. Inc. (Santa Cruz, CA). SB203580, the p38 inhibitor, was purchased from Cell Signaling (Boston, MA). Unless otherwise specified, all other reagents were of analytical grade, and were purchased from either Sigma-Aldrich Corp. or Fisher Scientific (Hanover Park, IL). Unless otherwise specified, all non-water soluble reagents were dissolved in DMSO and DMSO was used as a control.

HitHunter cAMP HS+ Assay and the IP<sub>3</sub> Assay were purchased from DiscoverX (Fremont CA). Human phosphokinase array kit was purchased from R&D systems (Minneapolis, MN). Rap Activation Assays were purchased from Cell Biolabs, Inc (San Diego, CA). Tissue culture plates, flasks, and transwells were purchased from Corning Inc, Life Sciences (Lowell, MA). Antibodies used: Phospho-specific and non-phospho specific antibodies to EGFR (Y1068), ERK1/2 (T202/Y204), and p38 (T180/Y182) were purchased from Cell Signaling (Boston, MA). Monoclonal mouse-anti-human CFTR COOH-terminus was purchased from R&D Systems (Minneapolis, MN). Polyclonal goat-anti-EGFP and rabbit-anti-TGR5 were from Abcam (Cambridge, MA). Monoclonal mouse-anti- $\alpha$ -tubulin was purchased from Sigma-Aldrich Corp. (St. Louis, MO). Polyclonal goat-anti-MRP4 and mouse monoclonal GAPDH were purchased from Novus Biologicals (Littleton, CO). Horseradish peroxidase (HRP) conjugated secondary antibodies used were goat-anti-rabbit, goat-anti-mouse, and bovine anti-goat purchased from Santa Cruz Biotechnology (Santa Cruz, CA). For immunofluorescence imaging, *SlowFade* Gold performance DAPI was purchased from Invitrogen (Carlsbad, CA). Wheat Germ Agglutinin, Alexa Fluor 594 conjugate, NucBlue Live Ready Probes Reagent were from Life Technologies (Grand Island, NY).

## **B. Tissue culture**

Human colon carcinoma T84 cells were acquired from the American Type Culture Collection (ATCC) (Manassas, VA, USA). T84 cells were cultured in media containing equivalent amounts of Dulbecco's Modified Eagle Medium and F-12, supplemented with 6% bovine calf serum, ampicillin (8 $\mu$ g/mL), penicillin (100 iU/mL) and streptomycin (100ug/mL). These cells are considered female as determined by amplification of the amelogenin gene (177). Cells from passages 39-50 were used for experimentation. For Ussing chamber studies, T84 cells were

seeded at a density of ~250,000 cells per Transwell insert (6.5-mm, 0.4  $\mu$ m pore size, 24-well plate) coated with rat-tail collagen. For immunoblot studies, cells were grown on 6-well plates or 6-well Transwells (24.5mm, 0.4 $\mu$ m pore size) at a density of  $1.5 \times 10^6$  cells per insert. T84 cells were serum starved overnight prior to immunoblot or Ussing chamber studies.

HEK-293 cells were kindly given to us by Dr. W.A. Alrefai (Jesse Brown VAMC and UIC Department of Medicine) and were grown in Minimum Essential Media supplemented with 10% FBS, 1% penicillin/streptomycin (100 iU/ml; 100  $\mu$ g/ml). Cultures of transfected HEK-293 cells were stabilized in the presence of G418 (see below). All cell cultures were incubated in a humidified atmosphere of 5% CO<sub>2</sub> at 37°C.

## **C. Transfection**

### **1. CFTR Expression**

A human CFTR/pEGFP (enhanced green fluorescent protein)-C1 plasmid consisting of wild-type human CFTR cDNA subcloned into the multiple cloning site of the pEGFP-C1 vector (Clontech, Mountain View, CA), resulted in EGFP plus a 2 amino acid linker fused to the N-terminus of human CFTR. This construct was originally generated in the laboratory of Dr. Kevin Foskett (University of Pennsylvania) and provided to Dr. Deborah J. Nelson (University of Chicago, our collaborator). The construct was sequenced and verified prior to transfection. The construct was amplified by transforming DH5alpha competent *E. coli*. For transfection studies, HEK-293 cells were seeded into 6-well plates in the presence of the human CFTR vector using X-tremeGENE 9 DNA Transfection Reagent. A total of 1 $\mu$ g DNA/well and 3 $\mu$ l of X-tremeGENE 9 reagent/well were used for each transfection in antibiotic free media. After 48 hours, cells were incubated with medium containing 0.8 mg/ml G418. Resistant clones of cells were trypsinized,

pooled, and maintained in medium containing the same concentration of G418 and designated as HEK-CFTR cells (77).

## **2. EGFR siRNA**

T84 cells were plated in 6-well plates until they reached ~50% confluency. They were then transiently transfected with 100pmol of scrambled siRNA or EGFR siRNA diluted in Opti-MEM medium and then combined in a 1:1 ratio with Opti-MEM diluted Lipofectamine 2000 transfection reagent. The mixture was allowed to incubate for at least 5 minutes before adding the siRNA-lipid complex to the cells. The scrambled siRNA, used as a nontargeting control, and EGFR siRNA were predesigned (Qiagen). After 24 hours, Opti-MEM media containing the transfection reagent was removed and replaced with regular Dulbecco's Modified Eagle Medium /F-12 as described above. After a further 48 hours (72 hours after transfection) cells were harvested for RNA, protein, or used to measure CDCA-stimulated Cl<sup>-</sup> transport by iodide efflux (described below). Ussing chambers (described below) are typically used to measure transepithelial Cl<sup>-</sup> secretion in T84 cells, and require confluent and resistive monolayers. This set up cannot be used with transfected cells because efficient transfection of siRNA requires subconfluent (~50% confluence) monolayers. The siRNA is most effective at 72 hours post transfection, (~7 days after plating), a time when the monolayers do not meet the minimal TER ( $\geq 1000 \Omega \cdot \text{cm}^2$ ) needed for studies in Ussing chambers. Thus we used the previously established method of iodide efflux (15, 77) which does not require resistive monolayers. After iodide efflux, cells were harvested for protein and expression of EGFR was assessed by immunoblotting using an EGFR specific antibody.

#### **D. RNA isolation and Reverse Transcriptase Polymerase Chain Reaction (RT-PCR)**

RT-PCR was performed as previously described (15). Cells were grown to confluence and then harvested in TRIzol reagent (1mL) and incubated for 5 minutes; incubations were at room temperature and centrifugations at 4°C unless otherwise specified. Chloroform (200µL) of was added to each sample and shaken for 15 seconds then incubated for 3 minutes. Samples were then centrifuged at 12,000 x g for 15 minutes. After centrifugation, the colorless liquid phase was removed and saved for RNA isolation. Samples were then incubated with isopropanol (500µL) for 10 minutes and centrifuged for 10 minutes at 12,000 x g. The supernatant was removed and the RNA pellet was washed with 1mL of 75% ethanol by vortexing and centrifuging for 5 minutes at 7,500 x g. The air-dried RNA pellet was resuspended in RNA-storage solution and stored at -80°C. RNA was treated with DNase prior to synthesis of cDNA. RNA concentrations and purity were measured by Nano-drop UV-Vis Spectrophotometer (Thermo Fisher Scientific; Asheville, NC) at 260nm. RNA (1µg) was used for cDNA synthesis by superscript II reverse transcriptase. **Table I** shows primer pairs used for PCR (36 cycles).

<b>Table I: PCR Primers</b>				
	<b>Forward</b>	<b>Reverse</b>	<b>Annealing Temp. (°C)</b>	<b>Estimated Size (bp)</b>
<b>FXR</b>	ATTTTGACGGAAATGGCAAC	AGCTAGACCCCTCCCCTGTA	55	591
<b>TGR5-IE</b>	AGCATCTTCCTTCCTCAGC	TTGTGTATCCCTGCCTCCAC	64	653
<b>TGR5-E2</b>	GCTGCTTCTCCTRAGCCTA	TGGGAGCTGCAGTTGGCA	50	321
<b>CFTR</b>	CAAGGAGGAACGCTCTATCG	GCCTCCGAGTCAGTTTCAG	59	558
<b>CIC-2</b>	AGTGGGAGGAGCAACTA	TGGGTCAGATTCCAGGTAGG	59	557
<b>TMEM16A</b>	GGCTTTCCTGCTGAAGTTTG	CGATGTCTTTGGCTCTGACA	59	505
<b>MRP2</b>	GAGCAAGTTTGAAACGCACA	AGCCGCAGTGAATAAGAGGA	59	397
<b>MRP3</b>	TGTGCTAGCTGATGGACAGG	TGTCACCTGCACCTTCTCTG	59	340
<b>MRP4</b>	CCATCTGTGCCATGTTTGTC	CCACAATGCCAACCTTTTCT	59	363
<b>TGR5-HEK</b>	CTCAGTCCTGGCCTATGAGC	TAACGGCCAGAGGAGCTTTA	59	399

### **E. Protein Isolation, SDS-PAGE, and Immunoblotting**

Cells were grown to confluence and washed with ice cold phosphate buffered saline (PBS) before being lysed in a buffer containing in mM: 25 Tris-HCl (pH 7.4), 1 EDTA, 2 MgCl<sub>2</sub>, 5 β-mercaptoethanol, 1 DTT, and 10μl protease inhibitor cocktail/mL lysis buffer. For protein isolated to assess phosphorylation state of kinases, phosphatase inhibitor cocktails 2 and 3 (Sigma) were also added to the lysis buffer. The lysates were sonicated on ice (30 seconds; Branson Sonifier Cell Disruptor Model 350) and centrifuged at 2,000 x g for 10 minutes (4°C). The pellet, containing nuclei and unlysed cells was discarded and the supernatant (total cell lysate) was saved. When needed, the cell lysates were further fractionated into membrane and cytosolic fractions, 30 minutes at 10,000 x g (4°C). The pelleted membrane fraction was resuspended in lysis buffer. Protein concentrations were measured using the Bio-Rad Protein Assay protocol. Cell fractions (30-50μg of protein) were separated by SDS-PAGE (7.5% or 4-15%) electrophoresis and the membranes subjected to Western blotting as described previously (9, 15). Blots were blocked with 5% milk or 3% bovine serum albumin for 1 hour at room temperature and incubated with primary antibodies (in 1% milk/bovine serum albumin, overnight (4°C). After washing with Tris-buffered saline (pH 7.4) containing 0.1% Tween 20, blots were exposed to HRP-conjugated secondary antibodies (1:10,000 dilution; 1 hour, room temperature) and visualized with Pierce SuperSignal West Pico or Femto Chemiluminescent Substrate kit (Thermo Scientific, Rockford, IL). When needed, mainly for blots where phosphorylation of proteins were screened first, membranes were stripped in a buffer containing 100 mM β-mercaptoethanol, 2% SDS, 62.5 mM Tris·HCl (pH 6.7) for 30 minutes, 55°C, and reprobed with different primary antibodies (not phospho-specific) as described above. The secondary antibody exposure and visualization of the reaction product were as described above. Immunoblot bands were quantified by ImageJ software after scanning densitometry. The concentrations of primary antibodies used are listed in the figure legends or within the text.

## **F. Human Phosphokinase Array**

A human phosphokinase array was performed according to the manufacturer's instructions. When T84 cells reached ~90% confluence in 100mm dishes, serum starved overnight, and were treated with either 500 $\mu$ M CDCA or 0.01% DMSO (as control) for 5 minutes to induce kinase phosphorylation. Cells were then washed with cold PBS and lysed with the lysis buffer provided. Cell lysates were centrifuged (14,000 x g, 5 minutes, 4°C) and the resulting supernatant was collected. Equal amounts of the supernatant were incubated overnight with the phosphokinase array membranes. The membranes have "capture" antibodies that bind to their respective proteins in the cell lysate. Similar to standard immunoblotting protocol (see above), membranes were washed and then exposed to a cocktail of detection antibodies. Signals were captured using streptavidin-HRP and chemiluminescent reagents provided by the manufacturer. The pixel density of each "spot" was determined using ImageJ, and duplicate spot signals were averaged.  $\beta$  catenin was used to normalize the kinase signals as its phosphorylation state remained unchanged. Normalized signals were compared between the DMSO and CDCA treated samples. If there were any indication that a kinase was involved in CDCA action, then further assessment was performed using specific primary antibodies as mentioned above.

## **G. Preparation of Detergent-Soluble and Insoluble Tubulin**

Detergent-soluble and -insoluble tubulin was prepared according to Yu et al. (272). To establish a protocol for destabilizing microtubules in HEK-CFTR cells, the distribution of detergent-soluble (monomeric) and detergent-insoluble (microtubule)  $\alpha$ -tubulin was examined under four conditions of nocodazole exposure. HEK-CFTR cells were grown in 10cm dishes and exposed to one of the following treatment regimens: I. 4°C, 30 minutes to destabilize microtubules followed by incubation with nocodazole on ice 30 minutes and then at room

temperature, 1 hour; II. Nocodazole on ice for 30 minutes followed by incubation at room temperature, 1 hour; III. 4°C for 30 minutes followed by incubation with nocodazole at room temperature, 1 hour; IV. Incubation with nocodazole at room temperature, 1 hour. After these regimens, the cells were rinsed with PBS and once with extraction buffer (in mM: 100 PIPES pH 6.75, 1 MgSO<sub>4</sub>, 2 EGTA, 0.1 EDTA, and 2000 glycerol). Cells were subsequently extracted twice for 8 minutes each with 750µl extraction buffer containing 0.1% Triton X-100 and protease inhibitors and the fractions collected to yield the detergent-soluble fraction. The detergent insoluble fraction remaining on the plate was treated with lysis buffer (in mM; 25 Na<sub>2</sub>HPO<sub>4</sub>, pH 7.2, 400 NaCl, and 0.5% SDS), sonicated and centrifuged for 10 minutes (2,000 x g), and the DNA-containing pellet was discarded. Equal amounts of detergent-soluble and insoluble proteins from each treatment group were subjected to SDS-PAGE and immunoblotting as described above using α-tubulin antibody (1:2,500 dilution).

#### **H. Cell Surface Biotinylation**

Cell surface biotinylation was performed as described by Gill et al. (97). Briefly, confluent HEK-CFTR cells were equilibrated in serum free media and treated with 10µM forskolin or DMSO (0.1%) for 1-10 minutes at room temperature. Cells were placed on ice, washed with a modified PBS (PBS+ 0.1mM CaCl<sub>2</sub> and 1mM MgCl<sub>2</sub>). and exposed to biotin (1.5mg/ml) in borate buffer (in mM: 10 boric acid pH 9.0, 154 NaCl, 7.2 KCl, and 1.8 CaCl<sub>2</sub>,) for 1 hour, 4°C, in the dark. The cells were treated with quenching buffer (modified PBS +100mM glycine, 20 minutes, 4°C) to bind any excess biotin, washed in modified PBS and collected by centrifugation at 13,000 x g (10 minutes, 4°C). The cells were lysed in RIPA buffer (in mM: 150 NaCl, 50 Tris-HCl pH 7.6, 5 EDTA, 1% Triton X-100, 0.1% SDS, protease inhibitor cocktail), sonicated (2 x 30 seconds) and centrifuged at 13,000 x g (4°C, 10 minutes) to yield the total cell lysate. Protein concentrations were determined by Bio Rad Protein Assay. One mg of protein from each

treatment group was added to Neutravidin beads (Thermo Scientific) that were pre-equilibrated with RIPA buffer. Samples were incubated overnight (4°C) in an Eppendorf rotoshaker. The beads were collected by centrifugation at 13,000 x g (4°C, 10 minutes) and the supernatant containing the non-biotinylated fraction was saved. The beads were washed with RIPA buffer (5,000 x g, 5 minutes, 4°C x3) and resuspended in 2X loading dye (Biorad). Non-biotinylated fractions were diluted in 2X loading dye. Nonbiotinylated, and biotinylated fractions were heated (60°C, 15 minutes) and resolved by SDS-PAGE, and immunoblotting as described above. The blots were probed with CFTR-COOH antibody (1:1,000) to assess CFTR expression. To check for non-biotinylated protein contamination of the biotinylated fraction, blots were stripped and reprobed with GAPDH antibody (1:2,000).

### **I. Live Cell Imaging and Vesicle Trafficking**

HEK-CFTR cells were seeded on 2-cm<sup>2</sup> glass bottom dishes (MatTek Corporation, MA, USA) for 3 to 4 days for ~90% confluence. The cells were washed with PBS, and incubated with 1ml of phenol free Dulbecco's Modified Eagle Medium containing 5µg Wheat Germ Agglutinin (WGA), Alexa Fluor 594 conjugate (Life Technologies, Grand Island, NY) for 10 minutes at 37°C in a tissue culture incubator. The cells were then washed five times with 1ml of phenol-free Dulbecco's Modified Eagle Medium. One ml of phenol-free Dulbecco's Modified Eagle Medium containing 2 drops of NucBlue Live Ready Probes Reagent (Life Technologies, Grand Island, NY) was then added to the dish. Next, the dish was mounted on a Zeiss LSM 710 confocal microscope (META) (Zeiss, Oberkochen, Germany) equipped with a PeCon temperature controller (PeCon GmbH, Erbach, Germany) to keep the temperature at 37°C. After a 2-minute incubation with NucBlue, 3 images were taken as baseline using diode UV laser, Exλ 405nm, Emλ 420-480nm; Argon laser, Exλ 488nm, Emλ 500-550nm and DPSS 561 laser, Exλ 561nm, Emλ 600-650nm. Then DMSO or forskolin were added to the cells, and images were captured

as time series using ZEISS microscope software Zen. A 63x/1.46 oil objective was used with a final magnification of 126X. For CFTR vesicle tracking, z-stack images were also acquired in addition to time series to generate 4D images. The vesicles were detected using the “spot detection” function of Imaris (Bitplane AG, Switzerland) and were tracked over time. To optimize sample size, vesicles  $\geq 0.71\mu\text{m}$  in diameter were tracked. Based on the relative size of the cells, vesicular tracking was done over a length of 1 to  $15\mu\text{m}$ . Vesicle speeds and other parameters were exported into Excel.

### **J. Intracellular $\text{Ca}^{2+}$ ( $[\text{Ca}^{2+}]_i$ ) Measurements**

T84, HEK, or HEK-CFTR cells (~one million cells) were seeded on 2-cm<sup>2</sup> glass bottom dishes (MatTek Corporation, MA, USA) for 3 to 4 days to achieve ~90% confluence. Dishes for HEK and HEK-CFTR cells were coated with Poly-L-lysine. The cells were loaded with  $5\mu\text{M}$  Fura2-AM (Molecular Probes) in serum-free Dulbecco's Modified Eagle Medium /F-12 (+0.02% F-127) for T84 cells, and in serum-free MEM for HEK/CFTR cells, for 1 hour in a tissue culture incubator at 37°C. To remove any extracellular or membrane bound Fura2-AM, cells were washed 3 times with Krebs–Ringer-Hepes buffer (in mM: 120 NaCl, 5.4 KCl, 0.8 MgCl<sub>2</sub>, 1 CaCl<sub>2</sub>, 11.1 glucose and 20 Hepes pH 7.4). For  $\text{Ca}^{2+}$  free buffer,  $\text{Ca}^{2+}$  was chelated with 2mM EGTA. After the final wash, the dishes were filled with fresh Krebs-Ringer-Hepes buffer and allowed to equilibrate at room temperature for 15 minutes for any remaining Fura2-AM cleavage. Dishes were next mounted on a dual channel temperature controlled (Warner Instruments, Hamden, CT) platform of a fluorescence microscope (Olympus IX51, Olympus America, Center Valley, PA).  $\text{Ca}^{2+}$  agonists (e.g. CDCA) made in Krebs-Ringer-Hepes buffer were delivered to the cells by a perfusion and vacuum system (Warner Instruments).  $\text{Ca}^{2+}$  signals were captured using a Q-8 spectrofluorometer system (Photon Technology International, Edison, NJ), and the fluorescence ratios (Ex $\lambda$ : 340/380 nm; Em $\lambda$ : 505 nm) were converted to nM concentrations

based on a standard curve using a calcium calibration buffer kit (Molecular Probes, Waltham, MA) (44, 250). If signaling inhibitors were required, the cells were pretreated with the inhibitor during the final 30 minutes of Fura2-AM loading and were present during the room temperature incubation in Krebs-Ringer-Hepes buffer. Agonists were then perfused in Krebs-Ringer-Hepes buffer containing the inhibitor.

### **K. Intracellular cAMP ([cAMP]<sub>i</sub>) Measurements**

HEK-CFTR cells were seeded in 96-well plates at a density of 35,000 cells per well, overnight prior to initiation of the assay. PBS with or without forskolin (10 $\mu$ M), LCA (50 $\mu$ M), MK571 (20 $\mu$ M), batimastat (20 $\mu$ M), DMSO (control), or a combination of the treatments was added to the cells and incubated at 37°C. [cAMP]<sub>i</sub> was measured using a HitHunter cAMP HS+ Assay as instructed by the manufacturer (DiscoverX). This assay uses enzyme fragment complementation technology with two fragments of *E. coli*  $\beta$ -galactosidase. The amount of luminescent signal produced is directly proportional to the amount of cAMP from the cell lysates. Briefly, cAMP HS+-antibody and lysis buffer were added to the standards and cells for an incubation of 1 hour at room temperature. The enzyme donor reagent was then added to the wells and incubated for 1 hour at room temperature. Finally, the enzyme acceptor and substrate mix were added to the wells and incubated at room temperature overnight in the dark. The luminescence was read on the second day using a luminescent microplate reader. The cAMP concentrations were determined from the standard curve.

### **L. IP<sub>3</sub> Measurements**

Generation of IP<sub>3</sub> was measured using the HitHunter IP<sub>3</sub> Assay from DiscoverX. As per the manufacturer's instructions, T84 cells were grown in a T25 flask (Corning) until confluency.

Cells were then trypsinized and counted. Cells were brought to a final concentration of  $2 \times 10^6$  cells/mL in PBS (without  $\text{CaCl}_2$  or  $\text{MgCl}_2$ ) and were aliquoted into microcentrifuge tubes for agonist treatment. Perchloric acid was added to stop the reaction. Cells were then distributed into a 96-well plate, which also included wells with  $\text{IP}_3$  assay standards.  $\text{IP}_3$  tracer and binding protein were added sequentially with a 5 minute incubation for each. The solutions were mixed using a microplate shaker at 650 RPM. The fluorescence polarization signal was read using the Tecan Infinite 200 Pro multimode reader (Tecan US Inc., Morrisville, NC) with the following settings: excitation filter fluorescein at 485nm, emission filter fluorescein at 530nm, and the dichroic fluorescein at 505nm. A standard curve was plotted using a 4 parameter best-fit analysis. With the DiscoverX fluorescence polarization technology,  $\text{IP}_3$  generated by the cells competes with the  $\text{IP}_3$  tracer for the  $\text{IP}_3$  binding protein. In principle, in the absence of additional  $\text{IP}_3$ , the tracer tumbles more slowly and results in a higher polarized signal. As  $\text{IP}_3$  in the sample increases, the unbound  $\text{IP}_3$  tracer will increase, making it tumble faster and thereby lower the polarized signal. Thus the polarization signal is inversely proportional to the  $\text{IP}_3$  produced by the cells.

### **M. Ussing Chambers**

Electrophysiological measurements were performed as previously described (15). T84 cells were seeded at a density of  $\sim 250,000$  cells per Transwell insert (6.5-mm, 0.4  $\mu\text{m}$  pore size, 24-well plate) coated with rat tail collagen. TER was measured after at least 2 weeks of seeding using an EVOM volt ohmmeter and a STX2 chopstick electrode (World Precision Instruments, Inc. Sarasota, FL). When cells reached sufficient confluency to establish a TER of at least  $1000 \Omega \cdot \text{cm}^2$  (approximately 14-28 days) they were serum starved overnight prior to experimentation. Transwell inserts were then mounted in Ussing chambers (area:  $0.33 \text{ cm}^2$ ; Physiologic Instruments, Inc., San Diego, CA) and bathed in 5mL (per reservoir) oxygenated buffer (95%

O<sub>2</sub>, 5% CO<sub>2</sub>). The transport buffer consisted of (in mM): NaCl 115.4; KCl 5.4; CaCl<sub>2</sub> 1.2; MgCl<sub>2</sub> 1.2; NaHCO<sub>3</sub> 21.0; NaH<sub>2</sub>PO<sub>4</sub> 0.6; Na<sub>2</sub>HPO<sub>4</sub> 2.4; pH 7.4, and D-glucose 10, at 37 °C. Transmural short-circuit current ( $I_{sc}$ ;  $\mu\text{A}/\text{cm}^2$ ) and TER were measured over the course of the experiment. For inhibitor studies, monolayers were pretreated for 30 minutes with bilateral addition of the inhibitor(s) unless otherwise stated. DMSO was used as a vehicle control for the inhibitors. Following equilibration with signaling inhibitors, CDCA (500 $\mu\text{M}$ ) was added to the basolateral reservoir, and subsequently forskolin (10 $\mu\text{M}$ ) and carbachol (100 $\mu\text{M}$ ) were added to ensure cell viability. **Figure 5** demonstrates the typical  $I_{sc}$  protocol for control treated wells.

For measurements of apical Cl<sup>-</sup> currents in the ESI-09 studies, a Cl<sup>-</sup> gradient was established by mounting monolayers in the regular transport buffer (containing 115.4mM NaCl), and a basolateral buffer where the NaCl was replaced with equimolar sodium gluconate. To account for potential Ca<sup>2+</sup> chelation by gluconate, the concentration of CaCl<sub>2</sub> was increased to 2mM in the basolateral buffer. The monolayers were then permeabilized by adding 200 $\mu\text{g}/\text{ml}$  nystatin to the basolateral surface (15). Once monolayers were equilibrated, they were treated with 0.1% DMSO as control or 10 $\mu\text{M}$  ESI-09 and stimulated with CDCA and forskolin. CFTRinh172 (10 $\mu\text{M}$ ) was added at the end to assess contribution of CFTR.

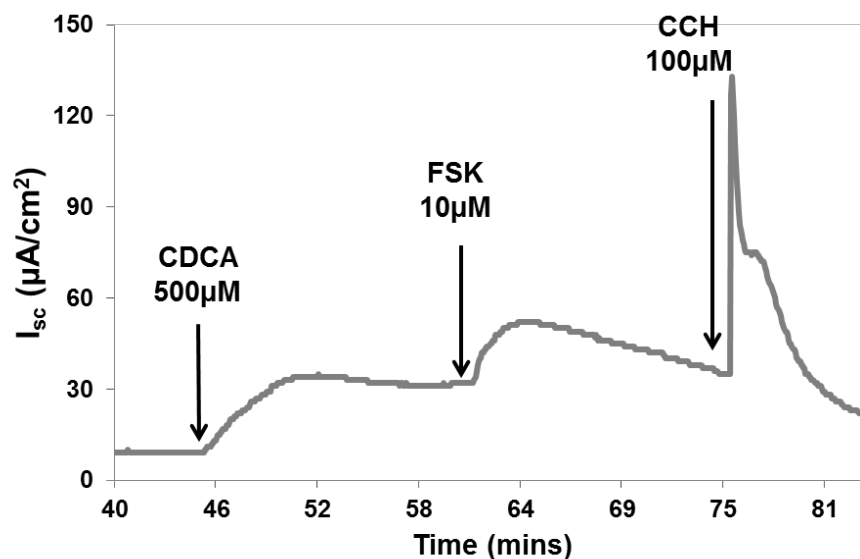


**Figure 5:** Typical Ussing chamber protocol. Confluent T84 monolayers are mounted in Ussing chambers and stimulated with basolateral addition of 500 $\mu\text{M}$  CDCA after the baseline current stabilizes. Forskolin (FSK; 10 $\mu\text{M}$ ) and carbachol (CCH; 100 $\mu\text{M}$ ) are used as positive controls for cAMP- and  $\text{Ca}^{2+}$ -induced  $\text{Cl}^-$  transport, and to demonstrate monolayer viability. Unless otherwise specified, when signaling inhibitor(s) are being used, the inhibitor(s) are added bilaterally at least 30 minutes before addition of CDCA.

## **N. Iodide Efflux**

Iodide efflux studies were performed as previously described by us (9, 15, 34) and are based on the method of Venglarik et al. (249) with modifications described by Chappe et al. (47). For T84 cells transfected with EGFR siRNA, iodide effluxes were used in place of  $I_{sc}$  measurements because efficient resistance could not be reached due to siRNA transfection. At 72 hours post transfection, media was removed and then cells were incubated with iodide containing buffer (in mM: 136 NaI, 3 KNO<sub>3</sub>, 2 Ca(NO<sub>3</sub>)<sub>2</sub>, 11 glucose and 20 HEPES, pH 7.4) for 1 hour at room temperature in the dark. After iodide loading, the iodide containing buffer was aspirated and wells were washed with iodide-free buffer three times (same as iodide-containing buffer but NaNO<sub>3</sub> replaced NaI; iodide efflux buffer). Cells were then exposed to iodide efflux buffer (1mL) containing DMSO, CDCA (500μM), or forskolin (10μM) after baseline efflux measurements. Efflux buffer was collected and saved at 2 minute intervals and replaced with fresh efflux buffer. Each sample saved contained the iodide released during the 2-minute period. At the end of the experiment the wells were washed with PBS and cells were harvested for protein. An iodide-sensitive electrode (Orion 96-53, Fisher Scientific) and a pH/mV meter were used to measure the amount of iodide in the buffer that was collected

In a similar manner, HEK-CFTR and HEK-293 cells were grown in 6-well plates coated with Poly-L-lysine. One million cells were seeded per well, and grown for 3 to 5 days for the cells to reach 90% confluence, at which time they were incubated with iodide loading buffer. Signaling inhibitors were added during the last 30 minutes of iodide loading and the inhibitors were present in the efflux buffer during the remainder of the experiment. After washing out any excess iodide, individual wells were exposed to DMSO, LCA (5-500μM), forskolin (2-50μM), or CDCA (100-500μM) ± inhibitors: CFTRinh172 (10-20μM), H89 (30μM), MK571 (20μM), BAPTA-AM (20μM), nocodazole (33μM), or AO1 (20μM).

Iodide concentration was calculated based on a standard curve as previously described (34) and depicted either as the mean rate of iodide efflux at each 2-minute interval or as fold change in mean cumulative iodide efflux  $\pm$  SEM relative to value at starting point.

### **O. Rap Activation Assay**

To assess CDCA activation of the small GTPase Rap2, Rap activation assays were performed on T84 cells grown on 10cm dishes to 80-90% confluence according to the manufacturer's instructions (Cell Biolabs, Inc.). Cells were serum starved overnight before stimulation with 500 $\mu$ M CDCA (0-20 minutes) and then washed with PBS. Plates were then incubated on ice with 1X lysis buffer provided by the manufacturer. Samples were transferred to microcentrifuge tube and centrifuged at 14,000 x g for 10 minutes at 4°C. Biorad Protein Assay was performed to calculate protein concentration in the supernatant fraction. An aliquot of protein from the total lysate (5mg) was then incubated with agarose beads conjugated to Ral guanine nucleotide dissociation stimulator for 1 hour at 4°C. The dissociation stimulator has a binding domain specific to GTP-bound Rap. Remaining lysate were prepared in the same manner as protein samples described above and used for input loading controls. After incubation, the beads were pelleted by centrifugation for 30 seconds at 14,000 x g at 4°C and supernatant was removed. Beads bound to activated Rap were then washed with 1X lysis buffer (3x) for 30s at 14,000 x g. After the final wash all excess lysis buffer was removed and beads were resuspended in 2X loading dye and boiled for 5 minutes. Samples were then loaded for SDS-polyacrylamide gel electrophoresis and immunoblotting for Rap2 (1:500 antibody dilution in 1% milk) as described above.

To test efficacy of the assay, a non-stimulated plate was harvested for protein in the same manner described above and protein concentration determined. Two aliquots (1.5mg each)

were incubated with 0.5M EDTA (20 $\mu$ L) and either 10 $\mu$ L of 10mM GTP $\gamma$ S (+ control) or 100mM GDP (- control) for 30 minutes at 30°C. Loading was stopped by addition of 65 $\mu$ L of MgCl<sub>2</sub>. Lysates were then incubated with the agarose beads as described for the stimulated samples and immunoblotted for Rap2.

## **P. Intestinal Organoids**

### **1. Generation and Maintenance**

Protocols for the generation and maintenance of organoids were established by our colleagues Drs. Hugo de Jonge and Marcel Bijvelds at Erasmus University, Rotterdam, Netherlands and are described in this section. Selected regions of mouse intestine (i.e. jejunum, ileum, and proximal colon) were harvested and kept in cold PBS on ice. Intestinal sections were cut open length wise and washed in PBS. For small intestinal tissue only, a cover slip was used to scrape off the villi; this was not necessary for colonic tissue. Surgical scissors were used to remove any remaining adipose tissue on all intestinal sections. Sections were then cut into small pieces using a scalpel and placed in fresh ice cold PBS (~30mL) in a 50mL conical tube. For further cleaning, a 10mL tip dipped in fetal calf serum was used to triturate the tissue, and after tissue sedimentation the PBS was discarded and further washed with fresh PBS (~5x). After the final wash, fresh cold PBS was supplemented with EDTA (2.5mM) and added to the tissue. The intestinal sections were then incubated on a rotating shaker (300 RPM) at 4°C for 30 minutes for small intestinal sections, and 1 hour for large intestinal sections. After EDTA incubation, the isolation procedure was continued under sterile conditions in a tissue culture hood. PBS+EDTA was removed and fresh cold PBS was added and the suspension was triturated (~20x) using a 10mL pipet tip (coated in serum). The cloudy supernatant was discarded and fresh PBS was added to further break up crypts by pipetting. The clean PBS

fraction was then passed through a 70 $\mu$ m filter into a clean 50mL conical tube until at least 50mL of PBS had been filtered. The filtrate was then split into two 50mL conical tubes and supplemented with 10% fetal calf serum. Samples were then centrifuged at 1200 RPM, 5 minutes, at 4°C. Supernatant was discarded and crypts were resuspended in Advanced Dulbecco's Modified Eagle Medium/F-12 media and transferred to a 15mL conical tube. Crypts were quantified to determine the yield and centrifuged at 600 RPM for 5 minutes at 4°C. Media was decanted and crypts were resuspended in thawed Matrigel (50 $\mu$ L/ well) and seeded ~100-500 crypts/ well in 24-well plates. Matrigel was allowed to stiffen at room temperature for 3-5 minutes before inversion of the plate and incubation at 37°C (~30 minutes) for full maturation of Matrigel, before addition of growth medium (**Figure 6**). Growth medium as described by Dekkers et al. contained: Dulbecco's Modified Eagle Medium/F-12 supplemented with penicillin and streptomycin, 10mM HEPES, 1X Glutamax (100X stock), 1X N2 (100X stock), 1X B27 (50X stock) (Invitrogen), 1 $\mu$ M N-acetylcysteine (Sigma), 16.3nM EGF, 50% Wnt3a-conditioned medium, 10% noggin-conditioned medium, 20% R-spondin1-conditioned medium, 10 $\mu$ M nicotinamide (Sigma), 500nM A83-01 (Tocris), and 10 $\mu$ M SB202190 (Sigma) (67). Wnt3a, noggin, and R-spondin1 conditioned media were harvested from individual cell lines that secreted the respective growth factor (e.g. stably transfected HEK-293 cell line expressing R-spondin1). The organoid medium was refreshed every 2–3 days, and organoids were passaged every 7–10 days. Briefly, media was aspirated and Matrigel/organoid suspensions were broken up by adding cold medium. Organoids were then transferred to a 15mL conical containing 2-3mL of cold medium and centrifuged for 5 minutes at 600 RPM, 4°C. The supernatant was then removed, organoids were resuspended in Matrigel and transferred to a warmed 24-well plate to incubate at room temperature. The plate was then incubated at 37°C until the Matrigel stiffened at which point growth medium was added. Organoids were cultured for at least 3 passages before use in swelling assays by confocal live-cell imaging.

In contrast to the small intestinal organoids, isolation of colonic crypts requires more rigorous EDTA exposure ( $\geq 1$  hour v. 30 minutes for small intestine), as well as increased supplementation with Wnt3A since the colonic epithelium does not produce sufficient amounts of Wnt3A to support the proliferative nature of the stem cells. Small intestinal derived organoids do produce sufficient amounts of Wnt3A to sustain their proliferative capacity, however we supplemented their growth as well in order to maintain the crypt-like character. For small intestinal organoids, withdrawal of Wnt3A results in organoid differentiation from crypt-like to villus-like characteristics (89).

## **2. Swelling Assay**

Organoid swelling assays were performed as described by Dekkers et al. (67). Mouse organoids from at least passage 3 were cultured for 7 days. On the 7<sup>th</sup> day, organoids were passaged and seeded in a flat-bottom 96-well culture plate in 5 $\mu$ l droplet of Matrigel and 100 $\mu$ l of culture medium. One day after plating, organoids were incubated for 1 hour with 100 $\mu$ l standard culture medium containing 10 $\mu$ M calcein green-AM (Invitrogen). After calcein green loading, organoids were mounted for confocal live-cell microscopy (Leica SP5 604, 10x objective). Organoids were stimulated with ethanol (vehicle control), CDCA (500 $\mu$ M), or forskolin (10 $\mu$ M). Organoid diameter or surface area was quantified by ImageJ, and data is displayed as increases relative to  $t=0$ . For quantification of surface area, the surface area threshold was set at 3000 $\mu$ m<sup>2</sup>, which excluded organoids that were considered too small and unviable.

## **P. Statistics**

Data from at least three individual experiments were analyzed and presented as means  $\pm$  SEM. Statistical significance was determined using paired Student's t-test or 1-way ANOVA. Values of  $p < 0.05$  were considered statistically significant and are denoted with an \* or # where indicated.

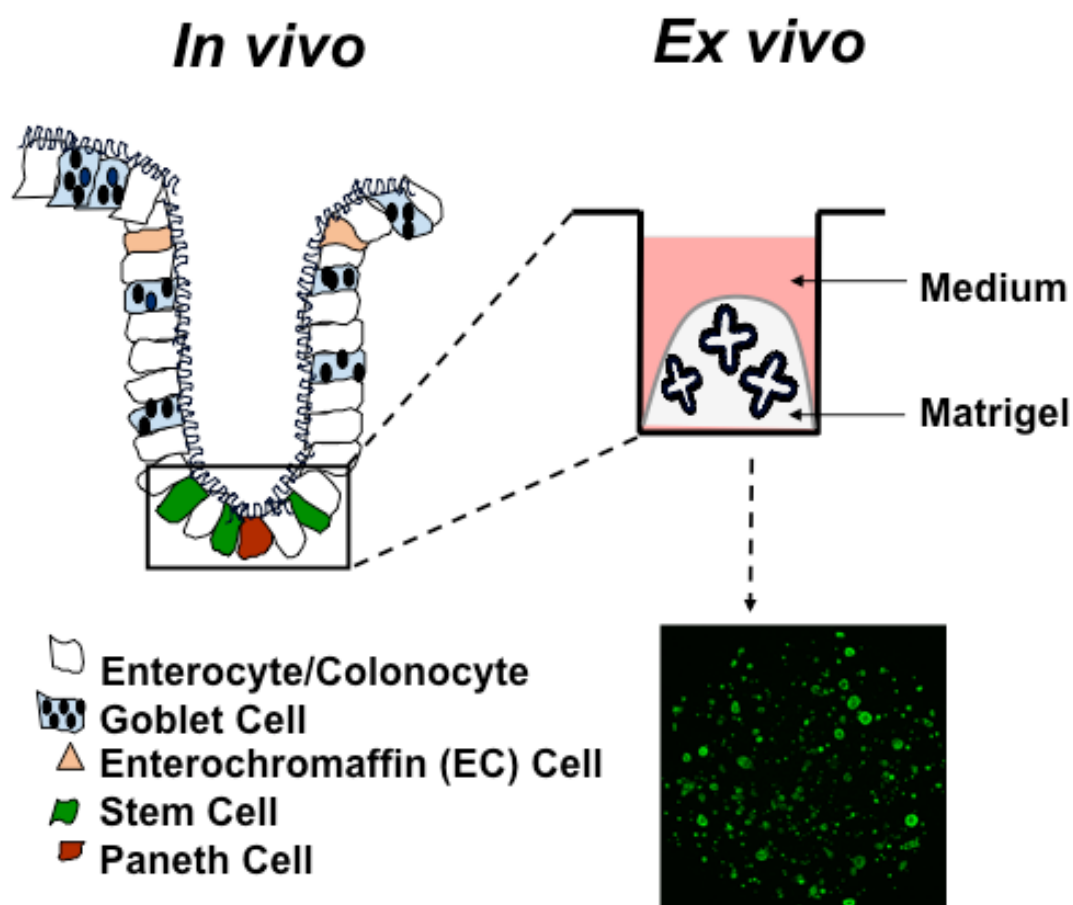


**Figure 6:** Depiction of crypt isolation to organoid maturation. The *in vivo* cartoon is representative of colonic crypts, but in general the intestinal crypts contain intestinal stem cells, which give rise to all the different epithelial cell types. Crypts can be isolated from intestinal tissues and cultured into organoids (*ex vivo*) in a 3D matrigel suspension with a specific combination of stem cell niche growth factors as described in the text. The bottom right image is a snapshot of individual mouse colonic organoids in matrigel suspension under a light microscope.

### **Chapter III. Results: Bile Acid Activation of Cl<sup>-</sup> Transport in T84 Cells**

**Parts of the work in this chapter were published as:**

Ao M, Sarathy J, **Domingue J**, Alrefai WA, and Rao MC. (2013). Chenodeoxycholic acid stimulates Cl<sup>-</sup> secretion via cAMP signaling and increases cystic fibrosis transmembrane conductance regulator phosphorylation in T84 cells. *Am J Physiol Cell Physiol.* 305:C447–C456.

## **A. Rationale and Aim**

High concentrations (0.5-1mM) of dihydroxy bile acids act on colonic epithelial cells in a rapid manner to activate CFTR, and the dose-dependency and sidedness of action suggest a receptor-mediated pathway (15, 118, 124, 250). While the presence and function of bile acid-activated receptors in intestinal epithelia has been reported, the bile acid receptor involved in the Cl<sup>-</sup> secretory response remains to be identified (56, 256). In addition, the structural specificity of the bile acids that stimulate the Cl<sup>-</sup> secretory cascade need to be further defined. Thus, the focus of this chapter was to determine the initial step by which CDCA acts to modulate Cl<sup>-</sup> secretion in a cell model of the human colonic epithelium (**Aim 1**). Based on the sidedness and rapidity of CDCA action, it was hypothesized that a receptor was mediating CDCA's activation of CFTR.

## **B. Bile Acid Specificity and Sidedness of Action**

The majority of studies have investigated the action of DCA and its taurine conjugates in the colon (49, 50, 118, 124, 202, 250) and we wanted to confirm the reported bile acid specific secretory action in human colonic T84 cells. We stimulated T84 cells with bilateral addition of CA, DCA, CDCA, and LCA (500 $\mu$ M) and measured changes in I<sub>sc</sub> ( $\mu$ A/cm<sup>2</sup>), indicative of Cl<sup>-</sup> secretion in these cells. In agreement with previous studies, only the 7 $\alpha$ -dihydroxy bile acids, DCA and CDCA, caused an increase in I<sub>sc</sub>, with CDCA having the strongest effect (**Figure 7**). One advantage of measuring I<sub>sc</sub> in Ussing chambers is the ability to assess sidedness of action of various regulators. Therefore, we assessed the effect of apical or basolateral addition of CDCA, DCA, their taurine conjugates, as well as CA and LCA on I<sub>sc</sub>. Consistent with previous studies (70, 72, 124, 166), both of the dihydroxy bile acids, and their taurine conjugates, had a stronger effect on Cl<sup>-</sup> secretion when administered to the basolateral surface (**Table II**).

Differences between basolateral (**Table II**) and bilateral bile acids (**Figure 7**) are reflective of variability in T84 responses, done at different times, but underscores the efficacy of DCA and CDCA as the pro-secretory bile acids, with CDCA being the most potent secretagogue in these cells. Although the average increase in  $I_{sc}$  was highest with tauro-CDCA, it was not statistically significantly different from that seen with CDCA. Additionally, tauro-CDCA is rapidly deconjugated by colonic bacteria, suggesting that in the normal colon, unconjugated CDCA may be the predominant species acting on the colonic epithelium. Therefore, the studies in this and the following chapters elucidate the signaling mechanisms activated by basolateral addition of 500 $\mu$ M CDCA.

$\Delta I_{sc}$	<b>Table II: Sidedness of Bile Acid (500<math>\mu</math>M) Action</b>					
$\mu$ A/cm <sup>2</sup> $\pm$ SEM (n $\geq$ 3)	CDCA	Tauro-CDCA	DCA	Tauro-DCA	CA	LCA
<b>Apical</b>	6.6 $\pm$ 1.6	6 $\pm$ 1.5	5.75 $\pm$ 2.1	3.0 $\pm$ 1.2	no effect	1.6 $\pm$ 0.9
<b>Basolateral</b>	24.3 $\pm$ 6.6	32.7 $\pm$ 4.7	18.3 $\pm$ 3.4	6.25 $\pm$ 1.9	no effect	-1.5 $\pm$ 1.1

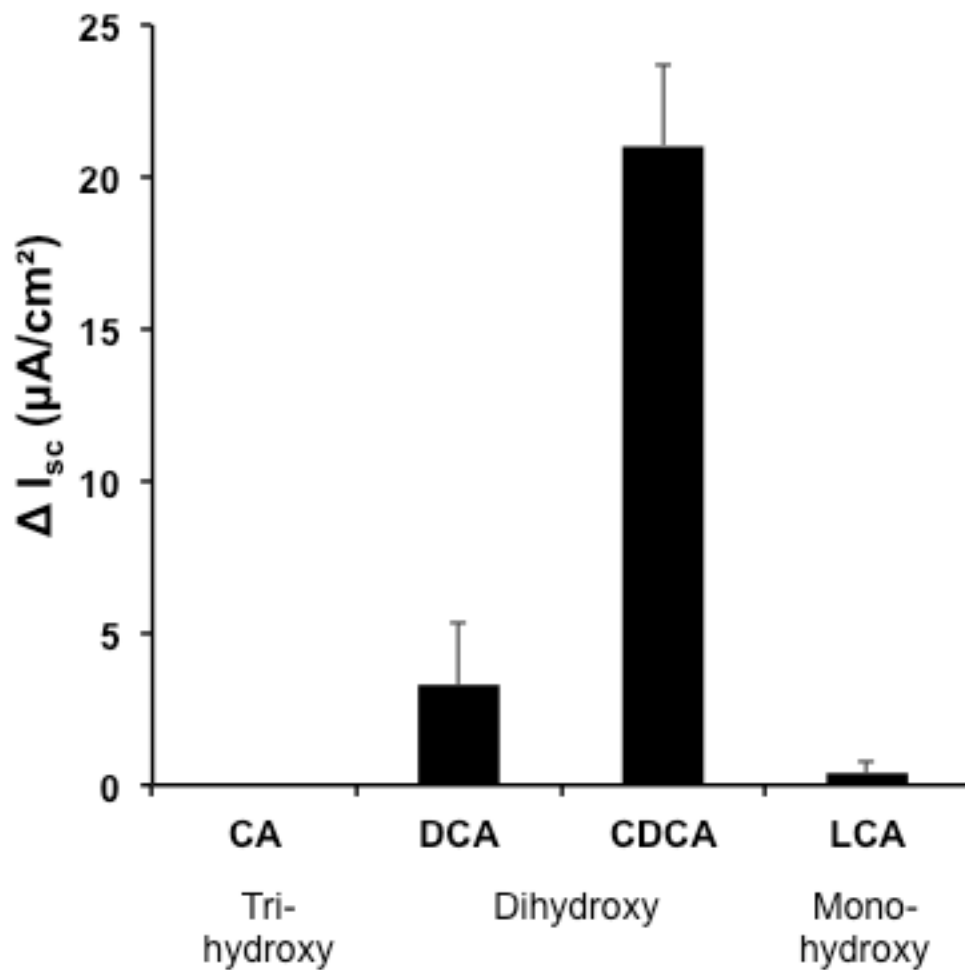


**Figure 7.** Specificity of bile acids on  $Cl^-$  secretion. 500 $\mu M$  of the bile acids, cholic acid (CA), deoxycholic acid (DCA), chenodeoxycholic acid (CDCA), and lithocholic acid (LCA), were added bilaterally to confluent T84 monolayers and changes in short circuit current ( $I_{sc}$ ,  $\mu A/cm^2$ ) were measured. Bar graphs display the average  $\Delta I_{sc} \pm SEM$ ,  $n=3$  for all bile acids.

## **C. Bile Acid Specific Receptor Expression and Activation**

### **1. FXR and TGR5 Expression**

CDCA's rapid and side-dependent effect on Cl<sup>-</sup> secretion (< 5 minutes; **Figure 5**) suggested the involvement of a receptor-mediated pathway. Two receptors have been described as being specific to bile acids, the GPCR, TGR5, as well as the nuclear receptor FXR. We first wanted to determine their expression in T84 cells. As shown in **Figure 8** [adapted from (15)], T84 cells expressed mRNA transcript for both FXR and TGR5. Two different primer sets were used to assess TGR5 expression. Since the mature protein is only encoded by a single exon, exon 2, one primer set included a portion of the intron upstream of exon 2 (TGR5-IE) while the second primer set was designed only for exon 2 (TGR5-E2). A band appearing in the cDNA samples using primer TGR5-IE would indicate DNA contamination. The representative image shows no DNA contamination in our cDNA samples. Additionally, expression of FXR or TGR5 was not affected by culturing on flat bottom dishes compared to collagen-coated Transwells. We also found that TGR5 protein was predominantly expressed in the membrane fraction of total cell lysates of T84 cells (**Figure 8**; (15)). We used rat distal colon, liver, and spleen as positive controls due to TGR5's reported expression in these tissues (121, 160, 256).

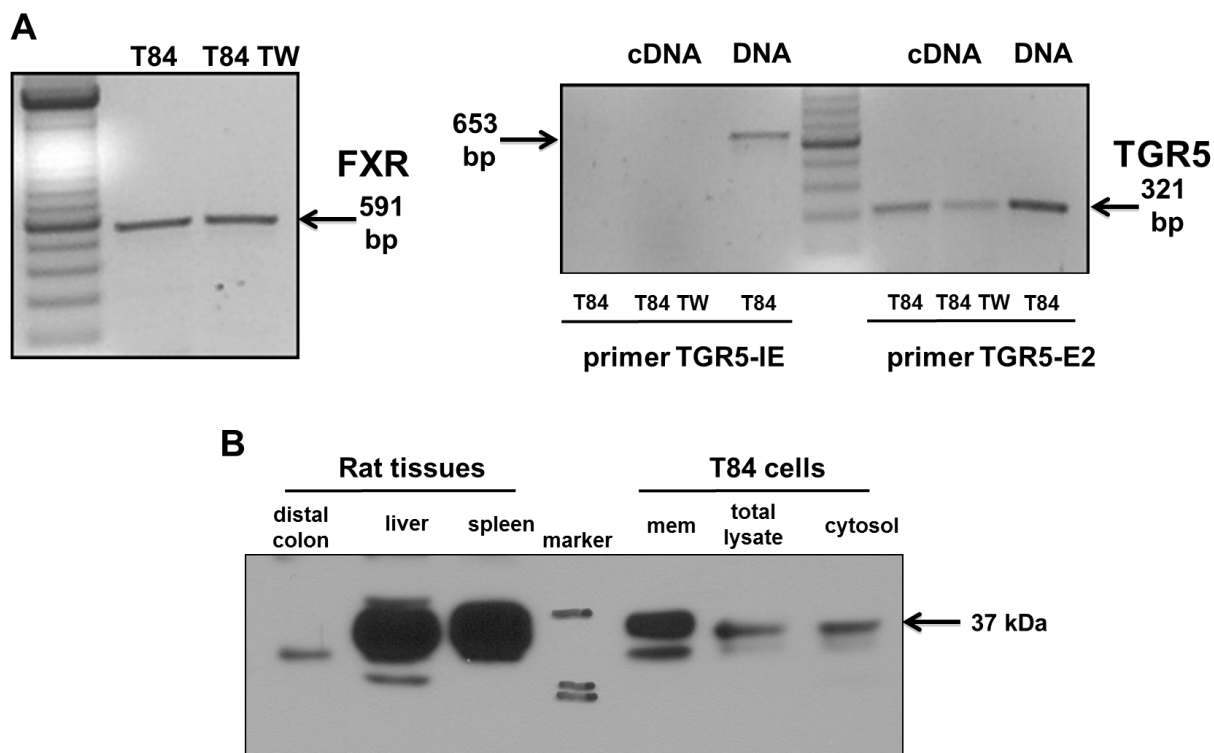


**Figure 8:** Bile acid receptor expression [adapted from (15)].

**A.** Representative RT-PCR of the bile acid specific receptors FXR (left) and TGR5 (right). FXR mRNA was estimated to be 591bp. Two different primer sets were used for TGR5; TGR5-IE spans a portion of the intron between exons 1 and 2, proving no DNA contamination in the cDNA. TGR5-E2 primers span only exon 2, which is the coding region for the protein. DNA and cDNA were harvested from T84 cells grown on cell culture dishes (T84) or from T84 cells grown on Transwells (TW);  $n \geq 3$ .

**B.** Representative ( $n=3$ ) western blot of TGR5 in T84 cell membrane fraction, total lysate, and cytosolic fraction. Rat distal colon, liver, and spleen were used as positive controls. TGR5 protein is estimated to be 37kDa.

## 2. Bile Acid Receptor Agonists and $I_{sc}$

Transcript and protein expression however do not always correlate with function of a protein. The role of these receptors in bile acid action have been previously investigated using specific agonists of the receptors (56, 173), implying that if either receptor is involved in a pro-secretory response, then their respective agonists should increase  $Cl^-$  secretion comparable to CDCA. However, addition of the TGR5 agonist ciprofloxacin (20 $\mu$ M) or the FXR agonist GW4064 (5 $\mu$ M) had little to no effect on  $I_{sc}$  (**Figure 9**). Lack of an effect with ciprofloxacin was not surprising, since another potent activator of TGR5, LCA, also does not alter  $I_{sc}$  (**Table II**). Interestingly, LCA actually inhibits cAMP-dependent  $Cl^-$  secretion, which suggests, either that LCA is not using TGR5 for its anti-secretory actions, or that in these cells LCA –TGR5 binding does not activate the canonical cAMP pathway, or that the TGR5 expressed in these cells is not functional (14). These results suggest that neither the membrane receptor TGR5, nor the nuclear receptor FXR are involved in CDCA-induced  $Cl^-$  secretion.

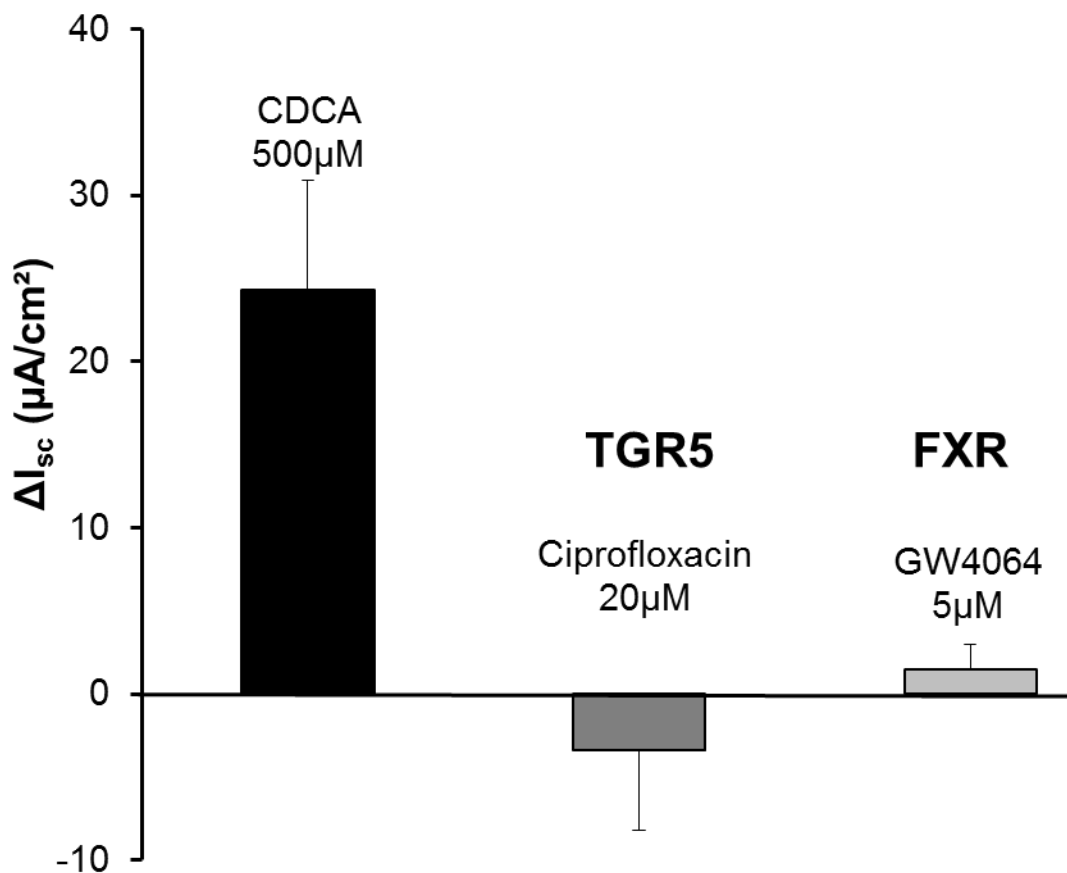


**Figure 9:** Effect of bile acid receptor agonists on  $I_{sc}$ . Agonists to the bile acid specific receptors were added to T84 monolayers and  $I_{sc}$  ( $\mu A/cm^2$ ) was measured. Ciprofloxacin (20 $\mu M$ ; n=7) was used as a TGR5 agonist and GW4064 (5 $\mu M$ ; n=3) was used as an agonist of FXR. These were compared to the effects of 500 $\mu M$  CDCA (n=4). Bar graphs represent the average changes in  $I_{sc}$  responses  $\pm$  SEM.

## **D. Role of Putative Bile Acid Receptors in CDCA Action**

It is well known that bile acids can also act via other receptors such as S1PR2 (236),  $\alpha 5\beta 1$ -integrin (98), M3R (49, 50), and via transactivation of EGFR. Signaling via S1PR2 and  $\alpha 5\beta 1$ -integrin have been implicated in hepatocytes, whereas activation of M3R and EGFR have been implicated in colonic epithelial cells lines (203).

### **1. Effect of Inhibition of Muscarinic Receptors by Atropine**

Investigation by Raufman et al. showed that DCA can bind to and activate M3R and induce transactivation of EGFR, leading to cell proliferation in H508 colonic cells (49, 50). They suggested activation of M3R could occur by other bile acids as well. In contrast to these earlier studies, CDCA-induced  $I_{sc}$  in T84 cells was not affected by atropine, an inhibitor of M3Rs [Figure 10A; adapted from (15)]. This does not mean that CDCA does not activate M3R, but that the M3R cascade is not involved in the pro-secretory effect of CDCA.

### **2. Effect of Inhibition of EGFR by AG1478**

Transactivation of EGFR is a mechanism employed by a number of GPCR activators to influence cell function, including VIP and carbachol in stimulation of  $Cl^-$  secretion in T84 cells (20, 25, 247). Although we ruled out involvement of the GPCRs TGR5 and M3R, we know that CDCA acts in a cAMP-PKA-dependent manner, implying involvement of a potentially unknown GPCR in CDCA action. Therefore, we determined if transactivation of EGFR could be mediating CDCA's activation of CFTR. T84 cells were pretreated with the EGFR inhibitor AG1478 (1 $\mu$ M) for 30 minutes then stimulated with CDCA. AG1478 is a tyrphostin that blocks activation of EGFR by inhibiting its kinase activity. Interestingly, AG1478 pretreatment resulted in a significant 58% inhibition of CDCA's increase in  $I_{sc}$  (Figure 10B).

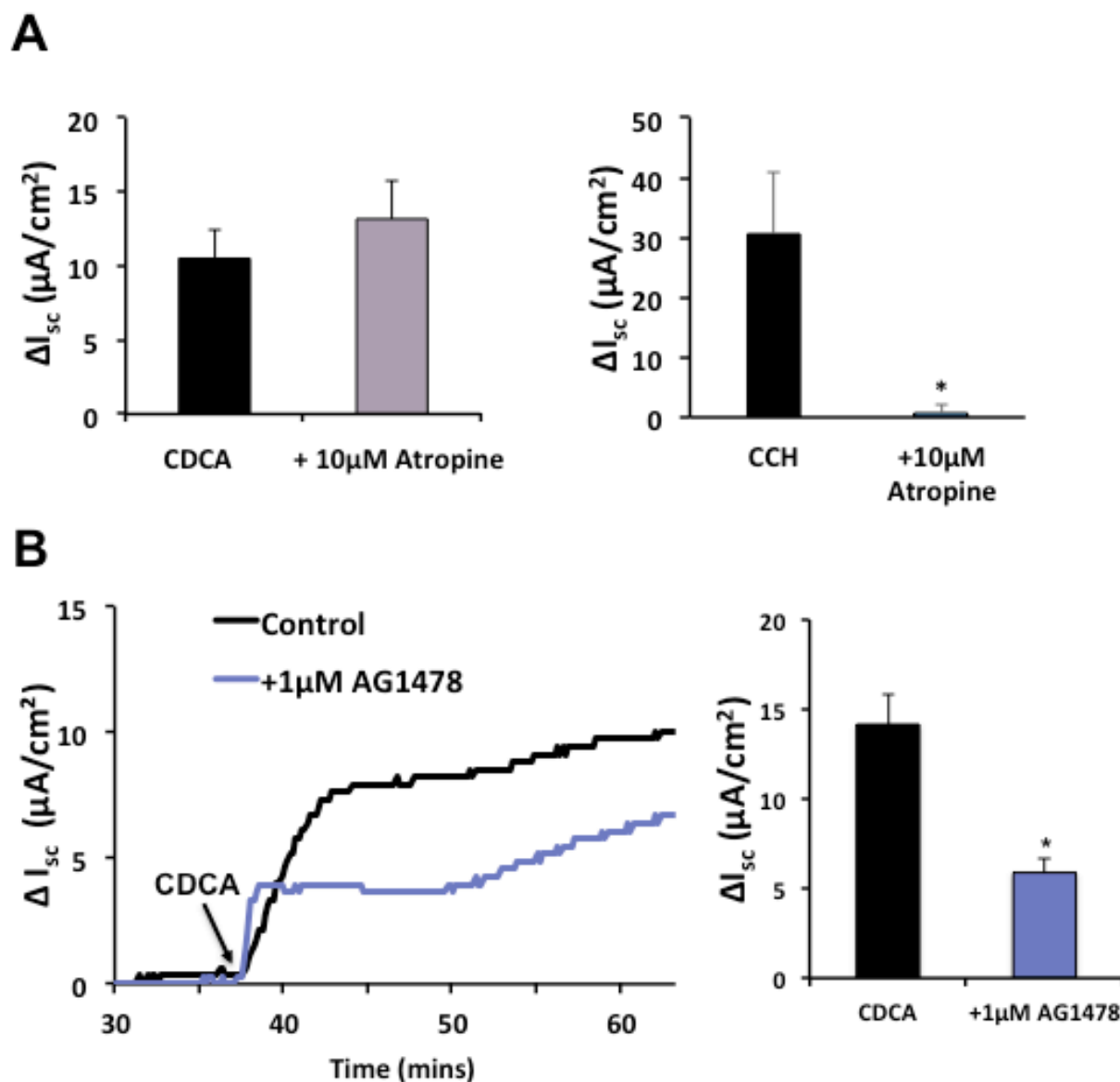


**Figure 10:** Effect of putative bile acid receptor antagonists on CDCA-induced  $I_{sc}$ .

**A.** T84 monolayers were pretreated for 30 minutes with bilateral addition of 0.1% DMSO or the muscarinic receptor antagonist atropine (10 $\mu M$ ) before stimulation with basolateral addition of 500 $\mu M$  CDCA or carbachol (CCH; 100 $\mu M$ ). \* denotes significance,  $p < 0.05$ ,  $n = 6$ . Bar graphs represent the average changes in  $I_{sc}$  responses  $\pm$  SEM.

**B.** In a similar manner, T84 monolayers were treated with the EGFR antagonist AG1478 (1 $\mu M$ ). Left panel: Representative tracing of  $I_{sc}$  ( $\mu A/cm^2$ ) in T84 cells pretreated with 0.1% DMSO (control; black line) or AG1478 (purple line) and then stimulated with CDCA. Right panel: Quantification of the effect of AG1478; \* denotes significance,  $p = 0.0005$ ,  $n = 8$ . Bar graphs represent the changes in  $I_{sc}$  responses mean  $\pm$  SEM.

## **E. CDCA Activation of EGFR**

### **1. CDCA and EGFR Phosphorylation**

EGFR is a receptor tyrosine kinase and is activated by autophosphorylation upon receptor dimerization. To assess if CDCA alters EGFR phosphorylation, T84 monolayers were stimulated with CDCA and immunoblotted for phosphorylated and total EGFR protein. The antibody used is specific to tyrosine 1068. **Figure 11A** shows that CDCA increased EGFR phosphorylation in a time dependent manner. Tyrphostin AG1478 inhibits EGFR by blocking its autophosphorylation activity to prevent downstream signaling. To assess if AG1478 would block CDCA-induced EGFR phosphorylation, similar to AG1478's inhibition of CDCA-induced  $I_{sc}$ , cells were pretreated with AG1478 before stimulation with CDCA, or carbachol, and immunoblotted for phosphorylated EGFR. Both CDCA and carbachol, used as a positive control, increased EGFR phosphorylation, and pretreatment with AG1478 reduced phosphorylation (**Figure 11B**).

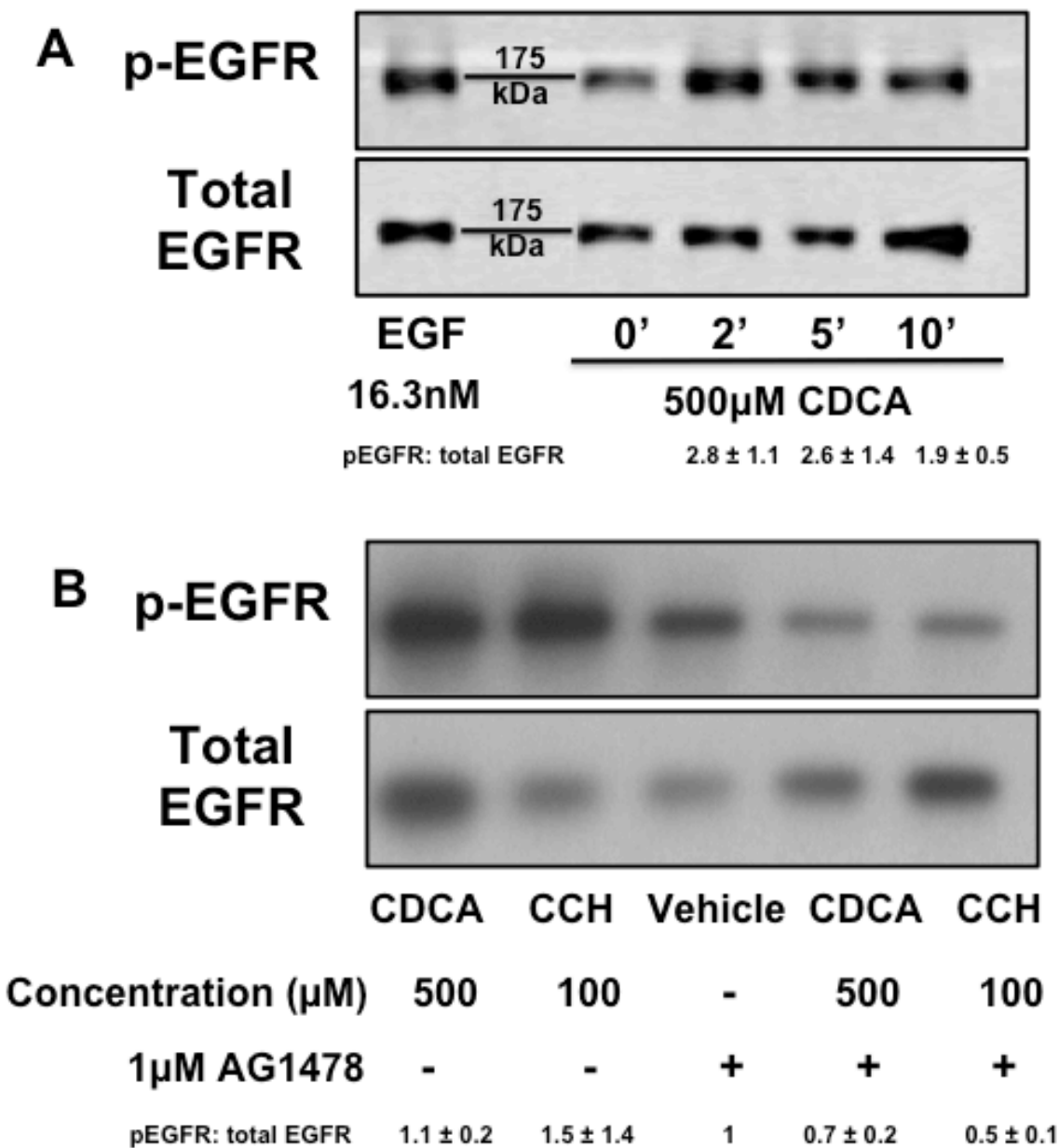


**Figure 11.** Effect of CDCA on EGFR phosphorylation.

**A.** T84 cells were grown to confluence and treated with 500µM CDCA for 0-10 minutes or EGF (16.3nM, 5 minutes) as a positive control. Protein was harvested and immunoblotted for phospho- and total EGFR protein (175 kDa); representative of n=4. The phosphor-EGFR (pEGFR) to total EGFR ratios normalized to t=0 are displayed below the representative blot for CDCA at 2-10 minutes.

**B.** EGFR phosphorylation by CDCA in the presence of AG1478. Cells were pretreated with AG1478 and then stimulated with CDCA or carbachol (CCH; 100µM) as a positive control. Vehicle is the effect of AG1478 alone without stimulation; representative of n=3. The pEGFR:total EGFR ratios normalized to vehicle are displayed below the representative blot.

## **2. Effect of EGFR Knockdown on CDCA-Induced Cl<sup>-</sup> Transport**

To validate the role that EGFR plays in CDCA action, we used siRNA methodology to knockdown EGFR expression. As shown in **Figure 12A**, EGFR siRNA, but not scrambled siRNA, decreased EGFR protein expression by 67% over 72 hours. Efficient transfection of siRNA requires sub-confluent monolayers transfected for  $\approx$  72 hours for the siRNA to have its optimal effect. Thus, the iodide efflux assay was used to study transport in siRNA treated cells, as this procedure does not require high resistance monolayers. We have previously published the efficacy of the iodide efflux assay, as another method to study CDCA-induced Cl<sup>-</sup> transport in T84 cells (15). We measured CDCA-stimulated iodide efflux in cells treated for 72 hours with EGFR siRNA or scrambled siRNA. As shown in **Figure 12B**, CDCA causes an increase in iodide efflux in cells transfected with scrambled siRNA. However, in cells transfected with EGFR specific siRNA, the CDCA response is decreased, confirming EGFR's role in CDCA-induced Cl<sup>-</sup> transport.

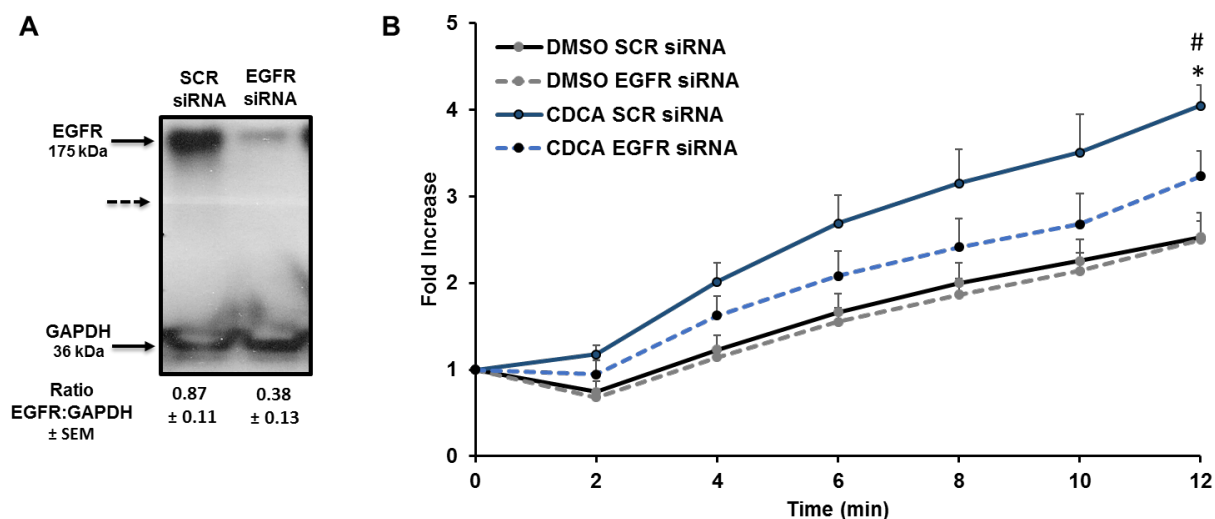


**Figure 12:** Effect of EGFR siRNA on EGFR expression and CDCA-induced Cl<sup>-</sup> transport. **A.** T84 cells were transfected with EGFR specific siRNA or scrambled (SCR) siRNA as a negative control for 72 hours and immunoblotted for EGFR protein (representative blot). The ratios of EGFR:GAPDH expression as determined by densitometry are provided below (n=7 for SCRsiRNA and n=6 for EGFRsiRNA). **B.** Cl<sup>-</sup> transport was measured by the iodide efflux assay. Transfected cells were loaded with iodide then placed in an iodide free buffer and stimulated with CDCA or 0.1% DMSO as a control. Tracing is the average cumulative iodide efflux (fold increase over t=0 minutes) from SCR (solid lines) or EGFR (dotted lines) siRNA transfected cells stimulated with CDCA (blue lines) or DMSO (black and gray lines); n=5. \*: p<0.05 to DMSO control; #: p<0.05 to treatment+EGFR siRNA.

### 3. Involvement of Matrix Metalloproteinases

Transactivation of EGFR can occur by activation of MMPs and cleavage of EGFR ligands such as EGF, transforming growth factor  $\alpha$ , and HB-EGF from their tethered pro-peptides. To assess if this mechanism is being activated by CDCA, we pretreated T84 cells with the general MMP inhibitor batimastat (20 $\mu$ M). Typically, the CDCA response is prolonged and can last > 30 minutes, often exhibiting a peak and a plateau phase. Interestingly, CDCA-stimulated  $I_{sc}$  in the presence of batimastat resulted in a transient CDCA response, in contrast to the sustained response in the untreated monolayers (**Figure 13**). Batimastat reduced the response (by 66%) to near baseline levels within 15 minutes. This suggests that MMPs are involved in the sustained phase of the CDCA response. Interestingly, a similar response occurs with pretreatment with the PKA inhibitor H89, suggesting that the sustained phase is dependent on cAMP-PKA signaling, as well as MMP activation (15). To investigate whether batimastat was affecting cAMP production, T84 cells treated with batimastat and  $[cAMP]_i$  was measured. Since CDCA's effect on cAMP is compartmentalized and difficult to capture (15), the effect of batimastat on forskolin-stimulated cAMP production was assessed instead. Batimastat did not significantly affect forskolin-stimulated cAMP production (cAMP, nmoles/well: 10 $\mu$ M forskolin:  $170 \pm 68$ ; 20 $\mu$ M batimastat:  $26 \pm 5$ ; batimastat+ forskolin:  $122 \pm 7$ ;  $n \geq 3$ ). These results implied that MMPs are not required for cAMP production. Furthermore, the laboratory had previously shown that EGF increased  $Cl^-$  transport in the rabbit colon (44), and thereby could potentially be a mechanism to mediate CDCA's transactivation of EGFR. However, bilateral addition of EGF (16.3nM) neither increased  $I_{sc}$  ( $-0.08 \pm 0.08$ ,  $n=4$ ), nor did it significantly alter CDCA's response (CDCA:  $19.3 \pm 1.7$ , EGF+CDCA  $15.7 \pm 1.2$ ;  $p=0.13$ ,  $n=4$ ).

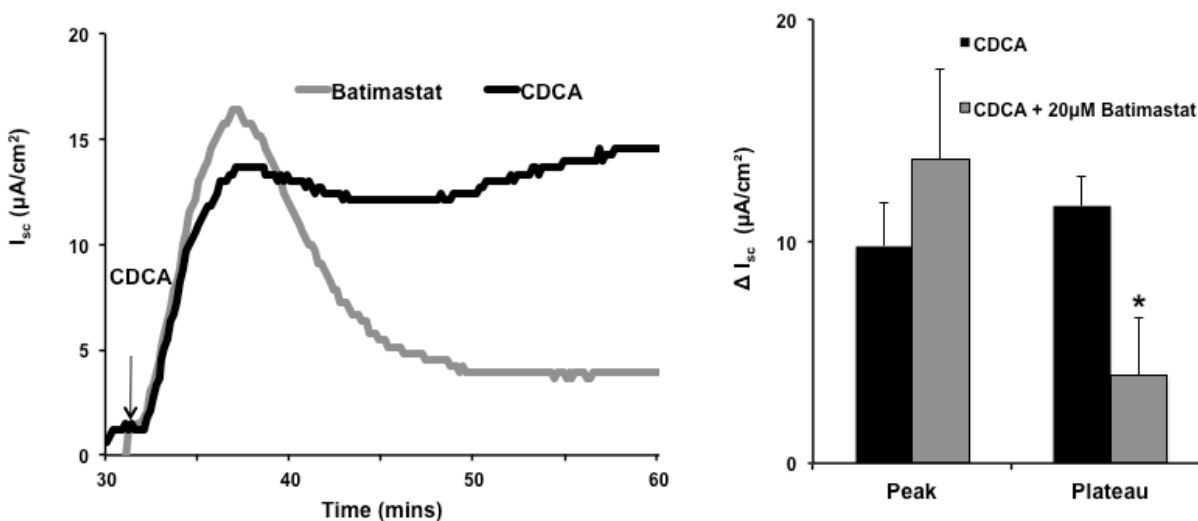


**Figure 13.** Effect of MMP inhibition on the CDCA response. Representative tracing of CDCA-induced  $I_{sc} \pm$  the MMP inhibitor batimastat ( $20\mu\text{M}$ ). The bar graph represents the average changes in the peak and plateau phases of CDCA-induced  $I_{sc} (\pm$  batimastat)  $\pm$  SEM. \* denotes  $p < 0.05$ ;  $n = 3$ .

## F. Membrane Perturbations

Since bile acids are cholesterol derivatives, they can incorporate into or pass through the plasma membrane, altering membrane dynamics and potentially activating membrane-bound proteins. Qiao et al. (196) showed that in primary hepatocytes, the dihydroxy bile acid, DCA, is capable of activating EGFR in a ligand-independent manner, causing a subsequent activation of MAPKs, resulting in apoptosis. The activation of EGFR was not blocked by neutralizing antibodies to EGFR ligands, suggesting that DCA's interaction with the plasma membrane was sufficient to activate EGFR (196). Additionally, Jean-Louis et al. (114) showed that DCA caused

an increase in cholesterol in the membrane and resulted in EGFR activation in colonic HCT116 cells. It was suggested that hydrophobic bile acids, such as DCA and CDCA, cause alterations in the membrane fluidity and can affect protein dynamics. Methyl- $\beta$ -cyclodextrin, a cholesterol sequestrant, has often been used to show involvement of lipid rafts in signaling cascades as they are largely composed of cholesterol. Jean-Louis et al. observed an inhibition of DCA's action on apoptosis in the presence of methyl- $\beta$ -cyclodextrin. However, when methyl- $\beta$ -cyclodextrin was washed out of their preparations there was less of an inhibition of DCA action, suggesting that methyl- $\beta$ -cyclodextrin was acting as a DCA and cholesterol sequestrant (114). Similarly, we observed that treatment of T84 cells with methyl- $\beta$ -cyclodextrin reduced the CDCA response, but rapidly washing the monolayers to remove methyl- $\beta$ -cyclodextrin restored CDCA's secretory response (Ao et al. unpublished observations). This does not rule out the possibility of CDCA acting as a membrane perturbant, but suggests the need to explore other mechanisms for studying CDCA action and membrane dynamics.

## **G. Discussion**

With the discovery of the bile acid specific receptors, FXR and TGR5, the majority of bile acid action has been attributed to activation of their related signaling cascades. FXR activation largely regulates bile acid synthesis in order to maintain the bile acid pool (52, 161). Previous studies have shown that activation of FXR by GW4064 for 24 hours lead to an inhibition of DCA, forskolin and carbachol responses. In that study FXR activation caused a reduction in CFTR expression, as well as an inhibition of  $\text{Na}^+/\text{K}^+$ -ATPase activity, without changing  $\text{Na}^+/\text{K}^+$ -ATPase expression (173). Interestingly, CDCA is the most potent natural agonist of FXR and results in **Figure 9** showed that acute activation of FXR with GW4064 had no effect on  $\text{Cl}^-$  secretion. We also found that prolonged treatment with GW4064 (24 hours) did not alter forskolin-induced  $I_{\text{sc}}$  responses or basal  $I_{\text{sc}}$  (14). This suggested that the immediate effect of CDCA on CFTR-

mediated  $I_{sc}$  does not involve FXR activation. Examining CDCA's effect in T84 cells transfected with FXR siRNA will help definitively determine the role, if any, of FXR in CDCA action both in the short term and long term.

CDCA acts in a rapid, sustained, and side-dependent manner to increase  $I_{sc}$  in T84 cells, suggesting involvement of a membrane bound receptor, rather than a nuclear receptor, in the CDCA-initiated signal transduction pathway necessary for  $Cl^-$  transport. TGR5, identified as the bile acid specific GPCR, is considered a major mediator between bile acids, metabolism, and insulin signaling (78, 146), however its role in  $Cl^-$  secretion varies with the cell type. The report that activation of TGR5 in cholangiocytes resulted in stimulation of CFTR, which was not present in TGR5 knockout mice (126), led us to hypothesize that it was mediating CDCA's activation of CFTR in T84 cells. However, we did not find an increase in  $I_{sc}$  in response to TGR5 agonists (**Figure 9** and (14)) comparable to CDCA. Our data suggests that TGR5 is not involved in CDCA's pro-secretory effect. Interestingly, in a study done by Ward et al., activation of TGR5, by INT-777 (a synthetic TGR5 agonist) or LCA (a potent natural TGR5 agonist), reduced the basal current and inhibited  $Ca^{2+}$ -dependent  $Cl^-$  secretion in rat distal colon (256). This further supports the idea that while TGR5 may regulate  $Cl^-$  transport in other epithelial preparations, its activation does not stimulate  $Cl^-$  secretion in T84 cells.

Several studies have shown that bile acids can activate other membrane bound and nuclear receptors, with broad specificities. For example, tauro-DCA activates M3Rs, to transactivate EGFR via MMP-7 and induce colonic epithelial cell proliferation (49, 50). Other studies have shown that bile acids can activate EGFR in cholangiocytes via cleavage of TGF $\alpha$  by MMPs (262). Additionally, Sommerfeld et al. (230) showed that bile acids activate EGFR in a Yes kinase-dependent manner in rat hepatic stellate cells. Results in **Figure 10A** showed that muscarinic receptors are not involved in CDCA action, however, CDCA signaling increases EGFR phosphorylation and requires its activation (**Figure 10B, 11-12**). Furthermore, inhibition

of MMPs (**Figure 13**) suggest that cleavage of an EGFR ligand may be required for CDCA-stimulated  $\text{Cl}^-$  transport, but the nature of the ligand is unknown. Alternatively, MMPs can also lead to cleavage of integrins (132), such that MMPs could mediate activation of  $\alpha 5\beta 1$ -integrin, but this receptor has only been shown to be activated by tauro-UDCA (98). Although our laboratory had demonstrated that EGF alone stimulates  $\text{Cl}^-$  secretion in the rabbit colon (44), EGF did not alter  $I_{\text{sc}}$  or the CDCA response in T84 cells. This suggests that either CDCA acts via another member of the EGFR ligand family, or that CDCA activates EGFR in a ligand-independent manner.

Although the results from the methyl- $\beta$ -cyclodextrin experiments are preliminary, undoubtedly hydrophobic bile acids are capable of altering membrane dynamics. LCA, the secondary bile acid formed from CDCA, has been shown to induce cholesterol accumulation in the canalicular membrane of hepatocytes (270, 271). DCA was shown to work in a similar manner and also altered caveolin-1 distribution in lipid raft domains (114). Interestingly, a recent report by Abu-Arish et al. showed that CFTR's localization in cholesterol enriched lipid rafts affects CFTR's stability and activity at the plasma membrane (1). When CFTR is localized to regions with low cholesterol, its turnover at the plasma membrane is faster, whereas in higher cholesterol containing regions (lipid rafts), CFTR was more stabilized in the membrane. It begs the question that changes in aggregation of cholesterol, or cholesterol "like" molecules (bile acids) in the plasma membrane could affect CFTR activity. Since CDCA is of similar hydrophobicity to DCA, albeit less so than LCA, it may be incorporating into the plasma membrane and enhance lipid raft-like structures that stabilize CFTR and sustain its activation. However, due to the sidedness of CDCA's action, being more potent at the basolateral membrane, and with CFTR located at the apical membrane, it seems more likely that CDCA could be acting through an unidentified, basolaterally localized, membrane-bound receptor (**Figure 14**). The two other potential receptors that could be mediating CDCA action are S1PR2

and  $\alpha 5\beta 1$ -integrin. However their involvement in the CDCA action in T84 cells is unlikely, since S1PR2 is not expressed in the colon, and even so is only activated by conjugated bile acids and  $\alpha 5\beta 1$ -integrin is only activated by UDCA (98).

To summarize (**Figure 14**), CDCA acted in a rapid manner, from the basolateral side, to increase activation of CFTR in T84 cells. CDCA action was independent of muscarinic receptors and likely does not involve the bile acid specific receptors TGR5 and FXR. To fully rule out their involvement in CDCA's pro-secretory response, future studies must investigate CDCA action in TGR5 and FXR knockdown cells. Furthermore, CDCA caused transactivation of EGFR, which may be mediated by MMPs, but does not require activation of EGFR by EGF. Studies using blocking antibodies to other EGFR ligands could identify the factor released by CDCA-induced activation of MMPs.

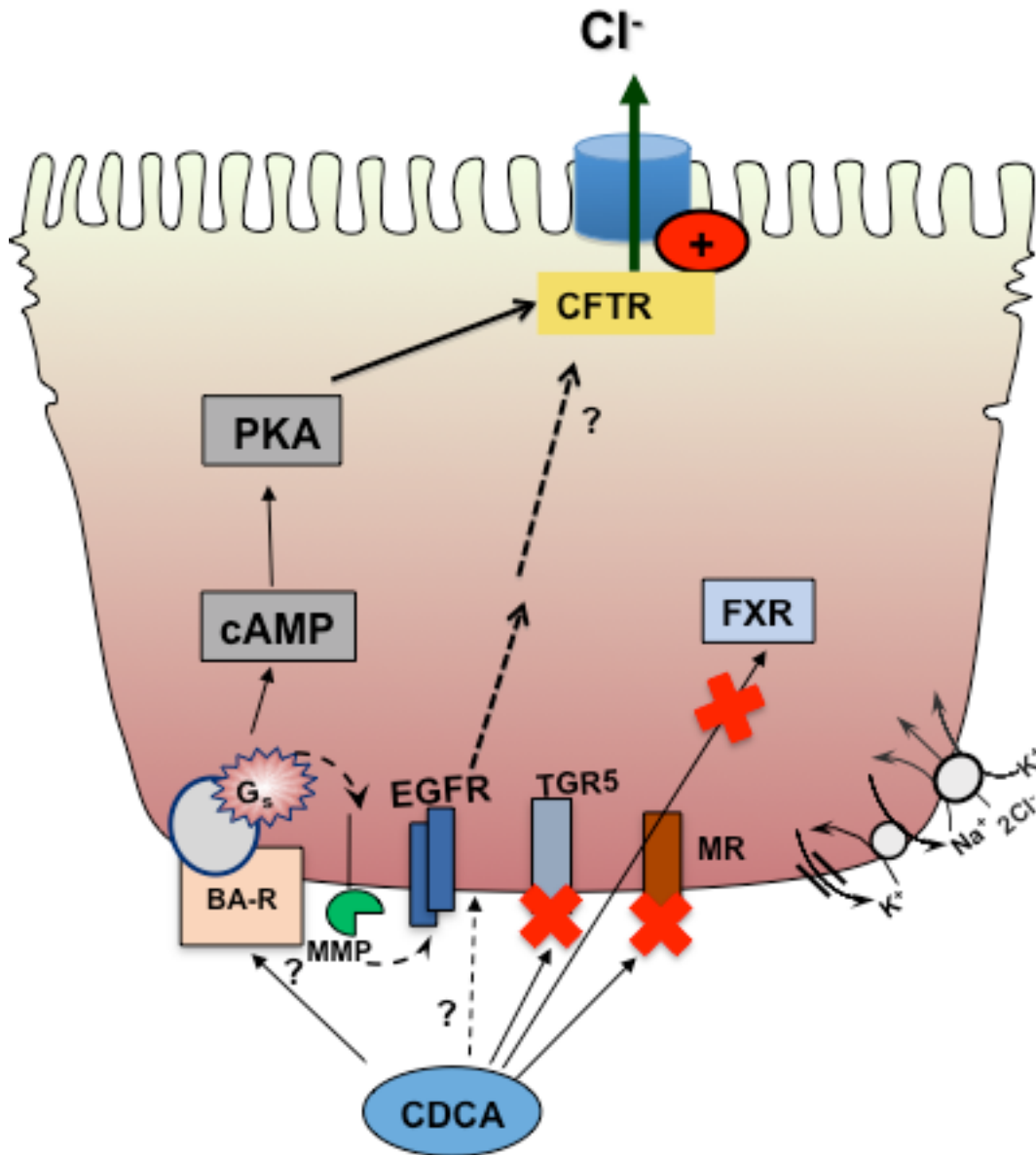


**Figure 14:** Receptor involvement in CDCA action. CDCA primarily acts from the basolateral membrane to increase CFTR-dependent Cl<sup>-</sup> secretion. CDCA does not require activation of the GPCRs, TGR5 and muscarinic receptors (MR), or activation of the nuclear receptor FXR. However, CDCA action requires MMPs, which mediate transactivation of EGFR that leads to Cl<sup>-</sup> secretion. This pathway may be initiated by an unidentified bile acid receptor (BA-R) or by membrane perturbations and activation of EGFR.

## Chapter IV. Results: CDCA Activation of 2<sup>nd</sup> Messenger Signaling Pathways

**Figure 23A was published in:**

Ao M, Sarathy J, **Domingue J**, Alrefai WA, and Rao MC. (2013). Chenodeoxycholic acid stimulates Cl<sup>-</sup> secretion via cAMP signaling and increases cystic fibrosis transmembrane conductance regulator phosphorylation in T84 cells. *Am J Physiol Cell Physiol.* 305:C447–C456.

## **A. Rationale and Aim**

Several 2<sup>nd</sup> messenger systems, including cAMP, PLC, IP<sub>3</sub>, and Ca<sup>2+</sup> have been implicated in the pro-secretory effects of dihydroxy bile acids in epithelial tissues across various mammalian species (95, 118, 124, 165, 250). The findings presented in **Chapter III**, regarding the involvement of EGFR, as well as our published study establishing the role for PKA in CDCA action (15), suggested that there could be a complex network of signaling cascades contributing to CDCA's activation of Cl<sup>-</sup> secretion in T84 cells. We have published that CDCA initiates a signaling cascade involving activation of adenylyl cyclase, PKA, a requirement of intact microtubules, and phosphorylation of CFTR to stimulate Cl<sup>-</sup> secretion in T84 cells (15). Interestingly, inhibition of PKA did not entirely block the CDCA response, suggesting the involvement of other signaling cascades in CDCA's effect on Cl<sup>-</sup> secretion. The studies implicating EGFR in the previous chapter suggest participation of its downstream effectors in CDCA action. In addition, other studies, including those from our laboratory in the rabbit colon (250), suggest Ca<sup>2+</sup> may be a candidate mediator for CDCA action. Thus, the focus of this chapter was to elucidate PKA-independent signaling cascades that contribute to CDCA's activation of Cl<sup>-</sup> secretion via CFTR, and are potentially involved with crosstalk of EGFR signaling (**Aim 2**).

## **B. The Role of Ca<sup>2+</sup> in CDCA Action**

Several studies, including our own in the rabbit (118, 250), and others in T84 cells (70, 72) demonstrated that tauro-DCA stimulates Ca<sup>2+</sup>-dependent colonic Cl<sup>-</sup> transport. In the adult rabbit colon, we demonstrated that tauro-DCA stimulates Cl<sup>-</sup> transport in an IP<sub>3</sub>-Ca<sup>2+</sup>-PKC $\delta$ -dependent manner (118, 250). Based on these data, we examined if PLC- Ca<sup>2+</sup> cascade is required for CDCA action. We began by measuring changes in [Ca<sup>2+</sup>]<sub>i</sub> induced by CDCA using

Fura2-AM. We found that addition of CDCA (navy blue bar) and ionomycin (positive control; blue bar) caused an increase in  $[Ca^{2+}]_i$  compared to basal values (black bar); determined as 340/380 ratio and calculated as nM values (**Figure 15A**). This increase in  $[Ca^{2+}]_i$  is partially dependent on extracellular  $Ca^{2+}$ , as its removal from the perfusion buffer (0mM  $[Ca^{2+}]_o$  by EGTA chelation) significantly decreased the CDCA-induced change in  $[Ca^{2+}]_i$  (light gray bar, **Figure 15B**). Additionally, chelation of free  $[Ca^{2+}]_i$  by BAPTA-AM (20 $\mu$ M) reduced the CDCA-induced change in  $[Ca^{2+}]_i$  (dark gray bar **Figure 15B**). Furthermore, pretreatment of T84 monolayers with BAPTA-AM significantly attenuated CDCA-induced  $I_{sc}$  responses (**Figure 15C**). These results suggest that rises in  $[Ca^{2+}]_i$  are necessary for CDCA's stimulation of  $Cl^-$  secretion.

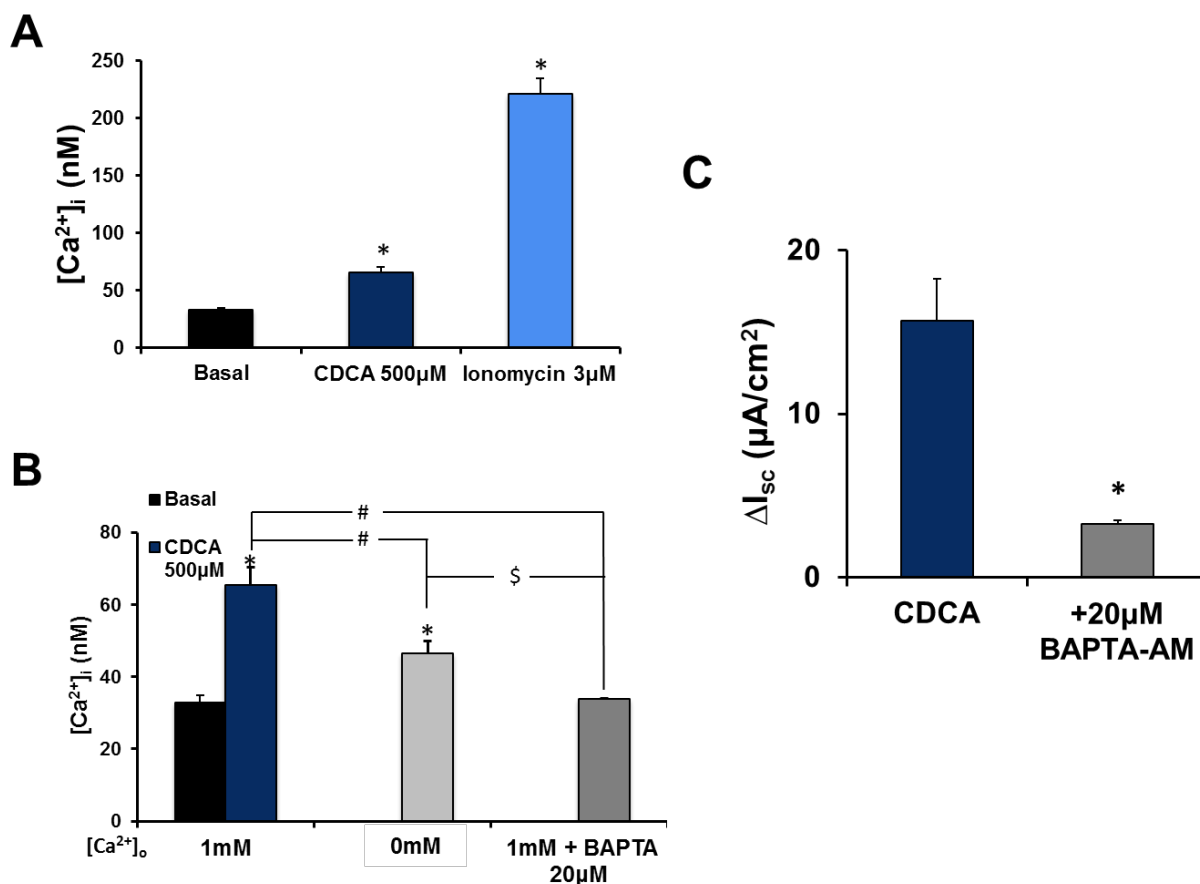


**Figure 15:** The role of Ca<sup>2+</sup> in CDCA action.

**A.** Summary of the change in [Ca<sup>2+</sup>]<sub>i</sub> in response to CDCA (500µM) and ionomycin (3µM); n=7, \*=p<0.05 compared to basal values.

**B.** CDCA's effect on [Ca<sup>2+</sup>]<sub>i</sub> in the presence of 1mM extracellular Ca<sup>2+</sup> ([Ca<sup>2+</sup>]<sub>o</sub>), 0mM [Ca<sup>2+</sup>]<sub>o</sub>, and 1mM [Ca<sup>2+</sup>]<sub>o</sub> + 30-minute pretreatment with the intracellular Ca<sup>2+</sup> chelator BAPTA-AM (20µM). For all conditions n≥5 and \* = p< 0.05 compared to CDCA in the presence of 1mM [Ca<sup>2+</sup>]<sub>o</sub>. # denotes p<0.05 compared to CDCA with 1mM [Ca<sup>2+</sup>]<sub>o</sub>, \$ denotes p=0.009 between CDCA in 0mM [Ca<sup>2+</sup>]<sub>o</sub> versus 1mM [Ca<sup>2+</sup>]<sub>o</sub> + BAPTA-AM.

**C.** The effect of 30-minute bilateral pretreatment of BAPTA-AM on CDCA-induced changes in I<sub>sc</sub>; n=4, \* denotes p=0.002 compared to CDCA alone.

### **C. PLC Activation in CDCA Action**

Within the cell,  $\text{Ca}^{2+}$  is sequestered in intracellular stores to regulate its effect on signaling cascades. Activation of PLC isoforms can be initiated by several different signals including GPCRs, tyrosine kinases,  $\text{Ca}^{2+}$ , and phospholipids (117). PLC converts phosphatidyl inositol bisphosphate to  $\text{IP}_3$  and diacyl glycerol.  $\text{IP}_3$  can bind to receptors on the endoplasmic reticulum and cause release of  $\text{Ca}^{2+}$  into the cytosol, while diacyl glycerol leads to activation of PKC. Based on these data, we examined whether PLC activity is required for the CDCA response. We pretreated T84 monolayers with the PLC inhibitor U73122, which blocks enzymatic activity of all PLC isoforms, and assessed the CDCA response. Inhibition of PLC by U73122 (10 $\mu\text{M}$ ) attenuated CDCA-induced  $I_{\text{sc}}$  (**Figure 16A**). Not surprisingly, the carbachol response was inhibited as expected since carbachol is known to activate  $\text{G}\alpha_q$  and PLC.

#### **1. The Role of $\text{IP}_3$ in CDCA Action**

To confirm the role of PLC, we measured production of  $\text{IP}_3$  and found that CDCA significantly increased  $\text{IP}_3$  compared to vehicle control at 10 minutes (**Figure 16B**). This effect on  $\text{IP}_3$  production was transient with an increase at 5 minutes ( $p=0.07$ ), and a maximal increase at 10 minutes ( $p=0.002$ ), and the response coming back to baseline by 20 minutes. Once  $\text{IP}_3$  is produced, binding to its receptor releases  $\text{Ca}^{2+}$  into the cytosol. To assess whether this  $\text{Ca}^{2+}$  release is necessary for CDCA action, we inhibited the  $\text{IP}_3\text{R}$  with 2-APB (50 $\mu\text{M}$ ) and found that the CDCA response was significantly attenuated, implying a role for  $\text{IP}_3\text{R}$  activation (**Figure 16C**). This data along with the increases in  $[\text{Ca}^{2+}]_i$ , and inhibition of the CDCA response with BAPTA-AM, confirms that  $\text{Ca}^{2+}$  signaling is essential for CDCA-stimulated  $\text{Cl}^-$  secretion in T84 cells.

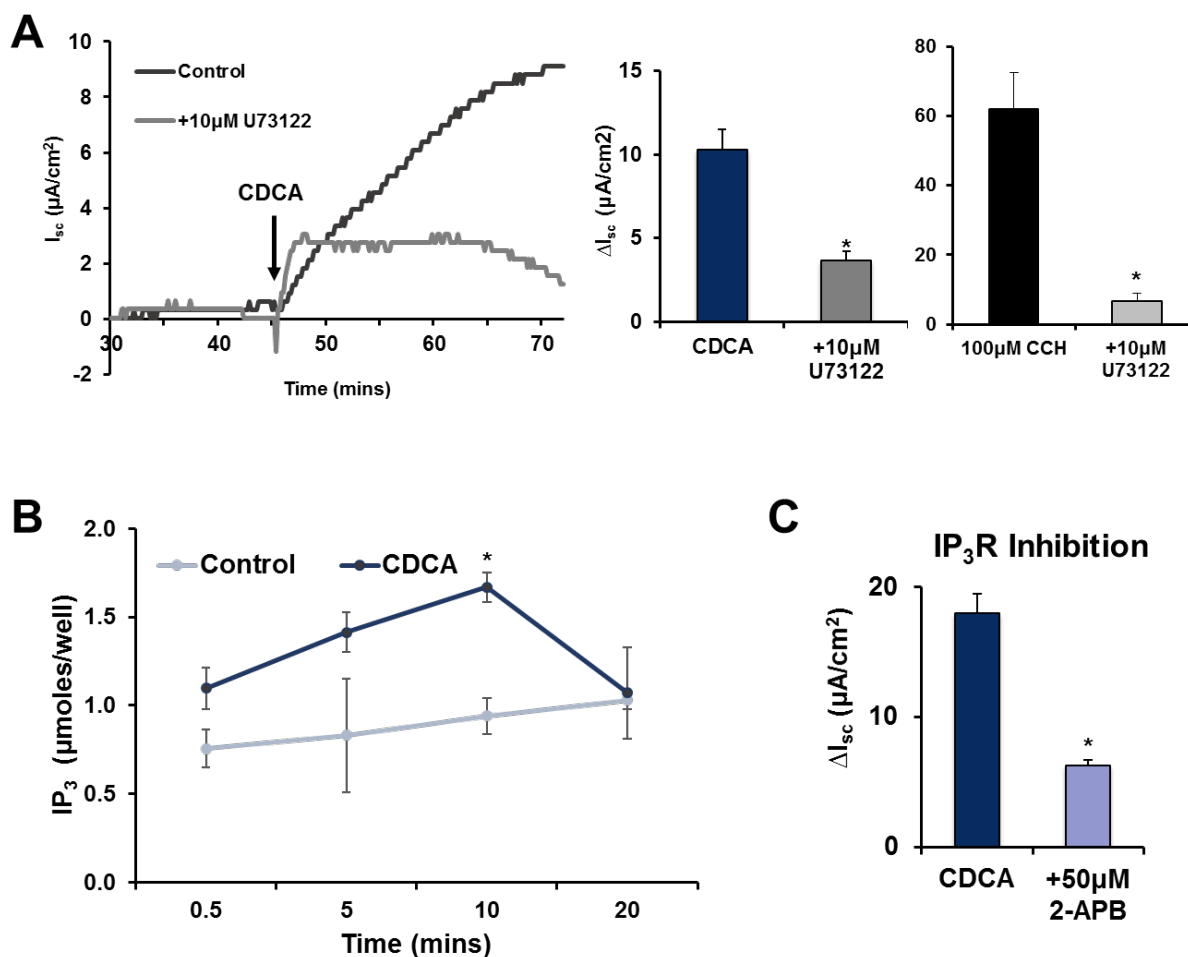


**Figure 16:** The role of PLC in CDCA action.

**A.** Representative tracing of  $I_{sc}$  when monolayers were pretreated bilaterally with the PLC inhibitor U73122 (10 $\mu\text{M}$ ) for 30 minutes and then stimulated with basolateral addition of 500 $\mu\text{M}$  CDCA. In the same set of experiments, carbachol (CCH; 100 $\mu\text{M}$ ) was added as a positive control for the inhibitor. The bar graphs represent the quantification of the secretagogue alone or + U73122;  $n=5$ , \* denotes  $p=0.0001$  compared to the secretagogue alone.

**B.** Measurement of  $\text{IP}_3$  production after cells were stimulated with CDCA for 0.5, 5, 10, and 20 minutes;  $n\geq 3$ ;  $p=0.07$  at 5 minutes and  $p=0.001$  at 10 minutes, different from control.

**C.** CDCA-induced change in  $I_{sc} \pm$  bilateral pretreatment (30 minutes) of 50 $\mu\text{M}$  2-APB ( $\text{IP}_3$ R inhibitor);  $n=3$ , \* denotes  $p=0.002$ , different from CDCA alone.

## 2. The Role of PKC in CDCA Action

In the adult rabbit colon, we demonstrated that tauro-DCA stimulated  $\text{Cl}^-$  transport was dependent on PKC $\delta$  (118). To determine if PKC was also involved in the CDCA response, T84 cells were treated with rottlerin, known to be a fairly specific inhibitor of PKC $\delta$ . While it inhibited tauro-DCA action in the rabbit colon (118), rottlerin (10 $\mu\text{M}$ ) had no effect on the CDCA-induced current in T84 cells ( $n=4$ ;  $p=0.99$ ; **Figure 17A**). There are three subfamilies of PKC, classical ( $\alpha$ ,  $\beta\text{I}$ ,  $\beta\text{II}$ , and  $\gamma$ ), novel ( $\delta$ ,  $\epsilon$ ,  $\eta$ , and  $\theta$ ), and the atypical ( $\text{M}\zeta$  and  $\text{I}/\lambda$ ) isoforms. Due to the variety of isoforms we next tested a general PKC inhibitor, chelerythrine. Pretreatment with chelerythrine at varying concentrations (2-10 $\mu\text{M}$ ) did not significantly affect the CDCA response (**Figure 17B**). The apparent decrease in the forskolin response in the presence of chelerythrine, seen in the tracing (**Figure 17B**), is not significant ( $p>0.05$ ,  $n>4$ ). These findings imply that CDCA acts via an  $\text{IP}_3$ - $\text{Ca}^{2+}$ -dependent manner, but independently of PKC activation, to stimulate  $\text{Cl}^-$  secretion in T84 cells.

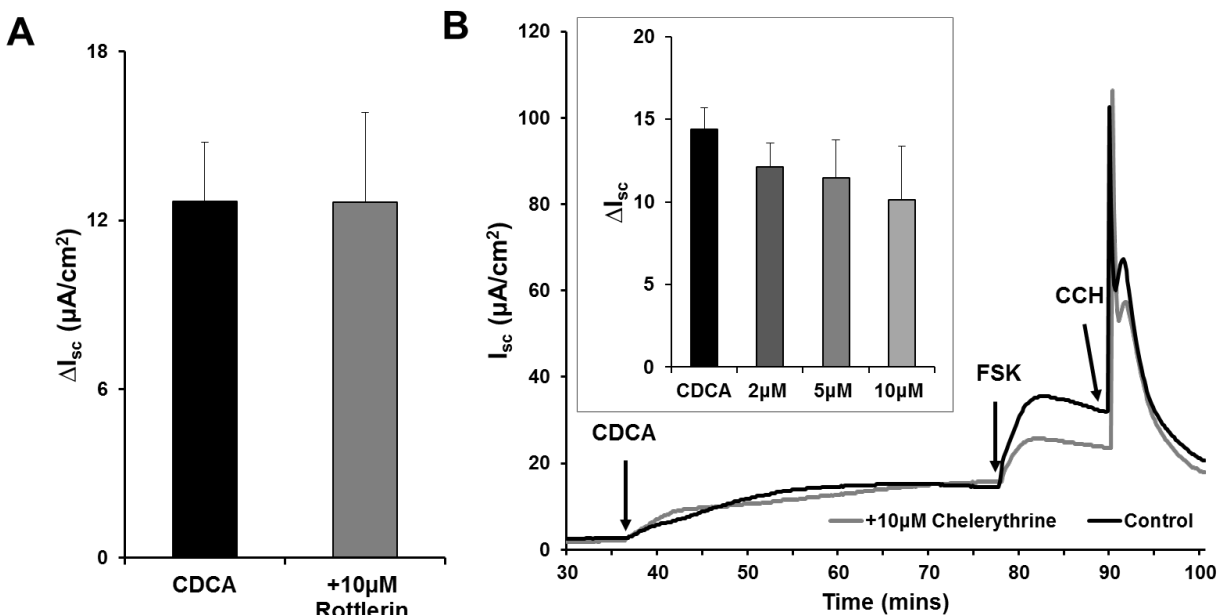


**Figure 17:** Effect of PKC inhibition on CDCA-induced  $I_{sc}$ .

**A.** T84 monolayers were pretreated for 30 minutes with the PKC-  $\delta$  specific inhibitor, rottlerin (10 $\mu M$ ), and then stimulated with 500 $\mu M$  CDCA;  $n \geq 4$ ;  $p = 0.99$ .

**B.** Representative tracing and quantification of  $I_{sc}$  with and without pretreatment with the general PKC inhibitor, chelerythrine (2-10 $\mu M$ ). Cells were stimulated with sequential addition of 500 $\mu M$  CDCA, 10 $\mu M$  forskolin (FSK), and 100 $\mu M$  carbachol (CCH);  $n \geq 3$  for all groups,  $p > 0.05$ .

## **D. Role of EGFR-Related Kinases in CDCA Action**

Results in **Chapter III** suggested a role for EGFR in CDCA action. EGFR signals via a multitude of pathways including Src kinase, the MAPKs ERK1/2 and p38, as well as PI3K and AKT (183). Thus, we wanted to elucidate the role of these effectors downstream of EGFR in the CDCA-stimulated secretory response.

### **1. Human Phosphokinase Array**

To get a broad overview of the activation of several kinases simultaneously, a human phosphokinase array was performed. The array consists of capture antibodies to specific phosphorylation sites of 43 different kinases spotted onto nitrocellulose membranes; some antibodies were specific to kinase isoforms as well as different sites on one kinase, e.g. AKT. The membranes were incubated with cell lysates followed by incubation with a cocktail of biotinylated detection antibodies. Streptavidin-HRP and chemiluminescent reagents are used to visualize the phosphorylated signals. The array included Src kinase, ERK 1/2, p38 kinase, and two specific phosphorylation sites (serine 473 and threonine 308) of AKT.  $\beta$ -catenin was used to normalize the signals as its phosphorylation remained unchanged between DMSO (control) and CDCA treatments. As shown in **Figure 18**, CDCA (500 $\mu$ M, 5 minutes) elicited a strong increase in EGFR and p38 phosphorylation, and a small increase in ERK 1/2 phosphorylation, but did not alter those of Src or AKT. The phosphokinase array validated the results on EGFR shown in **Figure 11**. To explore the array results further, we assessed the effects of specific kinase inhibitors on CDCA-induced Cl<sup>-</sup> current in Ussing chambers and performed immunoblot studies using phospho-specific and total kinase-specific antibodies.

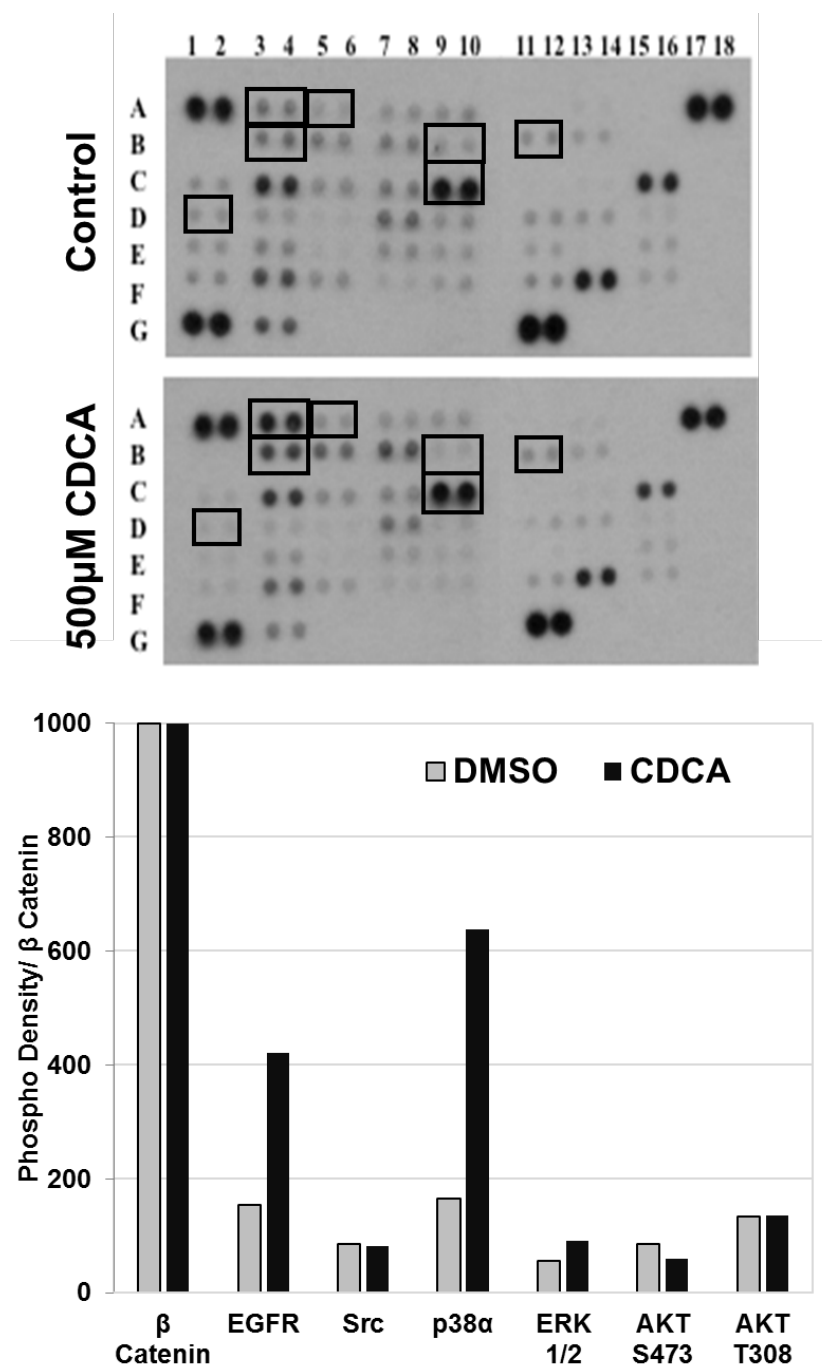


**Figure 18:** Kinase phosphorylation by CDCA. T84 cells were stimulated with 0.1% DMSO (control) or 500µM CDCA for 5 minutes and then harvested for protein lysates. Phosphorylation states of 43 kinases were compared in control (top image) and 500µM CDCA (5 min; bottom image) treated cell lysates. Boxes outline the phosphorylation signals of p38 (A-3,4), EGFR (B-3,4), ERK 1/2 (A-5,6), β-catenin (C-9,10), Src (D-1,2), AKT S473 (B-9,10), and AKT T308 (B-11,12). Results are quantified in the bar graph and phosphor density signals have been normalized to β-catenin.

## 2. Src Kinase and CDCA Activation of $I_{sc}$

Src kinase can act upstream and downstream of EGFR (33, 113, 131, 265). The phosphokinase array suggests that CDCA does not act via Src. However, we had shown that in the rabbit proximal colon both EGF- and neurotensin-induced  $Cl^-$  transport was inhibited by the Src inhibitor PP2 (192). To determine if Src had a role in CDCA action, T84 monolayers were pretreated with PP2 (10 $\mu$ M) and then stimulated with CDCA. In agreement with the array results, inhibition of Src did not affect CDCA's increase on  $I_{sc}$ , thus ruling out its involvement in CDCA action (**Figure 19**).

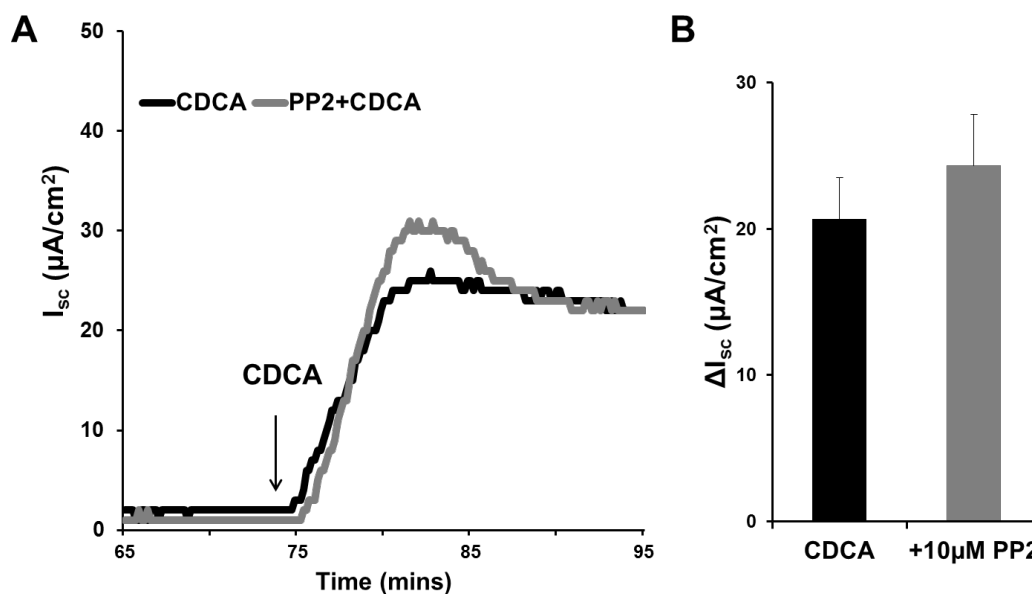


**Figure 19:** Effect of Src inhibition on CDCA-induced  $I_{sc}$ .  
**A.** Representative tracing of T84 monolayers pretreated bilaterally with the Src inhibitor PP2 (10 $\mu$ M) 30 minutes before stimulation with basolateral addition of CDCA (500 $\mu$ M).  
**B.** Quantification of CDCA-induced  $I_{sc}$   $\pm$  PP2; n=3; p=0.46.

### **3. p38 and ERK 1/2 Kinases in CDCA Signaling**

The phosphokinase array implied that p38 and ERK 1/2 MAPK cascades may be involved. In MAPK signaling, the proximal steps to ERK and p38 activation are the MAPK kinases, MKK and MEK, which phosphorylate p38 and ERK 1/2, respectively. As predicted by the array, CDCA caused a robust, time-dependent increase in p38 phosphorylation (**Figure 20A**; p38/total p38 normalized to t=0: 2 minutes:  $9.3 \pm 5.8$ ; 5 minutes:  $10.3 \pm 6$ ; 10 minutes:  $8.2 \pm 1.9$ ; EGF  $3.3 \pm 1.9$ ). Surprisingly, the p38 inhibitor, SB203580, had no effect on CDCA stimulation of  $I_{sc}$  (**Figure 20B**).

The CDCA increase in ERK 1/2 phosphorylation indicated by the phosphokinase array was confirmed in a time course using ERK-specific phospho and total antibodies. CDCA caused a transient increase in ERK 1/2 activation (**Figure 21A**). Both the CDCA-stimulated and epidermal growth factor-stimulated (positive control) phosphorylation of ERK 1/2 was inhibited by the MEK inhibitor PD98059 (**Figure 21B**), confirming activity of the inhibitor. This drastic effect of inhibition by PD98059 on ERK 1/2 phosphorylation is similar to our studies with LCA (14). Most striking was the fact that despite the efficacy of the MEK inhibitor on CDCA-induced ERK 1/2 phosphorylation, there was no effect of PD98059 on CDCA-stimulated  $Cl^-$  transport (**Figure 21C**). Studies by others (81, 225, 255) suggest that the actions of ERK 1/2 and p38 overlap, such that if one is rendered inactive, the other enzyme may compensate for its activity. To investigate if there is such an interaction on  $I_{sc}$ , T84 cells were pretreated with inhibitors of both pathways simultaneously. However, the combination also had no effect on CDCA action (**Figure 21D**). So although CDCA activated these kinases, they are not necessary for CDCA's action on  $Cl^-$  secretion.

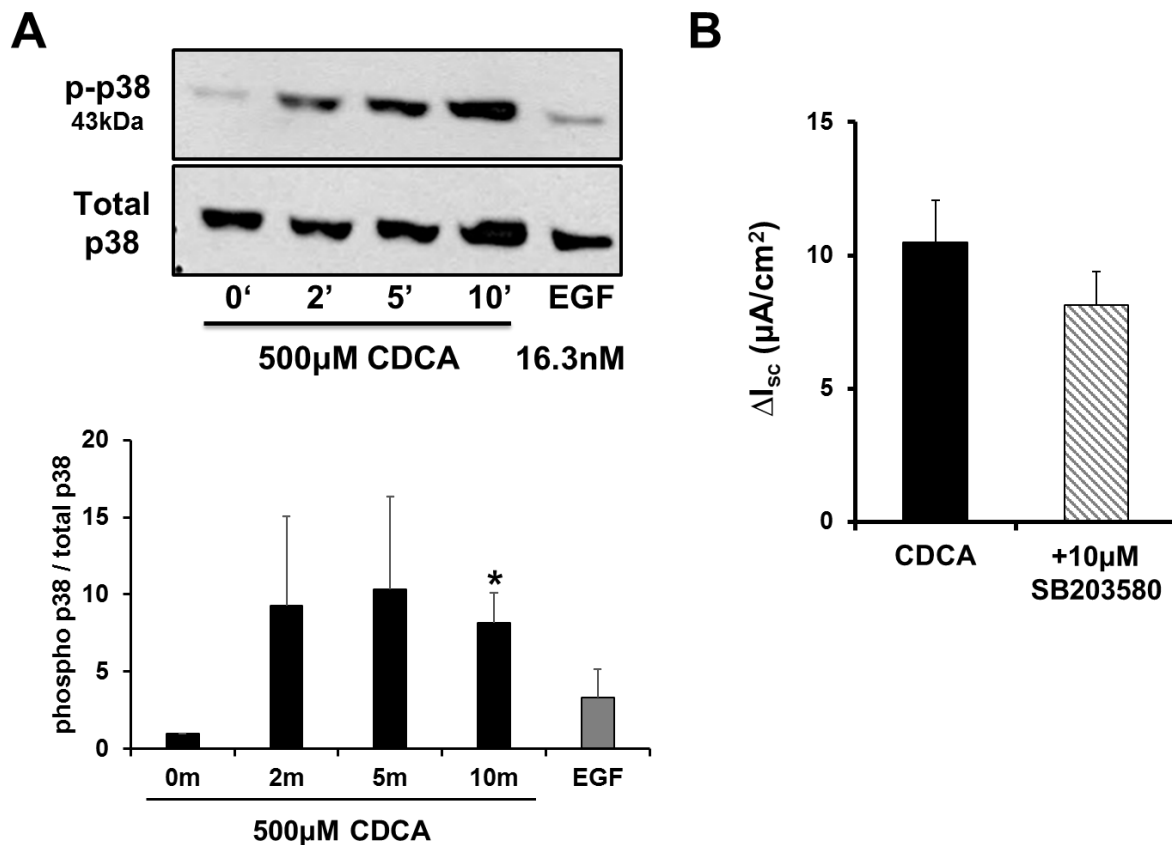


**Figure 20:** The role of p38 in CDCA action.

**A.** T84 cells were treated with 500µM CDCA (0-10 minutes) or EGF (16.3nM; positive control), then immunoblotted for phosphorylated (p-p38) and total p38 protein (43 kDa); Upper panel: Representative blot; Lower Panel: Densitometry of p-p38/total p38 (n=4); \*p<0.05 compared to t=0.

**B.** Quantification of the changes in  $I_{sc}$  measured in monolayers pretreated bilaterally with 0.1% DMSO (control) or 10µM SB203580 (p38 inhibitor) for 30 minutes and then stimulated with CDCA; n=7, p=0.26.

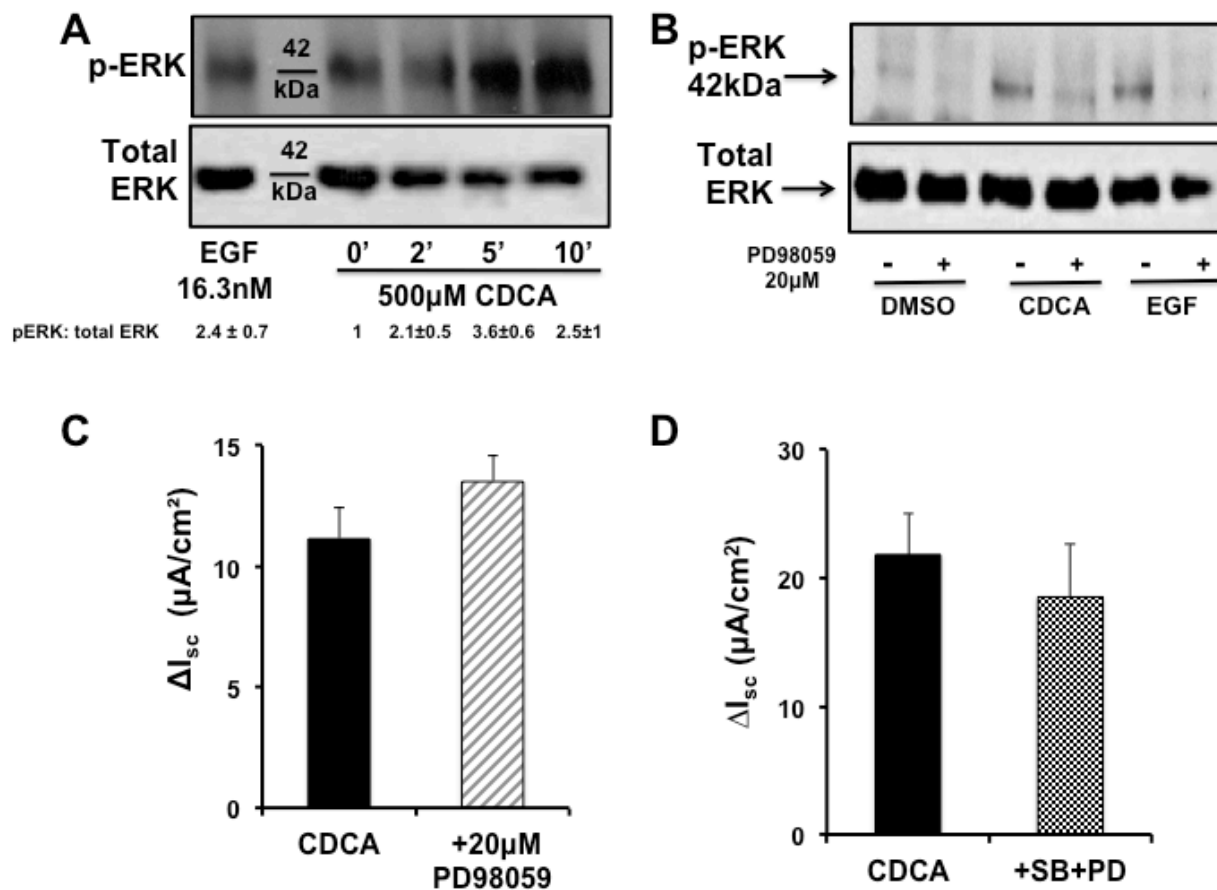


**Figure 21:** The role of ERK 1/2 signaling in CDCA action.

**A.** Representative blot of phospho (p)- and total ERK 1/2 protein (42 kDa) expression after treatment with 500μM CDCA (0-10 minutes) or 16.3nM epidermal growth factor (EGF; 5 minutes) as a positive control. Quantification of pERK/total ERK is provided below (n=3).

**B.** Representative blot of phospho and total ERK 1/2 protein expression after pretreatment with the MEK inhibitor PD98059 (20μM) for 30 minutes, then stimulated with EGF or CDCA for 5 minutes.

**C.** Change in  $I_{sc}$  by CDCA with or without 30 minute pretreatment of PD98059 (n=3, p>0.05).

**D.** Change in  $I_{sc}$  by CDCA with or without 30 minute pretreatment of a combination of SB203580 (SB; 10μM) and PD98059 (PD; 20μM) (n=5, p>0.05).

#### 4. PI3K and CDCA Action

Since Src, ERK 1/2, and p38 kinases did not appear to be involved in CDCA-induced Cl<sup>-</sup> secretion, the involvement of PI3K, another downstream effector of EGFR activation, was investigated. Using wortmannin and LY294002 as PI3K inhibitors, Bertelsen et al. had demonstrated that cAMP agonists (VIP and Bt<sub>2</sub>cAMP) stimulated PI3K via transactivation of EGFR in T84 cells, and from this also implied involvement of AKT (25). To see if CDCA may be acting in a similar manner to these agonists, T84 cells were pretreated first with wortmannin (25). Interestingly, we found that pretreatment with 500nM wortmannin significantly attenuated the CDCA response by 55% (**Figure 22A**). The literature suggests that this dose is over the specificity to PI3K (76, 80), with wortmannin having an IC<sub>50</sub> of 200-500nM for inhibition of forskolin-induced Cl<sup>-</sup> secretion, a 100-fold higher than the IC<sub>50</sub> of PI3K (2-4nM) demonstrated both in cell free lysates and in intact cell assays. These studies also reported that 100nM wortmannin, although higher than the IC<sub>50</sub>, was able to specifically target PI3K and reverse EGF's inhibition of thapsigargin-stimulated I<sub>sc</sub>. However, pretreatment with this dose (100nM) did not have a significant inhibition of the CDCA response (500μM CDCA: 7.9± 1.2; +100nM wortmannin: 6.5±1.1; n=6; p=0.4). Additionally, treatment with LY294002 (20-100μM) had no effect on the CDCA response (**Figure 22B**). Furthermore, inhibition of AKT, the downstream effector of PI3K, with MK2206 (1μM) had no effect on the CDCA response (**Figure 22C**). This was not surprising, as AKT phosphorylation was not increased by CDCA in the phosphokinase array (**Figure 18**). These data suggest that PI3K-AKT signaling is not involved in CDCA's activation of CFTR and that wortmannin could be having an effect on some other kinase or protein involved in CDCA action.

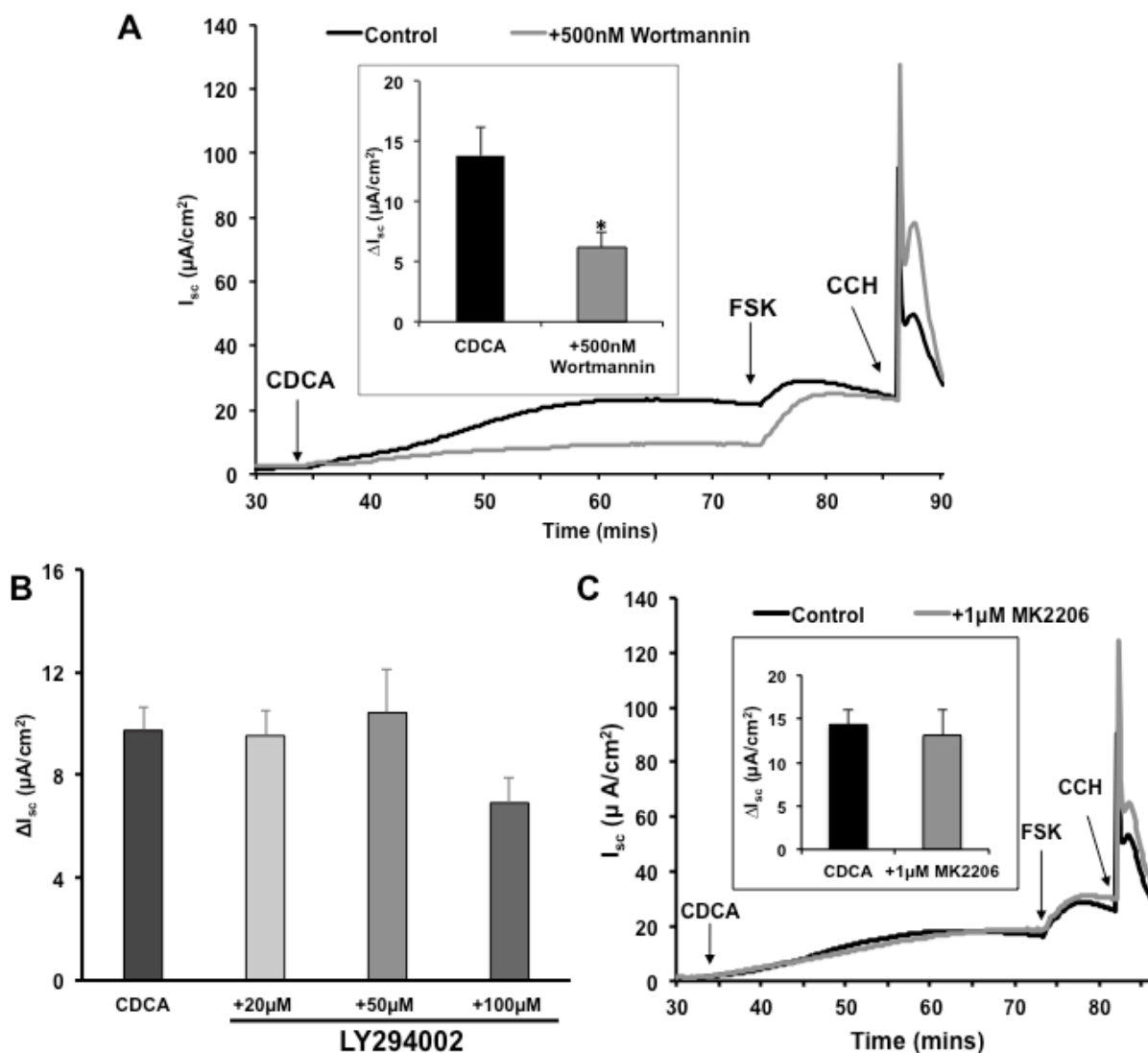


**Figure 22:** Effect of inhibition of PI3K and AKT on CDCA action.

**A.** Representative tracing and quantification (inset) of changes in  $I_{sc}$  when T84 monolayers were pretreated with wortmannin (500nM) or DMSO (0.1%) as control. The monolayers were then stimulated with basolateral addition of 500 $\mu M$  CDCA. Forskolin (FSK; 10 $\mu M$ ) and carbachol (CCH; 100 $\mu M$ ) were added sequentially to assess tissue viability;  $n=8$ ; \* denotes  $p=0.009$  compared to CDCA alone.

**B.** Quantification of CDCA-induced changes in  $I_{sc}$  ( $\mu A/cm^2 \pm SEM$ ) when T84 monolayers were pretreated with the PI3K inhibitor LY294002 (20-100 $\mu M$ ) for 30 minutes; DMSO was used as vehicle control;  $n=10$  for 20 $\mu M$ ;  $n=4$  for 50 $\mu M$ ;  $n=6$  for 100 $\mu M$ .

**C.** Representative tracing and quantification (inset) of changes in  $I_{sc}$  ( $\mu A/cm^2 \pm SEM$ ) when T84 monolayers were pretreated with the AKT inhibitor MK2206 (1 $\mu M$ ) for 30 minutes; DMSO was used as vehicle control. The monolayers were then stimulated with basolateral addition of CDCA. FSK and CCH were added sequentially to assess tissue viability;  $n=4$ ,  $p=0.58$ .

### E. The Role of cAMP Signaling in CDCA Action

We had previously shown that inhibition of PKA by H89 significantly attenuated CDCA action (15). However, this attenuation was not complete (**Figure 23**) [adapted from (15)]. As shown in this tracing, often the response to CDCA can be divided into an initial “peak” phase and a prolonged plateau phase. Inhibition of PKA with H89 had its strongest effect on the plateau phase of the CDCA response (**Figure 23B**), and when calculated as area under the curve (AUC) for the entire response, H89 inhibits the CDCA response by 69% (%AUC: CDCA: 100; +30 $\mu$ M H89: 38.3  $\pm$  8.8; n $\geq$ 8, p<0.0001) suggesting involvement of another signaling cascade. As there was sufficient evidence for the involvement of Ca<sup>2+</sup> in CDCA action, identifying a point of crosstalk between these second messengers was the next step.

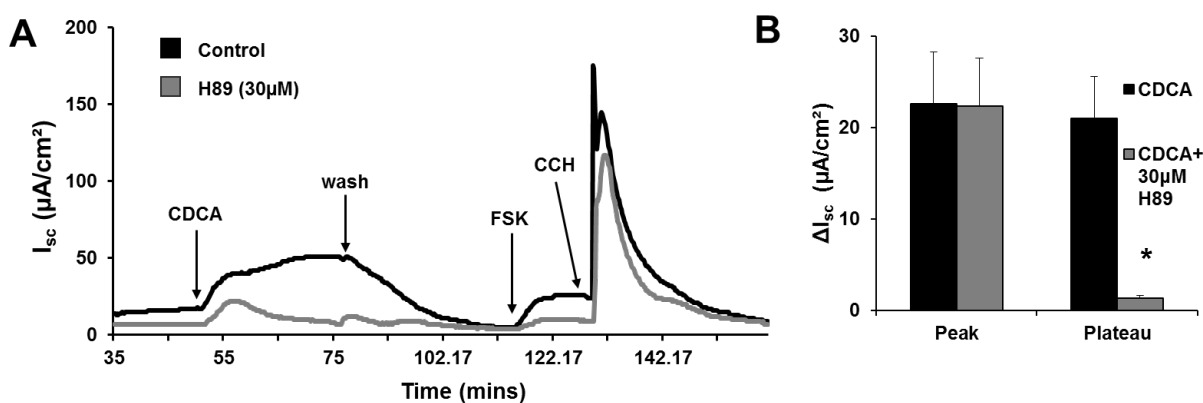


**Figure 23.** Effect of inhibition of PKA on  $I_{sc}$ .

**A.** Representative tracing [adapted from (15)] of T84 monolayers pretreated with the PKA inhibitor H89 (30 $\mu$ M) followed by addition of 500 $\mu$ M CDCA. Monolayers were then washed and stimulated with forskolin (FSK; 10 $\mu$ M) and carbachol (CCH; 100 $\mu$ M).

**B.** Quantification of the peak and plateau  $I_{sc}$  responses to CDCA  $\pm$  H89 pretreatment; n=5 for control monolayers and n=3 for H89 treated; \* denotes p<0.05 compared to CDCA alone for plateau.

The crosstalk between cAMP and  $\text{Ca}^{2+}$  has been studied in a variety of cell types, including T84 cells. Cartwright et al. showed that cAMP and  $\text{Ca}^{2+}$  agonists act on different basolateral  $\text{K}^+$  channels to increase the driving force for  $\text{Cl}^-$  transport, but only the cAMP signaling cascade activated robust apical  $\text{Cl}^-$  currents (45). Interestingly, when the  $\text{Ca}^{2+}$  and cAMP agonists were administered simultaneously, they had a synergistic effect on  $\text{Cl}^-$  secretion. Recently, EPAC has been described as a point of crosstalk between the cAMP and  $\text{Ca}^{2+}$  pathways. EPAC, a guanine nucleotide exchange factor, activates the small G-proteins, Rap 1 and 2, leading to downstream signaling cascades that modulate ion transport (108, 222). To investigate the potential role of EPAC in mediating the crosstalk between cAMP and  $\text{Ca}^{2+}$  in CDCA signaling, we inhibited EPAC with ESI-09 (10 $\mu\text{M}$ ). ESI-09 significantly attenuated CDCA-stimulated  $I_{\text{sc}}$  ( $p=0.0004$ ; **Figure 24A and C**). Interestingly, ESI-09 significantly increased the basal  $I_{\text{sc}}$  ( $\Delta\mu\text{A}/\text{cm}^2 \pm\text{SEM}$ : control:  $2.2\pm 0.8$ ; ESI-09:  $6.6\pm 0.4$ ;  $n=6$ ,  $p=0.0005$ ). Similar to the findings of Hoque et al. (108), ESI-09 also inhibited the forskolin response, but had no effect on the carbachol response (**Figure 24B and D**).

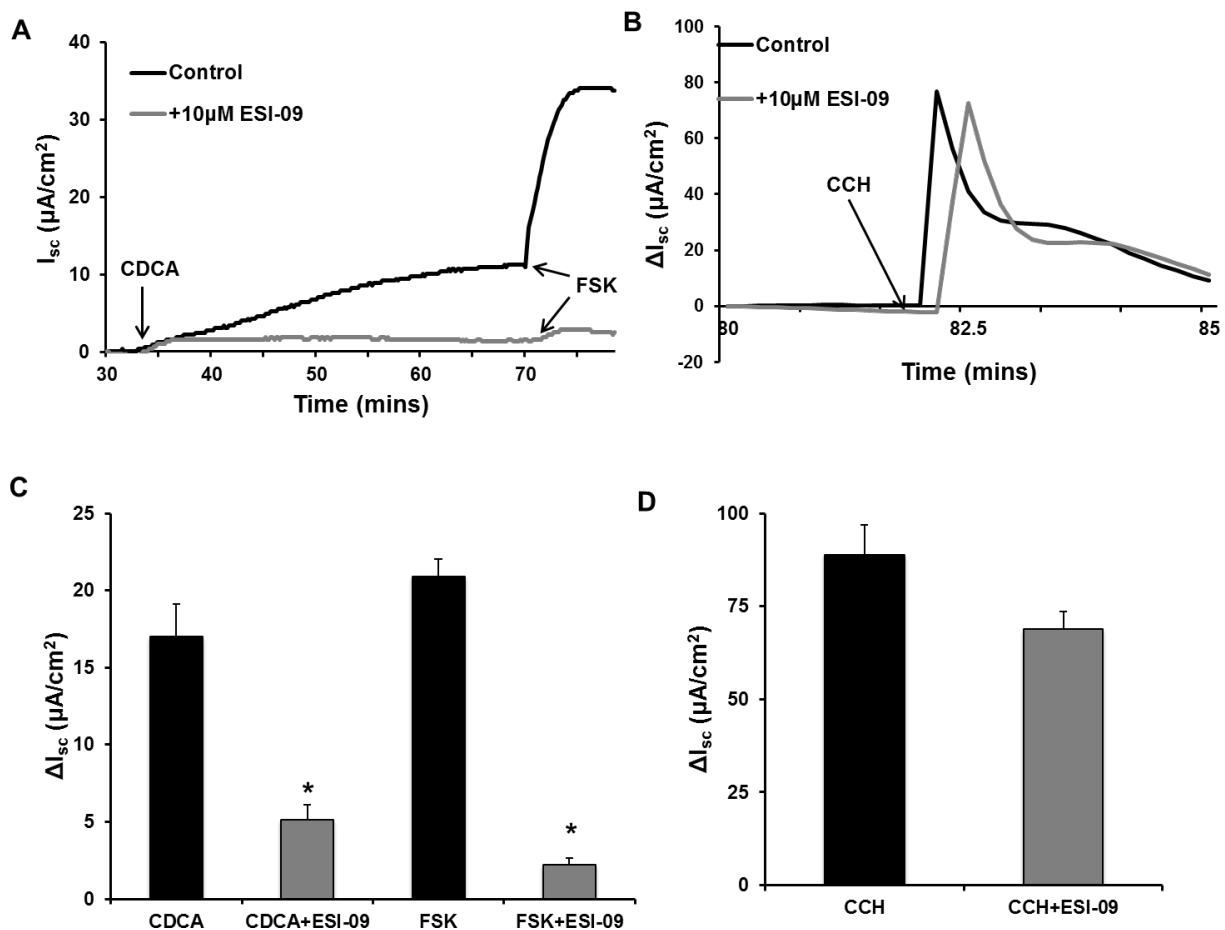


**Figure 24:** Effect of EPAC inhibition on the CDCA Response.

**A.** Representative tracing of  $I_{sc}$   $\pm$  bilateral pretreatment (30 minutes) with the EPAC inhibitor ESI-09 (10 $\mu M$ , gray line) in T84 monolayers grown to confluence and stimulated with basolateral addition of 500 $\mu M$  CDCA and 10 $\mu M$  forskolin (FSK).

**B.** Representative tracings of carbachol (CCH, 100 $\mu M$ )-induced  $\Delta I_{sc}$   $\pm$  ESI-09 pretreatment from the same experiment as **A**. Because the CCH response is very high, the tracings have been split from **A** and have been adjusted to begin at 0 $\mu A/cm^2$ .

**C.** Quantification of  $I_{sc}$  response to CDCA and FSK  $\pm$  ESI-09;  $n=6$ , \* denotes  $p \leq 0.001$  for inhibitor treatment compared to CDCA or FSK alone.

**D.** CCH-induced  $\Delta I_{sc}$   $\pm$  ESI-09;  $n=6$ ,  $p > 0.05$ .

To assess the ionic basis of EPAC involvement, ESI-09's effects on CDCA action on apical membrane  $\text{Cl}^-$  currents was examined. First, a  $\text{Cl}^-$  gradient was established by mounting monolayers in an apical buffer containing 115.4mM NaCl and an isotonic basolateral buffer with the NaCl replaced by equimolar sodium gluconate as described in methods. Monolayers were then basolaterally permabilized with nystatin (200 $\mu\text{g}/\text{mL}$ ) and treated with ESI-09 (gray line) or DMSO (black line, **Figure 25A**). Our recording electrode is in the basolateral medium with the reference electrode in the apical medium, and so changes in  $\text{Cl}^-$  entry across the apical membrane are recorded as a negative current. However, for ease of reading the  $I_{\text{sc}}$  tracings are inverted as shown in **Figure 25**. We have previously established that the apical  $\text{Cl}^-$  current activated by CDCA is largely due to CFTR activation, by demonstrating that CFTRinh172 attenuates the current (15). **Figure 25A** (black line) shows a representative tracing where basolateral permeabilization caused a slow and steady increase in the current due to the  $\text{Cl}^-$  gradient and addition of CDCA caused a robust increase in  $I_{\text{sc}}$ . Addition of forskolin further increased the current in a transient manner, and the current was inhibited by CFTRinh172. **Figure 25A** (gray line) demonstrated that the CDCA response was also significantly attenuated by ESI-09 ( $p < 0.0001$ ; **Figure 25C**). These data, taken with the results in intact monolayers, established EPAC's role in CDCA's activation of  $\text{Cl}^-$  transport via CFTR. Additionally, the representative tracing (**Figure 25B**) shows that inhibition of EPAC by ESI-09 stimulated a transient  $\text{Cl}^-$  current, consistent with the ESI-09-stimulated increase in basal  $I_{\text{sc}}$  stated above. This ESI-09-stimulated current was also inhibited by CFTRinh172 ( $p = 0.02$ ; **Figure 25B** and **C**). The current remaining after addition of CFTRinh172 to monolayers treated with ESI-09 alone, or after addition of ESI-09 to CDCA treated monolayers were not significantly different from addition of vehicle (0.1% DMSO; **Figure 25C**).

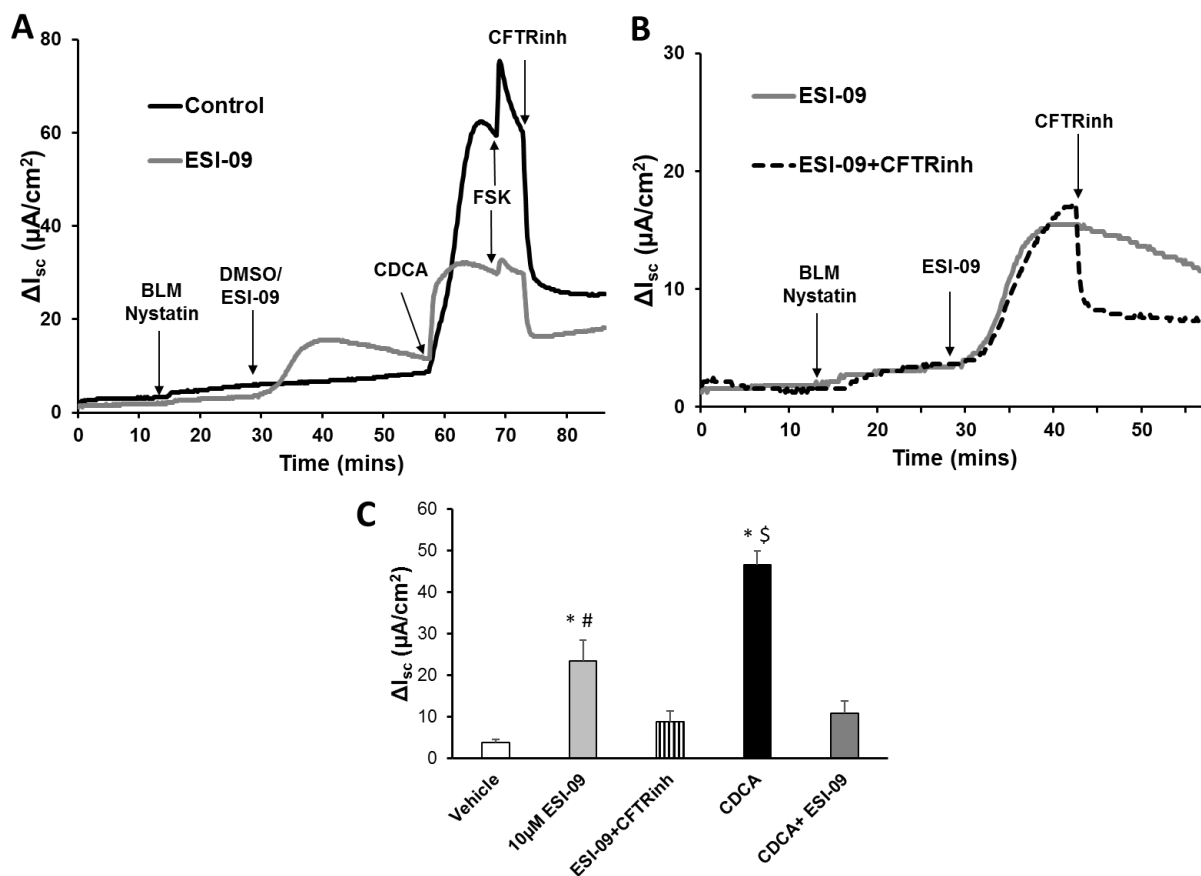


**Figure 25:** EPAC involvement in apical Cl<sup>-</sup> currents.

**A.** Apical Cl<sup>-</sup> currents were established as described in Methods. This is a representative tracing of I<sub>sc</sub> in basolateral permeabilized monolayers treated with bilateral addition of 0.1% DMSO (black line) or 10μM ESI-09 (gray line) and stimulated with 500μM CDCA, followed by forskolin (FSK; 10μM), and inhibition of the current by CFTRinh172 (10μM). The recordings depicted a negative current, and tracings have been inverted for ease of viewing.

**B.** Tracings of permeabilized monolayers treated with ESI-09. The black dotted line shows the addition of CFTRinh172 to ESI-09 treated monolayers. The gray line shows the ESI-09 response alone and is the same tracing used in A.

**C.** Quantification of the changes in apical Cl<sup>-</sup> I<sub>sc</sub> (μA/cm<sup>2</sup>) in response to vehicle (white bar), ESI-09 (light gray bar), ESI-09 +CFTRinh172 (striped bar), CDCA (black bar), and CDCA+ESI-09 (dark gray bar); n≥3 for all conditions, \* denotes p<0.05 compared to vehicle, # denotes p<0.05 compared to ESI-09+CFTRinh172, and \$ denotes p<0.05 compared to CDCA+ESI-09.

Since individual inhibition of PKA and EPAC pathways did not completely block the CDCA response, the effect of inhibiting these pathways simultaneously was studied. Pretreatment of T84 monolayers with H89 (30 $\mu$ M) and ESI-09 (10 $\mu$ M) for 30 minutes lead to an almost complete inhibition of the CDCA response (**Figure 26A**). Additionally, in a preliminary study, both inhibitors individually reduced the CDCA-induced increase in EGFR phosphorylation (**Figure 26B**). This implies that CDCA requires cAMP signaling, not only via PKA, but also via EPAC, in order to fully stimulate Cl<sup>-</sup> secretion. This data could also suggest a contribution of cAMP-gated ion channels; however, roles for such channels have only been described for Na<sup>+</sup> and Ca<sup>2+</sup> influx in rat colon (197), and their role in Cl<sup>-</sup> secretion has not been defined. Additionally, the reduced phosphorylation of EGFR suggests cAMP signaling is mediating CDCA-induced EGFR transactivation.

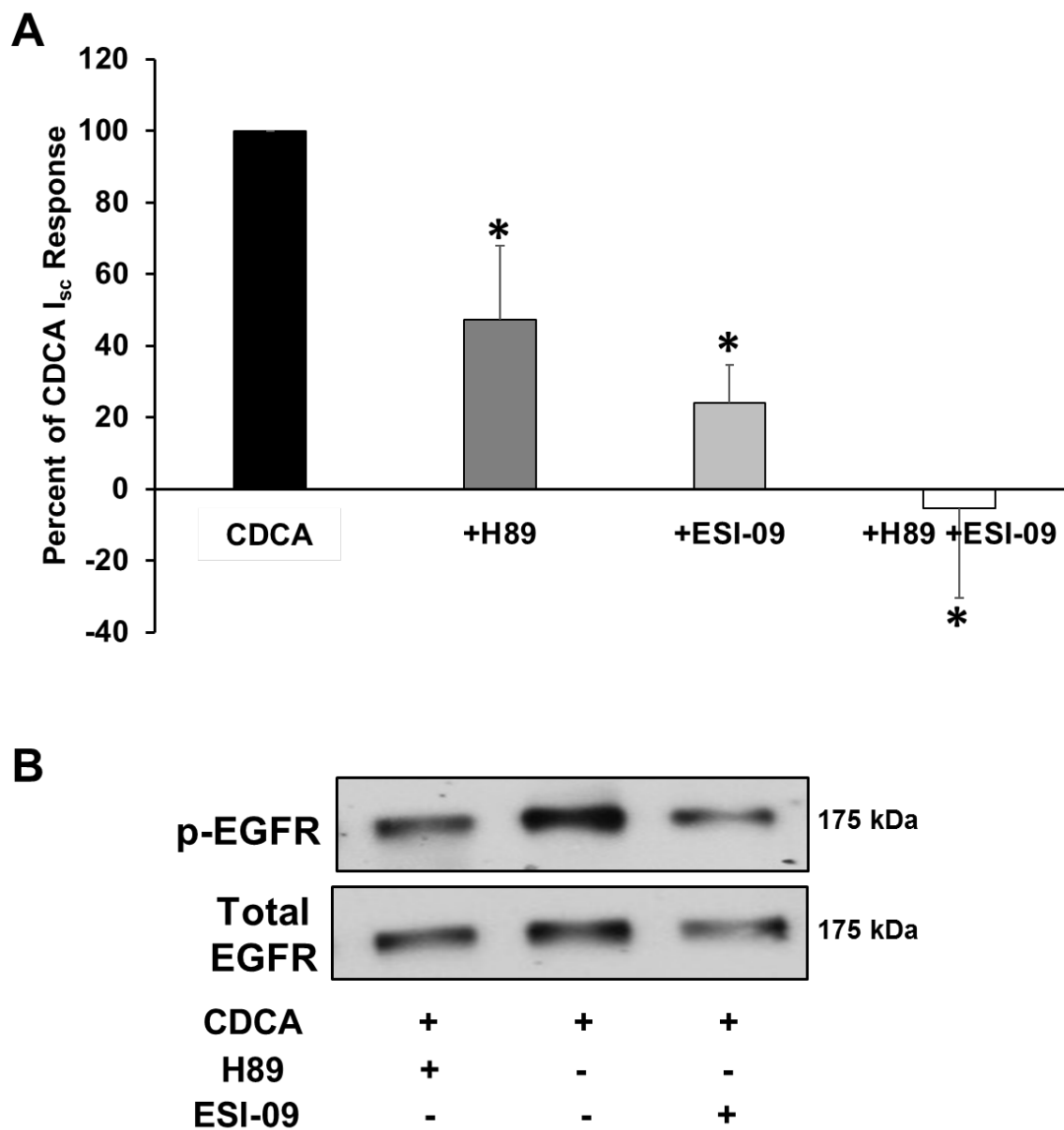


**Figure 26:** The effect of inhibition of PKA and EPAC on CDCA action.

**A.** Percent of the CDCA (500 $\mu$ M) I<sub>sc</sub> response  $\pm$  30 minute pretreatment with the PKA inhibitor H89 (30 $\mu$ M), the EPAC inhibitor ESI-09 (10 $\mu$ M), or both; n $\geq$ 3.

**B.** Effect of EPAC and PKA on CDCA-Induced EGFR activation. Phosphorylation of EGFR was determined after pretreatment (30 minutes) with H89 or ESI-09 (EPAC inhibitor) and stimulation by 500 $\mu$ M CDCA, n=2.

### 1. Rap1 Signaling in CDCA-Stimulation of $I_{sc}$

Sheikh et al. established that EPAC can lead to an activation of Rap1 and a subsequent activation of rho-associated protein kinase (ROCK). This Rap1-ROCK cascade was shown to modulate  $K^+$  transport, which is essential to maintain the driving force for  $Cl^-$  secretion (222). Interestingly, inhibition of Rap1 by GGTI298 (GGTI; 10 $\mu$ M) had no effect on the CDCA response (**Figure 27A**; n=4, p=0.78). Consistent with lack of effect with the Rap1 inhibitor, inhibition of ROCK did not affect CDCA-stimulated  $Cl^-$  secretion (**Figure 27B**; n=8, p=0.19). This was consistent with our earlier findings that CDCA increased  $Cl^-$  currents but not  $K^+$  currents (15), and thus ruled out involvement of Rap1 and ROCK in CDCA action.

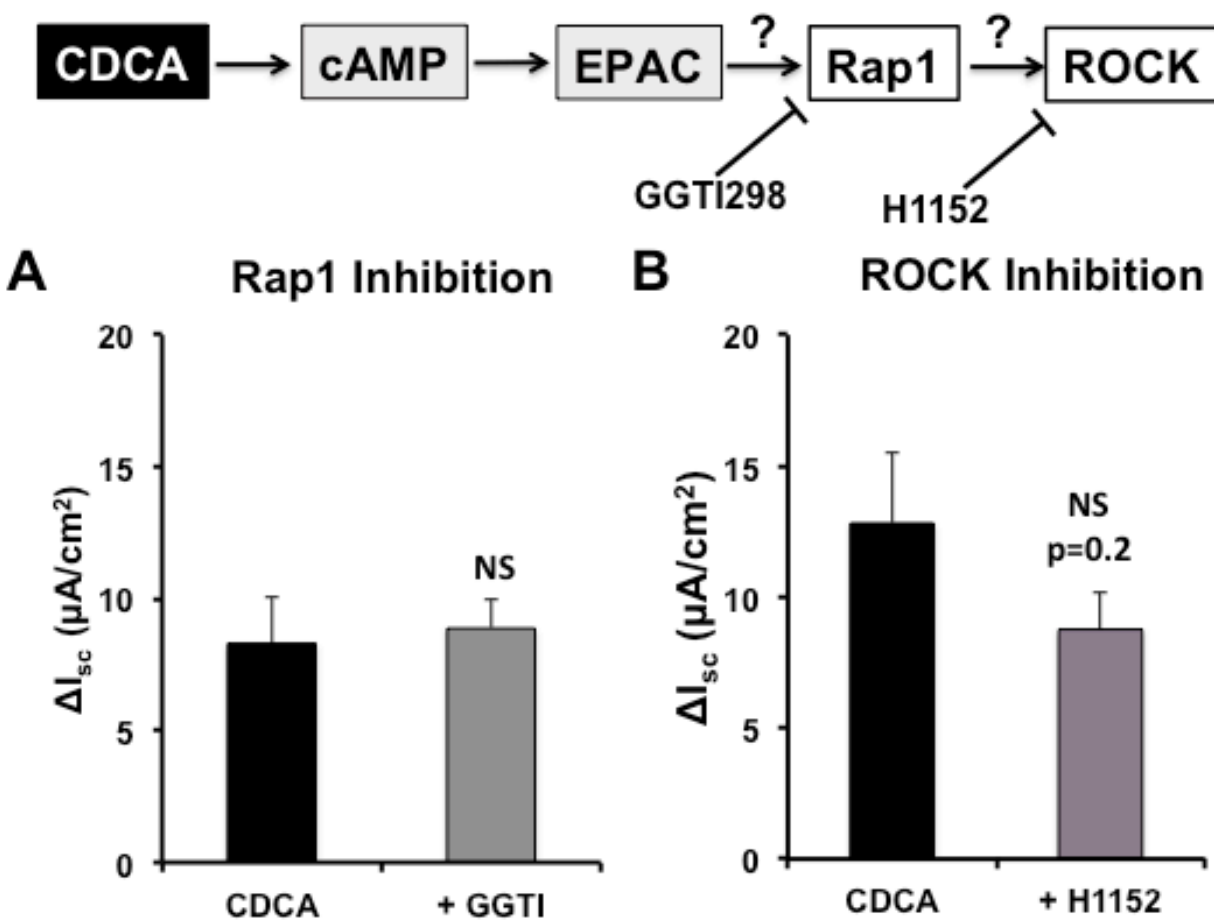


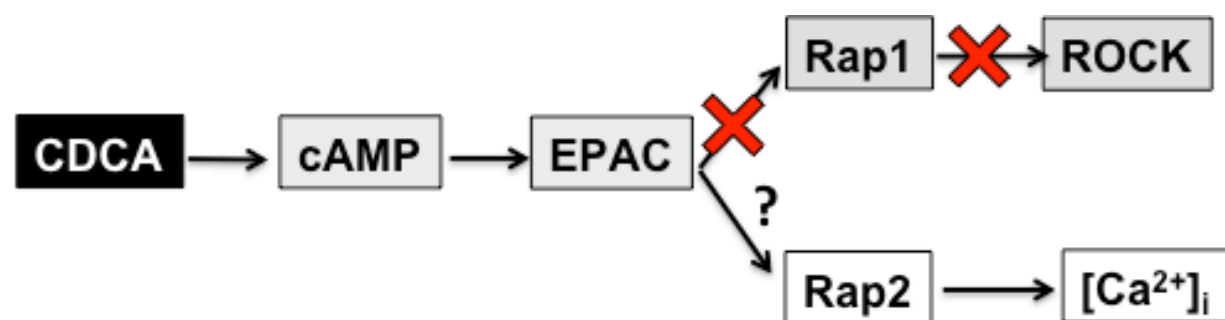
**Figure 27:** Rap1 signaling in CDCA action.

**A.** T84 monolayers were grown to confluence and then pretreated bilaterally for 30 minutes with Rap1 inhibitor, GGTI298 (GGTI; 10 $\mu$ M) before stimulation with basolateral addition of 500 $\mu$ M CDCA. Bar graph represents the  $\Delta I_{sc}$  responses to CDCA  $\pm$  GGTI (n=4).

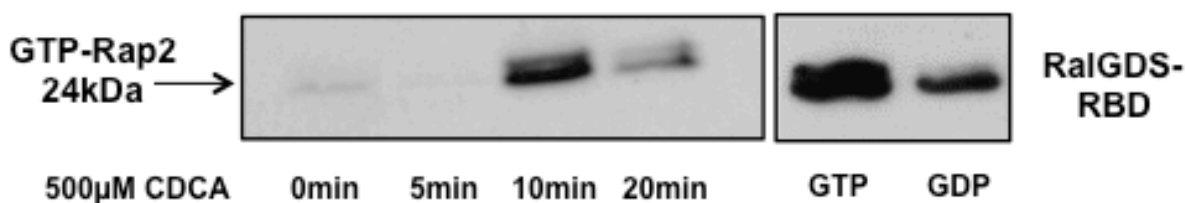
**B.** Monolayers were pretreated bilaterally for 30 minutes with the ROCK inhibitor, H1152 (20 $\mu$ M) and  $\Delta I_{sc}$  responses to CDCA  $\pm$  H1152 were measured (n=8).

## 2. Rap2 Signaling in CDCA Action

EPAC can also activate Rap2. EPAC activates the Raps by exchanging GDP for GTP, rendering the GTP-ases in their active confirmation. Hoque et al. showed that activation of EPAC by its specific activator, 8-pCPT-2'-O-Me-cAMP, increased GTP-bound Rap2, lead to an increase in  $Ca^{2+}$ , and the secretory response was sensitive to the PLC inhibitor U73122 (108). These results suggested that activation of EPAC-Rap2 contributes to a cAMP- $Ca^{2+}$ -dependent stimulation of  $Cl^-$  secretion. Since we know that CDCA action is dependent on cAMP, EPAC,  $Ca^{2+}$ , and is sensitive to U73122, we wanted to elucidate the involvement of Rap2. Unlike for Rap1, there are no commercially available inhibitors for Rap2, so the best way to assess its contribution is to perform activated Rap pull down assays. In this assay, T84 cells were stimulated with CDCA, and then total lysates were exposed to agarose beads conjugated to a Ral guanine nucleotide dissociation stimulator, which has a binding domain specific to activated, GTP-bound, Rap. Beads were used to pull down activated Rap, and then immunoblotted for Rap2. First, to confirm efficacy of the assay, a non-treated total cell lysate was split and loaded with GTP or GDP as positive and negative controls respectively, and then subjected to the pull down assay as described above (**Figure 28A**, right panel). Next in lysates from treated cells, CDCA caused a time-dependent increase in Rap 2 activation (**Figure 28A**, left panel), suggesting Rap2 involvement in CDCA action. Because activation of Rap2 leads to  $Ca^{2+}$  mobilization, we next determined if pretreatment with ESI-09 would affect CDCA-induced changes in  $[Ca^{2+}]_i$ . In control cells, CDCA caused an increase of  $22.4 \pm 3.2$  nM from basal  $[Ca^{2+}]_i$  levels. This was significantly reduced by ~50% in the presence of ESI-09 (**Figure 28B**). These data suggest that EPAC, most likely via the activation of Rap2, is involved in CDCA action on  $[Ca^{2+}]_i$  and  $Cl^-$  secretion.



A



B

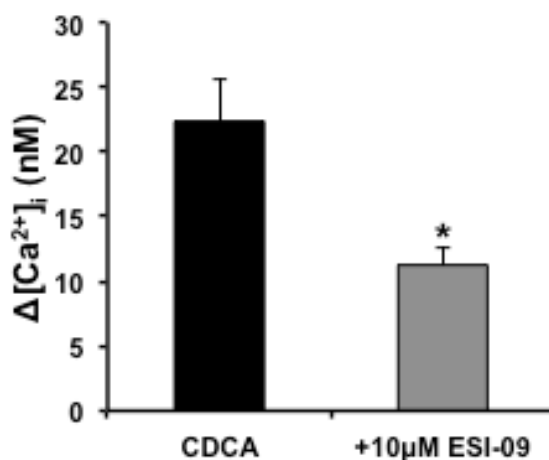


**Figure 28:** Rap 2 Activation in CDCA action.

**A.** Left panel: Representative western blot of Rap2 (24kDa) after T84 cells were stimulated with 500µM CDCA (0-20 minutes); n=3. Protein was harvested and incubated with RaIGDS-RBD agarose beads that pull down GTP-bound Rap which were then immunoblotted for Rap2; Right panel: Unstimulated cell lysates were incubated with either 0.1mM GTP (positive control) or 1mM GDP (negative control) and subjected to pull down assays and immunoblotting.

**B.** Quantification of CDCA-induced  $\Delta[Ca^{2+}]_i$   $\pm$  pretreatment (30 minutes) with 10µM ESI-09; n=4, \* denotes  $p=0.02$ .

## **F. Discussion**

Several studies established a role for  $\text{Ca}^{2+}$  in tauro-DCA regulated epithelial  $\text{Cl}^-$  transport and cell signaling. From these investigations it is known that tauro-DCA increases  $[\text{Ca}^{2+}]_i$  (71, 72), and activates  $\text{K}^+$  and  $\text{Cl}^-$  conductances via an  $\text{IP}_3$ -dependent release of  $\text{Ca}^{2+}$  in T84 cells (70). Studies in rabbit colon established that tauro-DCA's effect on  $\text{Cl}^-$  secretion is segment-specific (192), age dependent (191), mediated by  $[\text{Ca}^{2+}]_i$  and  $\text{IP}_3$  production (250), and requires  $\text{PKC}\delta$  activation (118). It has become evident that there is structural specificity to the signaling initiated by the dihydroxy bile acids. The rise in  $[\text{Ca}^{2+}]_i$  by tauro-DCA was not dependent on extracellular  $\text{Ca}^{2+}$  in both T84 cells and rabbit colon (70, 250); yet CDCA's action is dependent on  $[\text{Ca}^{2+}]_o$  (**Figure 15B**). Additionally, chelation of  $\text{Ca}^{2+}$  by BAPTA-AM significantly decreased both the CDCA-induced increase in  $[\text{Ca}^{2+}]_i$  and CDCA-induced  $\text{Cl}^-$  secretion (**Figure 15**). CDCA is dependent on PLC activation and  $\text{IP}_3$  production (**Figure 16**) similar to the findings of others in T84 cells (70) and rabbit (250). However, in contrast to tauro-DCA action in the adult rabbit colon (118), CDCA action is not dependent on PKC (**Figure 17**). These results suggest that CDCA is causing a rise in  $[\text{Ca}^{2+}]_i$  by releasing it from intracellular stores; the latter may then be replenished by SOCE via plasma membrane  $\text{Ca}^{2+}$  channels. Potential candidates for SOCE elicited by CDCA include the pore forming SOCE subunits Orais, and the transient receptor potential (TRP) proteins, which form cation channels in the membrane (229).

In addition to their effects on  $\text{Ca}^{2+}$  signaling, bile acids are known to activate a variety of kinases downstream of EGFR activation (115, 122, 198, 262). In T84 cells, Keating et al. reported that low doses of DCA (50 $\mu\text{M}$ ) attenuated forskolin- and carbachol-stimulated  $I_{sc}$  and increased EGFR, ERK 1/2, and p38 phosphorylation. However, only inhibition of EGFR by AG1478 attenuated DCA's anti-secretory effect (122). Similarly, high doses of CDCA increased the phosphorylation of these proteins over 10 minutes of stimulation (**Figures 11, 20, and 21**), and only inhibition of EGFR, and not ERK 1/2 and p38, resulted in decrease of the CDCA

response. The main difference between the Keating et al. study and the data presented here is that their studies investigated the effect of long-term exposure to DCA (24 hours) on  $I_{sc}$  and their phosphorylation studies investigated within 30 minutes of DCA treatment, while this study elucidated the short-term/immediate effects of CDCA. Nevertheless, both studies demonstrate that the effects of the dihydroxy bile acids on ERK 1/2 and p38 kinases are unrelated to  $Cl^-$  secretion.

Interestingly, our results (**Figures 10-11, 21-22, and 26**) share many but not all features of the cascade reported by Bertelsen et al. in studying VIP action in T84 cells (25). VIP stimulated EGFR phosphorylation in a PKA-dependent manner, and VIP-stimulated  $I_{sc}$  was inhibited by AG1478 (25). While VIP increased ERK 1/2 phosphorylation, inhibition of ERK 1/2 had no effect on VIP-stimulated  $I_{sc}$  (25), paralleling our findings in **Figure 21**. In contrast to the present results, Bertelsen et al. found VIP to activate PI3K, and VIP's action on  $I_{sc}$  was sensitive to both LY294002 and wortmannin (25). While CDCA action was sensitive to 500nM wortmannin (**Figure 22**), it was not inhibited by a lower dose (100nM, data in text) previously shown to inhibit PI3K action (76). This varied sensitivity to different doses of wortmannin suggests an inhibition of other signaling proteins that may be required for CDCA-induced  $Cl^-$  secretion. Dickson et al. (76) revealed that 500nM wortmannin (30 minutes) inhibited forskolin-induced  $I_{sc}$  in intact T84 cells, but did not inhibit forskolin activation of apical  $Cl^-$  currents in permeabilized monolayers. In a follow up study, Ecay et al. established that 500nM wortmannin inhibited  $Na^+/K^+$ -ATPase activity in intact monolayers, in an ERK 1/2 and p38-independent manner (80). However, use of a non-specific MAPK inhibitor mimicked the wortmannin inhibition of the forskolin response (80). Thus it is conceivable that another kinase, other than ERK 1/2 p38, and PI3K, may be inhibited by high doses of wortmannin, and contributes to cAMP-dependent regulation of  $Na^+/K^+$ -ATPase, an essential component of the  $Cl^-$  secretory mechanism. Wortmannin has also been shown to be a potent inhibitor of myosin light chain kinase (39, 178,

242). Whether one or more kinases are involved in the wortmannin effect, remains to be elucidated.

Clearly CDCA's effect on transepithelial  $I_{sc}$  in T84 cells requires contribution of several signaling pathways, leading us to investigate points of crosstalk. As cAMP (15) and  $Ca^{2+}$  (**Figure 15**) are the major contributors to CDCA action, the primary candidate bridging these two second messenger cascades was EPAC. Previous studies in T84 cells established the role of EPAC in forskolin-induced  $Cl^-$  transport by showing that knockdown of EPAC reduced the forskolin response, with the remaining response sensitive to the PKA inhibitor H89 (108). We have already shown that CDCA can be inhibited by H89 (15) (**Figure 23**), but here we show for the first time that CDCA-induced  $I_{sc}$  is dependent on EPAC as well (**Figures 24-25**). Inhibition of EPAC not only significantly attenuated the CDCA response in intact monolayers, it also inhibited the CDCA-induced apical  $Cl^-$  current, which we had previously attributed to CFTR (15). This implied that ESI-09 is regulating CDCA activation of CFTR. We also found that inhibition of EPAC unveils a transient activation of an apical  $Cl^-$  current (**Figure 25**) and this is significantly inhibited by CFTRinh172 (**Figure 25C**). It remains to be investigated if the apical current not sensitive to CFTRinh172 (**Figure 25C, white bar and striped bar**), is another  $Cl^-$  channel, such as the CaCC, TMEM16A. This current gradually increases with time either with or without the addition of inhibitor (compare grey and black lines in tracing at 12 min and 54 min, **Figure 25A**) and is probably a consequence of the nystatin permeabilization and electrically isolating the apical membrane. Nevertheless, we have significant evidence supporting the novel involvement of EPAC in CDCA action in T84 cells.

EPAC was also implicated in regulating the maintenance of the driving force for  $Cl^-$  secretion via  $K^+$  channel activation (222). Activation of EPAC by its specific agonist 8-pCPT-2'-O-Me-cAMP increased surface expression and activation of the KCNN4  $K^+$  channel in a Rap1-ROCK-dependent manner (222). To address if a similar mechanism was being initiated by CDCA via

EPAC, we inhibited Rap1 and ROCK and measured the resultant CDCA response. Their inhibition in T84 monolayers had no effect on the CDCA response (**Figure 27**). This was not surprising since we have previously shown that CDCA does not activate  $K^+$  conductances (15). Furthermore, EPAC, via Rap2 activation of PLC $\epsilon$ , activates  $Ca^{2+}$  signaling (215). Despite the lack of inhibitors to study Rap2, our data suggests that CDCA may be activating  $Ca^{2+}$  signaling in a Rap2-dependent manner. **Figures 15 and 16** establish CDCA's dependence on  $Ca^{2+}$  signaling, and **Figure 28A** indicated that CDCA increases Rap2 activity. Furthermore, CDCA's increase in  $[Ca^{2+}]_i$  was sensitive to inhibition of EPAC by ESI-09 (**Figure 28B**). Approximately 10nM of  $[Ca^{2+}]_i$  was insensitive to EPAC inhibition, suggesting involvement of an EPAC-independent activation of  $Ca^{2+}$  mobilization or that this concentration of ESI-09 is insufficient to block the response. It is also possible that the remaining response is due to EGFR activation of PLC $\gamma$  (158, 164) or is due to activation of PLC $\beta$  by a  $G\alpha_q$ -coupled mechanism.

Thus far, the involvement of PKC, the MAPKs (ERK 1/2 and p38), Src, PI3K and AKT have been ruled out, but the contributions of PKA,  $[Ca^{2+}]_i$  and EPAC in CDCA-induced  $Cl^-$  secretion has been implicated. The downstream effector of EGFR remains to be identified. However, preliminary data on the effect of cAMP signaling inhibitors on EGFR phosphorylation (**Figure 26**) suggests that cAMP signaling is mediating CDCA's transactivation of EGFR. Based on the findings in this chapter as shown in **Figure 29**, it can be summarized that CDCA increases cAMP, leading to activation of PKA and EPAC. PKA phosphorylates CFTR (15), while EPAC activates Rap2 to induce  $Ca^{2+}$  to further contribute to full activation of CFTR. Furthermore, cAMP signaling likely regulates EGFR activation, which further contributes to  $Ca^{2+}$  signaling via PLC.

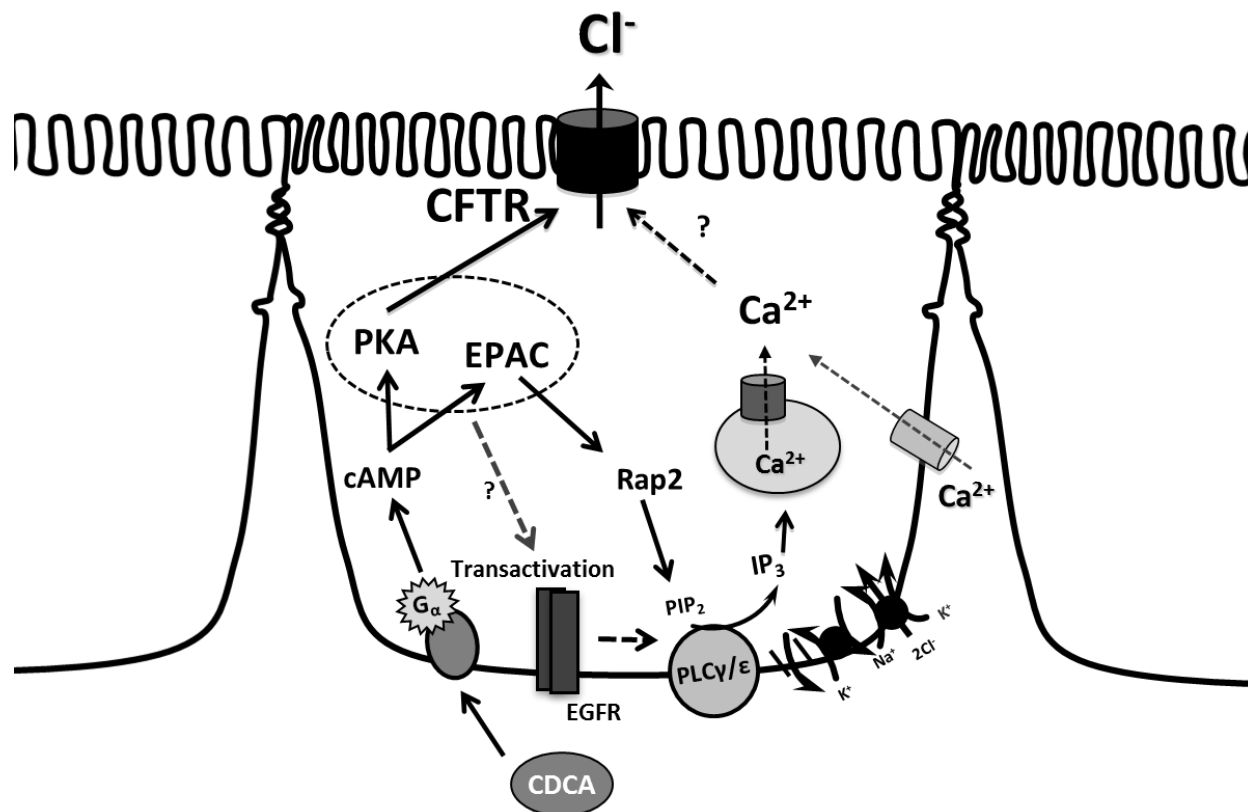


**Figure 29:** Summary of intracellular signaling initiated by CDCA. Based on the signaling described in this chapter, CDCA activates cAMP signaling leading to simultaneous activation of PKA and EPAC. PKA and EPAC modulate activation of EGFR, which may contribute to Ca<sup>2+</sup> signaling. EPAC activation leads to Rap2 signaling and stimulation of Ca<sup>2+</sup> release that contributes to CFTR-dependent Cl<sup>-</sup> secretion. Solid lines pertain to the evidence provided in the chapter and dotted lines are suggested pathways. Pathways that have been ruled out, such as Src and the MAPKs, are not shown.

## Chapter V. Results: Characterization of Cl<sup>-</sup> Transport in HEK-293 Cells

### Parts of the work in this chapter were published as:

**Domingue JC**, Ao M, Sarathy J, George A, Alrefai WA, Nelson DJ, and Rao MC. HEK-293 cells expressing the cystic fibrosis transmembrane conductance regulator (CFTR): a model for studying regulation of Cl<sup>-</sup> transport. *Physiological reports* 2: 2014.

Ao M, **Domingue JC**, Khan N, Javed F, Osmani K, Sarathy J, and Rao MC. Lithocholic acid attenuates cAMP-dependent Cl<sup>-</sup> secretion in human colonic epithelial T84 cells. *American journal of physiology Cell physiology* 310: C1010-1023, 2016.

## **A. Rationale and Aim**

As T84 cells do not lend themselves readily to genetic manipulation, we wanted to utilize a cell model that lends itself more readily to genetic alterations. HEK-293 cells are often considered a simple cell type and are typically utilized as a cell factory to express foreign DNA, leading to translation of specific proteins that can later be isolated, purified, and functionally characterized. Based on the usefulness of the HEK-293 cells, the focus of this chapter was to determine whether HEK-293 cells would be a useful model to study the molecular basis of CDCA regulation of Cl<sup>-</sup> transport as a supplementary component to **Aim 2** to further assess CDCA's regulation of Cl<sup>-</sup> transport. We have documented the expression of Cl<sup>-</sup> channels in these cells, investigated the regulation of stably transfected CFTR, and elucidated bile acid regulation of Cl<sup>-</sup> transport; we compared the findings in HEK-293 cells to those in T84 cells, including the secretagogue action of CDCA (15) and the inhibition of cAMP-induced Cl<sup>-</sup> transport by LCA (14).

## **B. Expression of Cl<sup>-</sup> Channels in HEK-293 Cells**

To establish the use of HEK-293 cells as a model for Cl<sup>-</sup> transport we first determined if the native cells express CFTR. As shown in **Figure 30**, HEK-293 cells neither express CFTR mRNA transcript (**Figure 30A**) nor CFTR protein (**Figure 30B**). We also examined if HEK-293 cells possess other Cl<sup>-</sup> channels and probed for CIC-2 and TMEM16A transcripts, using T84 cells as a positive control. HEK-CFTR cells (**Figure 30A**) express both CIC-2 and TMEM16A mRNA. Although HEK-293 cells were not shown, they also possessed CIC-2 and TMEM16A mRNA since they are the parent cells from which the HEK-CFTR cells were derived.

### **C. Establishment and Characterization of the HEK-CFTR Cell Line**

To further examine the regulation of CFTR function by bile acids, HEK-293 cells were stably transfected with human CFTR using a pEGFP-C1 vector (kindly provided by Dr. D.J. Nelson, The University of Chicago). Transfection resulted in robust expression of CFTR as demonstrated by mRNA transcript expression (**Figure 30A**), protein expression (**Figure 30B**), and epifluorescence microscopy (**Figure 30C**). Furthermore, the fluorescence and immunoblot data suggest that CFTR is expressed in membrane fractions of the CFTR transfected cells (**Figure 30B and C**). The EGFP-CFTR protein was also detectable with EGFP antibody (1:2,000). These cells will be referred to as HEK-CFTR cells.

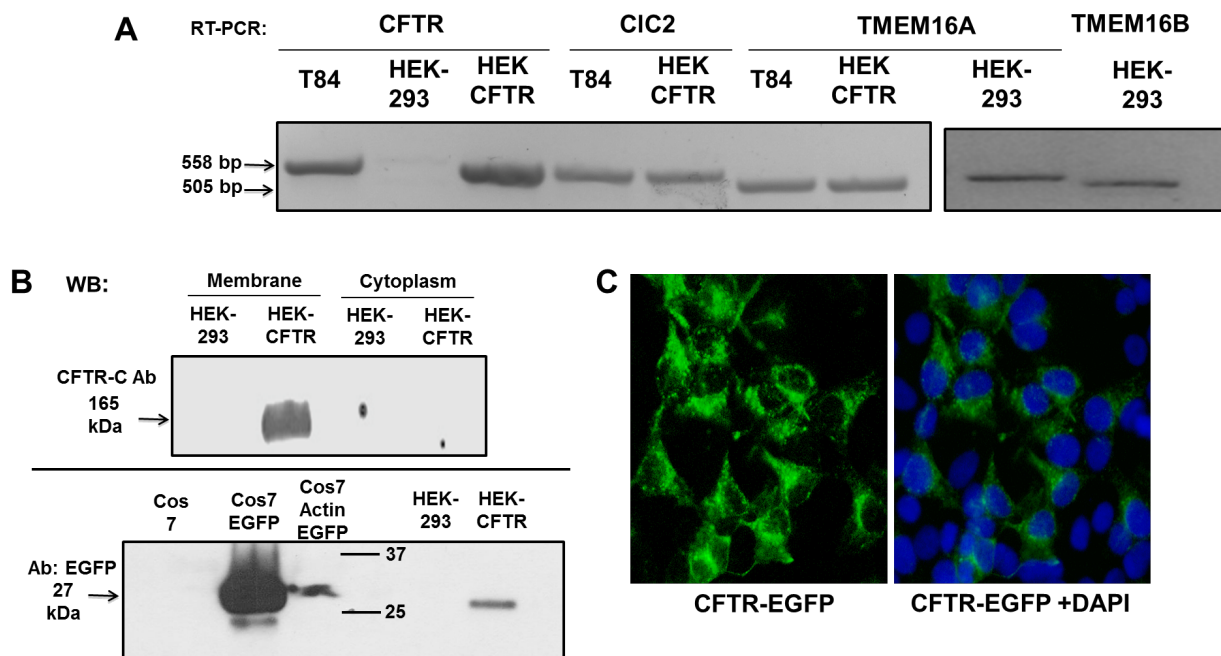


**Figure 30:** Cl<sup>-</sup> channel expression in HEK-293 and HEK-CFTR cells [adapted from (77)].  
**A.** Detection of mRNA for transcripts of Cl<sup>-</sup> channels CFTR, CIC-2 and TMEM16A by RT-PCR in HEK-CFTR cells. T84 colonic epithelial cells were used as a positive control. The anticipated size of the mRNA transcripts are as follows in base pairs: CFTR: 558; CIC-2: 557; and TMEM16A: 505.  
**B.** Detection of CFTR protein in HEK-293 and HEK-CFTR cells by Western blotting (WB). Top panel: CFTR in HEK-293 and HEK-CFTR membrane and cytosolic fractions (Ab: monoclonal mouse-anti-CFTR-COOH, 1:1,000 dilution, estimated size of CFTR is 165 kDa); Bottom panel: Cos7, Cos7 EGFP, and Cos7 Actin-EGFP used as controls for HEK-293 and HEK-CFTR cells; EGFP band is expressed in cell lines transfected with EGFP vectors (Ab: polyclonal goat-anti-EGFP, 1:2,000 dilution; estimated size of EGFP 27kDa).  
**C.** Representative epifluorescence image of CFTR-EGFP in HEK-CFTR cells stained with DAPI for nuclear visualization. Images in each figure are representative of n ≥ 3 experiments.

### 1. Forskolin Dose Response in HEK-CFTR Cells

Since HEK-CFTR cells are not polarized, the iodide efflux assay, a method originally described by Venglarik et al. (249), was used to determine if transfected CFTR was functional. This method was utilized in the siRNA transfected cells in **Chapter III**. Briefly, cells are loaded with iodide, then extracellular iodide is removed, and the rate of iodide efflux  $\pm$  putative activators or inhibitors of Cl<sup>-</sup> channels is determined. CFTR is activated primarily by cAMP, and 10 $\mu$ M forskolin has been shown to increase cAMP and to cause maximal Cl<sup>-</sup> secretion in T84 cells (15). To establish the optimal dose for forskolin action in HEK-293 cells, the effects of 2-50 $\mu$ M forskolin on iodide efflux were examined in HEK-CFTR cells. As shown in **Figure 31**, forskolin caused a dose-dependent increase in iodide efflux as compared to DMSO as control (n=4) in HEK-CFTR cells, with an estimated EC<sub>50</sub> of 3.5 $\mu$ M. Although 50 $\mu$ M forskolin resulted in the largest increase in iodide efflux, the rates were not statistically different from the effect of 10 $\mu$ M at the final time point. To avoid the non-specific effects of high concentrations of forskolin (279), in the remaining experiments 10 $\mu$ M forskolin was used to assess CFTR function.

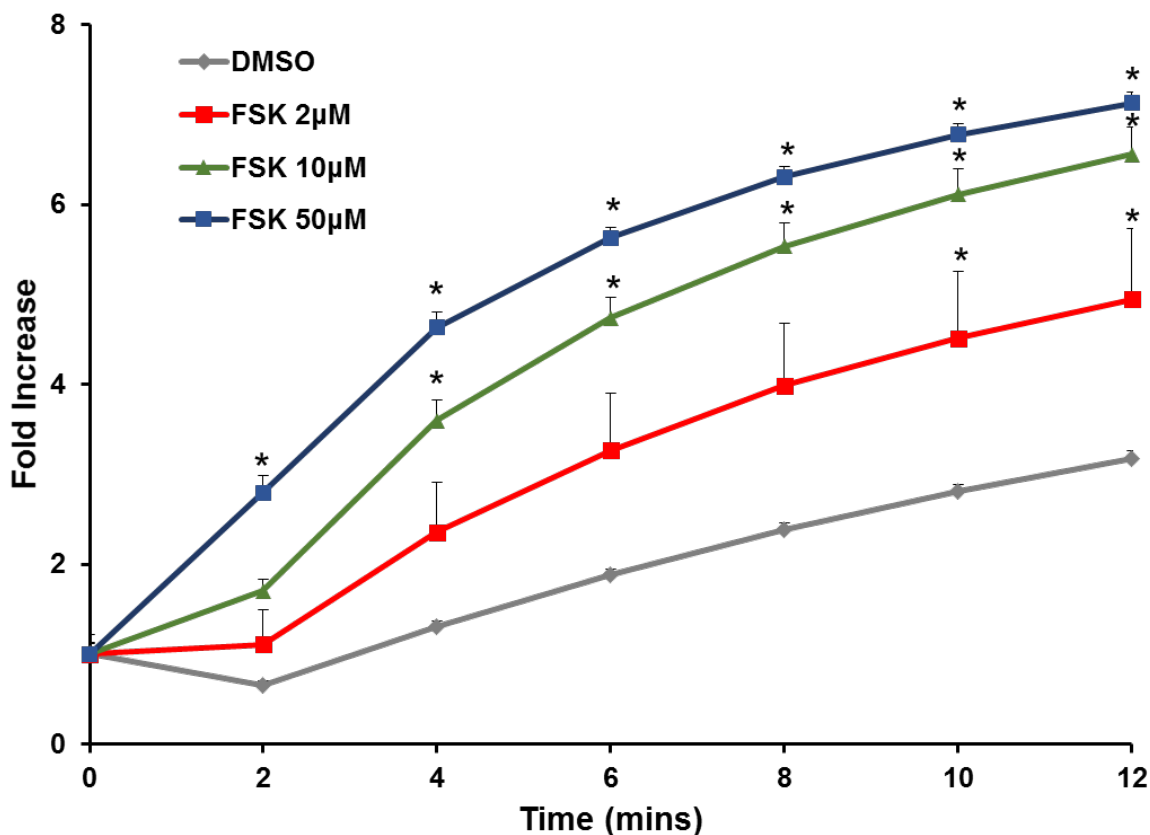


**Figure 31:** Forskolin-induced iodide efflux in HEK-CFTR cells [adapted from (77)]. Cells are loaded with iodide and then placed in an iodide free buffer before stimulation with a  $\text{Cl}^-$  channel activator. Dose-dependent effect of forskolin (FSK; 2-50 $\mu\text{M}$ ) on fold increase of iodide efflux;  $n \geq 3$  for all responses; \* denotes significant difference ( $p < 0.05$ ) compared to DMSO at the same time point. At 10 $\mu\text{M}$  the effect, was significantly different ( $p < 0.05$ ) from 2 $\mu\text{M}$  at 2 and 4 minutes, while at 50 $\mu\text{M}$ , the effect was significantly different from 2 $\mu\text{M}$  from 2 minutes onward. Additionally, 10 $\mu\text{M}$  was significantly different from 50 $\mu\text{M}$  between 2 and 8 minutes, but not at the 10 and 12 minute time points.

## **2. Forskolin Response in HEK-293 v. HEK-CFTR Cells**

To determine if the effects of forskolin reflected CFTR function, we compared its effects on iodide efflux in HEK-CFTR and non-transfected HEK-293 cells. As shown in **Figure 32A**, 10 $\mu$ M forskolin had no effect on the cumulative iodide efflux on HEK-293 cells over 12 minutes, as compared to DMSO, and in contrast to its action in HEK-CFTR cells. The rates of iodide efflux vary over the 12 minutes and as shown in **Figure 32B**, forskolin caused a sharp increase in iodide efflux beginning at 2 minutes and peaking at 4 minutes. These results demonstrate that the transfected CFTR is functional as measured by iodide efflux responses to forskolin, and that forskolin does not alter iodide efflux in non-transfected HEK-293 cells. Equally important these results suggest that although HEK-293 cells possess CIC-2 and TMEM16A transcript, forskolin-stimulated efflux occurs through CFTR, when present.

## **3. Effect of CFTRinh172 on Forskolin-Induced Iodide Efflux**

To further confirm that the iodide efflux stimulated by forskolin is CFTR-dependent, HEK-CFTR cells were pretreated with CFTRinh172 (20 $\mu$ M) for 30 minutes during iodide loading. CFTRinh172 was also present in the iodide efflux buffer during the experiment. In HEK-CFTR cells, forskolin significantly increased rates of iodide efflux compared to DMSO even in the presence of CFTRinh172, albeit to a lower extent (**Figure 33A**). CFTRinh172 inhibited the increase in the rate of forskolin-stimulated efflux at 2 and 4 minutes by 47% and 42% respectively (**Figure 33A**). Furthermore, CFTRinh172 attenuated the cumulative iodide efflux (**Figure 33B**) at all time points from 4 minutes on. However, forskolin, in the presence of CFTRinh172, was still able to significantly increase the cumulative iodide efflux response compared to DMSO at 8-12 minutes. CFTRinh172 had no effect on the iodide efflux in DMSO treated cells. Not surprisingly, there was also no difference in iodide efflux in HEK-293 cells  $\pm$  forskolin  $\pm$  CFTRinh172 ( $p > 0.05$ ,  $n = 3$ ).

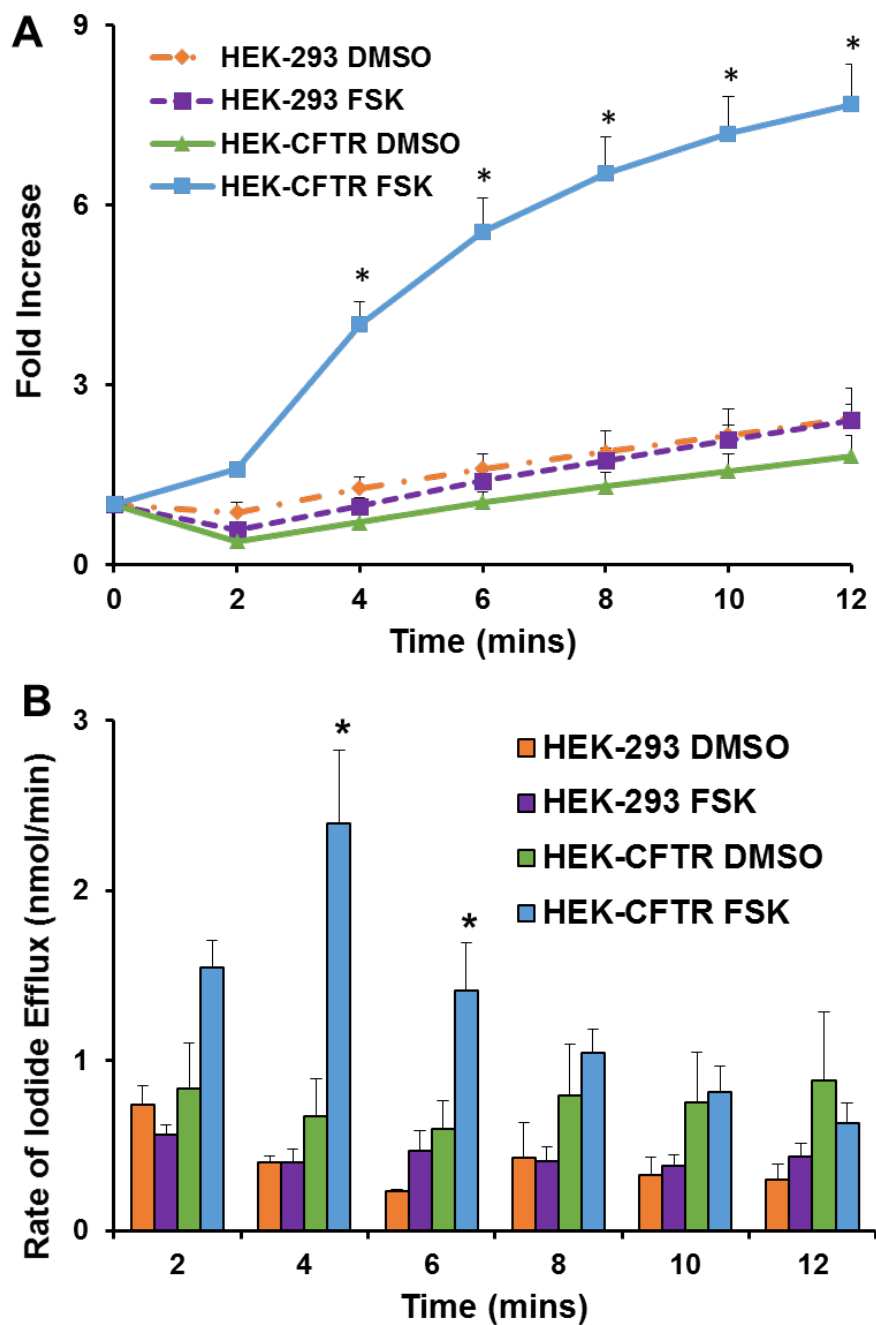


**Figure 32:** Effect of forskolin on iodide efflux in HEK-CFTR and HEK-293 cells [adapted from (77)].

**A.** Effect of forskolin (FSK; 10 $\mu$ M) on iodide efflux in HEK-293 and HEK-CFTR cells. Iodide efflux was measured at 2-minute intervals for 12 minutes and cumulative iodide efflux represented as fold increase over basal flux at time = 0 minutes.

**B.** Rate of iodide efflux (nmol/min) after addition of forskolin in HEK-293 and HEK-CFTR cells;  $n \geq 3$ ; \* denotes  $p < 0.05$  compared to DMSO of the same cell type, i.e. forskolin vs. DMSO in HEK-CFTR cells.

#### 4. Forskolin-Induced cAMP Signaling in HEK-CFTR Cells

To confirm that forskolin, a known activator of adenylyl cyclase, increases cAMP, HEK-CFTR cells were pretreated with forskolin for 5 minutes and intracellular cAMP was measured as described in Methods (**Chapter II**). Forskolin caused a robust increase in cAMP in HEK-CFTR cells (**Figure 33C**). To determine if PKA is involved in forskolin action, HEK-CFTR cells were pretreated with the PKA inhibitor H89 (30 $\mu$ M) for 30 minutes during iodide loading and continuously thereafter throughout the experiment, and then stimulated with DMSO as a negative control, or with forskolin. Interestingly, while DMSO alone did not lead to an increase in iodide efflux (**Figure 33D**), treatment with H89 and stimulation with DMSO was significantly increased from DMSO alone. This phenomenon may be due to the fact that the DMSO responses in these experiments were much lower than those in other experiments; i.e. the DMSO responses in **Figure 33A** are higher than those in **Figure 33D**, thus if the H89 response was compared to those values, they may not have been significantly different. More importantly, pretreatment with significantly inhibited the forskolin-stimulated efflux at 2 and 4 minutes by 43% and 33% respectively (**Figure 33D**).

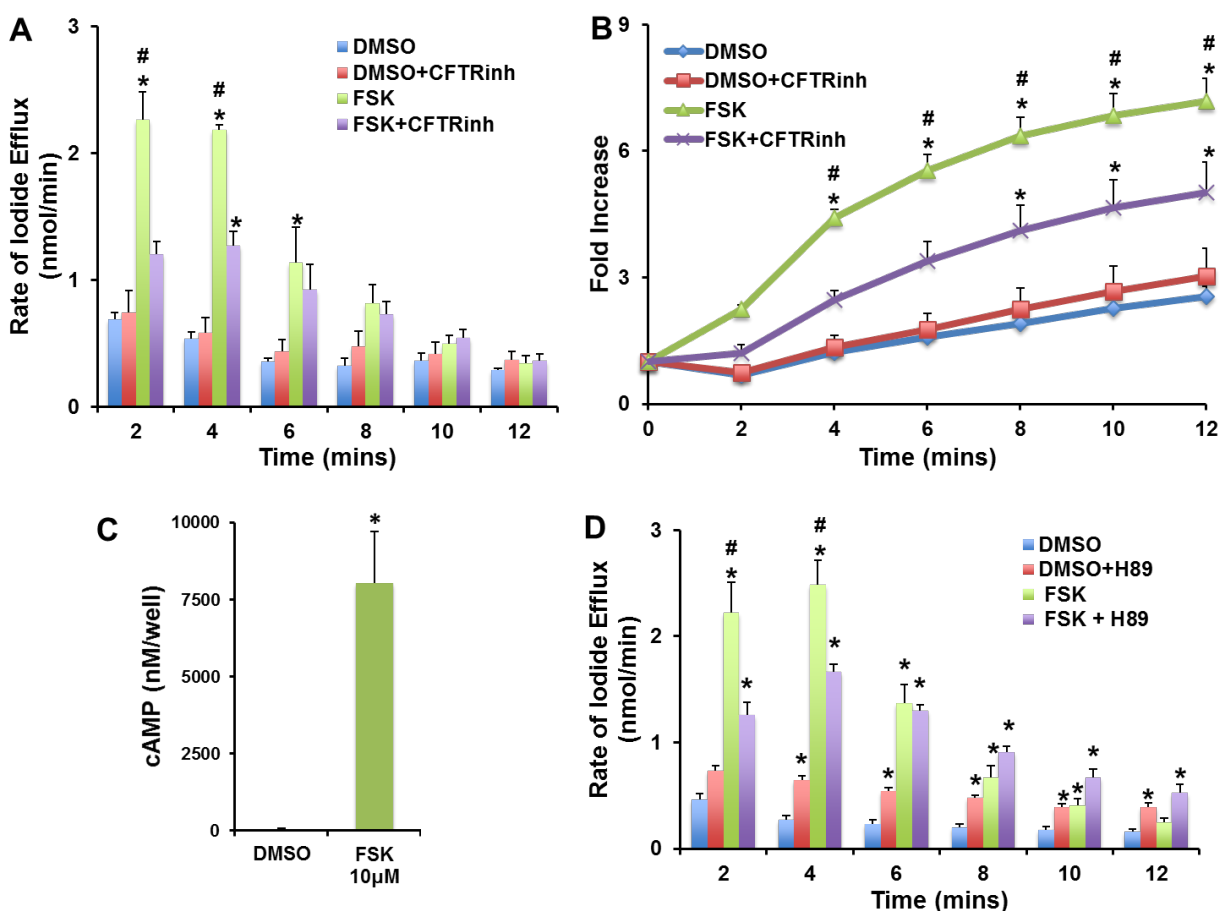


**Figure 33.** The role of CFTR and cAMP signaling in forskolin-induced iodide efflux [adapted from (77)].

**A and B.** Effect of CFTRinh172 (20µM) on iodide efflux in HEK-CFTR cells stimulated with forskolin (FSK; 10µM); HEK-CFTR cells were pretreated with DMSO (0.1%) or CFTRinh172 for 30 minutes during iodide loading. Effect of CFTRinh172 on rate of iodide efflux is shown in **A**, and on fold increase of the mean cumulative iodide efflux over 12 minutes is shown in **B**.

**C.** HEK-CFTR cells grown in 96 well-plates were incubated with 0.1% DMSO or 10 µM forskolin for 5 minutes for  $[cAMP]_i$  measurements. Cyclic AMP was measured using DiscoverX enzyme fragment complementation technology (see Methods) and is depicted as nM/well.

**D.** Effect of PKA inhibitor, H89 (30µM), on the rate of iodide efflux in HEK-CFTR cells stimulated with forskolin; HEK-CFTR cells were pretreated with DMSO or H89 for 30 minutes during iodide loading. Data represented are mean values  $\pm$  SEM relative to value at starting point of  $n \geq 3$  experiments.

\* denotes  $p < 0.05$  versus DMSO control; # denotes  $p < 0.05$  versus treatment+ inhibitor.

## 5. The Role of MRP4 in HEK-CFTR Cells

MRPs, members of the ATP-binding cassette transporter family, are involved in active transport of substrates out of cells. Specifically, MRP4, has been shown to act as a cAMP transporter and cause cAMP to efflux out of HT29 and T84 cells (141, 267). Furthermore, Li et al. (141) demonstrated that MRP4 forms a macromolecular complex with CFTR via the scaffolding protein PDZK1 allowing for local compartmentalized regulation. We screened for MRP expression in HEK-293 cells and found that they express the mRNA transcripts for MRP2 and MRP4, but not for MRP3; they also express MRP4 protein (**Figure 34A**). To determine if MRPs play a role in forskolin's activation of CFTR, we examined the effects of the MRP inhibitor MK571 (20 $\mu$ M) on forskolin-induced iodide efflux. HEK-CFTR cells were pretreated with MK571 for 30 minutes during iodide loading and the inhibitor was present in the efflux buffer during the experiment. While MK571 did not alter iodide efflux in DMSO-treated cells, it increased the rate of iodide efflux by forskolin at 2 minutes when compared to forskolin alone (**Figure 34B**). However, the effects of MK571 on total cell cAMP are unclear; initial experiments gave equivocal results. These results suggest that MRP4 is accentuating the forskolin's effects. Whether it did this by serving as a cAMP transporter into a specific microdomain remains to be determined.

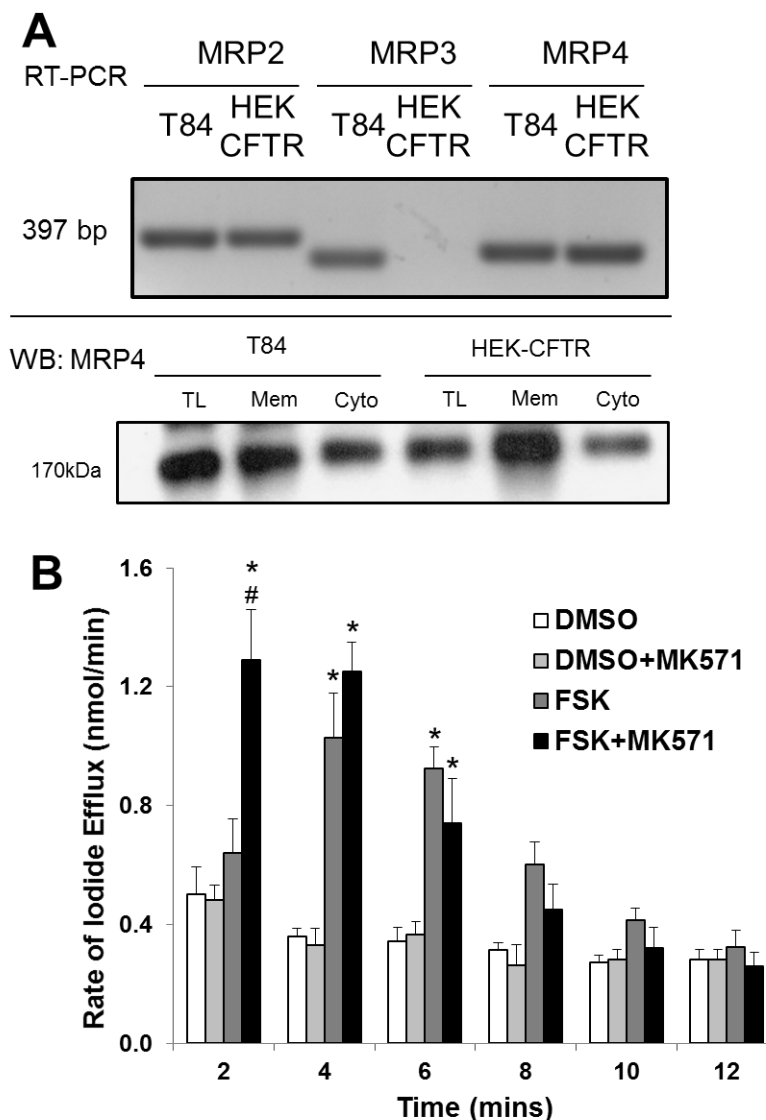


**Figure 34:** MRP expression and function in HEK-CFTR cells [adapted from (77)].

**A.** Upper Panel: Detection of mRNA for multidrug resistance associated proteins (MRPs) transcripts (MRP 2-4) by Reverse Transcriptase Polymerase Chain Reaction; transcript size for MRPs (in bp): MRP2: 397; MRP3: 340; MRP4: 363. Lower Panel: MRP4 protein in membrane, cytosolic and total lysate fractions of HEK-CFTR cells, determined by SDS-polyacrylamide gel electrophoresis, and western blotting (Ab: polyclonal goat-anti-MRP4; 1:750 dilution; estimated size: 170kDa). T84 cells were used as a positive control. Blots are representative of  $n \geq 3$ .

**B.** Effect of MRP inhibitor, MK571, on the rate of iodide efflux in DMSO- or forskolin- (FSK; 10 $\mu$ M) stimulated HEK-CFTR cells. Cells were pretreated with the MK571 (20 $\mu$ M) for 30 minutes during iodide loading, followed by stimulation with forskolin. The data represent the mean values of iodide efflux  $\pm$  SEM relative to value at starting point.  $n \geq 3$ ; \* denotes  $p < 0.05$  versus DMSO as a negative control; # denotes  $p < 0.05$  versus treatment + inhibitor.

## 6. Effect of $\text{Ca}^{2+}$ Chelation on the Forskolin Response in HEK-CFTR Cells

In a variety of cell types, some, but not all studies, show that forskolin may also signal via intracellular  $[\text{Ca}^{2+}]_i$  (108, 167). To test this possibility, HEK-CFTR cells were pretreated with the intracellular  $[\text{Ca}^{2+}]_i$  chelator BAPTA-AM (20 $\mu\text{M}$ ) and then stimulated with forskolin. In contrast to H89, BAPTA-AM had no effect on forskolin-stimulated ion transport (**Figure 35**). Furthermore, forskolin did not alter  $[\text{Ca}^{2+}]_i$  in these cells (**Figure 43**). These results suggest that the action of forskolin on iodide efflux was dependent on PKA but not on changes in  $[\text{Ca}^{2+}]_i$ .

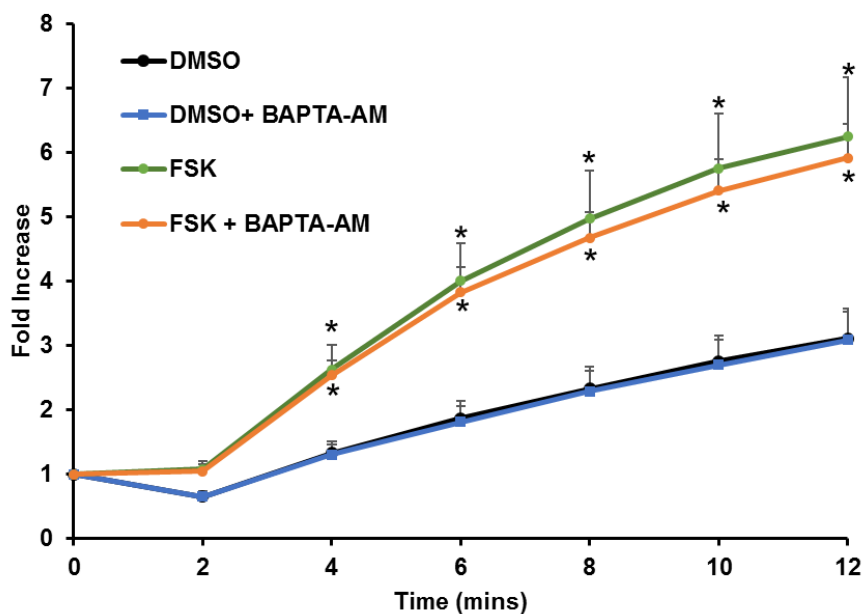


**Figure 35:** Effect of BAPTA-AM on forskolin-induced iodide efflux [adapted from (77)]. HEK-CFTR cells were pretreated with the  $\text{Ca}^{2+}$  chelator BAPTA-AM (20 $\mu\text{M}$ ) and then stimulated with 10 $\mu\text{M}$  forskolin (FSK). The data represents the fold increase in cumulative iodide efflux from basal efflux  $\pm$  SEM relative to value at starting point;  $n \geq 3$ . \* denotes  $p < 0.05$  versus DMSO as a negative control.

## 7. Effect of Forskolin on CFTR Surface Expression

In addition to activation of transporters present in the apical membrane, stimulation of ion transport processes, in some cell types, involves recruitment of intracellular vesicles carrying the transporter to the plasma membrane, as has been shown for CFTR (92, 151, 243, 246). These processes may or may not be dependent on microtubule polymerization. Two approaches were used to assess vesicular transport, surface biotinylation and live cell imaging, to determine if forskolin causes an increase in surface expression of CFTR. First, HEK-CFTR cells were treated with DMSO or forskolin for 1, 4, or 10 minutes and then biotinylated to capture the CFTR expressed at the plasma membrane. CFTR-COOH antibody was used to screen for the proteins in the biotinylated and non-biotinylated fractions. As shown in **Figure 36A**, forskolin did not cause an increase in cell surface biotinylation of CFTR at any time point, although there was a slight decrease in surface expression (10 minutes). No GAPDH was detected in the biotinylated fractions, confirming the efficacy of the separation. The biotinylation results suggest that in HEK-CFTR cells, stimulation of Cl<sup>-</sup> transport did not involve an appreciable increase in CFTR recruitment to the plasma membrane, but was due to activation of CFTR already present in the membrane.

To further confirm that forskolin was not affecting CFTR dynamics, live cell imaging was used to detect the time dependent effects of forskolin on EGFP-CFTR distribution. Cells were counter stained with WGA (red) for plasma membrane and DAPI (blue) for nuclei, and images were captured by confocal microscopy at 25 second intervals over 10 minutes. As shown in **Figure 36B**, the majority of EGFP-CFTR was localized in intracellular vesicles with some expression on the plasma membrane. It is important to note that the images are cross sections of membrane, not at the membrane surface, hence CFTR at the membrane will overlap with the red WGA staining and show as yellow fluorescence (white arrows). We next quantified the speed of vesicular movement at different time points (5s, 3, 6, and 9 minutes). In cells treated

with forskolin the vesicular movement was significantly faster at 3 (DMSO:  $0.008 \pm 0.0002 \mu\text{m/s}$ ; forskolin:  $0.016 \pm 0.003 \mu\text{m/s}$ ) and 6 minutes (DMSO:  $0.006 \pm 0.0002 \mu\text{m/s}$ ; forskolin:  $0.014 \pm 0.001 \mu\text{m/s}$ ), and seemed to come to a halt by 9 minutes (DMSO:  $0.005 \pm 0.0003 \mu\text{m/s}$ ; forskolin:  $0.000 \mu\text{m/s}$ ). Over the time course, vesicular movement in the DMSO treated cells steadily decreased. No increases were detected in EGFP-CFTR in the plasma membrane as a consequence of forskolin's effects on vesicular movement.

## **8. Effect of Nocodazole in HEK-CFTR cells**

### **i. Effect of Nocodazole on Tubulin**

Previous studies examining the activation of CFTR have shown an involvement of microtubules, and that this may be tissue-specific (246) and we recently reported that the microtubule destabilizer nocodazole, disrupts microtubules and inhibits CFTR mediated ion transport in T84 cells (15). Thus, we explored the role of microtubules in forskolin-induced iodide efflux in HEK-CFTR cells. To achieve and maintain microtubule disruption, T84 cells need to be pre-incubated at  $4^\circ\text{C}$  prior to exposure to  $33 \mu\text{M}$  nocodazole while on ice based on the protocol defined by Tousson et al. (246) and modified by us (15). However, this pre-treatment in conjunction with the loading conditions of the iodide efflux (protocol I below), were too harsh for HEK-CFTR cells as they sloughed off during the efflux measurements. Therefore, to establish a protocol for destabilizing microtubules in HEK-CFTR cells the distribution of detergent-soluble (monomeric) and detergent-insoluble (microtubule)  $\alpha$ -tubulin was examined by immunoblot under four conditions as described in methods: (I)  $4^\circ\text{C}$ , 30' to destabilize microtubules followed by incubation with nocodazole on ice 30 minutes and then at room temperature, 1 hour; (II) Nocodazole on ice for 30 minutes followed by incubation at room temperature, 1 hour; (III)  $4^\circ\text{C}$  for 30 minutes followed by incubation with nocodazole at room temperature, 1 hour; (IV) Incubation with nocodazole at room temperature for 1 hour. In all

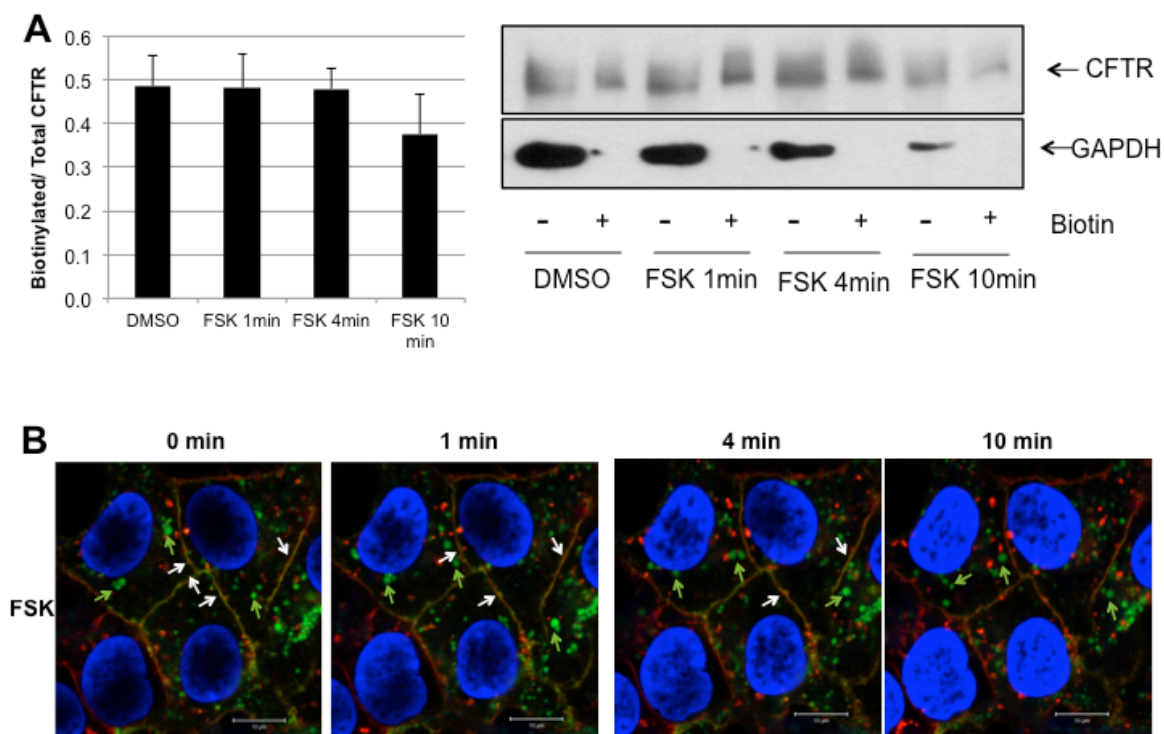


**Figure 36:** Effect of forskolin on the surface expression of CFTR [adapted from (77)].

**A.** Quantitation and representative blot of cell surface biotinylation of CFTR in HEK-CFTR cells that were treated with forskolin (FSK; 10 $\mu$ M) for 1, 4, and 10 minutes. GAPDH was used as a control to determine if there was any contamination of biotinylated protein in the nonbiotinylated fractions (Ab: monoclonal mouse-anti-CFTR-COOH and anti-GAPDH; 1:1000 and 1:2000 dilution, respectively; estimated sizes: for CFTR: 165 kDa and GAPDH: 36 kDa).

**B.** Effect of forskolin on CFTR location in live HEK-CFTR cells grown in 35-mm glass-bottom dishes and stained as described in Methods. Images were captured before and after the treatment of forskolin as time series. Snapshots at 0, 1, 4, and 10 min are shown. Green: CFTR; red: WGA; and blue: Dapi. White arrows: colocalization of CFTR and WGA; green arrows: CFTR vesicles.  $n \geq 3$  for all experiments.

conditions, control cells were exposed to DMSO instead of nocodazole. As shown in **Figure 37A**, in all conditions, treatment with nocodazole resulted in no detectable tubulin in the detergent-soluble fraction. These results established that in HEK-CFTR cells, nocodazole treatment does destabilize microtubules into tubulin monomers, and that protocol IV is sufficient for microtubule disruption (bottom panel in **Figure 37A**). **Figure 37B** shows a representative quantification of the proportion of soluble tubulin compared to total tubulin (insoluble + soluble). All treatment protocols showed similar densitometric ratios, and the values of the 4°C+Ice+RT treatment protocol (top panel) are shown as an example.

#### **ii. Effect of Nocodazole on Forskolin-Induced Iodide Efflux**

Protocol IV was used to determine if microtubule disruption affected forskolin-induced iodide efflux. In addition to the 1 hour pre-treatment, nocodazole was present in the efflux buffer during the entirety of the experiment. **Figure 37C** shows that nocodazole had no effect on iodide efflux either in the presence or absence of forskolin. Therefore, in HEK-CFTR cells, activation of CFTR by forskolin was independent of microtubule interaction.

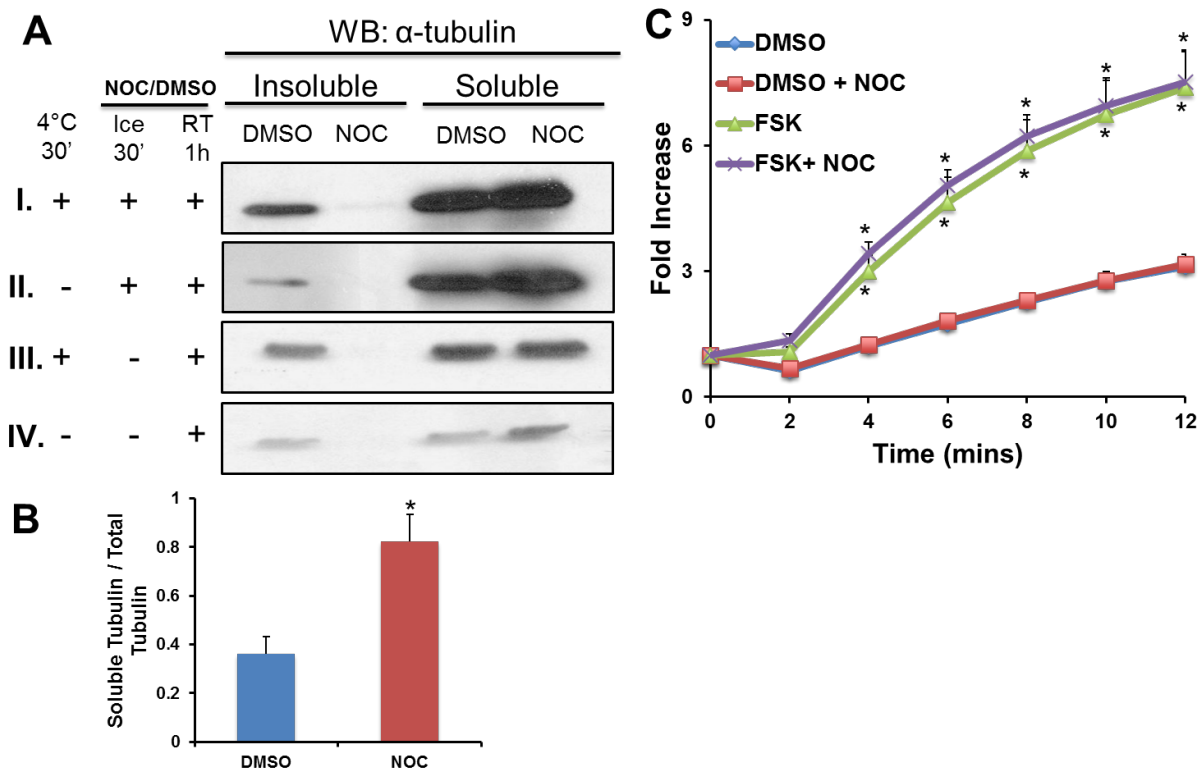


**Figure 37:** Effect of nocodazole treatment on HEK-CFTR cells [adapted from (77)].

**A.** HEK-CFTR cells were pretreated with nocodazole (NOC; 33 $\mu$ M) for 1h at room temperature (RT) preceded by either incubation at 4°C for 30', or addition of NOC for 30' on ice, or a combination of the two. Representative blots show the 0.1% Triton X-100 soluble and insoluble  $\alpha$ -tubulin (Ab: mouse-anti- $\alpha$ -tubulin; 1:2,500 dilution; estimated size: 50kDa).

**B.** The ratio of soluble tubulin to total tubulin (insoluble + soluble tubulin) was analyzed by densitometry of the DMSO and NOC signals for all four conditions. Representative values for protocol 'I' (4°C for 30' + NOC for 30' on ice + NOC for 1h at RT) are shown (data not shown for "II to IV").

**C.** Effect of NOC (1h, RT) on iodide efflux in HEK-CFTR cells. Cells were pretreated with NOC during iodide loading and then stimulated with forskolin (FSK; 10 $\mu$ M). The data represents the fold change of mean cumulative iodide efflux from basal efflux  $\pm$  SEM relative to value at starting point;  $n \geq 3$  for A-C. DMSO (0.1%) was used as a negative control for NOC and forskolin. \* denotes  $p < 0.05$  v. DMSO.

## **D. Bile Acid Signaling in HEK-293 Cells**

One of the main goals in establishing the HEK-CFTR cell line was to use it as a model to examine the modulation of CFTR activity by secretagogues, including bile acids. To use HEK-CFTR as a comparative model to the T84 cell line we needed to confirm that the bile acids initiated the same signaling pathways, such as PKA-dependent activation of CFTR by CDCA (15) and inhibition of cAMP-dependent pathways by LCA (14) in the HEK-CFTR cells.

### **1. Expression of TGR5 in HEK Cells**

HEK-293 cells stably transfected with TGR5 ( $G\alpha_s$ -coupled GPCR), were reported to respond to tauro-LCA with an increase in cAMP (115). HEK-293 cells were first examined for endogenous expression of TGR5. As shown in **Figure 38A** both HEK-293 and HEK-CFTR cells express the transcript and protein for TGR5 and the protein is localized to the membrane fraction. Additionally, immunofluorescence images in HEK-293 cells showed punctate expression of TGR5 (**Figure 38B**).

### **2. CDCA-Induced Iodide Efflux in HEK and HEK-CFTR Cells**

#### **i. CDCA Dose Response**

Since TGR5 has been shown to activate CFTR-dependent  $Cl^-$  secretion in cholangiocytes (126), we assessed activation of  $Cl^-$  transport by CDCA in HEK-CFTR cells. HEK-CFTR cells were incubated with varying concentrations of CDCA (100-500 $\mu$ M), and iodide efflux measured. At 250 $\mu$ M and 500 $\mu$ M CDCA caused a significant increase in the cumulative iodide efflux compared to DMSO from 4 minutes onward (**Figure 39A**). The 100 $\mu$ M dose did cause an increase but this was not significant compared to DMSO at any time point (**Figure 39A**). Interestingly, unlike forskolin, CDCA also caused a significant increase in iodide efflux in normal HEK-293 cells (**Figure 39B**). Additionally, CDCA required a longer stimulation of HEK-293 cells (~20 minutes) to induce maximal iodide efflux compared to the shorter time for

forskolin (~12 minutes; **Figure 31**). For the remainder of the experiments 500 $\mu$ M CDCA was used, to mimic the dose studied in T84 cells.

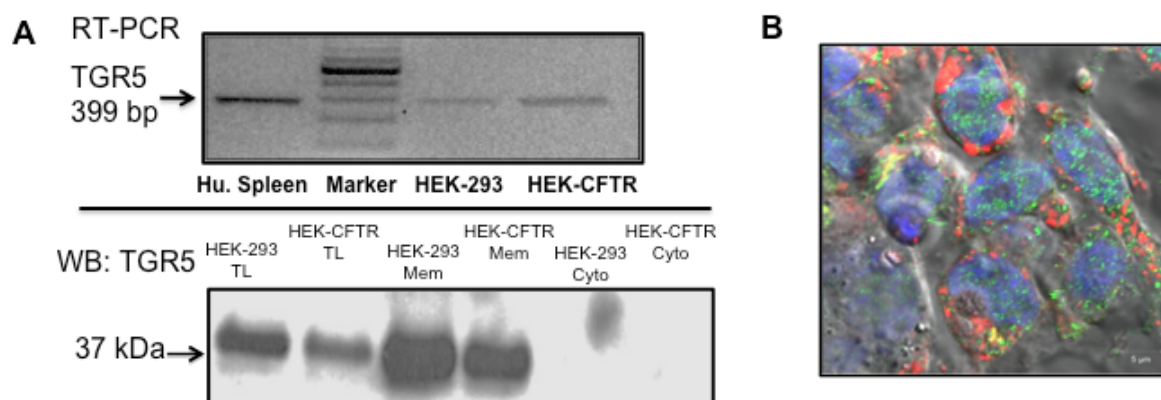


**Figure 38:** Expression of TGR5 in HEK-293/CFTR cells [adapted from (77)].

**A.** Top Panel: Detection of mRNA transcript by RT-PCR and protein by immunoblot for TGR5 expression in HEK-293 and HEK-CFTR cells. Human spleen (Hu.spleen) was used as a positive control.

Bottom Panel: The cytosolic, membrane and total lysate protein fractions were screened by SDS-PAGE and immunoblotting for the presence of TGR5 protein using a polyclonal rabbit-anti-TGR5 antibody (1:2,500 dilution; estimated size: 37kDa).

**B.** Immunofluorescence image of TGR5 (green), actin (red), and nuclei (blue; DAPI) in HEK cells overlaid on the DIC image.

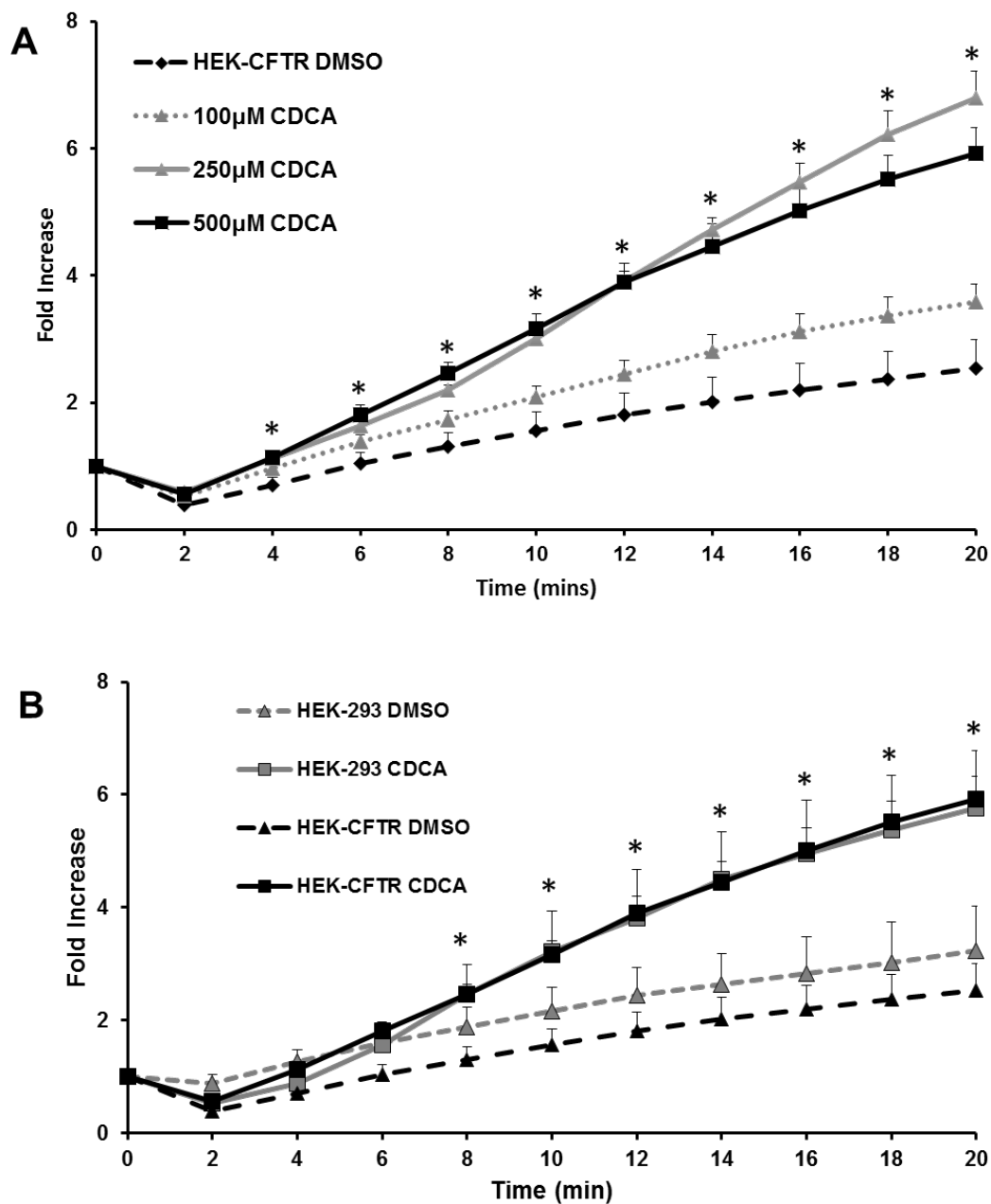


**Figure 39.** CDCA-induced iodide efflux in HEK-293 and HEK-CFTR cells.

**A.** Dose response of CDCA in HEK-CFTR cells. Cells were stimulated with 100µM (gray dotted line), 250µM (gray solid line), and 500µM (black solid line) CDCA and 0.1% DMSO (black dotted line) as a negative control. \* denotes significance between 250µM and 500µM compared to DMSO control.

**B.** Effect of 500µM CDCA (solid lines) on iodide efflux in HEK (gray lines) and HEK-CFTR (black lines) cells compared to DMSO (dotted lines). The data represent the fold increase of mean cumulative iodide efflux from basal efflux  $\pm$  SEM relative to value at starting point;  $n \geq 3$ ; \* denotes  $p < 0.05$  compared to DMSO in the same cell type at that time point.

### **ii. Effect of Microtubule Destabilization on CDCA Action in HEK-CFTR Cells**

Since nocodazole treatment inhibited CDCA action in T84 cells, the effect of nocodazole on CDCA-induced  $\text{Cl}^-$  transport in HEK-CFTR cells was next determined (15). Interestingly, destabilization of microtubules with 1 hour of nocodazole ( $33\mu\text{M}$ ) treatment had no effect on the CDCA response in HEK-CFTR cells (**Figure 40A**). This finding, in addition to the lack of microtubule involvement in the forskolin response in these cells, suggests that  $\text{Cl}^-$  transport in HEK-CFTR cells occurs independently of intact microtubules.

### **iii. Effect of CFTRinh172 on CDCA Action in HEK Cells**

The findings that CDCA increased iodide efflux in non-CFTR expressing HEK-293 cells, and that  $\text{Cl}^-$  transport was independent of intact microtubules were intriguing. In contrast to the effect of CFTRinh172 on forskolin action in HEK-CFTR cells (**Figure 33**), and not surprisingly, pretreatment of cells with CFTRinh172 ( $20\mu\text{M}$ ) had no effect on the CDCA response in either HEK-CFTR cells (**Figure 40B**), or in HEK-293 cells (data not shown). Cumulatively these studies suggest that CFTR does not play a role in CDCA-induced iodide efflux in HEK-293 cells and that the iodide-efflux in HEK-CFTR cells by CDCA is due to activation of another  $\text{Cl}^-$  transporter.

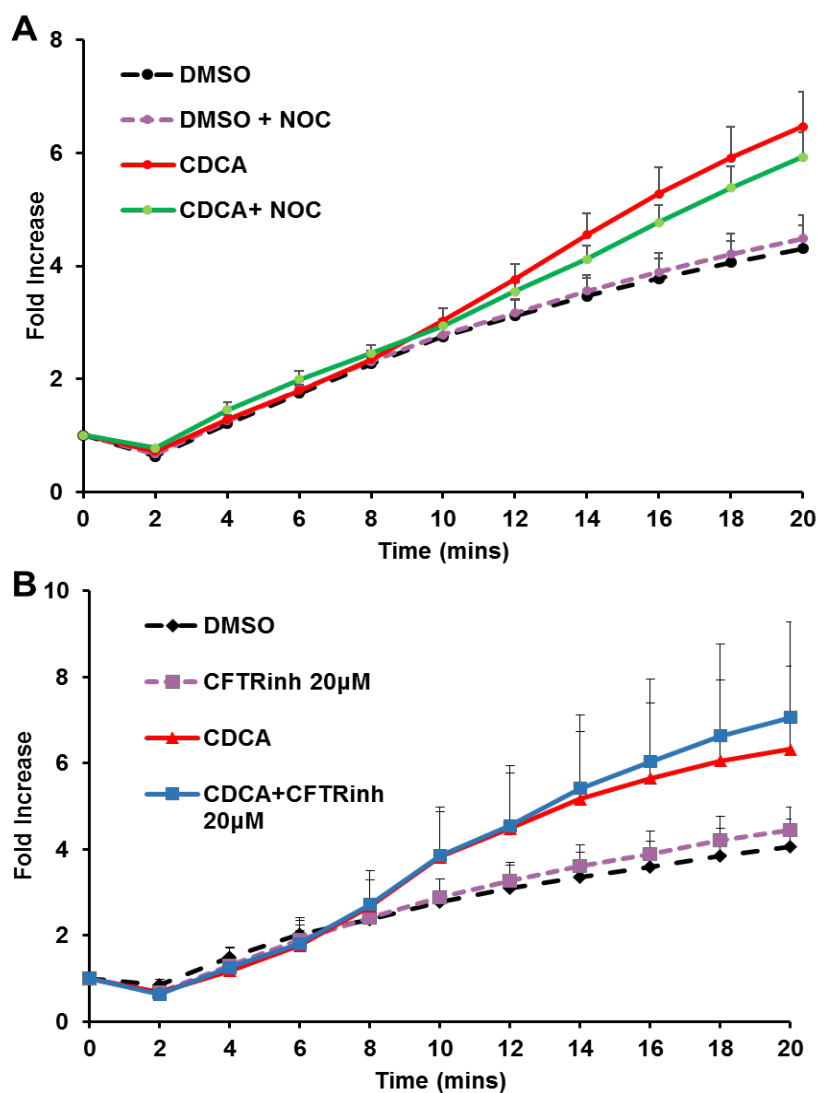


**Figure 40.** Effects of nocodazole and CFTRinh172 on CDCA action in HEK-CFTR cells.

**A.** Effect of nocodazole (NOC; 33 $\mu$ M; protocol IV) on CDCA-induced iodide efflux in HEK-CFTR cells. Cells were pretreated with NOC or 0.1% DMSO during iodide loading and then stimulated with CDCA (500 $\mu$ M).

**B.** Effect of CFTRinh172 on CDCA-induced iodide efflux in HEK-CFTR cells. Cells were pretreated for 30 minutes with 20 $\mu$ M CFTRinh172 (CFTRinh172) and then stimulated with 500 $\mu$ M CDCA.

The data represents the fold change of mean cumulative iodide efflux from basal efflux  $\pm$  SEM relative to value at starting point;  $n \geq 3$  for all conditions.

#### iv. CDCA and Ca<sup>2+</sup> Signaling in HEK-293 Cells

CFTR-independent Cl<sup>-</sup> transport in HEK-293 cells by CDCA suggested that another second messenger signaling pathway may be involved. Thus, changes in [Ca<sup>2+</sup>]<sub>i</sub> by CDCA were measured in HEK-293 cells using Fura2-AM. Addition of CDCA caused a significant increase in [Ca<sup>2+</sup>]<sub>i</sub> compared to basal Ca<sup>2+</sup> levels (**Figure 41A**). The CDCA-stimulated increase in Ca<sup>2+</sup> implied that CDCA could be activating the Ca<sup>2+</sup>-activated Cl<sup>-</sup> channel, TMEM16A. HEK-293 cells were pretreated with the TMEM16A inhibitor AO1 (20μM), and iodide efflux was measured. AO1 reduced the CDCA-stimulated iodide efflux by 27%, although this was not significant (**Figure 41B**). It is important to note that inhibition of TMEM16A in T84 cells had no effect on CDCA-induced I<sub>sc</sub>. (ΔI<sub>sc</sub>, μA/cm<sup>2</sup>; CDCA: 7.9±1.4; +AO1: 10.2±2.5; n=7, p=0.44). To determine if the increase in Ca<sup>2+</sup> was necessary for CDCA-induced iodide efflux, HEK-293 cells were pretreated with 40μM BAPTA-AM to chelate [Ca<sup>2+</sup>]<sub>i</sub>. However, as shown in **Figure 41B**, there was considerable variability in the response to CDCA ± BAPTA-AM making it difficult to ascertain if [Ca<sup>2+</sup>]<sub>i</sub> played a role in CDCA action. Interestingly, CDCA-induced changes in [Ca<sup>2+</sup>]<sub>i</sub> were significantly reduced in the presence of 1mM EGTA to chelate extracellular Ca<sup>2+</sup> (data not shown), suggesting that CDCA requires extracellular Ca<sup>2+</sup> influx to increase [Ca<sup>2+</sup>]<sub>i</sub>. Furthermore, pretreatment of HEK-293 cells with AG1478 did not significantly affect the CDCA response (maximal cumulative normalized to t=0: CDCA:3.4±0.5; +AG1478: 4.6±0.6; n=4, p>0.05). In summary, while CDCA increases Ca<sup>2+</sup>, at this juncture our results are equivocal as to whether [Ca<sup>2+</sup>]<sub>i</sub> or TMEM16A play a role in CDCA action in HEK-293 cells. It is also possible that there may be a Cl<sup>-</sup> transporter other than TMEM16A that was involved in CDCA-induced iodide efflux in HEK-293 cells, and the regulation of Cl<sup>-</sup> channel activation by CDCA varies between T84 and HEK-293 cells.

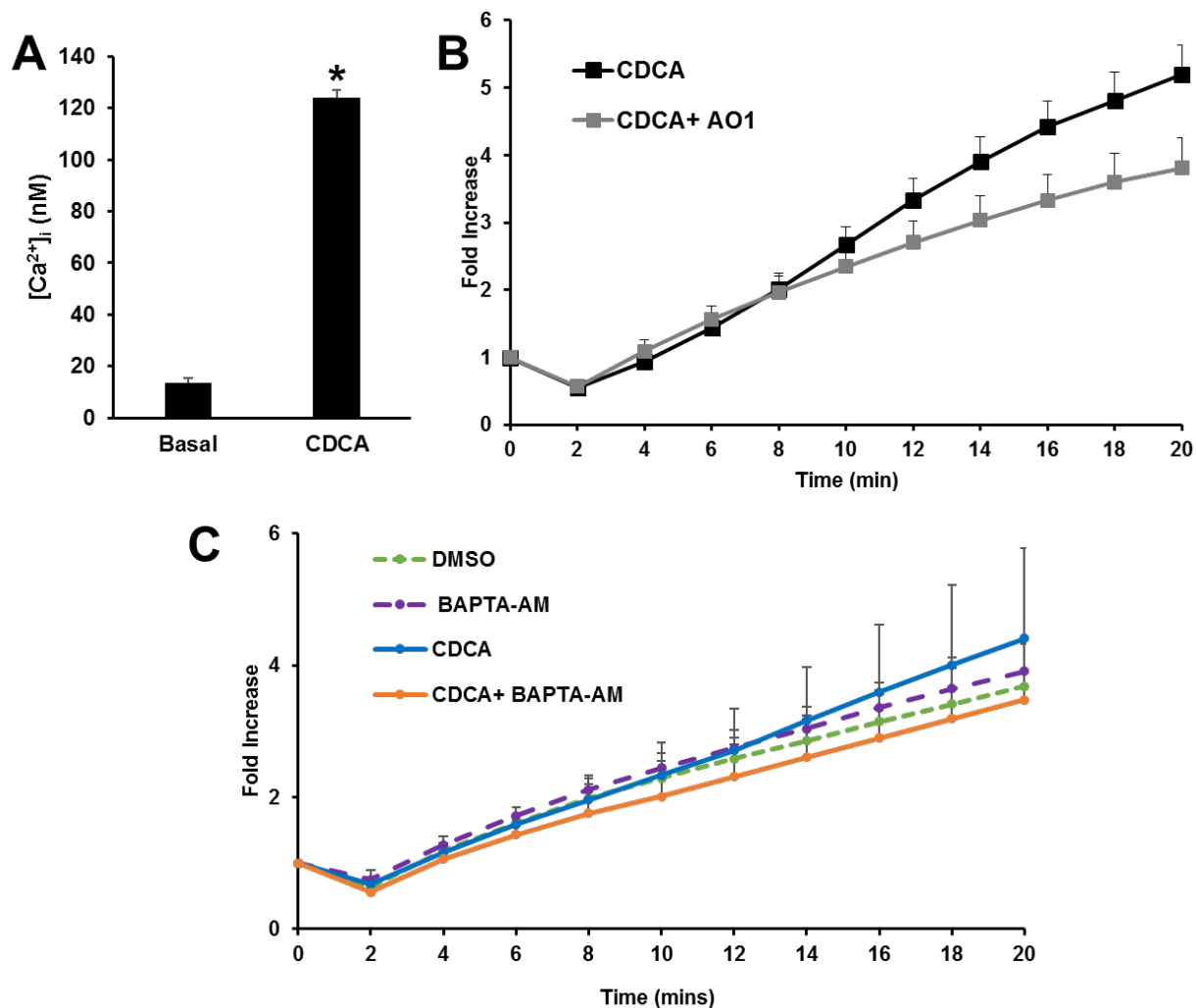


**Figure 41.** Ca<sup>2+</sup> in CDCA action in HEK-293 cells.

**A.** Fura2-AM was used to assess CDCA-induced changes in intracellular Ca<sup>2+</sup>. Data is represented as [Ca<sup>2+</sup>]<sub>i</sub> before (basal) and after addition of 500μM CDCA; n=5; \* denotes p<0.05.

**B.** Fold increase in cumulative iodide efflux by 500μM CDCA (black line) ± the TMEM16A inhibitor AO1 (20μM; gray line); n=4, p>0.05.

**C.** Fold increase in cumulative iodide efflux from t=0 in response to 0.1% DMSO (green dotted line), 40μM BAPTA-AM (purple dotted line), 500μM CDCA (blue line), and CDCA + BAPTA-AM (orange line); n=3.

### 3. LCA Action in HEK and HEK-CFTR Cells

#### i. LCA Dose Response

Thus far, these data suggest distinct cell type differences in responsiveness to bile acids between HEK-293/CFTR and T84 cells. Considering the prominent expression of TGR5 in HEK-293/CFTR cells, and because LCA is the most potent physiological agonist of TGR5, LCA's effect on iodide efflux was assessed in these cells. As shown in **Figure 42A**, increasing doses of LCA (5-500 $\mu$ M) had no effect on iodide efflux, indicating that, as in T84 cells, LCA does not have a pro-secretory effect in HEK-CFTR (**Figure 42A**) or HEK-293 cells (data not shown). All values were not statistically significant from DMSO as control.

#### ii. Effect of LCA Pretreatment on Iodide Efflux

We have recently published that although LCA did not elicit a secretory response, it did attenuate forskolin-stimulated  $I_{sc}$  in T84 cells (**Table III** reported in (14)). To determine whether this inhibitory effect of LCA was conserved across cell types, HEK-CFTR cells were pretreated with LCA and examined its effect on forskolin- and CDCA-induced iodide efflux. Similar to its action in T84 cells (**Table III** reported in (14)), LCA significantly reduced both the forskolin (**Figure 42B**) and CDCA (**Figure 42C**) responses in HEK-CFTR cells. LCA significantly inhibited forskolin's rate of iodide efflux at 2, 4, and 6 minutes (**Figure 42B**). and the CDCA-induced iodide efflux at the later time points of 14-20 minutes (**Figure 42C**). This was similar to LCA action in T84 cells, wherein LCA caused the CDCA response to become transient (Area under curve: CDCA:  $258 \pm 36$  v +LCA:  $104 \pm 26$ ;  $n=3$ ;  $p=0.03$ ; **Table III**) and **Figure 42C** shows that CDCA alone is significantly higher than CDCA in the presence of LCA at the later time points. Collectively, these results suggest that LCA inhibits forskolin- and CDCA-activated Cl<sup>-</sup> transport in both HEK-293 and T84 cells. However, there may be differences in the inhibitory mechanisms since CDCA action in HEK cells is CFTR-independent.

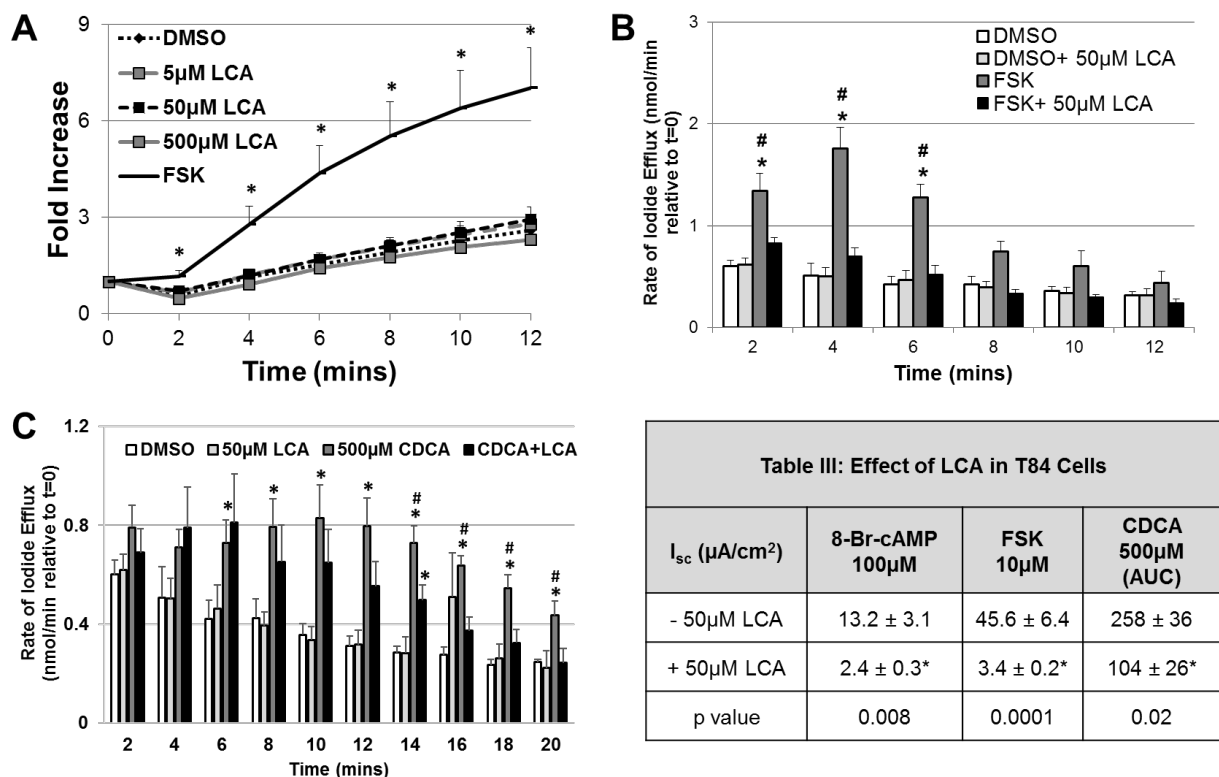


**Figure 42.** LCA action in HEK-CFTR cells [adapted from (14 and 77)].

**A.** Dose response of LCA (5-500 $\mu\text{M}$ ) on the fold increase of cumulative iodide efflux; forskolin (FSK; 10 $\mu\text{M}$ ) was used as positive control. The data are represented as the fold change of mean cumulative iodide efflux from basal efflux  $\pm$  SEM relative to value at starting point in HEK-CFTR cells;  $n \geq 3$ .

**B.** Effect of LCA on FSK-induced iodide efflux. Bars are the rate of iodide efflux stimulated with FSK  $\pm$  LCA (50 $\mu\text{M}$ ) in HEK-CFTR cells. Cells were pretreated with or without LCA for 15 minutes during iodide loading. DMSO was used as control. Data represent the mean rate of efflux (nmol/min)  $\pm$  SEM relative to value at starting point.  $n=4$ . \* denotes  $p < 0.05$  versus DMSO; # denotes  $p < 0.05$  versus FSK+LCA.

**C.** Effect of LCA on CDCA-Induced Iodide Efflux. Iodide efflux was measured in the presence of LCA (50 $\mu\text{M}$ ), and then stimulated with 500 $\mu\text{M}$  CDCA. The data are represented as the mean rate of iodide efflux (nmol/min)  $\pm$  SEM relative to value at starting point HEK-CFTR cells;  $n \geq 3$ . \* denotes  $p < 0.05$  versus DMSO; # denotes  $p < 0.05$  versus CDCA +LCA.

**Table III:** Effect of LCA in T84 cells on  $\text{Cl}^-$  secretion by 8-Br-cAMP (100  $\mu\text{M}$ ), forskolin (10 $\mu\text{M}$ ) and CDCA (500 $\mu\text{M}$ ).

### iii. LCA and 2<sup>nd</sup> Messenger Production

The effect of LCA on cAMP production and  $[Ca^{2+}]_i$  were measured since TGR5 may be coupled to  $G\alpha_s$  or  $G\alpha_q$ . Despite the expression of TGR5, exposure to 50 $\mu$ M LCA for 15 minutes did not alter intracellular cAMP concentrations but completely inhibited the forskolin-stimulated production of cAMP (**Figure 43A**). As we have demonstrated in T84 cells (14), LCA also increased  $[Ca^{2+}]_i$  in HEK-CFTR cells, (**Figure 43B**). Whether this rise in  $Ca^{2+}$  contributes to its inhibitory effect in HEK-CFTR cells remains to be determined; however in T84 cells, chelation of  $Ca^{2+}$  by BAPTA-AM did not reverse LCA's inhibitory effect (14).

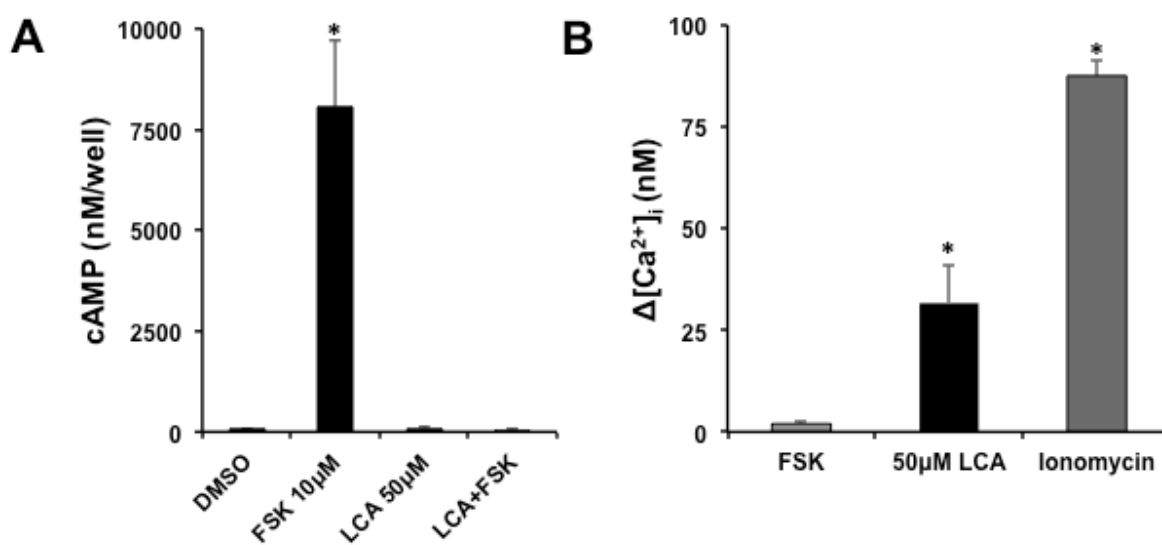


**Figure 43:** Measurements of 2<sup>nd</sup> messenger production by LCA in HEK-CFTR cells [adapted from (77)].

**A.** HEK-CFTR cells grown in 96 well-plates were incubated with 0.1% DMSO, 50 $\mu$ M LCA for 15 minutes, or 10 $\mu$ M forskolin for 5 minutes, or a combination of LCA pretreatment then stimulation with forskolin for  $[cAMP]_i$  measurements; cAMP is depicted as nM/well;  $n \geq 3$ .

**B.** Effect of LCA on Intracellular  $Ca^{2+}$ . HEK-CFTR cells grown in 35-mm glass-bottom dishes were loaded with Fura2-AM as described in the Methods, and the effects of 10 $\mu$ M forskolin, 50 $\mu$ M LCA and 3 $\mu$ M ionomycin on  $[Ca^{2+}]_i$  were assessed and displayed as  $\Delta[Ca^{2+}]_i$  (nM);  $n=4$ .

\* denotes  $p < 0.05$  versus forskolin as a negative control.

## **E. Discussion**

Epithelial Cl<sup>-</sup> transport and its regulation have been characterized in a number of reductionist human cell line models derived from a variety of tissues. A composite picture is emerging with the caveat that there is considerable tissue and cell line variation in the underlying regulatory cascades. The additional caveat is the complexity in translating this information from reductionist models into what occurs in human physiological and pathophysiological states. Nevertheless, the information from cell lines is invaluable and cell lines can be readily manipulated biochemically, genetically and pharmacologically. However, some cell lines, in particular those of intestinal origin, do not lend themselves readily to genetic manipulations, such as stable transfections, while retaining polarity and function. Therefore, to better understand the molecular regulation of Cl<sup>-</sup> secretion, we explored the utility of HEK-293 cells, well established for their versatility as a model for molecular manipulations.

HEK-293 cells are frequently used to study CFTR function and regulation in an over-expression system (189). Generally, HEK-293 cells have been used as a tool to explore specific steps in a series of regulatory interactions. Thus, although Cheng et al. used HEK-293 cells transfected with GFP-CFTR to examine CFTR interaction with CFTR associated ligand, the accompanying transport studies were done in CFBE14o-, a bronchial derived cell line (48). However, Mondini et al. used HEK-293 cells to examine the effect of a hypertension-linked mutation of  $\alpha$ -adducin on CFTR surface expression and channel activity (171). In these studies, HEK-293 cells stably transfected with wild type or mutant  $\alpha$ -adducin, and transiently transfected with pIRES2-CFTR-EGFP, which expressed separate EGFP and CFTR proteins, were used to assess CFTR activity by whole cell patch experiments. Additionally, HEK-293 cells have been used as a system to study the physical and functional interactions between phosphodiesterase 3A and CFTR by measuring adenosine-induced iodide efflux in cells overexpressing HA-tagged CFTR (189).

Studies in the present chapter have further validated these findings by developing a stably transfected HEK-(EGFP)-CFTR cell line, which allowed us to perform consistent measurements over time. Data presented in **Figure 32** demonstrated that the EGFP-CFTR is functional since HEK-CFTR but not HEK-293 cells respond to forskolin with a robust increase in iodide efflux as a measure of Cl<sup>-</sup> transport. The lack of a forskolin response in HEK-293 cells was likely because they neither expressed CFTR transcript nor CFTR protein (**Figure 30**). In HEK-CFTR cells the protein is associated with membrane and intravesicular compartments and can be readily visualized (**Figure 30**). These data demonstrate that the effects of forskolin on iodide efflux are due to its action on CFTR and not on other endogenously expressed Cl<sup>-</sup> channels. Minimally, HEK-293 cells possess transcripts for three other Cl<sup>-</sup> channels, CIC-2 and the Ca<sup>2+</sup>-activated Cl<sup>-</sup> channels, TMEM16A and TMEM16B (**Figure 30**) (96). There is evidence that these channels may be involved in Cl<sup>-</sup> secretion (64, 135), though if they were being activated by forskolin, then we would have observed forskolin-induced iodide efflux in both HEK-293 and HEK-CFTR cells. The use of the iodide efflux assay in assessing CIC-2 or TMEM16A function is less well documented compared to its use for assessing CFTR activation. Iodide efflux studies in Caco-2 cells with transfected antisense CIC-2 showed less iodide efflux compared to control transfected cells, suggesting that CIC-2s partially contribute to Cl<sup>-</sup> transport in these cells (170). Additionally, studies examining the action of TMEM16A using iodide influx with a halide-sensitive yellow fluorescent protein, established that TMEM16A can effectively transport iodide (111). Expression of TMEM16A in Axolotl oocytes showed halide permeabilities of iodide (3.8) > bromide (2.0) > chloride (1.0) (217). Finally, in HEK-293 cells transfected with endothelin receptor subtype-A and mouse TMEM16A, the latter showed the following halide permeabilities: iodide (1.85) > bromide (1.74) > chloride (1.0) > fluoride (0.43) (268). Thus, TMEM16A is capable of transporting iodide, however treatment with AO1 did not significantly inhibit CDCA-induced iodide efflux (**Figure 41B**).

In HEK-CFTR cells, forskolin increased intracellular cAMP but not  $\text{Ca}^{2+}$  (**Figure 43**).

Therefore, it was not surprising that the  $\text{Ca}^{2+}$  chelator BAPTA did not inhibit forskolin-stimulated iodide efflux (**Figure 35**). Interestingly, in T84 cells, the reports of forskolin increasing  $[\text{Ca}^{2+}]_i$  are variable, thus while we did not find forskolin to increase  $[\text{Ca}^{2+}]_i$  (14), others reporter a small, significant increase in  $[\text{Ca}^{2+}]_i$  (108, 167). The actions of forskolin in HEK-CFTR cells were inhibited by CFTRinh172 and by H89 (**Figure 33**). However, neither of these compounds completely inhibited the actions of forskolin in HEK-CFTR cells. Variability in the efficacy of CFTRinh172 to block CFTR-dependent iodide efflux in different cell types has been reported (223). While, Mondini et al. reported that CFTRinh172 completely blocked the forskolin-induced whole cell current in transiently CFTR transfected HEK-293 cells (171), Stahl et al. (233) demonstrated that different orthologs of CFTR respond differently to CFTR inhibitors. Thus, the variability in the efficacy of CFTRinh172 to inhibit CFTR-dependent responses in the HEK-CFTR cells may be due to the structure function relationship of the EGFP-CFTR protein, or due to differences in the source of the inhibitor, the relative insolubility of the compound in aqueous solution, or because in a stable over expression system this dose is insufficient to completely nullify the response.

Many elegant studies have demonstrated that CFTR, via protein-protein interactions with scaffolding and regulatory proteins, exists in a macromolecular complex. This allows for fine-tuning and spatiotemporal coupling of responses. One such coupling is between CFTR and MRP4 in HT29 colon carcinoma cells, where MRP4 functions as a cAMP transporter (141). In HT-29 cells, adenosine increases cAMP and activates CFTR, and inhibiting MRP4 accentuates this response by preventing cAMP extrusion. Findings in **Figure 34** suggest that MRP4 may be acting in a similar manner, though its inhibition only caused a moderate increase in iodide efflux and its effect on forskolin-stimulated cAMP production is equivocal. It is possible that the discrepancy between our findings and those of Li et al. is that the cAMP assay used in these

studies assessed global cAMP production whereas their study measured cAMP production in localized regions of the cell (141). Future studies using the FRET based EPAC-cAMP sensor will be needed to clarify increases in cAMP in microdomains of the cell.

Other studies demonstrate that in some, but not all cell types, activation of CFTR includes membrane trafficking and involves microtubules interaction and remodeling. Thus, Loffing et al. showed that cAMP activation of CFTR involves increased exocytosis in intestinal but not airway epithelial cells (149). We demonstrated that in T84 cells, the stimulation of Cl<sup>-</sup> transport by CDCA is partially inhibited by disruption of microtubules (15). However, in HEK-CFTR cells, despite the fact that nocodazole disrupts microtubules (**Figure 37A**), nocodazole had no effect on forskolin-stimulated Cl<sup>-</sup> transport (**Figure 37B**). In view of the known differences in microtubule dependent regulation of CFTR in intestinal versus respiratory epithelial cells, it is not surprising that HEK-CFTR cells behave like respiratory epithelia. However, microtubule-independent membrane trafficking can occur. Surprisingly, it appears that forskolin's activation of Cl<sup>-</sup> transport in HEK-CFTR does not cause any measurable changes in trafficking to the plasma membrane (**Figure 36A**). A time course of surface biotinylation could not detect a change in trafficking in response to forskolin. Similarly, we were unable to detect increased EGFP-CFTR in the plasma membrane in response to forskolin with live cell imaging (**Figure 36B**). The lack of trafficking is not due to a paucity of CFTR containing membrane vesicles, since EGFP-CFTR is prominently distributed in intracellular vesicles in HEK-CFTR cells. However, forskolin clearly increased the rate of vesicular movement in the cell. A further characterization of the molecular basis of this vesicular movement or its biphasic regulation by forskolin is warranted. For example, it remains to be determined if the inability of this increased movement to result in increased plasma membrane expression is a function of HEK-293 cell scaffolding machinery or the EGFP-CFTR construct per se. It is conceivable that the EGFP

moiety at the N-terminus of CFTR, despite a 2 amino acid spacer, may hinder some aspects of CFTR's interaction with other protein partners, such as syntaxin and thereby prevent trafficking.

The initial characterization of the HEK-CFTR cells with forskolin-induced iodide efflux measurements established the major signaling components that contribute to CDCA-induced  $\text{Cl}^-$  secretion in T84 cells. Therefore, we explored the use of HEK-CFTR cells to further elucidate bile acid regulation of CFTR activity. Similar to T84 cells (15), CDCA increased iodide efflux in HEK-CFTR cells (**Figure 39A**). Surprisingly, CDCA had the same effect on iodide efflux in the parent HEK-293 cells, suggesting CDCA-induced iodide efflux was independent of CFTR (**Figure 39B**). Furthermore, the CDCA response was not inhibited by CFTRinh172 (**Figure 40B**). The CFTR-independent response to CDCA, as well as the lack of increase in cAMP by CDCA in these cells ( $p > 0.05$ ,  $n = 3$ ), suggested contribution of another intracellular messenger and perhaps another  $\text{Cl}^-$  channel. As we established that CDCA could increase  $\text{Ca}^{2+}$  in T84 cells (**Chapter IV, Figure 15**), we assessed changes in  $[\text{Ca}^{2+}]_i$  by CDCA in HEK-293 cells. CDCA caused a robust increase in  $[\text{Ca}^{2+}]_i$  (**Figure 41A**) and therefore we speculated that TMEM16A (**Figure 30A**) could be mediating CDCA-induced iodide efflux. Pretreatment with the TMEM16A inhibitor A01 decreased the CDCA response, but this was not significant (**Figure 41B**). It is possible that TMEM16A is involved in the CDCA response, but it is not the major contributor, suggesting that another  $\text{Cl}^-$  transporter may be involved. This hypothesis is also supported by the lack of significant effect of BAPTA-AM on CDCA-induced iodide efflux (**Figure 41C**). Baseline efflux values in HEK-293 cells were not as robust as those in HEK-CFTR cells, so future studies will elucidate CDCA action in HEK-293 cells transfected with TMEM16A to get a better understanding of its role in CDCA action in these cells.

In addition to the regulation of  $\text{Cl}^-$  transport by CDCA, HEK-CFTR cells were used to corroborate our recent findings on LCA's inhibition of  $\text{Cl}^-$  transport in T84 cells (**Table III** reported in (14)). Similar to T84 cells (**Chapter III, Figure 8**), HEK-CFTR cells express transcript

and protein of TGR5 (**Figure 38**). Despite TGR5 expression, LCA as a potent TGR5 agonist failed to increase cAMP (**Figure 43A**) and to stimulate iodide efflux (**Figure 42A**) in these cells. However, LCA caused a modest increase in  $[Ca^{2+}]_i$  (**Figure 43B**). These findings were all consistent with LCA action in T84 cells (14). It is possible that in this cell line, the endogenous TGR5 is functionally coupled to G $\alpha_q$ , however this link is less well characterized than TGR5 being linked to production of cAMP. It remains to be elucidated whether the rise in  $[Ca^{2+}]_i$  by LCA contributes to its inhibitory response and studies of the effect of BAPTA-AM in LCA action in HEK-CFTR cells may confirm the role of  $[Ca^{2+}]_i$ . Studies performed in the human enteroendocrine cell line NCI-H716 showed that the synthetic TGR5 agonist INT-777 increased  $Ca^{2+}$  influx, which was reduced by TGR5 RNA interference. This study suggested that activation of TGR5 and production of cAMP was upstream of  $Ca^{2+}$  influx, as inhibition of adenylyl cyclase significantly reduced the calcium influx induced by INT-777 (244). The lack of an effect on cAMP by LCA is in contrast to the reports of Jensen et al. that HEK-293 cells stably transfected with TGR5 show increases in cAMP in response to LCA (115). There are perhaps two reasons for this discrepancy: first, the stably transfected cells probably have many more receptors than are present in the non-transfected cells; second, our confocal microscopy studies suggest that although present, TGR5 appears to be largely confined to intracellular vesicles (**Figure 38B**). However, while TGR5 in HEK-CFTR cells may not be “functionally-linked” to G $\alpha_s$  it remains to be determined if it still plays a role in the inhibitory effects of LCA on forskolin-stimulated iodide efflux in these cells. In other words, could LCA act via TGR5 to activate G $\alpha_q$ , increase  $[Ca^{2+}]_i$  and thereby completely inhibit forskolin-stimulated iodide efflux and production of cAMP? This inhibitory effect may not be specific to cAMP-dependent secretagogues as it is in T84 cells since LCA was also able to inhibit the CDCA-induced iodide efflux (**Figure 42C**). These findings suggest that LCA is negatively regulating a process that is required for forskolin and CDCA-induced iodide efflux, and it is possible that LCA is acting as a membrane perturbant. Explorations of the mechanism by which LCA is acting, the cross talk between the LCA and

forskolin signaling cascades, and whether this involves spatio-temporal coupling and macromolecular complexes could be the focus of future studies.

In summary, this chapter characterized the HEK-(EGFP)-CFTR cell line as a viable model for studying the regulation of forskolin-, but not CDCA-, induced Cl<sup>-</sup> transport, to mimic our findings in T84 cells. We are cognizant that this may not be entirely representative of a native epithelium. First, HEK-293 cells are not polarized. Second, there is the issue of the cellular origin of HEK-293 cells; some studies have revealed them to be of epithelial origin (46), and others debate their kidney nomenclature, or if they are more fibroblast like in nature. Through a serendipitous series of studies, Shaw et al have provided evidence that they were more similar to differentiating neurons in early stages (220). Therefore, when designing experiments using this cell line as a tool to study exogenous proteins, the endogenous signaling machinery and their possible origin should be taken into consideration.

## **Chapter VI. Results: CDCA Action in Intestinal Organoids**

### **A. Rationale and Aim**

Thus far, the data accumulated in this thesis has been in human-derived transformed cell lines. Although these findings are beneficial to our knowledge of bile acid signaling, there is a need to corroborate these findings in more physiologically relevant models. Intestinal organoid methodology is becoming one of the hallmark techniques in the field of gastrointestinal physiology as the organoids are derived from primary mammalian tissues (e.g. human, pig, and murine tissues) and can be used as long-term in vitro culture systems. Thus the focus of this chapter is to delineate CDCA activation *ex vivo* using intestinal organoids (**Aim 3**) as a proof of concept to our findings in **Aim 2**.

### **B. Relevance of Organoid Cultures**

Organoid cultures derived from primary tissues are able to be maintained at length (>1 year) in vitro, compared to previous methodologies of intestinal primary cultures where the cells are limited to a much shorter (a few days at the most) life span (200). The long-term culturing of organoids is based on the proliferative capacity of the stem cells (66, 209, 210). To maintain their proliferative capacity, organoids require a lamin-rich Matrigel suspension and media containing Wnt signaling growth factors. The organoids described in this chapter are composed only of epithelial cells and were derived from stem cells of adult mouse small and large intestine.

The development of assays to examine CFTR function by Liu et al. (147) and Dekkers et al. (67) validated the use of organoids to study ion and fluid transport. Since the organoids have an enclosed, epithelial-lined lumen, changes in the diameter or surface area (organoid swelling) of the organoids are indicative of fluid transport into the lumen. CFTR is highly expressed in the apical membrane of crypt cells, and since organoids are crypt-like in nature soon after

passaging, any changes in swelling of the organoids is representative of CFTR activation. This was verified in both human and mouse derived organoids where addition of forskolin only induced swelling in normal human and mouse organoids but not in mouse CFTR<sup>-/-</sup> or human CF derived organoids (67, 147). Thus, utilization of the organoid methodology and the swelling assay will allow elucidation of CDCA action in a more physiological model compared to the T84 and HEK cells lines. Generation of the organoids was previously established by the laboratory of Dr. Hugo de Jonge at Erasmus University Medical Center, Rotterdam, Netherlands. Organoid maintenance and swelling assays were performed under the guidance and supervision of the Erasmus collaborators, as described in methods (**Chapter II**).

### **C. Region Specific Organoid Swelling**

Elucidation of CDCA was first assessed in organoids derived from different regions of the mouse intestine. Organoids isolated from jejunum, ileum, and proximal colon were cultured for at least three passages before assaying, as described in the methods. One day after passaging and seeding in a 96-well plate, organoids were loaded with calcein green-AM. The acetoxymethyl ester attached to the calcein was cleaved by intracellular esterases in live cells and converted to a green-fluorescent calcein. Organoids were stimulated with ethanol (negative control), 500 $\mu$ M CDCA, or 10 $\mu$ M forskolin; swelling was imaged by confocal microscopy and analyzed using ImageJ. Since the apical membrane faces the organoid lumen, this preparation allows for addition of CDCA to the basolateral membrane, recapitulating our studies in T84 cells. **Figure 44** displays organoid swelling as the maximal increase in organoid diameter, with each point representing an individual organoid. In each region CDCA and forskolin slightly increased swelling compared to the negative control. Swelling in jejunal organoids were not significantly different from each other ( $p > 0.05$ ). Forskolin was significantly different from ethanol in both ileal and proximal colonic organoids ( $p < 0.05$ ), but was not different from CDCA ( $p > 0.05$ ) by 1-way

ANOVA. Although CDCA increased swelling in ileal and proximal colonic organoids, it was significantly different from control only in the proximal colonic organoids ( $p=0.08$  and  $0.05$ , respectively) by unpaired t-test.

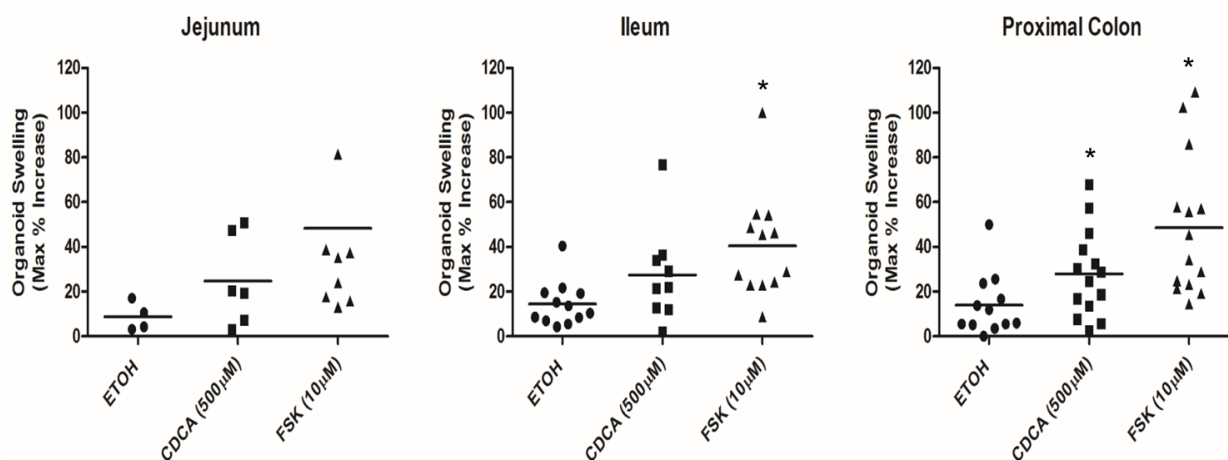


**Figure 44:** Mouse intestinal region specific organoid swelling. Mouse jejunum, ileum, and proximal colon organoids were loaded with calcein green-AM and imaged by confocal microscopy at 37°C according to Dekkers et al. (67). Organoids were imaged at  $t=0$  and then treated with ethanol (ETOH), 500µM CDCA, or 10µM forskolin (FSK). Images were taken over 1 hour. Data is represented as maximal increase in organoid diameter (organoids swelling) relative to diameter at  $t=0$ . Lines represent the average maximal diameter increase and comparisons were made by 1-way ANOVA. \* denotes significance compared to ETOH.

#### **D. EPAC and CDCA-Induced Organoid Swelling**

The effects of CDCA in colonic organoids was further studied as the colon is the predominant region where CDCA acts to increase electrolyte and fluid secretion leading to secretory diarrhea. To validate the role of EPAC in CDCA action, mouse colonic organoids were pretreated with ESI-09 (10 $\mu$ M) for 2 hours, and then stimulated with ethanol, CDCA, and forskolin as described above. As change in diameter is a 2 dimensional analysis and organoids are 3-dimensional spheroid structures, our collaborators and we pursued the notion that swelling is better represented as changes in surface area over time. Thus, **Figure 45** displays the change in surface area relative to surface area at t=0. The tracings are the average swelling of at least 3 wells per treatment, with each well containing at least 20 viable organoids. The dark blue and orange lines represent increases in organoid swelling by CDCA and forskolin, respectively. CDCA, and forskolin,  $\pm$  ESI-09 were significantly different from ethanol control and ESI-09 alone at all time points after t=0; ESI-09 was not different from control at any time point. Interestingly, ESI-09 decreased both the forskolin (yellow line) and the CDCA response (green line), however this decrease of the forskolin response was not statistically significant. In contrast, ESI-09 significantly decreased the CDCA (CDCA vs CDCA+ESI-09) response at all time points except at 54 minutes ( $p=0.07$ ). These results indicate that EPAC partially contributed to the CDCA-stimulated mouse colonic organoid swelling.

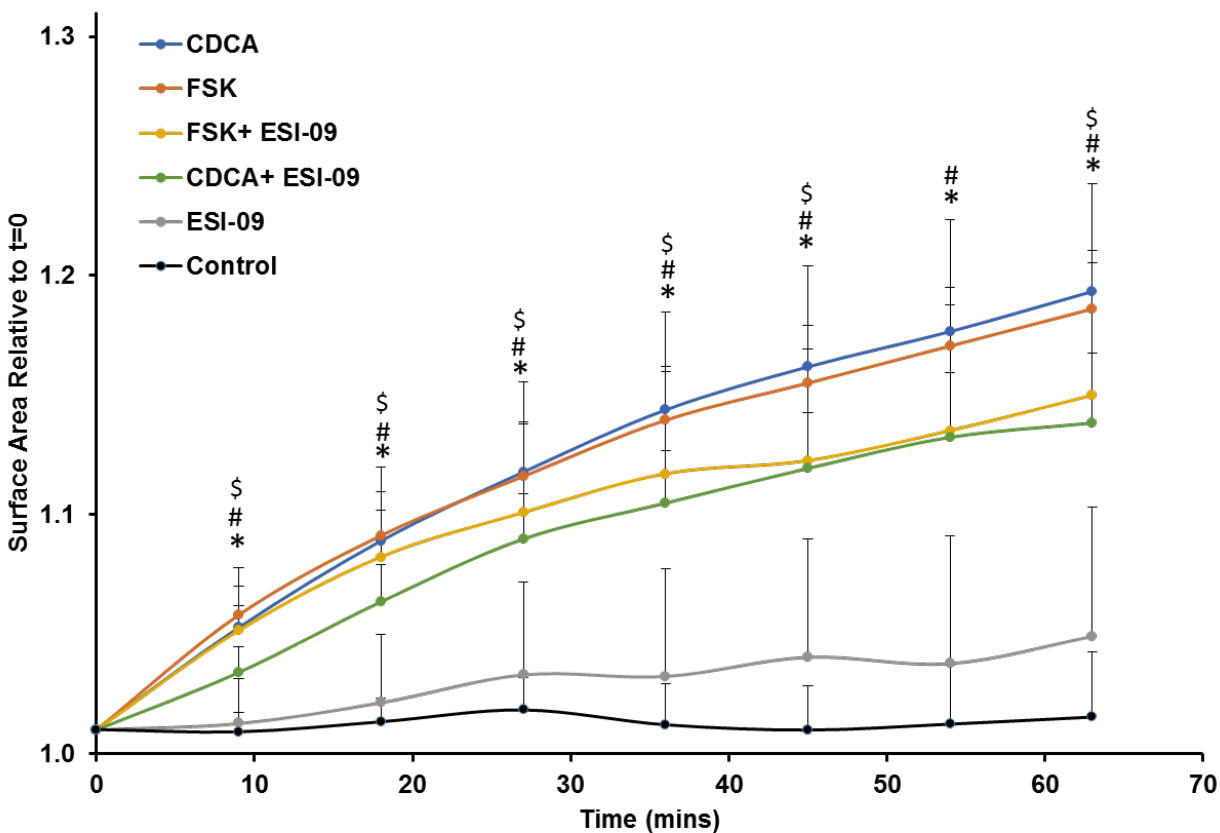


**Figure 45:** Effect of ESI-09 on mouse colonic organoid swelling. Tracings represent the changes in surface area over time relative to  $t=0$  in response to ethanol (control), forskolin (FSK;  $10\mu\text{M}$ ) and CDCA ( $500\mu\text{M}$ ), and treatments +ESI-09 ( $10\mu\text{M}$ ; 2 hour pretreatment) in mouse colonic organoids. Tracings are the average of at least 3 wells per treatment with at least 20 organoids per well. ESI-09 was not different from control.

\* denotes significance ( $p < 0.05$ ) compared to control for CDCA, FSK, and treatments + ESI-09; # denotes significance compared to ESI-09 alone for CDCA and FSK;

\$ denotes CDCA's significance compared to CDCA + ESI-09. FSK was not different from FSK+ESI-09 at any time point.

## **E. Discussion**

Transformed *in vitro* intestinal cell lines have been extremely useful models of intestinal transport functions for several decades. Prior to the development of intestinal organoid methodology, use of intestinal cell lines were limited due to their derivation from cancerous tissues, their possible immortalization by viral infection, and their expression of oncogenes. While these characteristics allowed for easy proliferation, other non-physiological phenotypic characteristics may have been introduced. These conditions restricted the usefulness of cell lines for recapitulating the normal gastrointestinal environment. While explanted intestinal tissue cultures were more physiological than cell lines, they were limited by their short-term survival (<2 weeks) in culture (66, 200).

Intestinal organoids have broken these limitations as long-term culture systems that can be derived from a variety of mammalian sources including from mouse tissue, human biopsies, and from pluripotent stem cells. Tissue-derived epithelial/mesenchymal organoids can be grown from both neonatal and adult tissue. This type of organoid was established by Ootani et al. using small pieces of small intestine and colon cultured in a collagen matrix and expanded in an air-liquid interface system to improve oxygenation *in vitro* (184). These cultures include the intestinal epithelium and the underlying myofibroblasts, and can be maintained for up to one year. Human embryonic stem cells, and induced pluripotent stem cells derived from human skin keratinocytes, can be differentiated into intestinal tissues in a step-by-step manner using specific growth factors that mimic embryonic development. This protocol included definitive endoderm formation, posterior endoderm patterning, hindgut development, and pro-intestinal growth factors to form intestinal organoids. This culturing method has the advantage of presence of supportive mesenchymal cells, but lacks neuronal and immune cells (232). This system is limited by its strict maintenance protocol, and that the organoid characteristics are more fetal-like in nature; for example, gene profiling demonstrated the similarity between these

cultures and organoids derived from human fetal intestine in contrast to adult intestinal-derived organoids (88). Furthermore, the mesenchymal cells provide proliferative support to the epithelial cells but due to the restrictive geometry of the organoid structures, hinder the ability of the epithelium to properly differentiate and function similar to the *in vivo* epithelium (275).

In contrast to the mesenchymal containing organoids, tissue-derived epithelial organoids, as described by Sato et al., can be generated from fetal or adult tissues and are established very rapidly but lack the underlying mesenchymal layer (66, 210, 275). This organoid methodology was used to assess CDCA's effects on ion transport as a more physiological model compared to the T84 and HEK-293 cell lines. One benefit of this culture system is the access to the basolateral side. The organoid develops such that the apical membranes of the epithelium are facing inward towards the lumen, leaving the basolateral membrane accessible. Some studies have utilized microinjection to administer agents or bacteria into the lumen of organoids (21, 263). Sidedness of bile acid action remains to be elucidated in the organoid cultures, but it may be predicted that the dihydroxy bile acids will elicit a stronger secretory response from the basolateral surface of the organoids compared to luminal exposure. This prediction is supported by our findings and others in T84 cells (**Chapter III**, (15, 72, 124), and studies in the rat colon (32).

These studies were preliminary but a definite proof of concept as CDCA induced organoid swelling comparable to the action of forskolin used as a positive control (**Figure 44**). Previous studies using mouse ileal tissues demonstrated that bile acids could have a pro-secretory effect dependent on CFTR (29). This effect was also dependent on bile acid uptake via ASBT. It still remains to be investigated if the same mechanism is occurring in ileal organoids. Studies will continue to investigate the CDCA response in other intestinal segments (**Figure 44**), and will seek to compare the effects of unconjugated and conjugated dihydroxy bile acids. It will also be interesting to investigate whether LCA's effect on organoid swelling mimics its anti-secretory

actions in T84 and HEK-CFTR cells. Furthermore, to definitively prove CDCA's activation of CFTR-dependent  $\text{Cl}^-$  secretion, studies must be done in CFTR<sup>-/-</sup> intestinal organoids.

As T84 cells were used as a model to examine the regulation of colonic  $\text{Cl}^-$  secretion, it was necessary to examine if similar regulatory mechanisms were in place in colonic organoids. The role of EPAC in regulating ion transport has been of interest in recent years, considering cAMP's effects had largely been attributed to PKA. Studies by Hoque and colleagues (108, 222) demonstrated the role of EPAC in regulating  $\text{Cl}^-$  and  $\text{K}^+$  conductances in T84 cells. Findings in the previous chapter demonstrated a role for EPAC in CDCA action, and we sought to mimic this novel finding in the mouse colonic organoids. Indeed, we found that EPAC inhibition decreased both the CDCA and forskolin responses, although only the CDCA response was significant, paralleling our findings in T84 cells (**Figure 45**). The inhibitory effect of ESI-09 was smaller in the colonic organoids, suggesting that the  $\text{Cl}^-$  secretory responses in this model may be more PKA-dependent. It is also possible that the partial inhibition was due to the Matrigel limiting direct access of ESI-09 to the organoids. This is true for CFTRinh172, which requires ~2 hour pretreatment for organoid swelling inhibition (67), while its effect in intestinal cell lines is immediate (15). Future studies will aim to elucidate the CDCA-induced signaling pathways in the colonic organoids and determine if they are similar or distinct from those we have described for T84 cells. If CDCA action in colonic organoids (in mouse and human) is dependent on CFTR, cAMP (PKA and EPAC), EGFR and  $\text{Ca}^{2+}$  then the organoid models could prove useful in identifying novel therapeutic target for bile acid-associated diarrheal diseases.

## **Chapter VII. General Conclusions and Future Directions**

It has been well established in a variety of species, including humans, that the 7 $\alpha$ -dihydroxy bile acids stimulate Cl<sup>-</sup> secretion. However, the underlying mechanisms were not fully elucidated (16, 17, 72, 118, 124, 250, 259). The objective of this thesis was to further investigate the signaling mechanisms by which CDCA induces pro-secretory responses from the colonic epithelium. This body of work demonstrates that, in human colonic T84 cells, CDCA action involves intricate crosstalk between cAMP (PKA and EPAC), Ca<sup>2+</sup>, and EGFR signaling cascades to fully activate CFTR (**Chapters III-IV**), while CDCA acts independently of CFTR in HEK-293 cells to stimulate Cl<sup>-</sup> transport (**Chapter V**). Finally, part of the CDCA signaling pathway established in T84 cells was corroborated in the more physiologically relevant intestinal organoid model (**Chapter VI**).

**Aim 1** was to determine the initial step by which CDCA acts to modulate Cl<sup>-</sup> secretion in T84 cells (**Chapter III**). As regulators, bile acids have been shown to activate nuclear receptors (FXR, PXR, VDR), GPCRs (TGR5 and M3R), as well as multiple signaling pathways in the gastrointestinal tract (51). Despite the expression of several of these receptors (FXR, TGR5, VDR, and M3R) in T84 cells, CDCA seemed to act independently of their activation. The muscarinic antagonist atropine eliminated the possibility of M3R's role and the lack of involvement of FXR and TGR5 was implied based on the use of pharmacological agonists since antagonists were not available. Agonists to various receptors are known to exhibit biased ligand binding (264) and it is possible that the FXR and TGR5 agonists used signal in a different manner than CDCA. Ultimately, knockdown of specific receptors individually, or in combination, would allow for the validation of their contribution to the acute action of CDCA on T84 cells. Interestingly, TGR5 knockout mice display defunct defecation due to decreased serotonin release and decreased peristalsis (5) and they also exhibit decreased activation of CFTR in cholangiocytes (126). Since T84 cells serve as a model of secretory colonocytes, it is possible that TGR5 is uncoupled from activation of CFTR due to lack of proper trafficking to the membrane, as is suggested by the punctate expression of TGR5 in immunofluorescence

localization in both T84 and HEK-293 cells. Taken together, in the intact colon under normal physiological conditions, TGR5 activation is required for normal peristaltic contractions to move the luminal contents towards the rectum for defecation. However, under pathological conditions, when there are increased bile acids in the colonic lumen, dihydroxy bile acids are likely acting on secretory colonocytes to stimulate Cl<sup>-</sup> secretion, while simultaneously activating TGR5 on enterochromaffin cells to increase serotonin releases and peristalsis, leading to bile acid associated-diarrhea.

Additionally, CDCA can exert transcriptional effects via FXR, which often requires a longer time frame (140) than the <30 minute window which we used in these studies. It would be intriguing to compare the effects of short-term exposure (<30 minutes) vs. chronic exposure (~24 hours) to CDCA on FXR-related genes that contribute to ion transport. Mroz et al. (173) showed that exposure to GW4064 (5μM) for 24 hours inhibited secretagogue-induced ion transport in an FXR-dependent manner. Furthermore, exposure to low doses of DCA (10-200μM) for 24 hours, inhibited cAMP- and Ca<sup>2+</sup>-dependent Cl<sup>-</sup> secretion, which may have been in an FXR-dependent manner (122). It is possible that long-term exposure to high doses of CDCA, considered pathophysiological, may have a similar effect since FXR has a higher affinity for CDCA. On the other hand, low versus high doses of dihydroxy bile acids may have different effects and CDCA-FXR regulated genes may be different from DCA-FXR related genes. Thus, while low doses decrease transporters that contribute to Cl<sup>-</sup> secretion, perhaps high doses may increase these transporters as a protective mechanism to increase flushing of the colonic lumen under pathological conditions.

While tauro-DCA transactivates EGFR via M3R in H508 colon cancer cells (49, 50), in T84 cells CDCA action is independent of M3R, but dependent on EGFR. Inhibition of MMPs, which mediate cleavage of EGFR ligands such as EGF, reduced the CDCA response. If CDCA was acting in an EGF-dependent manner, EGF alone should have been able to increase Cl<sup>-</sup> secretion, however EGF did not mimic CDCA action. Several other ligands have been

implicated in transactivation of EGFR, such as HB-EGF or TGF $\alpha$ , and their involvement in Cl<sup>-</sup> secretion can be elucidated by using ligand specific blocking antibodies and measuring the response to CDCA. This can then be confirmed by screening the media and cell lysates of CDCA-stimulated T84 cells for the presence of the specific EGFR-ligands.

EGFR has several phosphorylation sites including tyrosine 992, 1045, 1068, 1148, and 1173 that lie within its autophosphorylation domain. Specific phosphorylation of these autophosphorylation sites serve as a docking mechanism for binding of EGFR adaptor proteins. These include growth factor receptor-bound protein 2, SH2 domain containing transforming protein, and the growth factor receptor-bound protein 2-associated binding protein. Furthermore, EGFR has several more phosphorylation sites within the kinase domain that regulate downstream signaling cascades. For example, phosphorylation of tyrosines 992, 1101, and 1148 lead to activation of PLC $\gamma$ , PI3K/AKT, and MAPKs, respectively (183). Our studies examined CDCA-induced phosphorylation of tyrosine 1068, a site commonly associated with EGFR activation. The role of the other phosphorylation sites, or of the EGFR adaptor proteins, have yet to be identified in CDCA signaling. Although we ruled out involvement of MAPKs and PI3K/AKT activation in CDCA-induced Cl<sup>-</sup> secretion, it is conceivable that CDCA may activate PLC $\gamma$  in an EGFR-dependent manner, and thus CDCA would increase phosphorylation of tyrosine 992. If so, site specific mutagenesis of tyrosine 992 would decrease CDCA-induced production of IP<sub>3</sub> and [Ca<sup>2+</sup>].

Aside from ligand-dependent activation of EGFR, CDCA could be activating EGFR by altering membrane dynamics, presumably by intercalating into the plasma membrane, as suggested for DCA-induced ligand-independent EGFR activation (114, 196). In these studies, DCA increased EGFR phosphorylation which was blocked by AG1478, similar to our findings. However, neutralizing antibodies to EGF and TGF $\alpha$  did not block DCA's activation of EGFR (114). Interestingly, LCA and DCA have been shown to alter plasma membrane cholesterol, and alter membrane dynamics (114, 270, 271). While CFTR can be stabilized in lipid rafts and can

potentially be altered by hydrophobic bile acids incorporating into the membrane (1), it is unlikely that this is the case in the present studies. We showed that CDCA exerted its effects primarily from the basolateral membrane, while CFTR is localized to the apical membrane. It is possible to consider CDCA's stabilization of CFTR in lipid rafts in cases of bile acid malabsorption *in vivo*, but the influence of CDCA on membrane dynamics in T84 cells has yet to be investigated. However, due to the sidedness of CDCA action, it is more plausible that CDCA is acting on basolaterally localized EGFR (162, 269), and possibly on distinct phospholipids that are in high concentration in the basolateral membrane; the basolateral membranes of epithelial cells have a much higher concentration of phosphatidylcholine (~30%) compared to the apical membrane (<10%) (228).

CDCA initiated a complex signaling cascade (**Chapter IV**) that is likely mediated by an unknown, basolaterally localized, membrane bound receptor as hypothesized above. While S1PR2 and  $\alpha 5\beta 1$ -integrin have been implicated in bile acid action in hepatocytes, their function in intestinal epithelia, including T84 cells, remain to be investigated. While the protein expression of the GPCR S1PR2, is highest in the duodenum, it is minimally expressed in the colon (53). Moreover, the cAMP-dependency of CDCA action suggests a GPCR coupled to  $G\alpha_s$  rather than an integrin receptor, and there may be an orphan-GPCR that is specific to CDCA and mediating its effects on EGFR and  $Cl^-$  secretion. To investigate expression of potential GPCRs in T84 cells, we could screen their expression using T84 RNA in Taqman real time-PCR GPCR arrays, which have primers specific to more than 50 different GPCR subfamilies. Alternatively, CDCA could be conjugated to beads using CarboxyLink Coupling Gel, similar to the production of cholesterol-conjugated beads described by Takahashi et al. (241). CDCA-conjugated beads can then be exposed to T84 lysates to pull down any proteins that may bind to CDCA. Proteins in the pull down fraction can then be eluted with non-conjugated CDCA followed by mass spectrometry sequence analysis of CDCA-bound proteins. Receptors can

then be identified and specific shRNA can be used to knockdown the receptors and assess CDCA responses (163).

While **Chapter III** delineated receptor involvement, **Chapters IV** and **V** served to elucidate the intracellular signaling mechanisms underlying CDCA action, proposed in **Aim 2**. With the substantial evidence for the role of  $\text{Ca}^{2+}$  signaling in bile acid action from our laboratory (118, 250), and others (70-72, 191), it was no surprise that in addition to cAMP/PKA signaling,  $\text{Ca}^{2+}$  was also necessary for CDCA's full activation of  $\text{Cl}^-$  secretion. CDCA's increase of  $[\text{Ca}^{2+}]_i$  was dependent on intracellular stores as well as influx from the extracellular compartment, implying that CDCA may activate SOCE via plasma membrane  $\text{Ca}^{2+}$  channels (229). Orai and TRP  $\text{Ca}^{2+}$  channels have been shown to mediate SOCE in a variety of cells types (107). While Orais have yet to be described in T84 cells, TRPV6, a TRP channel highly selective for  $\text{Ca}^{2+}$ , has been shown to contribute to  $\text{Ca}^{2+}$  entry activated by  $17\beta$ -estradiol in T84 cells (112). To assess involvement of TRPV6-dependent  $\text{Ca}^{2+}$  entry in CDCA action, Ussing chamber studies can be performed using the TRPV6 inhibitor ruthenium red. Similarly, iodide efflux studies using T84 cells with siRNA knockdowns to Orai or TRP channels will allow for the determination of their contribution to CDCA-induced  $\text{Cl}^-$  transport. Interestingly, studies elucidating apical versus basolateral-dependent activation of  $\text{Cl}^-$  secretion showed that basolateral addition of carbachol lead to rises in  $[\text{Ca}^{2+}]_i$  and  $\text{Cl}^-$  secretion, and this was blocked by removal of  $\text{Ca}^{2+}$  from the basolateral buffers. This finding suggested that  $\text{Ca}^{2+}$  entry in T84 cells occurs across the basolateral membrane and contributes to activation of apical  $\text{Cl}^-$  channels (127). Comparable studies can be done with CDCA to determine if side-specific removal of  $\text{Ca}^{2+}$  affects CDCA-induced  $I_{sc}$ .

Use of the pharmacological agent 2-APB ( $50\mu\text{M}$ ) in Ussing chamber studies implied that  $\text{IP}_3\text{Rs}$  and subsequent  $\text{Ca}^{2+}$  release from intracellular stores were involved in CDCA-induced  $I_{sc}$ , however this inhibitor has also been shown to block SOCE. Maruyama et al. (159) first described 2-APB as an inhibitor of  $\text{IP}_3\text{Rs}$  with an  $\text{IC}_{50}$  of  $42\mu\text{M}$  in rat cerebellar microsomal

preparations. Bootman et al. described the inconsistency of 2-APB as an inhibitor of IP<sub>3</sub>Rs, with more consistency in inhibition of SOCE (35). To definitively prove if the inhibitor is acting on IP<sub>3</sub>Rs or SOCE in CDCA action in T84 cells, Fura2-AM measurements can be performed in the presence of 2-APB without [Ca<sup>2+</sup>]<sub>o</sub>. Since removal of [Ca<sup>2+</sup>]<sub>o</sub> partially decreased CDCA-induced [Ca<sup>2+</sup>]<sub>i</sub>, we assumed the remaining Ca<sup>2+</sup> response was due to release from intracellular stores. Thus, addition of 2-APB should completely block the remaining CDCA-induced Δ[Ca<sup>2+</sup>]<sub>i</sub> if it is indeed acting on IP<sub>3</sub>Rs. However, if there is no difference in CDCA-induced Δ[Ca<sup>2+</sup>]<sub>i</sub> in the absence of [Ca<sup>2+</sup>]<sub>o</sub> ± 2-APB, this would suggest that 2-APB is inhibiting SOCE.

It was assumed that Ca<sup>2+</sup> signaling occurred in a linear manner, such that CDCA increased IP<sub>3</sub>, which then activated IP<sub>3</sub>Rs on intracellular stores leading to release of Ca<sup>2+</sup>, depletion of the stores, and activation of SOCE, to increase [Ca<sup>2+</sup>]<sub>i</sub> and activate Cl<sup>-</sup> secretion. With this assumption, clearly an inhibition of store depletion would also inhibit SOCE. Since we assessed the need for [Ca<sup>2+</sup>]<sub>i</sub> in the presence of [Ca<sup>2+</sup>]<sub>o</sub>, treatment with 2-APB could have been inhibiting IP<sub>3</sub>R-dependent store release or SOCE. To determine if CDCA-induced I<sub>sc</sub> is dependent on Ca<sup>2+</sup> from intracellular stores, Ca<sup>2+</sup> entry, or a combination of both, measurements of I<sub>sc</sub> can be performed with removal of [Ca<sup>2+</sup>]<sub>o</sub> as described by Nichols et al. (182). If extracellular Ca<sup>2+</sup> is removed (to exclude SOCE contribution in CDCA-induced I<sub>sc</sub>), and addition of 2-APB further reduces the CDCA response (inhibition of IP<sub>3</sub>Rs), then the residual current should be solely PKA-dependent as all pathways contributing to cytosolic Ca<sup>2+</sup> increase have been negated. Alternatively, if the CDCA response is the same in preparations without [Ca<sup>2+</sup>]<sub>o</sub> ± 2-APB, then this would suggest that 2-APB is acting as a SOCE inhibitor and the residual current would be PKA and IP<sub>3</sub>R (release of Ca<sup>2+</sup> from intracellular stores)-dependent. In this case buffering the cell with BAPTA and 2-APB, should leave a residual current that is solely PKA-dependent.

In cases when there is no extracellular Ca<sup>2+</sup> and the store is depleted, there can be activation of SOcAMPS as recently described by A.M. Hofer and colleagues in NCM460 colonic cells (138, 154) as well as in T84 cells (182). It is possible that CDCA could also be acting

through SOcAMPS, but this would suggest that there are local regions with very low  $[Ca^{2+}]_o$ , and when CDCA acts in these areas there is a compartmentalized increase in cAMP. However, it is more likely that SOCE, rather than SOcAMPS, is involved in CDCA action in T84 cells since CDCA's increases in  $[Ca^{2+}]_i$  were dependent on both intracellular and extracellular  $Ca^{2+}$ . Furthermore, SOcAMPS was independent of rises in  $[Ca^{2+}]_i$ , such that BAPTA-AM did not affect SOcAMPS-dependent  $I_{sc}$ . This cannot be the case with CDCA since pretreatment with BAPTA-AM significantly decreased CDCA-induced  $I_{sc}$ , thus if CDCA was working in a SOcAMPS-dependent manner, then it would be insensitive to BAPTA-AM. Additionally, if the experiments described above reveal a contribution of SOCE to CDCA-induced  $I_{sc}$ , then SOcAMPS would not be activated.

In addition to the involvement of  $Ca^{2+}$  signaling, as well as our previous findings on the contribution of PKA and CDCA-induced CFTR phosphorylation (15), the role of EGFR delineated in **Chapter III** implied that CDCA activated a variety of signaling cascades. Stimulation of T84 cells with CDCA led to an increase in the activation of several kinases that are associated with EGFR. Although CDCA significantly increased p38 and ERK 1/2, their individual inhibition, or combined inhibition had no effect on the CDCA-secretory response. Thus, p38 and ERK 1/2 may be involved in other physiological aspects of bile acid signaling, but not  $Cl^-$  secretion. These MAPKs are considered survival kinases, and are typically activated when cells are stressed. In hepatocytes, bile acids activate both of these pathways as well as the FAS-receptor, such that anti- and pro-apoptotic pathways are activated simultaneously. Inhibition of the MAPKs potentiates bile acid-induced apoptosis (195, 196, 216). Unpublished results by our colleagues show that CDCA increases cytotoxicity and epithelial permeability (91), thus it is possible that p38 and ERK 1/2 kinases are activated because CDCA is inducing a stress response similar to bile acid action in hepatocytes. Furthermore, DCA and CDCA have been shown to increase IL-8 production in a p38-dependent manner in squamous epithelial cells

(219). Interestingly, our colleagues have also found that CDCA induces IL-8 release from T84 cells (69), and it is conceivable that this may be via a p38-dependent mechanism.

The lack of involvement of the MAPKs in CDCA-induced  $\text{Cl}^-$  secretion lead us to hypothesize that PI3K may mediate CDCA signaling downstream of EGFR, however LY294002 had no effect. Interestingly 500nM wortmannin, another PI3K inhibitor, did attenuate the CDCA response. This implies that other target kinases for wortmannin, such as myosin light chain kinase, may be involved in CDCA action (39, 178, 242). To test the involvement of myosin light chain kinase,  $I_{\text{sc}}$  can be measured in the presence of myosin light chain kinase inhibitors ML-7 and ML-9. Alternatively, EGFR may be modulating activation of PLC (183), since PLC activation is implicated in CDCA action. As mentioned above, phosphorylation of tyrosine 992 on EGFR leads to activation of PLC $\gamma$ . Therefore, it would be intriguing to measure the CDCA-induced  $\text{IP}_3$  production in the presence of the EGFR inhibitor or in EGFR silenced cells. If PLC signaling is leading to  $\text{IP}_3$ -dependent  $[\text{Ca}^{2+}]_i$  increases, then Fura2-AM measurements can be performed in EGFR inhibited or silenced cells.

Our results implicated the role of EPAC-Rap2 signaling as a bridge between cAMP and  $\text{Ca}^{2+}$  in CDCA action. Additionally, CDCA may be causing a cAMP-dependent transactivation of EGFR. EPAC bridges cAMP and  $\text{Ca}^{2+}$  cascades by activation of Rap2 (108). If so, it is also possible that the EPAC-dependent increases in  $\text{Ca}^{2+}$  are mediating transactivation of EGFR. CDCA required MMP activation for full  $I_{\text{sc}}$  responses, and MMP cleavage of EGFR ligands is dependent on  $\text{Ca}^{2+}$  (68, 193, 280). If such is the case in T84 cells, then CDCA-induced activation of EPAC would lead to increases in  $[\text{Ca}^{2+}]_i$ , activation of MMPs and ligand cleavage to transactivate EGFR.

Although it is well known that  $\text{Ca}^{2+}$  contributes to  $\text{Cl}^-$  secretion, how  $\text{Ca}^{2+}$  modulates CFTR activation is undefined. T84 cells express all 9 membrane bound adenylyl cyclases (129), thus it is possible that  $\text{Ca}^{2+}$  may be activating the  $\text{Ca}^{2+}$ -dependent adenylyl cyclases to increase cAMP and activation of CFTR. In addition to  $\text{Ca}^{2+}$ -dependent adenylyl cyclases, Billet and Hanrahan

proposed that CFTR could also be modulated by  $\text{Ca}^{2+}$ -dependent activation of tyrosine kinases, which can inhibit phosphatases or which can phosphorylate CFTR directly (30), suggesting a possible role for EGFR inhibition of phosphatases or direct phosphorylation of CFTR. Moreover, cAMP is known to act in two ways to increase activation of CFTR: 1) PKA-dependent phosphorylation; and 2) increase in CFTR at the apical membrane via exocytosis (8, 99, 240, 246). Recruitment of CFTR has yet to be related to EPAC action specifically but there is some evidence that cAMP-PKA are involved in CFTR regulation (36, 246), however exocytosis is often considered a  $\text{Ca}^{2+}$ -dependent process. Based on the data presented here, one could hypothesize that in T84 cells, CDCA's induction of  $\text{Ca}^{2+}$  signaling contributes to CFTR activation by increasing exocytosis of CFTR to the plasma membrane. Thus, while PKA phosphorylates CFTR, increases its open probability and contributes to membrane exocytosis, EPAC-Rap2- $\text{Ca}^{2+}$  signaling may further increase CFTR incorporation into the membrane. This could be determined by measuring changes in cell surface biotinylated CFTR induced by CDCA  $\pm$  ESI-09 to inhibit EPAC, as well as  $\pm$  H89 to assess the involvement of PKA-dependent processes. If the CDCA-induced biotinylated fraction of CFTR is decreased in the presence of either ESI-09 or H89, it would suggest that both EPAC and PKA are involved in CFTR exocytosis.

In an effort to better understand bile acid regulation of CFTR, we developed and characterized a HEK-CFTR cell line in **Chapter V** (77). Forskolin action in HEK-CFTR cells was dose-, CFTR-, and PKA- dependent. While H89 significantly reduced the forskolin response, the remaining response was still significantly higher than vehicle control for most time points. It is possible that forskolin-induced iodide efflux may also involve EPAC, such that ESI-09 may block the H89 insensitive iodide efflux. Similar to a partial inhibition with H89, CFTRinh172 did not fully block forskolin's effect. It is unlikely that this is due to the activation of another channel, since forskolin was unable to increase iodide efflux in parental HEK-293 cells. It is conceivable that the inhibitor's efficacy is reduced in an over-expression system as compared to one in which CFTR is endogenously expressed, such as T84 cells. The HEK-CFTR model may require

the combined addition of CFTRinh172 and another CFTR inhibitor such as GlyH-101, to fully attenuate the forskolin response. Based on the initial characterization with forskolin, the HEK-CFTR cell line seemed useful to further study CDCA action. It was surprising to find that CDCA increased iodide efflux in both HEK-293 and HEK-CFTR cells, which suggested that CDCA was acting via another  $\text{Cl}^-$  channel expressed in HEK-293 cells. Although CDCA caused a significant rise in  $[\text{Ca}^{2+}]_i$ , CDCA-induced iodide efflux was not significantly decreased by inhibition of TMEM16A with 20 $\mu\text{M}$  AO1 or by BAPTA-AM. Although these data suggest that TMEM6A may not be involved, it would nevertheless be intriguing to examine CDCA action in HEK-293 cells either over-expressing TMEM16A or in which TMEM16A has been silenced. It is also possible that CIC-2 may be contributing to  $\text{Cl}^-$  transport in these cells. Finally it is possible that HEK-293 cells may be more sensitive to the detergent properties of CDCA compared to T84 cells, and maybe membrane perturbations are sufficient to increase non-specific iodide efflux.

Unlike CDCA's cell type-dependent signaling, LCA's effects in HEK-CFTR cells parallel our recently published findings in T84 cells (14). LCA did not stimulate iodide efflux, but it did significantly inhibit both the forskolin- and CDCA-induced iodide efflux in HEK-CFTR cells (77). These findings, taken with the findings in T84 cells (14), suggest that LCA is modulating a common mechanism required for  $\text{Cl}^-$  transport in general. In T84 cells LCA inhibited  $\text{K}^+$  channel activity, which will block the driving force for  $\text{Cl}^-$  secretion regardless of the identity of the  $\text{Cl}^-$  channel. It is possible that this is also occurring in the HEK-CFTR cells. In polarized epithelial monolayers it is easy to determine the contribution of specific ion transporters on the apical and basolateral membranes. HEK-293 cells are not epithelial cells, and either indirect measurements of channel activity or patch clamp methodology will need to be utilized to better understand transport functions. For example, if forskolin is activating a  $\text{K}^+$  channel in HEK-CFTR cells, and this is inhibited by LCA,  $\text{K}^+$  channel activation may be measured using the FluxOR Potassium Ion Channel assay from Molecular Probes. In brief,  $\text{K}^+$  channels are permeable to thalium, such that when a  $\text{K}^+$  channel becomes activated, thalium will enter the cytosol and

fluorescence of FluxOR will increase. Using this assay, if LCA inhibits  $K^+$  channel activity, then the forskolin-induced change in fluorescence should be decreased compared to forskolin alone.

Taken together, these findings further confirmed the differences in bile acid specificity being pro (CDCA)- and anti (LCA)-secretory. However, they demonstrated cell type-specificity of CDCA action, where CDCA activates CFTR in epithelial cells, but not in non-epithelial cells. It would be intriguing to elucidate CDCA action in other cell types typically used for genetic manipulations such as CHO and HeLa cells to see if CDCA also works in a CFTR-independent manner. It is also possible that the HEK-293 cells don't express the same "receptor" as T84 cells, such that CDCA action is not linked CFTR-dependent iodide efflux. If a CDCA receptor can be identified by GPCR-array screening, then HEK-293 and HEK-CFTR cells can again be used to assess CDCA-stimulated iodide efflux while overexpressing the GPCR.

Findings from **Chapters III** and **IV** were partially validated using *ex vivo* intestinal epithelial organoids in **Chapter VI**. Organoids used in this study were of small intestinal and colonic crypt origin, and formed a simple spheroid structure with an enclosed lumen surrounded by an epithelial monolayer. This model was very useful as we were able to demonstrate that CDCA could induce organoid swelling, paralleling CDCA's activation of  $Cl^-$  secretion in T84 cells. Furthermore, we found that EPAC was involved in CDCA-induced colonic organoid swelling. These studies were preliminary and ongoing investigations will elucidate bile acid specificity and sidedness of action. Furthermore, EPAC is one aspect of the CDCA signaling cascade in T84 cells, and it would be intriguing to measure the role of PKA and  $Ca^{2+}$  in the CDCA-induced changes in these cells. Additionally, LCA's inhibition of organoid swelling would validate our results in T84 (14) and HEK-CFTR cells (77).

As is the case of validating new models, the organoids need to be characterized, specifically by examining the expression of known transporters, as well as cell type-specific proteins. Results suggested that CDCA's effect on organoid swelling may be specific to the region of the intestine, with its strongest pro-secretory effects in the colon. Our lab has previously shown both

region and age-specific differences in bile acid action in the rabbit intestine (118, 250, 259) and it would be interesting to see similar responses in intestinal organoids. Though mouse studies are more physiological than *in vitro* cell lines, recapitulating the CDCA signaling in human-derived organoids would be ideal. Since organoids express all the cell types of the intestinal epithelium, their use will allow for the elucidation of bile acid action on all the cell types, rather than just focusing on the secretory cells modeled by the T84 cell line.

The goal of this thesis was to elucidate potential mechanisms that contribute to bile acid-associated diarrhea. Diarrhea is not only the consequence of excessive secretion, but is also the consequence of a decrease in absorptive processes. Interestingly, a recent study by Pallagi-Kunstar et al. demonstrated that bile acids, specifically CDCA, inhibit NHEs and  $\text{Cl}^-/\text{HCO}_3^-$  exchangers in a  $\text{Ca}^{2+}$ -dependent manner, contributing to the development of diarrhea (187). This finding substantiated the study by Alrefai et al. (7) where tauro-DCA and glycol-CDCA inhibited  $\text{Cl}^-/\text{OH}^-$  exchange in Caco-2 cells. Specifically, tauro-DCA action was dependent on  $\text{Ca}^{2+}$ , PKC $\beta$ , and PI3K. Furthermore, unpublished studies in collaboration with our colleague Dr. J. Sarathy at Benedictine University (Lisle, IL), have demonstrated that apical addition of high concentrations of CDCA disrupt epithelial barrier integrity, redistribute tight junction proteins, and increase pro-inflammatory cytokine release from T84 cells (69, 91, 128).

Taking the findings in this body of work, with the above cited studies, and with the previous work done on bile acid signaling, I propose that under conditions of increased colonic bile acids, such as that of irritable bowel syndrome or inflammatory bowel diseases, there is bile acid-associated disruption of the epithelial barrier and increased pro-inflammatory cytokine production. Loosening of tight junctions (69, 91, 128) allows for bile acids to reach the basolateral surface where they can initiate signaling cascades to inhibit absorptive processes (7, 187) and activate secretory processes, manifesting in bile acid-induced diarrhea. CDCA specifically acts via a basolaterally localized receptor to induced cAMP-dependent activation of PKA and EPAC. PKA leads to an increase in phosphorylation of CFTR (15), while EPAC

activates Rap2 and PLC $\epsilon$ -dependent production of Ca<sup>2+</sup>. This initial increase in Ca<sup>2+</sup> can then activate MMPs which will lead to transactivation of EGFR (**Chapter III and IV**). EGFR will then stimulate PLC $\gamma$  to further increase Ca<sup>2+</sup> signaling (**Chapter IV and VI**), contributing to a robust increase in Cl<sup>-</sup> secretion via CFTR (**Figure 46**).

All of these studies look at the action of one bile acid at a time, which is not fully representative of the *in vivo* environment, as other bile acid species will be present in the colon. Thus it would be intriguing to look at the regulation of the bile acid signaling pathways when there is more than one type of bile acid present. These studies would be performed with bile acid combinations that mimic their *in vivo* concentrations under normal and pathophysiological conditions. It is conceivable that the fine tuning of the pathways resulting in hyper- or hypo-activation of transport processes is controlled by the relative concentrations of the different bile acids. Currently, bile acid sequestrants are useful for people that suffer from bile acid malabsorption, but they are known to cause constipation, diarrhea, bloating, flatulence, and interference of lipid-soluble vitamin absorption. Hence, there is a need for identifying more direct therapies, which will not have adverse side effects, and could be based on the signaling mechanisms described in this work. For example, identification of a receptor related to bile acid activation of Cl<sup>-</sup> secretion or inhibition of absorption could be a therapeutic target for patients that suffer from bile acid-associated diarrheas. This investigation has provided a framework for bile acid signaling and will lay the foundation for future studies in understanding bile acid-associated diarrheas.

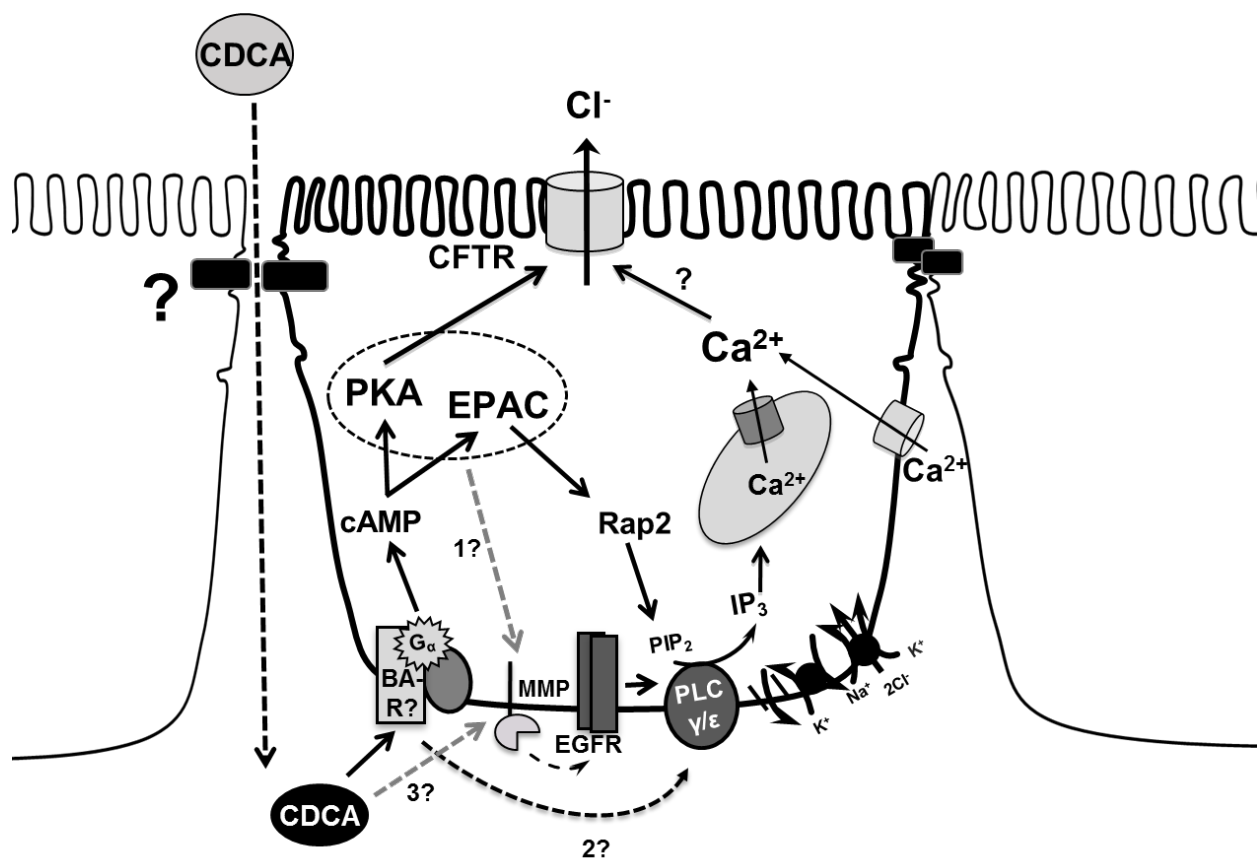


**Figure 46:** Summary of the complex network of signaling cascade induced by CDCA. CDCA activates Cl $^-$  secretion in a rapid manner from the basolateral side. Activation of an unidentified bile acid receptor (BA-R) results in cAMP activation of PKA and EPAC. PKA phosphorylates CFTR (15) and EPAC activates Rap2 to lead to an increase in Ca $^{2+}$  which further contributes to activation of CFTR. PKA and EPAC may also be transactivating EGFR (dotted line 1) which further modulates the signaling pathways that contribute to CDCA-induced Cl $^-$  secretion. CDCA may be initiating this signaling cascade through an unidentified bile acid receptor that may be activating PLC directly (dotted line 2), or CDCA may be acting via membrane perturbations (dotted line 3).

## CHAPTER VII. CITED LITERATURE

1. **Abu-Arish A, Pandzic E, Goepf J, Matthes E, Hanrahan JW, and Wiseman PW.** Cholesterol modulates CFTR confinement in the plasma membrane of primary epithelial cells. *Biophysical journal* 109: 85-94, 2015.
2. **Ahlberg J, Angelin B, Bjorkhem I, and Einarsson K.** Individual bile acids in portal venous and systemic blood serum of fasting man. *Gastroenterology* 73: 1377-1382, 1977.
3. **Ajouz H, Mukherji D, and Shamseddine A.** Secondary bile acids: an underrecognized cause of colon cancer. *World journal of surgical oncology* 12: 164, 2014.
4. **Alberts B, Johnson A, Lewis J, Morgan D, Raff M, Roberts K, Walter P, Wilson J, and Hunt T.** *Molecular biology of the cell*. p. xxxiv, 1342, 1334, 1353, 1341 pages.
5. **Alemi F, Poole DP, Chiu J, Schoonjans K, Cattaruzza F, Grider JR, Bunnett NW, and Corvera CU.** The receptor TGR5 mediates the prokinetic actions of intestinal bile acids and is required for normal defecation in mice. *Gastroenterology* 144: 145-154, 2013.
6. **Alrefai WA, and Gill RK.** Bile acid transporters: structure, function, regulation and pathophysiological implications. *Pharm Res* 24: 1803-1823, 2007.
7. **Alrefai WA, Saksena S, Tyagi S, Gill RK, Ramaswamy K, and Dudeja PK.** Taurodeoxycholate modulates apical Cl<sup>-</sup>/OH<sup>-</sup> exchange activity in Caco2 cells. *Digestive diseases and sciences* 52: 1270-1278, 2007.
8. **Ameen NA, Marino C, and Salas PJ.** cAMP-dependent exocytosis and vesicle traffic regulate CFTR and fluid transport in rat jejunum in vivo. *American journal of physiology Cell physiology* 284: C429-438, 2003.
9. **Anantamongkol U, Ao M, Sarathy Nee Venkatasubramanian J, Devi YS, Krishnamra N, and Rao MC.** Prolactin and dexamethasone regulate second messenger-stimulated Cl<sup>-</sup> secretion in mammary epithelia. *Journal of signal transduction* 2012: 192142, 2012.
10. **Anbzhagan AN, Priyamvada S, Kumar A, Maher DB, Borthakur A, Alrefai WA, Malakooti J, Kwon JH, and Dudeja PK.** Translational repression of SLC26A3 by miR-494 in intestinal epithelial cells. *American journal of physiology Gastrointestinal and liver physiology* 306: G123-131, 2014.
11. **Annaba F, Ma K, Kumar P, Dudeja AK, Kineman RD, Shneider BL, Saksena S, Gill RK, and Alrefai WA.** Ileal apical Na<sup>+</sup>-dependent bile acid transporter ASBT is upregulated in rats with diabetes mellitus induced by low doses of streptozotocin. *American journal of physiology Gastrointestinal and liver physiology* 299: G898-906, 2010.
12. **Annaba F, Sarwar Z, Gill RK, Ghosh A, Saksena S, Borthakur A, Hecht GA, Dudeja PK, and Alrefai WA.** Enteropathogenic Escherichia coli inhibits ileal sodium-dependent bile acid transporter ASBT. *American journal of physiology Gastrointestinal and liver physiology* 302: G1216-1222, 2012.

13. **Annaba F, Sarwar Z, Kumar P, Saksena S, Turner JR, Dudeja PK, Gill RK, and Alrefai WA.** Modulation of ileal bile acid transporter (ASBT) activity by depletion of plasma membrane cholesterol: association with lipid rafts. *American journal of physiology Gastrointestinal and liver physiology* 294: G489-497, 2008.
14. **Ao M, Domingue JC, Khan N, Javed F, Osmani K, Sarathy J, and Rao MC.** Lithocholic acid attenuates cAMP-dependent Cl<sup>-</sup> secretion in human colonic epithelial T84 cells. *American journal of physiology Cell physiology* 310: C1010-1023, 2016.
15. **Ao M, Sarathy J, Domingue J, Alrefai WA, and Rao MC.** Chenodeoxycholic acid stimulates Cl<sup>-</sup> secretion via cAMP signaling and increases cystic fibrosis transmembrane conductance regulator phosphorylation in T84 cells. *American journal of physiology Cell physiology* 305: C447-456, 2013.
16. **Ao M, Venkatasubramanian J, Boonkaewwan C, Ganesan N, Syed A, Benya RV, and Rao MC.** Lubiprostone activates Cl<sup>-</sup> secretion via cAMP signaling and increases membrane CFTR in the human colon carcinoma cell line, T84. *Digestive diseases and sciences* 56: 339-351, 2011.
17. **Bajor A, Gillberg PG, and Abrahamsson H.** Bile acids: short and long term effects in the intestine. *Scandinavian journal of gastroenterology* 45: 645-664, 2010.
18. **Bali M, Lipecka J, Edelman A, and Fritsch J.** Regulation of ClC-2 chloride channels in T84 cells by TGF- $\alpha$ . *American journal of physiology Cell physiology* 280: C1588-1598, 2001.
19. **Barker N, van Es JH, Kuipers J, Kujala P, van den Born M, Cozijnsen M, Haeghebarth A, Korving J, Begthel H, Peters PJ, and Clevers H.** Identification of stem cells in small intestine and colon by marker gene Lgr5. *Nature* 449: 1003-1007, 2007.
20. **Barrett KE.** Positive and negative regulation of chloride secretion in T84 cells. *The American journal of physiology* 265: C859-868, 1993.
21. **Bartfeld S, Bayram T, van de Wetering M, Huch M, Begthel H, Kujala P, Vries R, Peters PJ, and Clevers H.** In vitro expansion of human gastric epithelial stem cells and their responses to bacterial infection. *Gastroenterology* 148: 126-136 e126, 2015.
22. **Bayerdorffer E, Mannes GA, Ochsenkuhn T, Dirschedl P, Wiebecke B, and Paumgartner G.** Unconjugated secondary bile acids in the serum of patients with colorectal adenomas. *Gut* 36: 268-273, 1995.
23. **Bayerdorffer E, Mannes GA, Richter WO, Ochsenkuhn T, Wiebecke B, Kopcke W, and Paumgartner G.** Increased serum deoxycholic acid levels in men with colorectal adenomas. *Gastroenterology* 104: 145-151, 1993.
24. **Berne RM, and Levy MN.** *Principles of physiology*. St. Louis: Mosby, 2000, p. xix, 680 p.
25. **Bertelsen LS, Barrett KE, and Keely SJ.** Gs protein-coupled receptor agonists induce transactivation of the epidermal growth factor receptor in T84 cells: implications for epithelial secretory responses. *The Journal of biological chemistry* 279: 6271-6279, 2004.

26. **Bevins CL, and Salzman NH.** Paneth cells, antimicrobial peptides and maintenance of intestinal homeostasis. *Nature reviews Microbiology* 9: 356-368, 2011.
27. **Bhalla S, Ozalp C, Fang S, Xiang L, and Kemper JK.** Ligand-activated pregnane X receptor interferes with HNF-4 signaling by targeting a common coactivator PGC-1alpha. Functional implications in hepatic cholesterol and glucose metabolism. *The Journal of biological chemistry* 279: 45139-45147, 2004.
28. **Bijvelds MJ, Bot AG, Escher JC, and De Jonge HR.** Activation of intestinal Cl<sup>-</sup> secretion by lubiprostone requires the cystic fibrosis transmembrane conductance regulator. *Gastroenterology* 137: 976-985, 2009.
29. **Bijvelds MJ, Jorna H, Verkade HJ, Bot AG, Hofmann F, Agellon LB, Sinaasappel M, and de Jonge HR.** Activation of CFTR by ASBT-mediated bile salt absorption. *American journal of physiology Gastrointestinal and liver physiology* 289: G870-879, 2005.
30. **Billet A, and Hanrahan JW.** The secret life of CFTR as a calcium-activated chloride channel. *The Journal of physiology* 591: 5273-5278, 2013.
31. **Binder HJ, Filburn C, and Volpe BT.** Bile salt alteration of colonic electrolyte transport: role of cyclic adenosine monophosphate. *Gastroenterology* 68: 503-508, 1975.
32. **Binder HJ, and Rawlins CL.** Effect of conjugated dihydroxy bile salts on electrolyte transport in rat colon. *The Journal of clinical investigation* 52: 1460-1466, 1973.
33. **Biscardi JS, Maa MC, Tice DA, Cox ME, Leu TH, and Parsons SJ.** c-Src-mediated phosphorylation of the epidermal growth factor receptor on Tyr845 and Tyr1101 is associated with modulation of receptor function. *The Journal of biological chemistry* 274: 8335-8343, 1999.
34. **Boonkaewwan C, Ao M, Toskulkao C, and Rao MC.** Specific immunomodulatory and secretory activities of stevioside and steviol in intestinal cells. *Journal of agricultural and food chemistry* 56: 3777-3784, 2008.
35. **Bootman MD, Collins TJ, Mackenzie L, Roderick HL, Berridge MJ, and Peppiatt CM.** 2-aminoethoxydiphenyl borate (2-APB) is a reliable blocker of store-operated Ca<sup>2+</sup> entry but an inconsistent inhibitor of InsP<sub>3</sub>-induced Ca<sup>2+</sup> release. *FASEB journal : official publication of the Federation of American Societies for Experimental Biology* 16: 1145-1150, 2002.
36. **Borthwick LA, McGaw J, Conner G, Taylor CJ, Gerke V, Mehta A, Robson L, and Muimo R.** The formation of the cAMP/protein kinase A-dependent annexin 2-S100A10 complex with cystic fibrosis conductance regulator protein (CFTR) regulates CFTR channel function. *Molecular biology of the cell* 18: 3388-3397, 2007.
37. **Bright-Asare P, and Binder HJ.** Stimulation of colonic secretion of water and electrolytes by hydroxy fatty acids. *Gastroenterology* 64: 81-88, 1973.
38. **Brunner H, Northfield TC, Hofmann AF, Go VL, and Summerskill WH.** Gastric emptying and secretion of bile acids, cholesterol, and pancreatic enzymes during digestion. Duodenal perfusion studies in healthy subjects. *Mayo Clinic proceedings* 49: 851-860, 1974.

39. **Burdyga TV, and Wray S.** The effect of inhibition of myosin light chain kinase by Wortmannin on intracellular  $[Ca^{2+}]$ , electrical activity and force in phasic smooth muscle. *Pflugers Archiv : European journal of physiology* 436: 801-803, 1998.
40. **Calmus Y, Guechot J, Podevin P, Bonnefis MT, Giboudeau J, and Poupon R.** Differential effects of chenodeoxycholic and ursodeoxycholic acids on interleukin 1, interleukin 6 and tumor necrosis factor-alpha production by monocytes. *Hepatology* 16: 719-723, 1992.
41. **Camilleri M.** Advances in understanding of bile acid diarrhea. *Expert review of gastroenterology & hepatology* 8: 49-61, 2014.
42. **Camilleri M, and Gores GJ.** Therapeutic targeting of bile acids. *American journal of physiology Gastrointestinal and liver physiology* 309: G209-215, 2015.
43. **Caputo A, Caci E, Ferrera L, Pedemonte N, Barsanti C, Sondo E, Pfeffer U, Ravazzolo R, Zegarra-Moran O, and Galletta LJ.** TMEM16A, a membrane protein associated with calcium-dependent chloride channel activity. *Science* 322: 590-594, 2008.
44. **Carlos MA, Nwagwu C, Ao M, Venkatasubramanian J, Boonkaewwan C, Prasad R, Chowdhury SA, Vidyasagar D, and Rao MC.** Epidermal growth factor stimulates chloride transport in primary cultures of weanling and adult rabbit colonocytes. *Journal of pediatric gastroenterology and nutrition* 44: 300-311, 2007.
45. **Cartwright CA, McRoberts JA, Mandel KG, and Dharmasathaphorn K.** Synergistic action of cyclic adenosine monophosphate- and calcium-mediated chloride secretion in a colonic epithelial cell line. *The Journal of clinical investigation* 76: 1837-1842, 1985.
46. **Chan CW, Song Y, Ailenberg M, Wheeler M, Pang SF, Brown GM, and Silverman M.** Studies of melatonin effects on epithelia using the human embryonic kidney-293 (HEK-293) cell line. *Endocrinology* 138: 4732-4739, 1997.
47. **Chappe V, Hinkson DA, Zhu T, Chang XB, Riordan JR, and Hanrahan JW.** Phosphorylation of protein kinase C sites in NBD1 and the R domain control CFTR channel activation by PKA. *The Journal of physiology* 548: 39-52, 2003.
48. **Cheng J, Cebotaru V, Cebotaru L, and Guggino WB.** Syntaxin 6 and CAL mediate the degradation of the cystic fibrosis transmembrane conductance regulator. *Molecular biology of the cell* 21: 1178-1187, 2010.
49. **Cheng K, and Raufman JP.** Bile acid-induced proliferation of a human colon cancer cell line is mediated by transactivation of epidermal growth factor receptors. *Biochemical pharmacology* 70: 1035-1047, 2005.
50. **Cheng K, Xie G, and Raufman JP.** Matrix metalloproteinase-7-catalyzed release of HB-EGF mediates deoxycholytaurine-induced proliferation of a human colon cancer cell line. *Biochemical pharmacology* 73: 1001-1012, 2007.
51. **Chiang JY.** Bile acid metabolism and signaling. *Comprehensive Physiology* 3: 1191-1212, 2013.

52. **Chiang JY.** Regulation of bile acid synthesis: pathways, nuclear receptors, and mechanisms. *Journal of hepatology* 40: 539-551, 2004.
53. **Chiang JY.** Sphingosine-1-phosphate receptor 2: a novel bile acid receptor and regulator of hepatic lipid metabolism? *Hepatology* 61: 1118-1120, 2015.
54. **Chin D, and Means AR.** Calmodulin: a prototypical calcium sensor. *Trends in cell biology* 10: 322-328, 2000.
55. **Chow JY, Uribe JM, and Barrett KE.** A role for protein kinase cepsilon in the inhibitory effect of epidermal growth factor on calcium-stimulated chloride secretion in human colonic epithelial cells. *The Journal of biological chemistry* 275: 21169-21176, 2000.
56. **Cipriani S, Mencarelli A, Chini MG, Distrutti E, Renga B, Bifulco G, Baldelli F, Donini A, and Fiorucci S.** The bile acid receptor GPBAR-1 (TGR5) modulates integrity of intestinal barrier and immune response to experimental colitis. *PloS one* 6: e25637, 2011.
57. **Cipriani S, Mencarelli A, Palladino G, and Fiorucci S.** FXR activation reverses insulin resistance and lipid abnormalities and protects against liver steatosis in Zucker (fa/fa) obese rats. *Journal of lipid research* 51: 771-784, 2010.
58. **Clarke LL, and Harline MC.** CFTR is required for cAMP inhibition of intestinal Na<sup>+</sup> absorption in a cystic fibrosis mouse model. *The American journal of physiology* 270: G259-267, 1996.
59. **Clevers H.** The intestinal crypt, a prototype stem cell compartment. *Cell* 154: 274-284, 2013.
60. **Conley DR, Coyne MJ, Bonorris GG, Chung A, and Schoenfield LJ.** Bile acid stimulation of colonic adenylate cyclase and secretion in the rabbit. *The American journal of digestive diseases* 21: 453-458, 1976.
61. **Cooper DM.** Regulation and organization of adenylyl cyclases and cAMP. *The Biochemical journal* 375: 517-529, 2003.
62. **Cowen AE, Korman MG, Hofmann AF, and Cass OW.** Metabolism of lithocholate in healthy man. I. Biotransformation and biliary excretion of intravenously administered lithocholate, lithocholyglycine, and their sulfates. *Gastroenterology* 69: 59-66, 1975.
63. **Cremers CM, Knoefler D, Vitvitsky V, Banerjee R, and Jakob U.** Bile salts act as effective protein-unfolding agents and instigators of disulfide stress in vivo. *Proceedings of the National Academy of Sciences of the United States of America* 111: E1610-1619, 2014.
64. **Cuppoletti J, Malinowska DH, Tewari KP, Li QJ, Sherry AM, Patchen ML, and Ueno R.** SPI-0211 activates T84 cell chloride transport and recombinant human CIC-2 chloride currents. *American journal of physiology Cell physiology* 287: C1173-1183, 2004.
65. **Dawson PA, and Karpen SJ.** Intestinal transport and metabolism of bile acids. *Journal of lipid research* 56: 1085-1099, 2015.

66. **Dedhia PH, Bertaux-Skeirik N, Zavros Y, and Spence JR.** Organoid Models of Human Gastrointestinal Development and Disease. *Gastroenterology* 2016.
67. **Dekkers JF, Wiegerinck CL, de Jonge HR, Bronsveld I, Janssens HM, de Winter-de Groot KM, Brandsma AM, de Jong NW, Bijvelds MJ, Scholte BJ, Nieuwenhuis EE, van den Brink S, Clevers H, van der Ent CK, Middendorp S, and Beekman JM.** A functional CFTR assay using primary cystic fibrosis intestinal organoids. *Nature medicine* 19: 939-945, 2013.
68. **Dethlefsen SM, Raab G, Moses MA, Adam RM, Klagsbrun M, and Freeman MR.** Extracellular calcium influx stimulates metalloproteinase cleavage and secretion of heparin-binding EGF-like growth factor independently of protein kinase C. *Journal of cellular biochemistry* 69: 143-153, 1998.
69. **Detloff SJ, Khan N, Ao M, Movva B, Nair T, Sirajuddin H, Domingue J, Rao MC, and Sarathy J.** The Yin and Yang of Bile Acid Action on Tight Junctions in Colonic Epithelia: A Putative Role for Pro-inflammatory Cytokines. *FASEB journal : official publication of the Federation of American Societies for Experimental Biology* 30: 1223.1229, 2016.
70. **Devor DC, Sekar MC, Frizzell RA, and Duffey ME.** Taurodeoxycholate activates potassium and chloride conductances via an IP<sub>3</sub>-mediated release of calcium from intracellular stores in a colonic cell line (T84). *The Journal of clinical investigation* 92: 2173-2181, 1993.
71. **Dharmsathaphorn K, Cohn J, and Beuerlein G.** Multiple calcium-mediated effector mechanisms regulate chloride secretory responses in T84-cells. *The American journal of physiology* 256: C1224-1230, 1989.
72. **Dharmsathaphorn K, Huott PA, Vongkovit P, Beuerlein G, Pandol SJ, and Ammon HV.** Cl<sup>-</sup> secretion induced by bile salts. A study of the mechanism of action based on a cultured colonic epithelial cell line. *The Journal of clinical investigation* 84: 945-953, 1989.
73. **Dharmsathaphorn K, and Madara JL.** Established intestinal cell lines as model systems for electrolyte transport studies. *Methods in enzymology* 192: 354-389, 1990.
74. **Dharmsathaphorn K, McRoberts JA, Mandel KG, Tisdale LD, and Masui H.** A human colonic tumor cell line that maintains vectorial electrolyte transport. *The American journal of physiology* 246: G204-208, 1984.
75. **DiBaise IRa.** Bile Acids: An Underrecognized and Underappreciated Cause of Chronic Diarrhea. *Practical Gastroenterology* 110: 32-44, 2012.
76. **Dickson JL, Conner TD, and Ecay TW.** Inhibition of phosphatidylinositol 3-kinase does not alter forskolin-stimulated Cl<sup>-</sup> secretion by T84 cells. *American journal of physiology Cell physiology* 278: C865-872, 2000.
77. **Domingue JC, Ao M, Sarathy J, George A, Alrefai WA, Nelson DJ, and Rao MC.** HEK-293 cells expressing the cystic fibrosis transmembrane conductance regulator (CFTR): a model for studying regulation of Cl<sup>-</sup> transport. *Physiological reports* 2: 2014.

78. **Duboc H, Tache Y, and Hofmann AF.** The bile acid TGR5 membrane receptor: from basic research to clinical application. *Digestive and liver disease : official journal of the Italian Society of Gastroenterology and the Italian Association for the Study of the Liver* 46: 302-312, 2014.
79. **Duran C, and Hartzell HC.** Physiological roles and diseases of Tmem16/Anoctamin proteins: are they all chloride channels? *Acta pharmacologica Sinica* 32: 685-692, 2011.
80. **Ecay TW, Dickson JL, and Conner TD.** Wortmannin inhibition of forskolin-stimulated chloride secretion by T84 cells. *Biochimica et biophysica acta* 1467: 54-64, 2000.
81. **Estrada Y, Dong J, and Ossowski L.** Positive crosstalk between ERK and p38 in melanoma stimulates migration and in vivo proliferation. *Pigment cell & melanoma research* 22: 66-76, 2009.
82. **Eyssen H, Van Eldere J, Parmentier G, Huijghebaert S, and Mertens J.** Influence of microbial bile salt desulfation upon the fecal excretion of bile salts in gnotobiotic rats. *Journal of steroid biochemistry* 22: 547-554, 1985.
83. **Fallah G, Romer T, Detro-Dassen S, Braam U, Markwardt F, and Schmalzing G.** TMEM16A(a)/anoctamin-1 shares a homodimeric architecture with CLC chloride channels. *Molecular & cellular proteomics : MCP* 10: M110 004697, 2011.
84. **Fasano A, Budillon G, Guandalini S, Cuomo R, Parrilli G, Cangioti AM, Morroni M, and Rubino A.** Bile acids reversible effects on small intestinal permeability. An in vitro study in the rabbit. *Digestive diseases and sciences* 35: 801-808, 1990.
85. **Field M.** Intestinal ion transport and the pathophysiology of diarrhea. *The Journal of clinical investigation* 111: 931-943, 2003.
86. **Fiorotto R, Spirli C, Fabris L, Cadamuro M, Okolicsanyi L, and Strazzabosco M.** Ursodeoxycholic acid stimulates cholangiocyte fluid secretion in mice via CFTR-dependent ATP secretion. *Gastroenterology* 133: 1603-1613, 2007.
87. **Fiorucci S, and Distrutti E.** Bile Acid-Activated Receptors, Intestinal Microbiota, and the Treatment of Metabolic Disorders. *Trends in molecular medicine* 21: 702-714, 2015.
88. **Fordham RP, Yui S, Hannan NR, Soendergaard C, Madgwick A, Schweiger PJ, Nielsen OH, Vallier L, Pedersen RA, Nakamura T, Watanabe M, and Jensen KB.** Transplantation of expanded fetal intestinal progenitors contributes to colon regeneration after injury. *Cell stem cell* 13: 734-744, 2013.
89. **Foulke-Abel J, In J, Yin J, Zachos NC, Kovbasnjuk O, Estes MK, de Jonge H, and Donowitz M.** Human Enteroids as a Model of Upper Small Intestinal Ion Transport Physiology and Pathophysiology. *Gastroenterology* 150: 638-649 e638, 2016.
90. **Freel RW, Hatch M, Earnest DL, and Goldner AM.** Dihydroxy bile salt-induced alterations in NaCl transport across the rabbit colon. *The American journal of physiology* 245: G808-815, 1983.

91. **French S, Framarin N, Badar A, Akhtar I, Ao M, Domingue J, Rao MC, and Sarathy J.** Effect of the Bile Acids Unconjugated and Conjugated, Chenodeoxycholic Acid and Deoxycholic Acid, on Epithelial Tight Junction Barrier Function in a Human Colon Carcinoma Cell Line, T84. *FASEB journal : official publication of the Federation of American Societies for Experimental Biology* 28: 1113.1113, 2014.
92. **Fuller CM, Bridges RJ, and Benos DJ.** Forskolin- but not ionomycin-evoked Cl<sup>-</sup> secretion in colonic epithelia depends on intact microtubules. *Am J Physiol* 266: C661-668, 1994.
93. **Gadsby DC, and Nairn AC.** Control of CFTR channel gating by phosphorylation and nucleotide hydrolysis. *Physiological reviews* 79: S77-S107, 1999.
94. **Garcia-Canaveras JC, Donato MT, Castell JV, and Lahoz A.** Targeted profiling of circulating and hepatic bile acids in human, mouse, and rat using a UPLC-MRM-MS-validated method. *Journal of lipid research* 53: 2231-2241, 2012.
95. **Gelbmann CM, Schteingart CD, Thompson SM, Hofmann AF, and Barrett KE.** Mast cells and histamine contribute to bile acid-stimulated secretion in the mouse colon. *The Journal of clinical investigation* 95: 2831-2839, 1995.
96. **George A, Domingue J, Ao M, Sarathy J, and Rao MC.** Chenodeoxycholate (CDCA) activation of Ca<sup>2+</sup>-dependent Cl<sup>-</sup> transport in human embryonic kidney-293 cells (HEK\_293) is CFTR-independent. *FASEB journal : official publication of the Federation of American Societies for Experimental Biology* 29: LB764, 2015.
97. **Gill RK, Borthakur A, Hodges K, Turner JR, Clayburgh DR, Saksena S, Zaheer A, Ramaswamy K, Hecht G, and Dudeja PK.** Mechanism underlying inhibition of intestinal apical Cl<sup>-</sup>/OH exchange following infection with enteropathogenic E. coli. *The Journal of clinical investigation* 117: 428-437, 2007.
98. **Gohlke H, Schmitz B, Sommerfeld A, Reinehr R, and Haussinger D.** alpha5 beta1-integrins are sensors for tauroursodeoxycholic acid in hepatocytes. *Hepatology* 57: 1117-1129, 2013.
99. **Golin-Bisello F, Bradbury N, and Ameen N.** STa and cGMP stimulate CFTR translocation to the surface of villus enterocytes in rat jejunum and is regulated by protein kinase G. *American journal of physiology Cell physiology* 289: C708-716, 2005.
100. **Graham FL, Smiley J, Russell WC, and Nairn R.** Characteristics of a human cell line transformed by DNA from human adenovirus type 5. *The Journal of general virology* 36: 59-74, 1977.
101. **Greve JW, Gouma DJ, and Buurman WA.** Bile acids inhibit endotoxin-induced release of tumor necrosis factor by monocytes: an in vitro study. *Hepatology* 10: 454-458, 1989.
102. **Halpern MD, and Dvorak B.** Does abnormal bile acid metabolism contribute to NEC? *Seminars in perinatology* 32: 114-121, 2008.

103. **Head BP, Patel HH, Roth DM, Murray F, Swaney JS, Niesman IR, Farquhar MG, and Insel PA.** Microtubules and actin microfilaments regulate lipid raft/caveolae localization of adenylyl cyclase signaling components. *The Journal of biological chemistry* 281: 26391-26399, 2006.
104. **Herbst RS.** Review of epidermal growth factor receptor biology. *International journal of radiation oncology, biology, physics* 59: 21-26, 2004.
105. **Hofmann AF.** Bile acids: trying to understand their chemistry and biology with the hope of helping patients. *Hepatology* 49: 1403-1418, 2009.
106. **Hofmann AF.** The continuing importance of bile acids in liver and intestinal disease. *Archives of internal medicine* 159: 2647-2658, 1999.
107. **Hogan PG, and Rao A.** Store-operated calcium entry: Mechanisms and modulation. *Biochemical and biophysical research communications* 460: 40-49, 2015.
108. **Hoque KM, Woodward OM, van Rossum DB, Zachos NC, Chen L, Leung GP, Guggino WB, Guggino SE, and Tse CM.** Epac1 mediates protein kinase A-independent mechanism of forskolin-activated intestinal chloride secretion. *The Journal of general physiology* 135: 43-58, 2010.
109. **Huang C, Hepler JR, Chen LT, Gilman AG, Anderson RG, and Mumby SM.** Organization of G proteins and adenylyl cyclase at the plasma membrane. *Molecular biology of the cell* 8: 2365-2378, 1997.
110. **Inagaki T, Choi M, Moschetta A, Peng L, Cummins CL, McDonald JG, Luo G, Jones SA, Goodwin B, Richardson JA, Gerard RD, Repa JJ, Mangelsdorf DJ, and Kliewer SA.** Fibroblast growth factor 15 functions as an enterohepatic signal to regulate bile acid homeostasis. *Cell metabolism* 2: 217-225, 2005.
111. **Iosco C.** Characterization of new molecular targets involved in iodide flux in the thyroid gland: the anoctamins. In: *Biochemistry* University of Bologna, 2012, p. 172.
112. **Irnaten M, Blanchard-Gutton N, and Harvey BJ.** Rapid effects of 17beta-estradiol on epithelial TRPV6 Ca<sup>2+</sup> channel in human T84 colonic cells. *Cell calcium* 44: 441-452, 2008.
113. **Irwin ME, Bohin N, and Boerner JL.** Src family kinases mediate epidermal growth factor receptor signaling from lipid rafts in breast cancer cells. *Cancer biology & therapy* 12: 718-726, 2011.
114. **Jean-Louis S, Akare S, Ali MA, Mash EA, Jr., Meuillet E, and Martinez JD.** Deoxycholic acid induces intracellular signaling through membrane perturbations. *The Journal of biological chemistry* 281: 14948-14960, 2006.
115. **Jensen DD, Godfrey CB, Niklas C, Canals M, Kocan M, Poole DP, Murphy JE, Alemi F, Cottrell GS, Korbmacher C, Lambert NA, Bunnnett NW, and Corvera CU.** The bile acid receptor TGR5 does not interact with beta-arrestins or traffic to endosomes but transmits sustained signals from plasma membrane rafts. *The Journal of biological chemistry* 288: 22942-22960, 2013.

116. **Joyce SA, MacSharry J, Casey PG, Kinsella M, Murphy EF, Shanahan F, Hill C, and Gahan CG.** Regulation of host weight gain and lipid metabolism by bacterial bile acid modification in the gut. *Proceedings of the National Academy of Sciences of the United States of America* 111: 7421-7426, 2014.
117. **Kadamur G, and Ross EM.** Mammalian phospholipase C. *Annual review of physiology* 75: 127-154, 2013.
118. **Kanchanapoo J, Ao M, Prasad R, Moore C, Kay C, Piyachaturawat P, and Rao MC.** Role of protein kinase C-delta in the age-dependent secretagogue action of bile acids in mammalian colon. *American journal of physiology Cell physiology* 293: C1851-1861, 2007.
119. **Kang G, Chepurny OG, and Holz GG.** cAMP-regulated guanine nucleotide exchange factor II (Epac2) mediates Ca<sup>2+</sup>-induced Ca<sup>2+</sup> release in INS-1 pancreatic beta-cells. *The Journal of physiology* 536: 375-385, 2001.
120. **Katsuma S, Hirasawa A, and Tsujimoto G.** Bile acids promote glucagon-like peptide-1 secretion through TGR5 in a murine enteroendocrine cell line STC-1. *Biochemical and biophysical research communications* 329: 386-390, 2005.
121. **Kawamata Y, Fujii R, Hosoya M, Harada M, Yoshida H, Miwa M, Fukusumi S, Habata Y, Itoh T, Shintani Y, Hinuma S, Fujisawa Y, and Fujino M.** A G protein-coupled receptor responsive to bile acids. *The Journal of biological chemistry* 278: 9435-9440, 2003.
122. **Keating N, Mroz MS, Scharl MM, Marsh C, Ferguson G, Hofmann AF, and Keely SJ.** Physiological concentrations of bile acids down-regulate agonist induced secretion in colonic epithelial cells. *Journal of cellular and molecular medicine* 13: 2293-2303, 2009.
123. **Keely SJ, and Barrett KE.** p38 mitogen-activated protein kinase inhibits calcium-dependent chloride secretion in T84 colonic epithelial cells. *American journal of physiology Cell physiology* 284: C339-348, 2003.
124. **Keely SJ, Scharl MM, Bertelsen LS, Hagey LR, Barrett KE, and Hofmann AF.** Bile acid-induced secretion in polarized monolayers of T84 colonic epithelial cells: Structure-activity relationships. *American journal of physiology Gastrointestinal and liver physiology* 292: G290-297, 2007.
125. **Keely SJ, Uribe JM, and Barrett KE.** Carbachol stimulates transactivation of epidermal growth factor receptor and mitogen-activated protein kinase in T84 cells. Implications for carbachol-stimulated chloride secretion. *The Journal of biological chemistry* 273: 27111-27117, 1998.
126. **Keitel V, Cupisti K, Ullmer C, Knoefel WT, Kubitz R, and Haussinger D.** The membrane-bound bile acid receptor TGR5 is localized in the epithelium of human gallbladders. *Hepatology* 50: 861-870, 2009.
127. **Kerstan D, Thomas J, Nitschke R, and Leipziger J.** Basolateral store-operated Ca<sup>2+</sup>-entry in polarized human bronchial and colonic epithelial cells. *Cell calcium* 26: 253-260, 1999.

128. **Khan N, Hung D, Javed F, Shukla P, Detloff SJ, Ao M, Domingue J, Rao MC, and Sarathy J.** Bile Acid, Lithocholic Acid, Reverses Chenodeoxycholate- and Cytokine-Induced Loss in Epithelial Barrier Function in Human Colon Carcinoma T84 Cells. *FASEB journal : official publication of the Federation of American Societies for Experimental Biology* 29: 998.991, 2015.
129. **Kolachala VL, Obertone TS, Wang L, Merlin D, and Sitaraman SV.** Adenosine 2b receptor (A2bR) signals through adenylate cyclase (AC) 6 isoform in the intestinal epithelial cells. *Biochimica et biophysica acta* 1760: 1102-1108, 2006.
130. **Kovacs E, Zorn JA, Huang Y, Barros T, and Kuriyan J.** A structural perspective on the regulation of the epidermal growth factor receptor. *Annual review of biochemistry* 84: 739-764, 2015.
131. **Kraus S, Benard O, Naor Z, and Seger R.** c-Src is activated by the epidermal growth factor receptor in a pathway that mediates JNK and ERK activation by gonadotropin-releasing hormone in COS7 cells. *The Journal of biological chemistry* 278: 32618-32630, 2003.
132. **Kryczka J, Stasiak M, Dziki L, Mik M, Dziki A, and Cierniewski C.** Matrix metalloproteinase-2 cleavage of the beta1 integrin ectodomain facilitates colon cancer cell motility. *The Journal of biological chemistry* 287: 36556-36566, 2012.
133. **Kuipers F, and Groen AK.** FXR: the key to benefits in bariatric surgery? *Nature medicine* 20: 337-338, 2014.
134. **Kumar DP, Asgharpour A, Mirshahi F, Park SH, Liu S, Imai Y, Nadler JL, Grider JR, Murthy KS, and Sanyal AJ.** Activation of Transmembrane Bile Acid Receptor TGR5 Modulates Pancreatic Islet alpha Cells to Promote Glucose Homeostasis. *The Journal of biological chemistry* 291: 6626-6640, 2016.
135. **Kunzelmann K, Schreiber R, Kmit A, Jantarajit W, Martins JR, Faria D, Kongsuphol P, Ousingsawat J, and Tian Y.** Expression and function of epithelial anoctamins. *Experimental physiology* 97: 184-192, 2012.
136. **Kurdi P, Kawanishi K, Mizutani K, and Yokota A.** Mechanism of growth inhibition by free bile acids in lactobacilli and bifidobacteria. *Journal of bacteriology* 188: 1979-1986, 2006.
137. **Lavoie B, Balemba OB, Godfrey C, Watson CA, Vassileva G, Corvera CU, Nelson MT, and Mawe GM.** Hydrophobic bile salts inhibit gallbladder smooth muscle function via stimulation of GPBAR1 receptors and activation of KATP channels. *The Journal of physiology* 588: 3295-3305, 2010.
138. **Lefkimmiatis K, Srikanthan M, Maiellaro I, Moyer MP, Curci S, and Hofer AM.** Store-operated cyclic AMP signalling mediated by STIM1. *Nature cell biology* 11: 433-442, 2009.
139. **Leslie JL, Huang S, Opp JS, Nagy MS, Kobayashi M, Young VB, and Spence JR.** Persistence and toxin production by *Clostridium difficile* within human intestinal organoids result in disruption of epithelial paracellular barrier function. *Infection and immunity* 83: 138-145, 2015.

140. **Lew JL, Zhao A, Yu J, Huang L, De Pedro N, Pelaez F, Wright SD, and Cui J.** The farnesoid X receptor controls gene expression in a ligand- and promoter-selective fashion. *The Journal of biological chemistry* 279: 8856-8861, 2004.
141. **Li C, Krishnamurthy PC, Penmatsa H, Marrs KL, Wang XQ, Zaccolo M, Jalink K, Li M, Nelson DJ, Schuetz JD, and Naren AP.** Spatiotemporal coupling of cAMP transporter to CFTR chloride channel function in the gut epithelia. *Cell* 131: 940-951, 2007.
142. **Li C, and Naren AP.** CFTR chloride channel in the apical compartments: spatiotemporal coupling to its interacting partners. *Integrative biology : quantitative biosciences from nano to macro* 2: 161-177, 2010.
143. **Li T, and Chiang JY.** Mechanism of rifampicin and pregnane X receptor inhibition of human cholesterol 7 alpha-hydroxylase gene transcription. *American journal of physiology Gastrointestinal and liver physiology* 288: G74-84, 2005.
144. **Li T, and Chiang JY.** Nuclear receptors in bile acid metabolism. *Drug metabolism reviews* 45: 145-155, 2013.
145. **Li T, Holmstrom SR, Kir S, Umetani M, Schmidt DR, Kliewer SA, and Mangelsdorf DJ.** The G protein-coupled bile acid receptor, TGR5, stimulates gallbladder filling. *Molecular endocrinology* 25: 1066-1071, 2011.
146. **Lieu T, Jayaweera G, and Bunnett NW.** GPBA: a GPCR for bile acids and an emerging therapeutic target for disorders of digestion and sensation. *British journal of pharmacology* 171: 1156-1166, 2014.
147. **Liu J, Walker NM, Cook MT, Ootani A, and Clarke LL.** Functional Cftr in crypt epithelium of organotypic enteroid cultures from murine small intestine. *American journal of physiology Cell physiology* 302: C1492-1503, 2012.
148. **Liu R, Zhao R, Zhou X, Liang X, Campbell DJ, Zhang X, Zhang L, Shi R, Wang G, Pandak WM, Sirica AE, Hylemon PB, and Zhou H.** Conjugated bile acids promote cholangiocarcinoma cell invasive growth through activation of sphingosine 1-phosphate receptor 2. *Hepatology* 60: 908-918, 2014.
149. **Loffing J, Moyer BD, McCoy D, and Stanton BA.** Exocytosis is not involved in activation of Cl<sup>-</sup> secretion via CFTR in Calu-3 airway epithelial cells. *The American journal of physiology* 275: C913-920, 1998.
150. **Lorenzo-Zuniga V, Bartoli R, Planas R, Hofmann AF, Vinado B, Hagey LR, Hernandez JM, Mane J, Alvarez MA, Ausina V, and Gassull MA.** Oral bile acids reduce bacterial overgrowth, bacterial translocation, and endotoxemia in cirrhotic rats. *Hepatology* 37: 551-557, 2003.
151. **Lotscher M, Kaissling B, Biber J, Murer H, and Levi M.** Role of microtubules in the rapid regulation of renal phosphate transport in response to acute alterations in dietary phosphate content. *J Clin Invest* 99: 1302-1312, 1997.

152. **Ma K, Saha PK, Chan L, and Moore DD.** Farnesoid X receptor is essential for normal glucose homeostasis. *The Journal of clinical investigation* 116: 1102-1109, 2006.
153. **Maheshwari A, LL C, and Schelonka RL.** Neonatal Necrotizing Enterocolitis. *Research and Reports in Neonatology* 39-53, 2011.
154. **Maiellaro I, Lefkimmiatis K, Moyer MP, Curci S, and Hofer AM.** Termination and activation of store-operated cyclic AMP production. *Journal of cellular and molecular medicine* 16: 2715-2725, 2012.
155. **Makishima M, Okamoto AY, Repa JJ, Tu H, Learned RM, Luk A, Hull MV, Lustig KD, Mangelsdorf DJ, and Shan B.** Identification of a nuclear receptor for bile acids. *Science* 284: 1362-1365, 1999.
156. **Maran RR, Thomas A, Roth M, Sheng Z, Esterly N, Pinson D, Gao X, Zhang Y, Ganapathy V, Gonzalez FJ, and Guo GL.** Farnesoid X receptor deficiency in mice leads to increased intestinal epithelial cell proliferation and tumor development. *The Journal of pharmacology and experimental therapeutics* 328: 469-477, 2009.
157. **Marchiando AM, Graham WV, and Turner JR.** Epithelial barriers in homeostasis and disease. *Annual review of pathology* 5: 119-144, 2010.
158. **Margolis BL, Lax I, Kris R, Dombalagian M, Honegger AM, Howk R, Givol D, Ullrich A, and Schlessinger J.** All autophosphorylation sites of epidermal growth factor (EGF) receptor and HER2/neu are located in their carboxyl-terminal tails. Identification of a novel site in EGF receptor. *The Journal of biological chemistry* 264: 10667-10671, 1989.
159. **Maruyama T, Kanaji T, Nakade S, Kanno T, and Mikoshiba K.** 2APB, 2-aminoethoxydiphenyl borate, a membrane-penetrable modulator of Ins(1,4,5)P<sub>3</sub>-induced Ca<sup>2+</sup> release. *Journal of biochemistry* 122: 498-505, 1997.
160. **Maruyama T, Miyamoto Y, Nakamura T, Tamai Y, Okada H, Sugiyama E, Nakamura T, Itadani H, and Tanaka K.** Identification of membrane-type receptor for bile acids (M-BAR). *Biochemical and biophysical research communications* 298: 714-719, 2002.
161. **Mazuy C, Helleboid A, Staels B, and Lefebvre P.** Nuclear bile acid signaling through the farnesoid X receptor. *Cellular and molecular life sciences : CMLS* 72: 1631-1650, 2015.
162. **McCole DF, Rogler G, Varki N, and Barrett KE.** Epidermal growth factor partially restores colonic ion transport responses in mouse models of chronic colitis. *Gastroenterology* 129: 591-608, 2005.
163. **McFedries A, Schwaid A, and Saghatelian A.** Methods for the elucidation of protein-small molecule interactions. *Chemistry & biology* 20: 667-673, 2013.
164. **Meisenhelder J, Suh PG, Rhee SG, and Hunter T.** Phospholipase C-gamma is a substrate for the PDGF and EGF receptor protein-tyrosine kinases in vivo and in vitro. *Cell* 57: 1109-1122, 1989.
165. **Mekhjjan HS, Phillips SF, and Hofmann AF.** Colonic absorption of unconjugated bile acids: perfusion studies in man. *Digestive diseases and sciences* 24: 545-550, 1979.

166. **Mekjian HS, Phillips SF, and Hofmann AF.** Colonic secretion of water and electrolytes induced by bile acids: perfusion studies in man. *The Journal of clinical investigation* 50: 1569-1577, 1971.
167. **Merlin D, Jiang L, Strohmeier GR, Nusrat A, Alper SL, Lencer WI, and Madara JL.** Distinct Ca<sup>2+</sup>- and cAMP-dependent anion conductances in the apical membrane of polarized T84 cells. *The American journal of physiology* 275: C484-495, 1998.
168. **Merritt ME, and Donaldson JR.** Effect of bile salts on the DNA and membrane integrity of enteric bacteria. *Journal of medical microbiology* 58: 1533-1541, 2009.
169. **Moeser AJ, Haskell MM, Shifflett DE, Little D, Schultz BD, and Blikslager AT.** ClC-2 chloride secretion mediates prostaglandin-induced recovery of barrier function in ischemia-injured porcine ileum. *Gastroenterology* 127: 802-815, 2004.
170. **Mohammad-Panah R, Gyomory K, Rommens J, Choudhury M, Li C, Wang Y, and Bear CE.** ClC-2 contributes to native chloride secretion by a human intestinal cell line, Caco-2. *The Journal of biological chemistry* 276: 8306-8313, 2001.
171. **Mondini A, Sassone F, Civello DA, Garavaglia ML, Bazzini C, Rodighiero S, Vezzoli V, Conti F, Torielli L, Capasso G, Paulmichl M, and Meyer G.** Hypertension-linked mutation of alpha-adducin increases CFTR surface expression and activity in HEK and cultured rat distal convoluted tubule cells. *PLoS one* 7: e52014, 2012.
172. **Morris AP, Scott JK, Ball JM, Zeng CQ, O'Neal WK, and Estes MK.** NSP4 elicits age-dependent diarrhea and Ca<sup>2+</sup>-mediated I<sup>-</sup> influx into intestinal crypts of CF mice. *The American journal of physiology* 277: G431-444, 1999.
173. **Mroz MS, Keating N, Ward JB, Sarker R, Amu S, Aviello G, Donowitz M, Fallon PG, and Keely SJ.** Farnesoid X receptor agonists attenuate colonic epithelial secretory function and prevent experimental diarrhoea in vivo. *Gut* 63: 808-817, 2013.
174. **Mroz MS, and Keely SJ.** Epidermal growth factor chronically upregulates Ca<sup>2+</sup>-dependent Cl<sup>-</sup> conductance and TMEM16A expression in intestinal epithelial cells. *The Journal of physiology* 590: 1907-1920, 2012.
175. **Murer H, Ammann E, Biber J, and Hopfer U.** The surface membrane of the small intestinal epithelial cell. I. Localization of adenyl cyclase. *Biochimica et biophysica acta* 433: 509-519, 1976.
176. **Nagahashi M, Takabe K, Liu R, Peng K, Wang X, Wang Y, Hait NC, Wang X, Allegood JC, Yamada A, Aoyagi T, Liang J, Pandak WM, Spiegel S, Hylemon PB, and Zhou H.** Conjugated bile acid-activated S1P receptor 2 is a key regulator of sphingosine kinase 2 and hepatic gene expression. *Hepatology* 61: 1216-1226, 2015.
177. **Nakahori Y, Takenaka O, and Nakagome Y.** A human X-Y homologous region encodes "amelogenin". *Genomics* 9: 264-269, 1991.
178. **Nakanishi S, Kakita S, Takahashi I, Kawahara K, Tsukuda E, Sano T, Yamada K, Yoshida M, Kase H, Matsuda Y, and et al.** Wortmannin, a microbial product inhibitor of myosin light chain kinase. *The Journal of biological chemistry* 267: 2157-2163, 1992.

179. **Namkung W, Phuan PW, and Verkman AS.** TMEM16A inhibitors reveal TMEM16A as a minor component of calcium-activated chloride channel conductance in airway and intestinal epithelial cells. *The Journal of biological chemistry* 286: 2365-2374, 2011.
180. **Naren AP, Quick MW, Collawn JF, Nelson DJ, and Kirk KL.** Syntaxin 1A inhibits CFTR chloride channels by means of domain-specific protein-protein interactions. *Proceedings of the National Academy of Sciences of the United States of America* 95: 10972-10977, 1998.
181. **Natalini B, Sardella R, Gioiello A, Ianni F, Di Michele A, and Marinozzi M.** Determination of bile salt critical micellization concentration on the road to drug discovery. *Journal of pharmaceutical and biomedical analysis* 87: 62-81, 2014.
182. **Nichols JM, Maiellaro I, Abi-Jaoude J, Curci S, and Hofer AM.** "Store-operated" cAMP signaling contributes to Ca<sup>2+</sup>-activated Cl<sup>-</sup> secretion in T84 colonic cells. *American journal of physiology Gastrointestinal and liver physiology* 309: G670-679, 2015.
183. **Oda K, Matsuoka Y, Funahashi A, and Kitano H.** A comprehensive pathway map of epidermal growth factor receptor signaling. *Molecular systems biology* 1: 2005 0010, 2005.
184. **Ootani A, Li X, Sangiorgi E, Ho QT, Ueno H, Toda S, Sugihara H, Fujimoto K, Weissman IL, Capecchi MR, and Kuo CJ.** Sustained in vitro intestinal epithelial culture within a Wnt-dependent stem cell niche. *Nature medicine* 15: 701-706, 2009.
185. **Ousingsawat J, Martins JR, Schreiber R, Rock JR, Harfe BD, and Kunzelmann K.** Loss of TMEM16A causes a defect in epithelial Ca<sup>2+</sup>-dependent chloride transport. *The Journal of biological chemistry* 284: 28698-28703, 2009.
186. **Ousingsawat J, Mirza M, Tian Y, Roussa E, Schreiber R, Cook DI, and Kunzelmann K.** Rotavirus toxin NSP4 induces diarrhea by activation of TMEM16A and inhibition of Na<sup>+</sup> absorption. *Pflugers Archiv : European journal of physiology* 461: 579-589, 2011.
187. **Pallagi-Kunstar E, Farkas K, Maleth J, Rakonczay Z, Jr., Nagy F, Molnar T, Szepes Z, Venglovecz V, Lonovics J, Razga Z, Wittmann T, and Hegyi P.** Bile acids inhibit Na<sup>(+)</sup>/H<sup>(+)</sup> exchanger and Cl<sup>(-)</sup>/HCO<sup>(3-)</sup> exchanger activities via cellular energy breakdown and Ca<sup>(2+)</sup> overload in human colonic crypts. *Pflugers Archiv : European journal of physiology* 467: 1277-1290, 2015.
188. **Parks DJ, Blanchard SG, Bledsoe RK, Chandra G, Consler TG, Kliewer SA, Stimmel JB, Willson TM, Zavacki AM, Moore DD, and Lehmann JM.** Bile acids: natural ligands for an orphan nuclear receptor. *Science* 284: 1365-1368, 1999.
189. **Penmatsa H, Zhang W, Yarlagadda S, Li C, Conoley VG, Yue J, Bahouth SW, Buddington RK, Zhang G, Nelson DJ, Sonecha MD, Manganiello V, Wine JJ, and Naren AP.** Compartmentalized cyclic adenosine 3',5'-monophosphate at the plasma membrane clusters PDE3A and cystic fibrosis transmembrane conductance regulator into microdomains. *Molecular biology of the cell* 21: 1097-1110, 2010.
190. **Pols TW, Nomura M, Harach T, Lo Sasso G, Oosterveer MH, Thomas C, Rizzo G, Gioiello A, Adorini L, Pellicciari R, Auwerx J, and Schoonjans K.** TGR5 activation inhibits atherosclerosis by reducing macrophage inflammation and lipid loading. *Cell metabolism* 14: 747-757, 2011.

191. **Potter GD, Sellin JH, and Burlingame SM.** Bile acid stimulation of cyclic AMP and ion transport in developing rabbit colon. *Journal of pediatric gastroenterology and nutrition* 13: 335-341, 1991.
192. **Prasad R, Venkatasubramanian J, Amde M, and Rao MC.** Phospholipase C and src tyrosine kinases mediate neurotensin-stimulated Cl<sup>-</sup> secretion in rabbit proximal colon. *Digestive diseases and sciences* 49: 1318-1326, 2004.
193. **Prenzel N, Zwick E, Daub H, Leserer M, Abraham R, Wallasch C, and Ullrich A.** EGF receptor transactivation by G-protein-coupled receptors requires metalloproteinase cleavage of proHB-EGF. *Nature* 402: 884-888, 1999.
194. **Priyamvada S, Gomes R, Gill RK, Saksena S, Alrefai WA, and Dudeja PK.** Mechanisms Underlying Dysregulation of Electrolyte Absorption in Inflammatory Bowel Disease-Associated Diarrhea. *Inflammatory bowel diseases* 21: 2926-2935, 2015.
195. **Qiao D, Stratagouleas ED, and Martinez JD.** Activation and role of mitogen-activated protein kinases in deoxycholic acid-induced apoptosis. *Carcinogenesis* 22: 35-41, 2001.
196. **Qiao L, Studer E, Leach K, McKinstry R, Gupta S, Decker R, Kukreja R, Valerie K, Nagarkatti P, El Deiry W, Molkentin J, Schmidt-Ullrich R, Fisher PB, Grant S, Hylemon PB, and Dent P.** Deoxycholic acid (DCA) causes ligand-independent activation of epidermal growth factor receptor (EGFR) and FAS receptor in primary hepatocytes: inhibition of EGFR/mitogen-activated protein kinase-signaling module enhances DCA-induced apoptosis. *Molecular biology of the cell* 12: 2629-2645, 2001.
197. **Qiu W, Lee B, Lancaster M, Xu W, Leung S, and Guggino SE.** Cyclic nucleotide-gated cation channels mediate sodium and calcium influx in rat colon. *American journal of physiology Cell physiology* 278: C336-343, 2000.
198. **Raimondi F, Santoro P, Barone MV, Pappacoda S, Barretta ML, Nanayakkara M, Apicella C, Capasso L, and Paludetto R.** Bile acids modulate tight junction structure and barrier function of Caco-2 monolayers via EGFR activation. *American journal of physiology Gastrointestinal and liver physiology* 294: G906-913, 2008.
199. **Rajagopal S, Kumar DP, Mahavadi S, Bhattacharya S, Zhou R, Corvera CU, Bunnett NW, Grider JR, and Murthy KS.** Activation of G protein-coupled bile acid receptor, TGR5, induces smooth muscle relaxation via both Epac- and PKA-mediated inhibition of RhoA/Rho kinase pathway. *American journal of physiology Gastrointestinal and liver physiology* 304: G527-535, 2013.
200. **Randall KJ, Turton J, and Foster JR.** Explant culture of gastrointestinal tissue: a review of methods and applications. *Cell biology and toxicology* 27: 267-284, 2011.
201. **Rao MC, Sarathy J, and Ao M.** *Intestinal water and electrolyte transport in health and disease*. San Rafael, Calif . Morgan & Claypool, 2012, p. ix, 105 p.
202. **Raufman JP, Chen Y, Cheng K, Compadre C, Compadre L, and Zimniak P.** Selective interaction of bile acids with muscarinic receptors: a case of molecular mimicry. *European journal of pharmacology* 457: 77-84, 2002.

203. **Raufman JP, Cheng K, and Zimniak P.** Activation of muscarinic receptor signaling by bile acids: physiological and medical implications. *Digestive diseases and sciences* 48: 1431-1444, 2003.
204. **Raufman JP, Zimniak P, and Bartoszko-Malik A.** Lithocholytaurine interacts with cholinergic receptors on dispersed chief cells from guinea pig stomach. *The American journal of physiology* 274: G997-1004, 1998.
205. **Ridlon JM, Kang DJ, and Hylemon PB.** Bile salt biotransformations by human intestinal bacteria. *Journal of lipid research* 47: 241-259, 2006.
206. **Riordan JR.** CFTR function and prospects for therapy. *Annual review of biochemistry* 77: 701-726, 2008.
207. **Sadana R, and Dessauer CW.** Physiological roles for G protein-regulated adenylyl cyclase isoforms: insights from knockout and overexpression studies. *Neuro-Signals* 17: 5-22, 2009.
208. **Sassone-Corsi P.** The cyclic AMP pathway. *Cold Spring Harbor perspectives in biology* 4: 2012.
209. **Sato T, and Clevers H.** Growing self-organizing mini-guts from a single intestinal stem cell: mechanism and applications. *Science* 340: 1190-1194, 2013.
210. **Sato T, Vries RG, Snippert HJ, van de Wetering M, Barker N, Stange DE, van Es JH, Abo A, Kujala P, Peters PJ, and Clevers H.** Single Lgr5 stem cells build crypt-villus structures in vitro without a mesenchymal niche. *Nature* 459: 262-265, 2009.
211. **Savage DC.** Microbial ecology of the gastrointestinal tract. *Annual review of microbiology* 31: 107-133, 1977.
212. **Saxena K, Blutt SE, Ettayebi K, Zeng XL, Broughman JR, Crawford SE, Karandikar UC, Sastri NP, Conner ME, Opekun AR, Graham DY, Qureshi W, Sherman V, Foulke-Abel J, In J, Kovbasnjuk O, Zachos NC, Donowitz M, and Estes MK.** Human Intestinal Enteroids: a New Model To Study Human Rotavirus Infection, Host Restriction, and Pathophysiology. *Journal of virology* 90: 43-56, 2016.
213. **Sayin SI, Wahlstrom A, Felin J, Jantti S, Marschall HU, Bamberg K, Angelin B, Hyotylainen T, Oresic M, and Backhed F.** Gut microbiota regulates bile acid metabolism by reducing the levels of tauro-beta-muricholic acid, a naturally occurring FXR antagonist. *Cell metabolism* 17: 225-235, 2013.
214. **Schmidt M, Dekker FJ, and Maarsingh H.** Exchange protein directly activated by cAMP (epac): a multidomain cAMP mediator in the regulation of diverse biological functions. *Pharmacological reviews* 65: 670-709, 2013.
215. **Schmidt M, Evellin S, Weernink PA, von Dorp F, Rehmann H, Lomasney JW, and Jakobs KH.** A new phospholipase-C-calcium signalling pathway mediated by cyclic AMP and a Rap GTPase. *Nature cell biology* 3: 1020-1024, 2001.

216. **Schoemaker MH, Conde de la Rosa L, Buist-Homan M, Vrenken TE, Havinga R, Poelstra K, Haisma HJ, Jansen PL, and Moshage H.** Tauroursodeoxycholic acid protects rat hepatocytes from bile acid-induced apoptosis via activation of survival pathways. *Hepatology* 39: 1563-1573, 2004.
217. **Schroeder BC, Cheng T, Jan YN, and Jan LY.** Expression cloning of TMEM16A as a calcium-activated chloride channel subunit. *Cell* 134: 1019-1029, 2008.
218. **Shah VS, Meyerholz DK, Tang XX, Reznikov L, Abou Alaiwa M, Ernst SE, Karp PH, Wohlford-Lenane CL, Heilmann KP, Leidinger MR, Allen PD, Zabner J, McCray PB, Jr., Ostedgaard LS, Stoltz DA, Randak CO, and Welsh MJ.** Airway acidification initiates host defense abnormalities in cystic fibrosis mice. *Science* 351: 503-507, 2016.
219. **Shan J, Oshima T, Fukui H, Watari J, and Miwa H.** Acidic deoxycholic acid and chenodeoxycholic acid induce interleukin-8 production through p38 mitogen-activated protein kinase and protein kinase A in a squamous epithelial model. *Journal of gastroenterology and hepatology* 28: 823-828, 2013.
220. **Shaw G, Morse S, Ararat M, and Graham FL.** Preferential transformation of human neuronal cells by human adenoviruses and the origin of HEK 293 cells. *FASEB journal : official publication of the Federation of American Societies for Experimental Biology* 16: 869-871, 2002.
221. **Sheikh Abdul Kadir SH, Miragoli M, Abu-Hayyeh S, Moshkov AV, Xie Q, Keitel V, Nikolaev VO, Williamson C, and Gorelik J.** Bile acid-induced arrhythmia is mediated by muscarinic M2 receptors in neonatal rat cardiomyocytes. *PloS one* 5: e9689, 2010.
222. **Sheikh IA, Koley H, Chakrabarti MK, and Hoque KM.** The Epac1 signaling pathway regulates Cl<sup>-</sup> secretion via modulation of apical KCNN4c channels in diarrhea. *The Journal of biological chemistry* 288: 20404-20415, 2013.
223. **Sheppard DN.** CFTR channel pharmacology: insight from a flock of clones. Focus on "Divergent CFTR orthologs respond differently to the channel inhibitors CFTRinh-172, glibenclamide, and GlyH-101". *Am J Physiol Cell Physiol* 302: C24-26, 2012.
224. **Sheridan JT, Worthington EN, Yu K, Gabriel SE, Hartzell HC, and Tarran R.** Characterization of the oligomeric structure of the Ca(2+)-activated Cl<sup>-</sup> channel Ano1/TMEM16A. *The Journal of biological chemistry* 286: 1381-1388, 2011.
225. **Shimo T, Matsumura S, Ibaragi S, Isowa S, Kishimoto K, Mese H, Nishiyama A, and Sasaki A.** Specific inhibitor of MEK-mediated cross-talk between ERK and p38 MAPK during differentiation of human osteosarcoma cells. *Journal of cell communication and signaling* 1: 103-111, 2007.
226. **Shneider BL, Dawson PA, Christie DM, Hardikar W, Wong MH, and Suchy FJ.** Cloning and molecular characterization of the ontogeny of a rat ileal sodium-dependent bile acid transporter. *The Journal of clinical investigation* 95: 745-754, 1995.
227. **Simmonds N, Furman M, Karanika E, Phillips A, and Bates AW.** Paneth cell metaplasia in newly diagnosed inflammatory bowel disease in children. *BMC gastroenterology* 14: 93, 2014.

228. **Simons K, and van Meer G.** Lipid sorting in epithelial cells. *Biochemistry* 27: 6197-6202, 1988.
229. **Smyth JT, Hwang SY, Tomita T, DeHaven WI, Mercer JC, and Putney JW.** Activation and regulation of store-operated calcium entry. *Journal of cellular and molecular medicine* 14: 2337-2349, 2010.
230. **Sommerfeld A, Reinehr R, and Haussinger D.** Bile acid-induced epidermal growth factor receptor activation in quiescent rat hepatic stellate cells can trigger both proliferation and apoptosis. *The Journal of biological chemistry* 284: 22173-22183, 2009.
231. **Sorg JA, and Sonenshein AL.** Inhibiting the initiation of *Clostridium difficile* spore germination using analogs of chenodeoxycholic acid, a bile acid. *Journal of bacteriology* 192: 4983-4990, 2010.
232. **Spence JR, Mayhew CN, Rankin SA, Kuhar MF, Vallance JE, Tolle K, Hoskins EE, Kalinichenko VV, Wells SI, Zorn AM, Shroyer NF, and Wells JM.** Directed differentiation of human pluripotent stem cells into intestinal tissue in vitro. *Nature* 470: 105-109, 2011.
233. **Stahl M, Stahl K, Brubacher MB, and Forrest JN, Jr.** Divergent CFTR orthologs respond differently to the channel inhibitors CFTRinh-172, glibenclamide, and GlyH-101. *American journal of physiology Cell physiology* 302: C67-76, 2012.
234. **Staudinger JL, Goodwin B, Jones SA, Hawkins-Brown D, MacKenzie KI, LaTour A, Liu Y, Klaassen CD, Brown KK, Reinhard J, Willson TM, Koller BH, and Kliewer SA.** The nuclear receptor PXR is a lithocholic acid sensor that protects against liver toxicity. *Proceedings of the National Academy of Sciences of the United States of America* 98: 3369-3374, 2001.
235. **Stravitz RT, Hylemon PB, Heuman DM, Hagey LR, Schteingart CD, Ton-Nu HT, Hofmann AF, and Vlahcevic ZR.** Transcriptional regulation of cholesterol 7 alpha-hydroxylase mRNA by conjugated bile acids in primary cultures of rat hepatocytes. *The Journal of biological chemistry* 268: 13987-13993, 1993.
236. **Studer E, Zhou X, Zhao R, Wang Y, Takabe K, Nagahashi M, Pandak WM, Dent P, Spiegel S, Shi R, Xu W, Liu X, Bohdan P, Zhang L, Zhou H, and Hylemon PB.** Conjugated bile acids activate the sphingosine-1-phosphate receptor 2 in primary rodent hepatocytes. *Hepatology* 55: 267-276, 2012.
237. **Sun H, Harris WT, Kortyka S, Kotha K, Ostmann AJ, Rezayat A, Sridharan A, Sanders Y, Naren AP, and Clancy JP.** Tgf-beta downregulation of distinct chloride channels in cystic fibrosis-affected epithelia. *PloS one* 9: e106842, 2014.
238. **Sung JY, Shaffer EA, and Costerton JW.** Antibacterial activity of bile salts against common biliary pathogens. Effects of hydrophobicity of the molecule and in the presence of phospholipids. *Digestive diseases and sciences* 38: 2104-2112, 1993.
239. **Svensson L, Finlay BB, Bass D, von Bonsdorff CH, and Greenberg HB.** Symmetric infection of rotavirus on polarized human intestinal epithelial (Caco-2) cells. *Journal of virology* 65: 4190-4197, 1991.

240. **Takahashi A, Watkins SC, Howard M, and Frizzell RA.** CFTR-dependent membrane insertion is linked to stimulation of the CFTR chloride conductance. *The American journal of physiology* 271: C1887-1894, 1996.
241. **Takahashi S, Homma K, Zhou Y, Nishimura S, Duan C, Chen J, Ahmad A, Cheatham MA, and Zheng J.** Susceptibility of outer hair cells to cholesterol chelator 2-hydroxypropyl-beta-cyclodextrine is prestin-dependent. *Scientific reports* 6: 21973, 2016.
242. **Takayama M, Ozaki H, and Karaki H.** Effects of a myosin light chain kinase inhibitor, wortmannin, on cytoplasmic Ca<sup>2+</sup> levels, myosin light chain phosphorylation and force in vascular smooth muscle. *Naunyn Schmiedebergs Arch Pharmacol* 354: 120-127, 1996.
243. **Taylor A, Mamelak M, Reaven E, and Maffly R.** Vasopressin: possible role of microtubules and microfilaments in its action. *Science* 181: 347-350, 1973.
244. **Thomas C, Gioiello A, Noriega L, Strehle A, Oury J, Rizzo G, Macchiarulo A, Yamamoto H, Mataki C, Pruzanski M, Pellicciari R, Auwerx J, and Schoonjans K.** TGR5-mediated bile acid sensing controls glucose homeostasis. *Cell metabolism* 10: 167-177, 2009.
245. **Tian Y, Kongsuphol P, Hug M, Ousingsawat J, Witzgall R, Schreiber R, and Kunzelmann K.** Calmodulin-dependent activation of the epithelial calcium-dependent chloride channel TMEM16A. *FASEB journal : official publication of the Federation of American Societies for Experimental Biology* 25: 1058-1068, 2011.
246. **Tousson A, Fuller CM, and Benos DJ.** Apical recruitment of CFTR in T-84 cells is dependent on cAMP and microtubules but not Ca<sup>2+</sup> or microfilaments. *Journal of cell science* 109 ( Pt 6): 1325-1334, 1996.
247. **Uribe JM, Gelbmann CM, Traynor-Kaplan AE, and Barrett KE.** Epidermal growth factor inhibits Ca(2+)-dependent Cl- transport in T84 human colonic epithelial cells. *The American journal of physiology* 271: C914-922, 1996.
248. **Uribe JM, Keely SJ, Traynor-Kaplan AE, and Barrett KE.** Phosphatidylinositol 3-kinase mediates the inhibitory effect of epidermal growth factor on calcium-dependent chloride secretion. *The Journal of biological chemistry* 271: 26588-26595, 1996.
249. **Venglarik CJ, Bridges RJ, and Frizzell RA.** A simple assay for agonist-regulated Cl and K conductances in salt-secreting epithelial cells. *The American journal of physiology* 259: C358-364, 1990.
250. **Venkatasubramanian J, Selvaraj N, Carlos M, Skaluba S, Rasenick MM, and Rao MC.** Differences in Ca(2+) signaling underlie age-specific effects of secretagogues on colonic Cl(-) transport. *American journal of physiology Cell physiology* 280: C646-658, 2001.
251. **Vitek L.** Bile acid malabsorption in inflammatory bowel disease. *Inflammatory bowel diseases* 21: 476-483, 2015.
252. **Walker NM, Liu J, Stein SR, Stefanski CD, Strubberg AM, and Clarke LL.** Cellular chloride and bicarbonate retention alters intracellular pH regulation in Cftr KO crypt epithelium. *American journal of physiology Gastrointestinal and liver physiology* 310: G70-80, 2016.

253. **Walters JR.** Bile acid diarrhoea and FGF19: new views on diagnosis, pathogenesis and therapy. *Nature reviews Gastroenterology & hepatology* 11: 426-434, 2014.
254. **Wang YD, Chen WD, Yu D, Forman BM, and Huang W.** The G-protein-coupled bile acid receptor, Gpbar1 (TGR5), negatively regulates hepatic inflammatory response through antagonizing nuclear factor kappa light-chain enhancer of activated B cells (NF-kappaB) in mice. *Hepatology* 54: 1421-1432, 2011.
255. **Wang Z, Yang H, Tachado SD, Capo-Aponte JE, Bildin VN, Koziel H, and Reinach PS.** Phosphatase-mediated crosstalk control of ERK and p38 MAPK signaling in corneal epithelial cells. *Investigative ophthalmology & visual science* 47: 5267-5275, 2006.
256. **Ward JB, Mroz MS, and Keely SJ.** The bile acid receptor, TGR5, regulates basal and cholinergic-induced secretory responses in rat colon. *Neurogastroenterology and motility : the official journal of the European Gastrointestinal Motility Society* 25: 708-711, 2013.
257. **Watanabe M, Houten SM, Matakai C, Christoffolete MA, Kim BW, Sato H, Messaddeq N, Harney JW, Ezaki O, Kodama T, Schoonjans K, Bianco AC, and Auwerx J.** Bile acids induce energy expenditure by promoting intracellular thyroid hormone activation. *Nature* 439: 484-489, 2006.
258. **Wedlake L, A'Hern R, Russell D, Thomas K, Walters JR, and Andreyev HJ.** Systematic review: the prevalence of idiopathic bile acid malabsorption as diagnosed by SeHCAT scanning in patients with diarrhoea-predominant irritable bowel syndrome. *Alimentary pharmacology & therapeutics* 30: 707-717, 2009.
259. **Weihrauch D, Kanchanapoo J, Ao M, Prasad R, Piyachaturawat P, and Rao MC.** Weanling, but not adult, rabbit colon absorbs bile acids: flux is linked to expression of putative bile acid transporters. *American journal of physiology Gastrointestinal and liver physiology* 290: G439-450, 2006.
260. **Wells JE, Berr F, Thomas LA, Dowling RH, and Hylemon PB.** Isolation and characterization of cholic acid 7alpha-dehydroxylating fecal bacteria from cholesterol gallstone patients. *Journal of hepatology* 32: 4-10, 2000.
261. **Wells JE, and Hylemon PB.** Identification and characterization of a bile acid 7alpha-dehydroxylation operon in *Clostridium* sp. strain TO-931, a highly active 7alpha-dehydroxylating strain isolated from human feces. *Applied and environmental microbiology* 66: 1107-1113, 2000.
262. **Werneburg NW, Yoon JH, Higuchi H, and Gores GJ.** Bile acids activate EGF receptor via a TGF-alpha-dependent mechanism in human cholangiocyte cell lines. *American journal of physiology Gastrointestinal and liver physiology* 285: G31-36, 2003.
263. **Wilson SS, Tocchi A, Holly MK, Parks WC, and Smith JG.** A small intestinal organoid model of non-invasive enteric pathogen-epithelial cell interactions. *Mucosal immunology* 8: 352-361, 2015.
264. **Wisler JW, Xiao K, Thomsen AR, and Lefkowitz RJ.** Recent developments in biased agonism. *Curr Opin Cell Biol* 27: 18-24, 2014.

265. **Wu W, Graves LM, Gill GN, Parsons SJ, and Samet JM.** Src-dependent phosphorylation of the epidermal growth factor receptor on tyrosine 845 is required for zinc-induced Ras activation. *The Journal of biological chemistry* 277: 24252-24257, 2002.
266. **Xiao Q, Yu K, Perez-Cornejo P, Cui Y, Arreola J, and Hartzell HC.** Voltage- and calcium-dependent gating of TMEM16A/Ano1 chloride channels are physically coupled by the first intracellular loop. *Proceedings of the National Academy of Sciences of the United States of America* 108: 8891-8896, 2011.
267. **Xie M, Rich TC, Scheitrum C, Conti M, and Richter W.** Inactivation of multidrug resistance proteins disrupts both cellular extrusion and intracellular degradation of cAMP. *Mol Pharmacol* 80: 281-293, 2011.
268. **Yang YD, Cho H, Koo JY, Tak MH, Cho Y, Shim WS, Park SP, Lee J, Lee B, Kim BM, Raouf R, Shin YK, and Oh U.** TMEM16A confers receptor-activated calcium-dependent chloride conductance. *Nature* 455: 1210-1215, 2008.
269. **Yoo BK, He P, Lee SJ, and Yun CC.** Lysophosphatidic acid 5 receptor induces activation of Na(+)/H(+) exchanger 3 via apical epidermal growth factor receptor in intestinal epithelial cells. *American journal of physiology Cell physiology* 301: C1008-1016, 2011.
270. **Yousef IM, Lewittes M, Tuchweber B, Roy CC, and Weber A.** Lithocholic acid-cholesterol interactions in rat liver plasma membrane fractions. *Biochimica et biophysica acta* 796: 345-353, 1984.
271. **Yousef IM, and Tuchweber B.** Effect of lithocholic acid on cholesterol synthesis and transport in the rat liver. *Biochimica et biophysica acta* 796: 336-344, 1984.
272. **Yu JZ, Dave RH, Allen JA, Sarma T, and Rasenick MM.** Cytosolic G $\alpha$ s acts as an intracellular messenger to increase microtubule dynamics and promote neurite outgrowth. *The Journal of biological chemistry* 284: 10462-10472, 2009.
273. **Yu K, Zhu J, Qu Z, Cui YY, and Hartzell HC.** Activation of the Ano1 (TMEM16A) chloride channel by calcium is not mediated by calmodulin. *The Journal of general physiology* 143: 253-267, 2014.
274. **Yu Y, Kuan AS, and Chen TY.** Calcium-calmodulin does not alter the anion permeability of the mouse TMEM16A calcium-activated chloride channel. *The Journal of general physiology* 144: 115-124, 2014.
275. **Zachos NC, Kovbasnjuk O, Foulke-Abel J, In J, Blutt SE, de Jonge HR, Estes MK, and Donowitz M.** Human Enteroids/Colonoids and Intestinal Organoids Functionally Recapitulate Normal Intestinal Physiology and Pathophysiology. *The Journal of biological chemistry* 291: 3759-3766, 2016.
276. **Zdebik AA, Cuffe JE, Bertog M, Korbmacher C, and Jentsch TJ.** Additional disruption of the ClC-2 Cl(-) channel does not exacerbate the cystic fibrosis phenotype of cystic fibrosis transmembrane conductance regulator mouse models. *The Journal of biological chemistry* 279: 22276-22283, 2004.

277. **Zhang Y, Lee FY, Barrera G, Lee H, Vales C, Gonzalez FJ, Willson TM, and Edwards PA.** Activation of the nuclear receptor FXR improves hyperglycemia and hyperlipidemia in diabetic mice. *Proceedings of the National Academy of Sciences of the United States of America* 103: 1006-1011, 2006.
278. **Zhang YG, Wu S, Xia Y, and Sun J.** Salmonella-infected crypt-derived intestinal organoid culture system for host-bacterial interactions. *Physiological reports* 2: 2014.
279. **Zimmerman NP, Kumar SN, Turner JR, and Dwinell MB.** Cyclic AMP dysregulates intestinal epithelial cell restitution through PKA and RhoA. *Inflamm Bowel Dis* 18: 1081-1091, 2012.
280. **Zwick E, Daub H, Aoki N, Yamaguchi-Aoki Y, Tinhofer I, Maly K, and Ullrich A.** Critical role of calcium- dependent epidermal growth factor receptor transactivation in PC12 cell membrane depolarization and bradykinin signaling. *The Journal of biological chemistry* 272: 24767-24770, 1997.

## Chapter IX. APPENDICES

### APPENDIX A

7/14/2016

Physiological Reports - Permissions - Wiley Online Library



## Physiological Reports

### Permissions

All articles published in this journal are made available under the terms of the [Creative Commons Attribution License](#). Permission is therefore not required for academic or commercial reuse, provided that full attribution is included in the new work.

7/14/2016

American Physiological Society > Copyright



[About](#) | [Testimonial](#) | [Jobs](#) | [Store](#) | [FASEB Directory](#)

Search

Support APS

[Awards](#) | [Careers](#) | [Education](#) | [Meetings](#) | [Membership](#) | [Publications](#) | [Science Policy](#)

### » Copyright



[home](#) / [publications](#) / [information for authors](#) / [copyright](#)

#### Login

#### In this section

- [Cost of Publication](#)
- [Authorship Changes](#)
- [Manuscript Formatting Requirements](#)
- [Manuscript Composition](#)
- [Preparing Figures](#)
- [Data Repository Standards](#)
- [Data Supplements](#)
- [Special Instructions for Physiological Reviews](#)
- [Special Instructions for Physiology in Medicine](#)
- [Peer Review Policy](#)
- [Open Access](#)
- [Policy on Depositing Articles in PMC](#)
- [Copyright](#)
- [Permissions](#)

#### Copyright

The APS Journals are copyrighted for the protection of authors and the Society. The Mandatory Submission Form serves as the Society's official copyright transfer form.

#### Rights of Authors of APS Articles

- For educational purposes only:
  - Authors may republish parts of their final-published version articles (e.g., figures, tables), without charge and without requesting permission, provided that full acknowledgement of the source is given in the new work.
  - Authors may use their articles (in whole or in part) for presentations (e.g., at meetings and conferences). These presentations may be reproduced on any type of media in materials arising from the meeting or conference such as the proceedings of a meeting or conference. A copyright fee will apply if there is a charge to the user or if the materials arising are directly or indirectly commercially supported.
- Posting of the accepted or final version of articles or parts of articles is restricted and subject to the conditions below:
  - Theses and dissertations.** APS permits whole published articles to be reproduced without charge in dissertations and posted to thesis repositories. Full citation is required.

#### Discover the APS

- [Pay Your Membership Dues](#)
- [Apply for Membership](#)
- [APS Council/Leadership](#)
- [Visit the Journals of the APS](#)
- [Support the Society](#)
- [Explore the Living History of Physiology](#)
- [Visit PhysiologyInfo.org](#)
- [Join a Committee](#)
- [Read Our New I Spy Physiology Blog](#)
- [Network on the APS Connect Community](#)
- [Find Us on Social Media](#)

## APPENDIX B



Office of Animal Care and  
Institutional Biosafety Committees (MC 672)  
Office of the Vice Chancellor for Research  
206 Administrative Office Building  
1737 West Polk Street  
Chicago, Illinois 60612-7227

May 23, 2016

To: University of Illinois Graduate College

From: Dr. Mary Bowman, Director, Office of Animal Care and Institutional Biosafety

A handwritten signature in black ink that reads "Mary Bowman, PhD".

Re: Thesis work involving the use of tissue/cells obtained from vertebrate animals

This letter is to inform you that the work conducted by Jada Domingue as part of her thesis involved use of animal tissues that were obtained from Dr. Hugo de Jonge at Erasmus University in Rotterdam, Netherlands. The graduate student had no direct contact with any animals and only received excess tissues/cells for in vitro analysis; therefore, an IACUC protocol number and approval are not required for the thesis deposit. Should you have any questions regarding this matter, please contact the Office of Animal Care and Institutional Biosafety at the number listed below.

## CHAPTER X. VITA

### EDUCATION

- 2010-2016 Ph.D., Physiology and Biophysics, College of Medicine, University of Illinois at Chicago (UIC), Chicago, IL.
- 2006-2010 B.S., Biological Sciences, School of Biological Sciences, University of California Irvine (UCI), Irvine, CA.

### PUBLICATIONS

- **Domingue JC**, Ao M, Sarathy J, and Rao, MC. Chenodeoxycholic acid requires activation of EGFR, EPAC and  $Ca^{2+}$  to stimulate CFTR-dependent  $Cl^-$  secretion in human colonic T84 cells. *In Revision for Am J Physiol Cell Physiol*.
- Ao, M., **Domingue, J.C.**, Khan, N., Javed, F., Osmani, K., Sarathy, J., and Rao, MC. (2016). Lithocholic acid attenuates cAMP-dependent  $Cl^-$  secretion in human colonic epithelial T84 cells. *Am J Physiol Cell Physiol*. 310:C1010-1023.
- **Domingue JC** and Rao MC. Pyk and ERK your way to the hub by taking a RSK2 (Editorial Focus). 2015. *Am J Physiol Cell Physiol*. 309(1):C11-13.
- **Domingue JC**, Ao M, Sarathy J, George A, Alrefai WA, Nelson DJ, Rao MC. HEK-293 cells expressing the cystic fibrosis transmembrane conductance regulator (CFTR): a model for studying regulation of  $Cl^-$  transport. 2014. *Physiol Rep*. 2(9):e12158; 1-16.
- **Domingue JC** and Rao MC. CFTR and GM1 “gangl-ing” up to heal thy wound (Editorial Focus). 2014. *Am J Physiol Cell Physiol*. 306(9): C789-91.
- Ao M, Sarathy J, **Domingue J**, Alrefai WA, Rao MC. Chenodeoxycholic acid stimulates  $Cl^-$  secretion via cAMP signaling and increases cystic fibrosis transmembrane conductance regulator phosphorylation in T84 cells. 2013. *Am J Physiol Cell Physiol*. 305:C447–C456.

### MANUSCRIPTS IN PREPARATION

- **Domingue JC**, George AT, Ao M, Sarathy J, Rao MC. Chenodeoxycholic acid stimulates  $Cl^-$  secretion via the  $Ca^{2+}$ -activated  $Cl^-$  channel TMEM16A in HEK-293 cells.

### AWARDS/HONORS

- 2016 Chancellor’s Student Service and Leadership Award, UIC
- 2016 Semi-Finalist Robert Gunn Student Award, Cell and Molecular Physiology Section, American Physiological Society
- 2016 Minority Travel Fellowship Award, American Physiological Society
- 2016 Caroline tum Suden/Frances Hellebrandt Professional Opportunity Award, American Physiological Society
- 2015 College of Medicine Research Forum Honorable Mention, UIC
- 2015 Mark R. Lambrecht Award for Scholarship and Commitment, UIC Physiology and Biophysics
- 2015 Lambrecht Award for Research, UIC Physiology and Biophysics
- 2015 Porter Physiology Development Fellowship, American Physiological Society
- 2015 Abraham Lincoln Fellowship, UIC Graduate College; declined due to Porter Fellowship
- 2015 Poster Presentation Award, American Physiological Society GI & Liver Section for Experimental Biology 2015
- 2015 Meritorious Research Travel Award, American Physiological Society Epithelial Transport Group
- 2015 Undergraduate Mentoring Award, UIC Graduate College
- 2015 Poster of Distinction, American Physiological Society GI & Liver Section

- 2015 Minority Travel Fellowship Award, American Physiological Society
- 2014 Kate Barany Student Award, UIC Physiology and Biophysics
- 2014 Provost & Deiss Research Award, UIC Graduate College
- 2014 Dean's Scholar Award, UIC Graduate College
- 2014 Abraham Lincoln Fellowship, UIC Graduate College; declined due to Dean's Scholar
- 2014 Poster Presentation Award, American Physiological Society GI & Liver Section, Experimental Biology 2014
- 2014 Poster of Distinction, American Physiological Society GI & Liver Section

### **RESEARCH FELLOWSHIPS**

**Source:** American Physiological Society Porter Physiology Development Fellowship

**Dates:** August 2015-July 2016

**Title:** Molecular Mechanisms of Colonic Cl<sup>-</sup> Secreting Cells Contributing to Bile-Acid Associated Diarrhea

**Role:** PI

**Goals:** To elucidate chenodeoxycholic acid activation of Cl<sup>-</sup> secretion in *in vitro* and *ex vivo* models of the mammalian colon.

**Source:** University of Illinois at Chicago Graduate College Dean's Scholar Award

**Dates:** August 2014-July 2015

**Title:** Bile Acid Regulation of Cl<sup>-</sup> Secretion in the Human Colonic Epithelium

**Role:** PI

**Goals:** To determine the underlying signaling mechanisms of bile acid action in the regulation of fluid and electrolyte transport across the colonic epithelium.

### **TEACHING/MENTORING EXPERIENCE**

- 2014 to 2016 Co-Research Supervisor to Kashif Osmani, UIC Undergraduate GPA Student; Project: Phorbol esters and miRNA regulation of prostaglandin stimulated ion transport.
- 2013 to 2015 Research Supervisor to Alvin George, UIC Undergraduate GPA Student; Project: Examination of chloride channels in HEK cells.
- Jun. 2013, '14, '16 Gastrointestinal Physiology lecturer, Summer Pre-Matriculation Program Physiology Course, UIC Urban Health Program; Delivered lectures, developed study guides, and exam questions.
- Aug.- Dec. 2013 Lead Teaching Assistant/Tutor for UIC Graduate College Life Science Human Physiology Course. Conducted review sessions, office hours, and small group tutoring.
- 2012-2013 Research Supervisor for Shreya Shanker, Junior at Illinois Math and Science Academy; Project: Characterization of the role of multidrug resistance proteins in T84 cells.

### **RESEARCH EXPERIENCE**

- 2011-2016 Ph.D. Candidate; University of Illinois at Chicago, Chicago, IL.  
Advisor: Mrinalini Rao, Ph.D.  
Thesis: "CDCA Activation of CFTR-Dependent Cl<sup>-</sup> Secretion Requires a Complex Network of Signaling Cascades"
- Sep.- Nov. 2015 Visiting Research Scientist, Erasmus University MC, Rotterdam, Netherlands  
Advisor: Hugo de Jonge, Ph.D.

- Project: “CDCA-Induced Swelling in Human and Mouse Intestinal Organoids”

  - Jun.- Aug. 2010 Visiting Research Scientist, Minority Health and Health Disparities International Research Training Program; Centro Superior de Investigacion en Salud Publica, Valencia, Spain  
Advisors: Pilar Francino, Ph.D. & Yvonne Valles, Ph.D.
- Project: “The Transfer of the Gut Microbiome from Mother to Infant”

  - 2009-2010 Undergraduate Researcher, Minority Access to Research Careers Program; University of California Irvine, Irvine, CA.  
Advisor: Tom Carew, Ph.D.
- Project: “The Role of Serotonin in Tail-withdrawal Responses in *Aplysia*”

  - Jun.- Aug. 2009 Visiting Undergraduate Researcher, Minority Health and Health Disparities International Research Training Program; Instituto de Neurobiologia, Universidad Nacional Autonoma de Mexico, Juriquilla, Queretaro, Mexico  
Advisor: Gina Lorena Quirarte, Ph.D.
- Project: “The Effects of Corticosterone on Consolidation of Spatial Memory in the Dorsomedial Striatum”

  - Mar.-Jun. 2009 Undergraduate Researcher, Minority Biomedical Research Support Program; University of California Irvine, Irvine, CA.  
Advisor: Luis-Mota-Bravo, Ph.D.

### **LEADERSHIP EXPERIENCE**

#### **University of Illinois at Chicago:**

- 2013-2016 President, Physiology and Biophysics Graduate Student Association (PBGSA).
- 2013-2015 Co-founder and Event Organizer, GEMS Gives Back. *GEMS Gives Back helps the Chicago community and builds interdepartmental relationships through volunteer efforts.*
- 2013-2014 Vice-President and Co-founder, Graduate Education in Medical Sciences (GEMS) Student Association (GEMSSA).
- 2013-2014 Vice President, Women’s Club Soccer, University of Illinois at Chicago.
- 2012-2013 Physiology and Biophysics Representative to the Graduate Student Council
- 2012-2013 Vice President, Physiology and Biophysics Graduate Student Association

#### **University of California, Irvine:**

- 2009-2010 President, Women’s Club Soccer, University of California Irvine.

### **ABSTRACTS/PRESENTATIONS**

- **Domingue J**, George A, Ao M, Bijvelds M, de Jonge H, Rao M. Chenodeoxycholic acid (CDCA) initiates distinct signaling mechanisms to stimulate Cl<sup>-</sup> transport in intestinal and non-intestinal epithelial cells. 2016. *FASEB* 30:969.25. Presented at Experimental Biology, San Diego, CA. Oral and Poster Presentation.
  - Also presented as an Oral Presentation at 2016 Pre-EB Epithelial Transport Meeting
- Osmani K, Ao M, **Domingue J**, Sarathy J, Rao M. Phorbol dibutyrate (PDB) regulation of the cystic fibrosis transmembrane conductance regulator (CFTR) may involve down-regulation of

- microRNAs (miRs). 2016. *FASEB* 30:1223.21. Presented at Experimental Biology, San Diego, CA. Poster Presentation.
- Detloff SJ, Khan N, Ao M, Movva B, Nair T, Sirajuddin H, **Domingue J**, Rao M, Sarathy J. The yin and yang of bile acid (BA) action on tight junctions (TJ) in colonic epithelia: a putative role for pro-inflammatory cytokine. *FASEB* 30:1223.29. Presented at Experimental Biology, San Diego, CA. Poster Presentation.
  - Ao M, **Domingue J**, Osmani K, Alrefai W, Sarathy J, Rao MC. The bile acid (BA), lithocholic acid (LCA) alters multiple signaling cascades in human T84 colonic cells, but attenuates forskolin (FSK) induced Cl<sup>-</sup> secretion only via interfering with cAMP production and basolateral membrane (BLM) K<sup>+</sup> conductances. 2015. *Gastroenterology* 148: 5:S879. Presented at Digestive Diseases Week, Washington, DC. Poster Presentation
  - **Domingue J**, Ao M, Sarathy J, Alrefai W, Rao MC. Bile Acid (BA) Stimulation of Cl<sup>-</sup> secretion involves intricate crosstalk cascades in human colonic T84 cells. 2015. *FASEB* 29:855.1. Presented at Experimental Biology, Boston, MA. Poster Presentation. **Awarded Poster of Distinction to Gastrointestinal & Liver Section of the APS.**
    - Oral Presentation at 2015 Pre-EB Epithelial Transport Meeting
  - George A, **Domingue J**, Ao M, Sarathy J, Rao MC. Chenodeoxycholate (CDCA) activation of Ca<sup>2+</sup>-dependent Cl<sup>-</sup> transport in human embryonic kidney-293 cells (HEK) is CFTR-independent. 2015. *FASEB* 29:LB764. Presented at Experimental Biology, Boston, MA. Poster Presentation.
  - Osmani K, Ao M, **Domingue J**, Sarathy J, Rao MC. Phorbol Dibutyrate (PDB) Regulation of the Cystic Fibrosis Transmembrane Conductance Regulator (CFTR) Does Not Involve MicroRNAs. 2015. *FASEB* 29:855.5. Presented at Experimental Biology, Boston, MA. Poster Presentation.
  - Khan N, Hung D, Javed F, Shukla P, Detloff S, Ao M, **Domingue J**, Rao MC, Sarathy J. Bile acid (BA), lithocholic acid (LCA), reverses chenodeoxycholic (CDCA)- and cytokine- induced loss in epithelial barrier function in human colon carcinoma T84 cells. 2015. *FASEB* 29:998.1. Presented at Experimental Biology, Boston, MA. Poster Presentation.
  - **Domingue J**, Ao M, Sarathy J, Alrefai W, Rao MC. Bile acid (BA) chenodeoxycholate (CDCA) activation of Cl<sup>-</sup> transport involves epidermal growth factor receptor (EGFR) signal transduction in human colonic T84 cells. 2014. *FASEB* 28:908. Presented at Experimental Biology, San Diego, CA. Poster Presentation. **Awarded Poster of Distinction to Gastrointestinal & Liver Section of the APS**
    - Oral Presentation at 2014 Pre-EB Epithelial Transport Meeting
  - **Domingue J**, Ao M, Sarathy J, Nelson D, Alrefai W, Rao MC. HEK-293 cells expressing the cystic fibrosis transmembrane conductance regulator (CFTR): a model for studying bile acid (BA) regulation of Cl<sup>-</sup> transport. 2014. *FASEB* 28:LB720. Presented at Experimental Biology, San Diego, CA. Poster Presentation
  - French S, Farmarin N, Badar A, Akhtar I, Ao M, **Domingue J**, Rao MC, Sarathy J. Effect of the bile acids (BA), chenodeoxycholic acid (CDCA) and deoxycholic acid (DCA), on epithelial tight junction (TJ) barrier function in a human colon carcinoma cell line, T84. 2014. *FASEB* 28:1113.3. Presented at Experimental Biology, San Diego, CA. Poster Presentation
  - Ao M, **Domingue J**, Sarathy J, Alrefai W, Rao MC. A Potential Therapeutic Target: Lithocholic Acid-Specific Suppression of cAMP-Stimulated Chloride Secretion in Human Colonic Epithelial T84 Cells Involving Multiple Signals. 2014. *Gastroenterology* 146: Issue 5:S785. Digestive Diseases Week, Chicago, IL. Tu1213. Poster Presentation
  - Ao M, Sarathy J (nee Venkatasubramanian), **Domingue J**, Mathew J, Alrefai WA., Rao MC. Chenodeoxycholic Acid (CDCA) Stimulates Cl<sup>-</sup> Secretion Across the Apical Membrane of Human Colonic Epithelial T84 Cells via cAMP Signaling and Increases in the Phosphorylation of the Cystic Fibrosis Transmembrane Conductance Regulator (CFTR). 2013.

*Gastroenterology* 142: Issue 5: S268. Digestive Diseases Week, San Diego, CA. Sa1306.  
Poster Presentation

- **Domingue J**, Ao M, Sarathy J, Shanker S, Nelson D, Alrefai W, Rao MC. Chenodeoxycholate (CDCA) activates Cl<sup>-</sup> transport via CF transmembrane conductance regulator in T84 and HEK cells. 2013. *FASEB 27:LB788*. Presented at Experimental Biology, Boston, MA. Poster Presentation
  - Also presented in 2013 at ASPET Great Lakes Chapter, Chicago, IL.
- **Domingue J**, Ao M, Sarathy J, Alrefai WA, Rao MC. Second messenger signaling of bile acid induced Cl<sup>-</sup> secretion in human colonic epithelia. 2012. College of Medicine Research Forum, University of Illinois at Chicago, Chicago, IL. Poster Presentation
- **Domingue J**, Carew TJ. The role of temporal and spatial patterning of 5HT for memory formation in *Aplysia*. 2010. Excellence in Research Forum, University of California, Irvine, Irvine CA. Poster & Oral Presentation
- **Domingue J**, Lozano Y, Quirarte G. The effects of corticosterone into the dorsomedial striatum on the consolidation and selection of navigation strategies. 2010. American Association for the Advancement of Science, San Diego, CA. Poster Presentation
  - Also presented in 2009 at Sigma XI, The Woodlands, TX.
  - Also presented in 2009 at *the Annual Biomedical Research Conference for Minority Students, Phoenix, AZ*

#### **SOCIETY MEMBERSHIPS**

- 2015-Present      Student Member of the American Association for the Advancement of Science
- 2013-Present      Student Member of the American Physiological Society
- 2010-2011        Student Member of Sigma Xi